NEUTRONICS OF A COUPLED MULTIPLE CHAMBER GASEOUS CORE REACTOR POWER SYSTEM

By

MATHEW M. PANICKER

A DISSERTATION PRESENTED TO THE GRADUATE SCHOOL
OF THE UNIVERSITY OF FLORIDA IN PARTIAL FULFILLMENT
OF THE REQUIREMENTS FOR THE DEGREE
OF DOCTOR OF PHILOSOPHY

UNIVERSITY OF FLORIDA

1989

To my parents.

ACKNOWLEDGEMENTS

The author wishes to express his sincere thanks and appreciation to the members of his supervisory committee, Dr. Alan Jacobs, Dr. Nils Diaz, Dr. Calvin C. Oliver, and Dr. Robert Hanrahan for their willingness to assist in the preparation of this dissertation.

The author is particularly thankful to Dr. Edward T. Dugan, his supervisory committee chairman, for his guidance, patience, and understanding throughout this research. The author is grateful for having studied under the direction of such splendid personality as Dr. Edward Dugan whose knowledge in gaseous core neutronics has been truly invaluable to the preparation of this dissertation.

This research was supported by funds from the Frederick A. Hauck Fund, the University of Florida, and the Air Force Wright Aeronautical Laboratories (AFWAL). The AFWAL work was performed for the Innovative Science and Technology Directorate of the Strategic Defense Initiative Organization within the Innovative Nuclear Space Power Institute (INSPI) at the University of Florida. The author wishes to express sincere thanks to the Frederick A. Hauck fund, the University of Florida, and the Air Force for their support

of this research. The author also wishes to express special thanks and appreciation to Dr. Nils Diaz, Director of INSPI, for affording him the opportunity to work in INSPI as a research assistant.

Computations for this research work were done at the University of Florida facilities (Northeast Regional Data Center and the CAD/CAM center) and at the San Diego Supercomputer Center. The author is grateful to the College of Engineering for the local computer support and the National Science Foundation for computer time at the San Diego Supercomputer Center.

The author is thankful to fellow graduate students with whom he had many fruitful discussions on various aspects of this research. Special thanks go to Mrs. Mary Cole for her assistance in the final preparation of this dissertation.

Finally, an indescribable degree of appreciation goes to the author's wife, Annamma, and son, Dinesh, for their patience, support, and understanding throughout the author's stay at the University of Florida.

TABLE OF CONTENTS

ACKNOWLEDGEMENTS.. iii

LIST OF TABLES.. viii

LIST OF FIGURES.. xiii

ABSTRACT.. xx

CHAPTERS

1 INTRODUCTION.. 1

Brief Description of the Multiple Cavity Pulsed Gaseous Core Reactor Power System.............. 3
Aim and Scope of the Dissertation................ 7
Organization of the Dissertation................. 8

2 PREVIOUS STUDIES ON COUPLED CORE NEUTRONICS...... 11

Introduction.................................. 11
Choice of Weighting Functions.................. 15
Selection of Phase Space Regions............... 17
Treatment of Coupling Effects.................. 20
  Coupling Coefficients......................... 20
  Delay Time Effects........................... 28
Comments...................................... 32

3 PREVIOUS STUDIES ON PULSED GASEOUS CORE REACTOR AT THE UNIVERSITY OF FLORIDA.................. 34

Introduction.................................. 34
UF6 Piston Engine of Kylstra et al............. 36
  Neutronic Analysis........................... 37
  Energy Model................................. 38
  Results...................................... 39
Pulsed Nuclear Piston and Pulsed
  Gas Generator Systems........................ 45
  Pulsed Nuclear Piston System................. 46
  Summary of PNP Results....................... 46
  Gas Generator Pulsed Gas Core Nuclear System... 57
Comments...................................... 66

4 STATIC NEUTRONIC STUDIES ON COUPLED MULTIPLE CAVITY GASEOUS CORE REACTOR SYSTEM............. 68

Introduction.. 68
The Bimodal Gas Core Reactor System Description.. 69
Steady State Neutronic Analysis.................. 73
Steady State Calculations Procedure.............. 76
Discussion of Results............................ 81
  Effect of PGCR Core Loading and Inner Beryllium Thickness Variations When the BPGCR Core Is Unfueled.................. 81
  Effect of Outer Beryllium Thickness Variation.................................... 106
  Effect of BPGCR Core Fuel Loading and Inner Beryllium Thickness Variations When the PGCR Core Fuel Loading Is Fixed.................. 111
  Effect of PGCR Core Fuel Loading and Inner Beryllium Thickness Variations When the BPGCR Core Fuel Loading Is Fixed............. 128
  Effect of Unequal PGCR Core Fuel Loading When the BPGCR Core Is Unfueled.................. 140
Summary... 142

5 DYNAMIC NEUTRONIC STUDIES ON COUPLED MULTIPLE CAVITY GASEOUS CORE REACTOR SYSTEM............. 146

Introduction.. 146
Method of Solution of Coupled Core Point Reactor Kinetics Equations in COUPKIN... 149
Discussion of Results............................ 151
  Integral Parameters: Coupling Coefficients, Neutron Generation Time, and Reactivity...... 151
    Effect of PGCR core fuel loading and inner beryllium thickness variations when the BPGCR chamber is unfueled............... 153
    Effect of outer beryllium thickness variations.............................. 170
    Effect of BPGCR core fuel loading and inner beryllium thickness variations when PGCR gas loading is fixed.......... 176
    Effect of PGCR core fuel loading and inner beryllium thickness variations when the BPGCR core has a nominal fuel loading............................ 191
    Effect of unequal PGCR core fuel loading when the BPGCR core is unfueled......... 202
  Results from Coupled Core Kinetics Analysis: Core Neutron Level and Delayed Neutron Precursor Concentration Variations........... 211
    Fueled PGCR cores and unfueled BPGCR core.. 212

Fueled PGCR cores and nominally fueled BPGCR core.............................. 236
Summary... 244

6 CONCLUSIONS, RECOMMENDATIONS AND AREAS OF FURTHER RESEARCH............................ 247

Introduction...................................... 247
Summary of Conclusions............................ 248
Variation in PGCR Fuel Loading (20-60 atm) and Inner Be Thickness (10-40 cm), Unfueled BPGCR Chamber.......................... 249
Effect of Outer Be Thickness Variation (20-70 cm).................................... 249
Variation in BPGCR Fuel Loading (25-100 atm) and Inner Be Thickness (10-40 cm), Fixed PGCR Fuel Loading (10 atm).................. 250
Variation in PGCR Core Loading (10-50 atm) and Inner Be Thickness (20-30 cm), Fixed BPGCR Chamber Loading (25 atm)..................... 251
Unequal PGCR Core Loading........................ 252
Static and Dynamic Neutronic Models for the Bimodal Gaseous Core Reactor System............ 256
Steady State Neutronic Analysis................ 256
Integral Kinetics Parameters for Individual Coupled Cores............................... 259
Neutron Kinetics Calculations.................. 260
Feedbacks due to Temperature Changes........... 261
Moderator Reflector Studies.................... 262
Fuel Studies................................... 263
Gas Flow/Heat Transfer Studies for the Bimodal Gaseous Core Reactor.......................... 264
Summary... 265

APPENDICES

A MCNP-A GENERAL MONTE CARLO CODE FOR NEUTRON AND PHOTON TRANSPORT............................. 268

B COUPLED CORE POINT REACTOR KINETICS EQUATIONS AND THE SOLUTION PROCEDURE....................... 319

C BENCHMARK CALCULATIONS WITH XSDRNPM AND MCNP CODES ON REFERENCE SPHERICAL AND CYLINDRICAL GAS CORE REACTOR SYSTEMS..................... 338

D COMPARISON OF RESULTS FROM COUPKIN AND ANCON CODES.. 351

REFERENCES.. 359

BIOGRAPHICAL SKETCH..................................... 363

LIST OF TABLES

Tables Pages

3-1 Summary of Results from the Different Neutron Kinetics Models for the PNP Configuration....... 59

3-2 Typical Equilibrium Cycle Pulsed Gas Generator System Operating Conditions........... 62

3-3 Typical Equilibrium Cycle Piston-Driven System Operating Conditions....................... 63

4-1 Core Physics Parameters for the Bimodal Gaseous Core Reactor System..................... 82

4-2 System Neutron Multiplication Factor (k_{eff}) and Neutron Removal Lifetime (ℓ) as a Function of PGCR Gas Loading for the Bimodal Gas Core Reactor System with Inner Beryllium Thickness of 10 cm................................ 83

4-3 System Neutron Multiplication Factor (k_{eff}) and Neutron Removal Lifetime (ℓ) as a Function of PGCR Gas Loading for the BGCR System with TIBE of 20 cm................................... 84

4-4 System Neutron Multiplication Factor (k_{eff}) and Neutron Removal Lifetime (ℓ) as a Function of PGCR Gas Loading for the BGCR System with TIBE of 25 cm................................... 85

4-5 System Neutron Multiplication Factor (k_{eff}) and Neutron Removal Lifetime (ℓ) as a Function of PGCR Gas Loading for the BGCR System with TIBE of 30 cm................................... 86

4-6 System Neutron Multiplication Factor (k_{eff}) and Neutron Removal Lifetime (ℓ) as a Function of PGCR Gas Loading for the BGCR System with TIBE of 40 cm................................... 87

4-7 System Neutron Multiplication Factor (k_{eff}) from MCNP as a Function of Inner Beryllium Thickness (TIBE) for Various PGCR Core Gas Loadings.. 101

4-8 System Neutron Multiplication Factor (k_{eff}) from XSDRNPM as a Function of Inner Beryllium Thickness (TIBE) for Various PGCR Core Gas Loadings.. 102

4-9 Total PGCR Gas Loading and Neutron Removal Lifetime at Criticality for Various Inner Beryllium Thicknesses of the BGCR System........ 103

4-10 Neutron Removal Lifetime (ℓ) as a Function of Inner Beryllium Thickness for Various PGCRGas Loading as Predicted by MCNP............ 104

4-11 System Neutron Multiplication Factor (k_{eff}) and Neutron Removal Lifetime (ℓ) as a Function of Outer Beryllium Thickness (TOBE) for TIBE of 20 cm.................................. 107

4-12 System Neutron Multiplication Factor (k_{eff}) and Neutron Removal Lifetime (ℓ) as a Function of Outer Beryllium Thickness (TOBE) for TIBE of 30 cm.................................. 108

4-13 System Neutron Multiplication Factor (k_{eff}) and Neutron Removal Lifetime (ℓ) as a Function of BPGCR Gas Loading for TIBE of 10 cm.......... 112

4-14 System Neutron Multiplication Factor (k_{eff}) and Neutron Removal Lifetime (ℓ) as a Function of BPGCR Gas Loading for TIBE of 20 cm.......... 113

4-15 System Neutron Multiplication Factor (k_{eff}) and Neutron Removal Lifetime (ℓ) as a Function of BPGCR Gas Loading for TIBE of 30 cm.......... 114

4-16 System Neutron Multiplication Factor (k_{eff}) and Neutron Removal Lifetime (ℓ) as a Function of BPGCR Gas Loading for TIBE of 40 cm.......... 115

4-17 System Neutron Multiplication Factor (k_{eff}) from MCNP as a Function of Inner Beryllium Thickness (TIBE) for the Bimodal Gas Core Reactor for Various BPGCR Gas Loadings.......... 123

4-18 System Neutron Multiplication Factor (k_{eff}) from XSDRNPM as a Function of Inner Beryllium Thickness (TIBE) for the Spherical Mockup of BGCR System for Various BPGCR Gas Loadings...... 124

4-19 System Neutron Removal Lifetime (ℓ) as a Function of Inner Beryllium Thickness (TIBE) for the BGCR System at Various BPGCR Gas-Fuel Loadings.................................. 129

4-20 System Neutron Multiplication Factor (k_{eff}) from XSDRNPM as a Function of Inner Beryllium Thickness (TIBE) for the Spherical Mockup of BGCR System for Various BPGCR Gas Loadings.. 134

4-21 System Neutron Multiplication Factor (k_{eff}) and System Neutron Removal Lifetime (ℓ) of the BGCR System as Predicted by MCNP for Various Unequal PGCR Gas Loadings............... 141

5-1 Integral Kinetics Parameters as a Function of PGCR Core Fuel-Gas Loading for the BGCR System with Inner Beryllium Thickness of 10 cm......... 154

5-2 Integral Kinetics Parameters as a Function of PGCR Core Fuel-Gas Loading for the BGCR System with Inner Beryllium Thickness of 20 cm......... 155

5-3 Integral Kinetics Parameters as a Function of PGCR Core Fuel-Gas Loading for the BGCR System with Inner Beryllium Thickness of 25 cm......... 156

5-4 Integral Kinetics Parameters as a Function of PGCR Core Fuel-Gas Loading for the BGCR System with Inner Beryllium Thickness of 30 cm......... 157

5-5 Integral Kinetics Parameters as a Function of PGCR Core Fuel-Gas Loading for the BGCR System with Inner Beryllium Thickness of 40 cm......... 158

5-6 Integral Kinetics Parameters as a Function of Outer Beryllium Thickness (TOBE) for the BGCR System with TIBE of 20 cm....................... 171

5-7 Integral Kinetics Parameters as a Function of Outer Beryllium Thickness (TOBE) for the BGCR System with TIBE of 30 cm....................... 172

5-8 Integral Kinetics Parameters as a Function of BPGCR Core Fuel-Gas Loading for the

BGCR System with TIBE of 10 cm.................. 177

5-9 Integral Kinetics Parameters as a Function of BPGCR Core Fuel-Gas Loading for the BGCR System with TIBE of 20 cm.............................. 178

5-10 Integral Kinetics Parameters as a Function of BPGCR Core Fuel-Gas Loading for the BGCR System with TIBE of 30 cm.................................. 179

5-11 Integral Kinetics Parameters as a Function of BPGCR Core Fuel-Gas Loading for the BGCR System with TIBE of 40 cm.................................. 180

5-12 Integral Kinetics Parameters as a Function of PGCR Core Fuel-Gas Loading for the BGCR System with TIBE of 20 cm.................................. 192

5-13 Integral Kinetics Parameters as a Function of PGCR Core Fuel-Gas Loading for the BGCR System with TIBE of 20 cm.................................. 193

5-14 Average Coupling Coefficients Among the PGCR Cores of the BGCR System with a TIBE of 20 cm When the PGCR Core Loading Pattern Is [60(4), 20(4), 10(4)]................................. 203

5-15 Average Coupling Coefficients Among the PGCR Cores for the BGCR System with a TIBE of 20 cm When the PGCR Core Loading Pattern Is [50(4), 30(4), 20(4)]................................. 204

5-16 Average Coupling Coefficients Among the PGCR Cores for the BGCR System with a TIBE of 20 cm When the PGCR Core Loading Pattern Is [70(4), 30(4), 20(4)]................................. 205

5-17 Average Coupling Coefficients Among the PGCR Cores for the BGCR System with a TIBE of 20 cm When the PGCR Core Loading Pattern Is [80(4), 40(4), 30(4)]................................. 206

5-18 Average Coupling Coefficients Among the PGCR Cores for the BGCR System with a TIBE of 20 cm When the PGCR Core Loading Pattern Is [70(6), 10(6)]... 207

5-19 Average Coupling Coefficients Among the PGCR Cores for the BGCR System with a TIBE of 30 cm When the PGCR Core Loading Pattern Is [80(4), 40(4), 30(4)]*............................... 210

A-1 MCNP Surface Cards.............................. 278

A-2 Basic MCNP Tallies................................ 289

A-3 Input Cards for the Bimodal Gaseous Core Reactor System............................... 301

A-4 MCNP Input for a Single Core PGCR................ 316

C-1 System k_{eff} from XSDRNPM Benchmark Calculations for the Reference Gaseous Core Reactor-Cylindrical Geometry... 340

C-2 System k_{eff} from XSDRNPM Benchmark Calculations for the Reference Gaseous Core Reactor-Spherical Geometry Mockup................................. 341

C-3 System k_{eff} from MCNP Benchmark Calculation for the Reference Gaseous Core Reactor System... 342

C-4 XSDRNPM Collapsed 26-Group Structures............. 344

C-5 XSDRNPM Collapsed 4-Group Structure............... 346

D-1 Relative Neutron Level (N(t)/N(0)) as a Function of Time as Predicted by ANCON and COUPKIN for a System of Neutron Multiplication Factor 1.0058.. 354

D-2 Relative Neutron Level (N(t)/N(0)) as a Function of Time as Predicted by ANCON and COUPKIN for a System of Neutron Multiplication Factor 0.9280.. 355

D-3 Relative Neutron Level (N(t)/N(0)) as a Function of Time as Predicted by ANCON and COUPKIN for a System of Neutron Multiplication Factor 1.0421.. 357

D-4 Relative Neutron Level (N(t)/N(0)) as a Function of Time as Predicted by ANCON and COUPKIN for a System of Neutron Multiplication Factor 1.1171.. 358

LIST OF FIGURES

1-1 Bimodal Gas Core Reactor Power System Schematic.... 4

1-2 Top and Side View of Bimodal Gas Core Reactor...... 5

2-1 Schematic Representation of Coupled Fast-Thermal Power Breeder; (a) Top View (b) Side View........ 13

3-1 Schematic Representation of UF_6 Piston Engine...... 35

3-2 Neutron Multiplication Factor Versus UF_6 Partial Pressure for an Infinite Graphite Reflector...... 40

3-3 Relative Thermal Flux in Core and Graphite Reflector for the UF_6 Piston Engine.............. 41

3-4 Average Core Thermal Neutron Flux and Neutron Multiplication Factor as a Function of Percent Travel Through the Piston Cycle for a Graphite-Reflected Engine................................ 42

3-5 UF_6 Piston Engine Performance for Thick Reflector Imposed at 10 Percent Cycle Position............ 44

3-6 General Schematic for a Piston-Driven Pulsed Gas Core Nuclear Power System.................... 47

3-7 Delayed Neutron and Photoneutron Precursor Concentration Buildup During Startup from Shutdown for Pulsed Nuclear Piston Engine................ 51

3-8 Peak Gas Temperature and Mechanical Power Versus Time During Startup from Shutdown for the Pulsed Nuclear Piston Engine......................... 52

3-9 Average Thermal Neutron Flux in the Core Versus Cycle Time for the PNP Engine When the Adiabatic Kinetics Model Is used.......................... 55

3-10 Average Thermal Neutron Flux in the Core Versus Cycle Time for the PNP Engine When the Point Kinetics Model Is Used with ℓ=2.557 msec........ 56

3-11 Average Thermal Neutron Flux in the Core Versus Cycle Time for the PNP Engine When the Point Kinetics Model Is Used with ℓ=1.718 msec......... 58

3-12 Pulsed Gas Generator Schematic..................... 60

3-13 Average Core Thermal Neutron Flux Versus Cycle Time for a Typical Gas Generator Pulsed Gas Core Nuclear System............................... 64

3-14 Average Core Thermal Neutron Flux Versus Cycle Time for a Typical Piston-Driven Pulsed Gas Core Nuclear System............................... 65

4-1 Cross-Sectional View of Cylindrical Bimodal Gas Core Reactor for MCNP and Spherical Mock-up of BGCR for XSDRNPM Calculation...................... 77

4-2 k_{eff} and ℓ as a Function of PGCR Gas Loading for TIBE of 10 cm................................ 89

4-3 k_{eff} and ℓ as a Function of PGCR Gas Loading for TIBE of 20 cm................................ 90

4-4 k_{eff} and ℓ as a Function of PGCR Gas Loading for TIBE of 25 cm................................ 91

4-5 k_{eff} and ℓ as a Function of PGCR Gas Loading for TIBE of 30 cm................................ 92

4-6 k_{eff} and ℓ as a Function of PGCR Gas Loading for TIBE of 40 cm................................ 93

4-7 System Neutron Multiplication Factor from XSDRNPM as a Function of PGCR Gas Loading........ 97

4-8 System Neutron Multiplication Factor, (k_{eff}) from MCNP as a Function of Inner Beryllium Thickness...................................... 98

4-9 System Neutron Multiplication Factor from XSDRNPM as a Function of Inner Beryllium Thickness...................................... 99

4-10 Neutron Removal Lifetime (ℓ) from MCNP as a Function of Inner Beryllium Thickness (TIBE) for Various PGCR Gas Loading..................... 105

4-11 System Neutron Multiplication Factor (k_{eff}) and Neutron Removal Lifetime (ℓ) as a Function of Outer Beryllium Thickness (TOBE) for TIBE of 20 cm.. 109

4-12 System Neutron Multiplication Factor (k_{eff}) and Neutron Removal Lifetime (ℓ) as a Function of Outer Beryllium Thickness (TOBE) for TIBE of 30 cm.. 110

4-13 System k_{eff} and ℓ as a Function of BPGCR Gas Loading for TIBE of 10 cm.......................... 117

4-14 System k_{eff} and ℓ as a Function of BPGCR Gas Loading for TIBE of 20 cm.......................... 118

4-15 System k_{eff} and ℓ as a Function of BPGCR Gas Loading for TIBE of 30 cm.......................... 119

4-16 System k_{eff} and ℓ as a Function of BPGCR Gas Loading for TIBE of 40 cm.......................... 120

4-17 System Neutron Multiplication Factor (k_{eff}) from MCNP as a Function of Inner Beryllium Thickness for Various BPGCR Chamber Fuel-Gas Loadings...... 125

4-18 System k_{eff} from XSDRNPM as a Function of Inner Beryllium Thickness for Various BPGCR Chamber Gas-Fuel Loadings.......................... 126

4-19 System Neutron Removal Lifetime (ℓ) as a Function of Inner Beryllium Thickness as Predicted by MCNP for BPGCR Chamber Gas Loadings.............. 130

4-20 System k_{eff} and ℓ as a Function of PGCR Gas Loading with 25 atmosphere of Fuel-Gas in BPGCR Chamber for TIBE of 20 cm.................. 132

4-21 System k_{eff} and ℓ as a Function of PGCR Gas Loading with 25 atmospheres of Fuel-Gas in BPGCR Chamber for TIBE of 30 cm.................. 133

4-22 System k_{eff} as a Function of Inner Beryllium Thickness Predicted by XSDRNPM for Various PGCR Gas Loadings................................ 135

4-23 Relative Radial Thermal Neutron Flux Distribution in the BGCR System with BPGCR Chamber at 75 Atmospheres and PGCR Core at 30 Atmospheres of Fuel-Gas Loading.............................. 138

4-24 Relative Radial Thermal Neutron Flux Distribution in the BGCR System with BPGCR Chamber at 100 Atmospheres and PGCR Cores at 10 Atmospheres Fuel-Gas Loading.................................. 139

5-1 Average Coupling Coefficients ($\alpha_{2\leftarrow k}$) as a Function of PGCR Gas Loading for a BGCR with TIBE of 10 cm.. 159

5-2 Average Coupling Coefficients ($\alpha_{2\leftarrow k}$) as a Function of PGCR Gas Loading for a BGCR with TIBE of 20 cm.. 160

5-3 Average Coupling Coefficients ($\alpha_{2\leftarrow k}$) as a Function of PGCR Gas Loading for a BGCR with TIBE of 25 cm.. 161

5-4 Average Coupling Coefficients ($\alpha_{2\leftarrow k}$) as a Function of PGCR Gas Loading for a BGCR with TIBE of 30 cm.. 162

5-5 Average Coupling Coefficients ($\alpha_{2\leftarrow k}$) as a Function of PGCR Gas Loading for a BGCR with TIBE of 40 cm.. 163

5-6 Average Coupling Coefficients ($\alpha_{2\leftarrow 3}$) as a Function of PGCR Gas Loading for Various Inner Beryllium Thickness...................................... 165

5-7 Average Coupling Coefficients ($\alpha_{2\leftarrow 3}$) as a Function of Inner Beryllium Thickness for Various PGCR Gas Loadings.................................... 166

5-8 Reactivity of BGCR System as a Function of PGCR Core Gas Loading for Various Inner Beryllium Thickness...................................... 168

5-9 Neutron Generation Time as a Function of Inner Beryllium Thickness for a BGCR with a BPGCR Chamber Gas Loading of 20 atm Helium Gas......... 169

5-10 Average Coupling Coefficients ($\alpha_{2\leftarrow k}$) as a Function of Outer Beryllium Thickness for TIBE of 20 cm and 30 cm...................................... 173

5-11 System Reactivity as a Function of Outer Beryllium Thickness 175

5-12 Average Coupling Coefficients (α_{jk}) due to Neutronic Contribution from PGCR Cores to BPGCR Chamber as a Function of BPGCR Core Fuel-Gas Loading.. 182

5-13 Average Coupling Coefficients (α_{jk}) due to Neutronic Contribution from PGCR Cores to BPGCR Chamber as a Function of Inner Beryllium Thickness.. 183

5-14 Average Coupling Coefficients Between Adjacent PGCR Cores ($\alpha_{2\leftarrow3,13}$) as a Function of Inner Beryllium Thickness for a BGCR with a PGCR Gas Loading of 10 atmospheres UF_6-He Mixture......... 185

5-15 Neutron Generation Time (Λ) as a Function of Inner Beryllium Thickness for a BGCR System with PGCR Core Gas Loading of 10 Atmospheres UF_6-He Mixture.................................. 187

5-16 Neutron Generation Time (Λ) as a Function of BPGCR Gas Loading for a BGCR System for Inner Beryllium Thickness of 10 cm and 40 cm..... 188

5-17 System Reactivity as a Function of BPGCR Gas Loading.. 190

5-18 Average Coupling Coefficients due to Neutronic Contribution from BPGCR Chamber to PGCR Cores as a Function of PGCR Gas Loading................ 194

5-19 Average coupling Coefficients due to Neutronic Contribution from PGCR Cores to BPGCR Chamber of the BGCR as a Function of PGCR Core Gas Loading.. 196

5-20 Average Coupling Coefficients Between Adjacent PGCR Cores as a Function of PGCR Gas Loading for the BGCR for both Unfueled and Fueled BPGCR Chamber.. 198

5-21 Neutron Generation Time as a Function of PGCR Core Gas Loading for the BGCR with Fueled and Unfueled BPGCR Chamber...................................... 200

5-22 System Reactivity as a Function of PGCR Core Gas Loading for the BGCR with Unfueled and Fueled BPGCR Chamber................................ 201

5-23 Relative PGCR Neutron Level and k_{eff} as a Function of Time for a TIBE of 20 cm............ 213

5-24 Relative PGCR Neutron Level and k_{eff} as a Function of Time for TIBE of 25 cm.............. 214

5-25 Relative PGCR Neutron Level and k_{eff} as a Function of Time for TIBE of 30 cm.............. 215

5-26 Relative PGCR Neutron Level and k_{eff} as a Function of Time for a TIBE of 40 cm............. 216

5-27 Relative PGCR Neutron Level as a Function of Time for a Cycle Time of 0.3 seconds for BGCR System with Inner Beryllium Thickness of 20 cm, 25 cm, 30 cm, and 40 cm with α_{jk}=0 During Exhaust....... 218

5-28 Relative PGCR Neutron Level and k_{eff} as a Function of Time for a TIBE of 30 cm and Cycle Time of 0.3 seconds with α_{jk}=0 During Exhaust.... 221

5-29 Relative PGCR Neutron Level and k_{eff} as a Function of Time for a TIBE of 40 cm with α_{jk}=0 During Exhaust.................................. 222

5-30 Relative PGCR Neutron Level as a Function of Cycle Time for a BGCR System with TIBE of 30 cm for Various Values of Coupling Coefficients (α_{jk}).... 224

5-31 Relative PGCR Neutron Level as a Function of Time for a BGCR with TIBE of 40 cm at Various Values of Coupling Coefficients................. 225

5-32 Relative PGCR Neutron Level as a Function of Cycle Time for a BGCR with a TIBE of 30 cm for Various Valies of Core-to-Core Delay Times (τ_{jk}).. 226

5-33 Relative PGCR Neutron Level as a Function of Cycle Time for a BGCR with a TIBE of 40 cm for Various Values of Core-to-Core Delay Times (τ_{jk}).. 227

5-34 Relative PGCR Neutron Level as a Function of Cycle Time for the BGCR System with TIBE of 20 cm, 25 cm, 30 cm, and 40 cm with Core-to-Core Delay Time, τ_{jk}=0.0 sec and α_{jk}=0 During Exhaust....... 229

5-35 $N_j(t)/N_j(0)$ and $C_j(t)/C_j(0)$ for Two Cycles for a BGCR with TIBE of 40 cm with the PGCR Cores Uncoupled (α_{jk}=0) During Exhaust Phase.. 230

5-36 $N_j(t)/N_j(0)$ and $C_j(t)/C_j(0)$ for Two Cycles for a BGCR with TIBE of 40 cm with Core-to-Core Coupling Reduced to 0.6 Times the Actual Values.................................. 232

5-37 $N_j(t)/N_j(0)$ and $C_j(t)/C_j(0)$ for Five Cycles for a BGCR with TIBE of 40 cm with Core-to-Core Coupling Coefficients Reduced to 0.55 times the Actual Values.............................. 234

5-38 $N_j(t)/N_j(0)$ and $C_j(t)/C_j(0)$ for Four Cycles for a BGCR with TIBE of 30 cm with Core-to-Core Coupling Reduced to 0.50 times the Actual Values. 235

5-39 Relative PGCR and BPGCR Neutron Levels as a Function of Cycle Time for a BGCR with a TIBE of 30 cm with Coupled PGCR and BPGCR Cores.. 237

5-40 PGCR Core Neutron Multiplication Factor as a Function of Cycle Time for a BGCR System with TIBE of 30 cm............................... 238

5-41 Relative PGCR and BPGCR Neutron Levels as a Function of Cycle Time for a BGCR with TIBE of 30 cm with PGCR Cores Uncoupled from BPGCR Core................................ 240

5-42 Relative PGCR and BPGCR Neutron Levels as a Function of Cycle Time for a BGCR with TIBE of 20 cm with Coupled PGCR and BPGCR Cores.................................... 241

5-43 PGCR Core Neutron Multiplication Factor as a Function of Cycle Time for a BGCR System with TIBE of 20 cm............................... 242

5-44 Relative PGCR and BPGCR Neutron Levels as a Function of Cycle Time for a BGCR with a TIBE of 20 cm with PGCR Cores Uncoupled from BPGGCR Core............................... 243

A-1 Geometry Splitting/Russian Roulette Technique in MCNP....................................... 282

A-2 Detail of the Weight Window......................... 285

A-3 Cross-Sectional View of Bimodal Gaseous Core Reactor; (a) Side View (b) Top View......................... 299

A-4 Cross-Sectional View of Single Core PGCR........... 315

Abstract of Dissertation Presented to the Graduate School
of the University of Florida in Partial Fulfillment
of the Requirements for the Degree of Doctor of Philosophy

NEUTRONICS OF A COUPLED MULTIPLE CHAMBER GASEOUS CORE REACTOR POWER SYSTEM

By

MATHEW M. PANICKER

May, 1989

Chairman: Dr. Edward T. Dugan
Major Department: Nuclear Engineering Sciences

Static and dynamic neutronics of an innovative, coupled, multiple chamber beryllium moderated bimodal gaseous core reactor (BGCR), capable of generating both low and high power for space applications are investigated. It is found that the core-to-core neutronic coupling effects contribute significantly to the power behavior of any chamber during both low power and high power operation. As a consequence of the strong coupling, steady state operation and even power increases can be achieved with all of the cores operating in a subcritical condition. The core power levels can be controlled by the core fuel loadings as well as the neutronic coupling effects among the cores.

The BGCR system consists of a large, central cylindrical high or burst power gaseous core reactor (BPGCR)

chamber and a surrounding annular ring of cylindrical low power pulsed gaseous core reactor (PGCR) chambers embedded in beryllium moderator. The BPGCR operates as an open flow system and employs an MHD generator for energy conversion. For the PGCR's the gaseous fuel mixture is cyclically injected into the PGCR chambers during the intake phase, heated during the power phase, and then discharged to an energy conversion system. With multiple PGCR chambers and proper timing of their operation, the conducted neutronics analysis indicates that the low power system should be able to provide a relatively continuous source of hot pressurized gas for the power conversion system.

The effects of PGCR and BPGCR core loadings and inner and outer beryllium thicknesses on the system neutron multiplication factor, system neutron removal lifetime, and the core-to-core neutronic coupling coefficients have been examined in the static (steady state) neutronic analysis of the BGCR. The dynamic behavior of the BGCR is evaluated by the program, COUPKIN, which was developed as part of this work. COUPKIN solves the coupled core point reactor kinetics equations. The integral kinetics parameters for the COUPKIN program are obtained from the static analysis of the system. The neutronic coupling effect among the cores is explicitly taken into account in the coupled core kinetics equations by means of the "effective source" term.

CHAPTER 1
INTRODUCTION

Pulsed cyclic gaseous core nuclear reactor systems have undergone extensive theoretical and experimental investigations at the University of Florida. Neutronics-energetics analyses of pulsed gas core reactor systems have lead to a basic scientific understanding of the behavior associated with the conceptual operation of these devices. The results of these research efforts indicate that the pulsed gaseous core reactor is a versatile and promising nuclear energy concept that has attractive features for space power generation as compared to conventional solid fueled nuclear reactor systems(1-2). These features include low critical mass, high fuel utilization, adaptability to different energy conversion systems, high operating temperature and efficiency, and good control and safety characteristics. They have additional advantages of compactness, relatively high power density, wide operating ranges, excellent dynamic response, and good operational flexibility. The high temperature of the coolant/working fluid in the core, which can be considerably hotter than the surrounding structure, is advantageous for both power cycle efficiency and heat rejection in space. The gaseous nature of the fuel gives the added advantage of rapid startup capabilities and the simple geometry of the core structure helps minimize the thermal shock and thermal stress especially during the rapid startup.

Pulsed gaseous core reactors (PGCR) are energy intensive, cyclic fission driven power systems that have uniquely attractive neutronic and energetic characteristics. In the power chamber or core of a single chamber PGCR, a fissionable circulating gas is pulsed from a predominantly far-subcritical state to a short lived, power rich near-critical, critical, or supercritical state and then the hot gas is exhausted. The energy released by the fissioning gas is extracted by any suitable power conversion system.

Previous analyses of pulsed, cyclic gaseous core reactor power systems have been performed for single or neutronically isolated chambers. These previous studies have not included the effects on system performance of the core-to-core neutronic coupling which would exist for array of pulsed gas core reactor chambers.

The pulsed gaseous core reactor system for space power generation investigated in this dissertation consists of a number of neutronically coupled, low-power PGCR chambers surrounding a large, high power cylindrical chamber embedded in beryllium moderator. The (low power)

PGCR's are expected to provide long term stationkeeping or surveillance power for a space based system. If a pulsed gaseous core reactor system with just one or two chambers is used for this purpose, flow discontinuities due to pulsation effects will make it difficult to extract a continuous supply of hot exhaust gas for any power conversion system. The multiple chamber design of the low power pulsed system will be capable of, as the analysis in Chapters 4 and 5 will show, delivering a relatively continuous source of high temperature, pressurized gas to any power conversion system associated with the reactor for uninterrupted power generation. This can be achieved by properly timing the operation of the individual chambers between the intake, power, and exhaust phases. Also the multiple cavity design should have a favorable impact on the system reliability since power can be generated even if a few of the individual chambers fail.

Brief Description of The Multiple Cavity Pulsed Gaseous Core Reactor Power System

The investigated gas core reactor power system consists of (Figures 1-1 and 1-2) a large, central burst power oscillating gas core reactor (BPGCR) chamber surrounded by an annular ring of small, cylindrical low power pulsed gaseous core reactor (PGCR) chambers embedded in beryllium moderator. The primary working fluid (fuel)

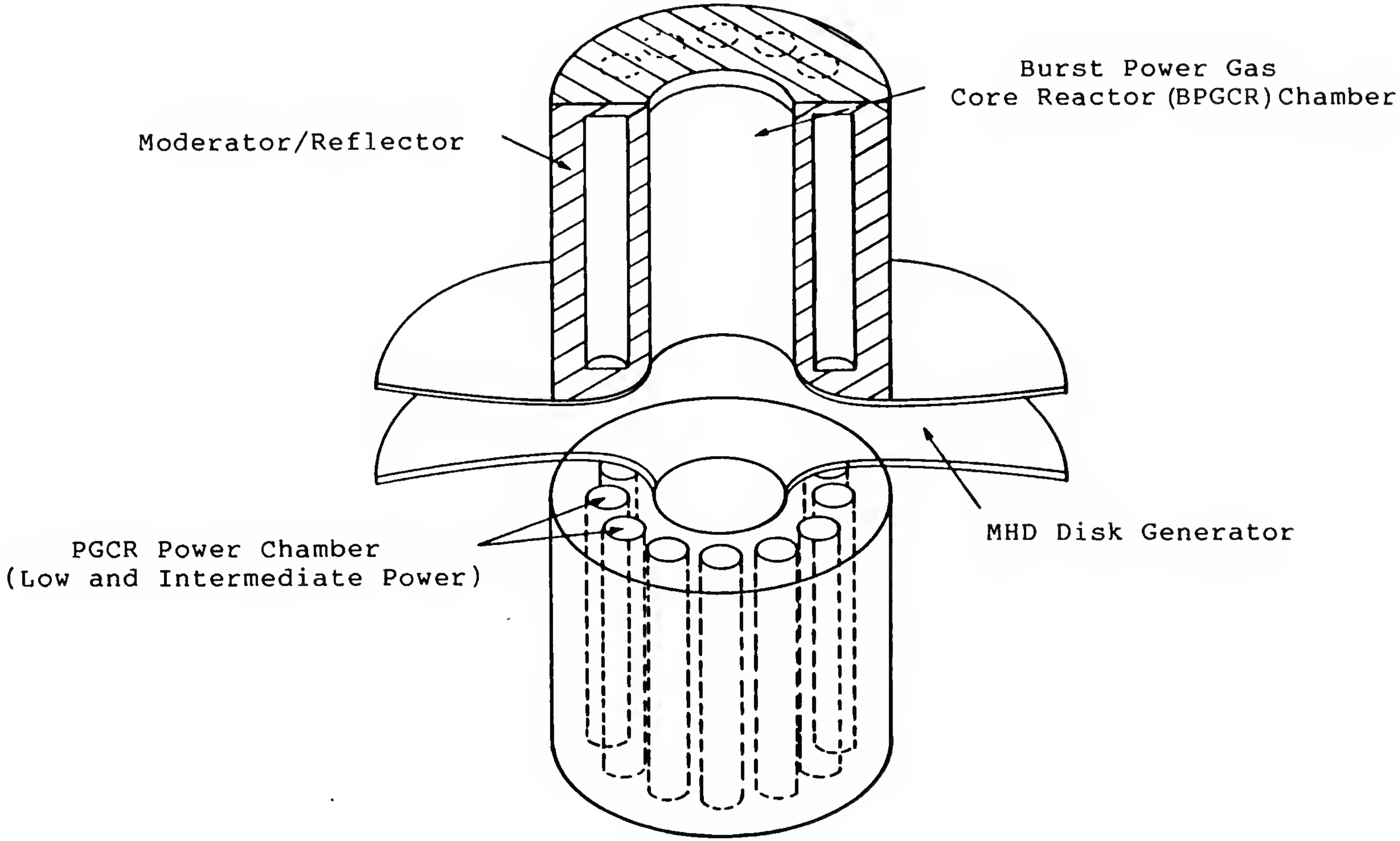

Figure 1-1. Bimodal Gas Core Reactor Power System Schematic

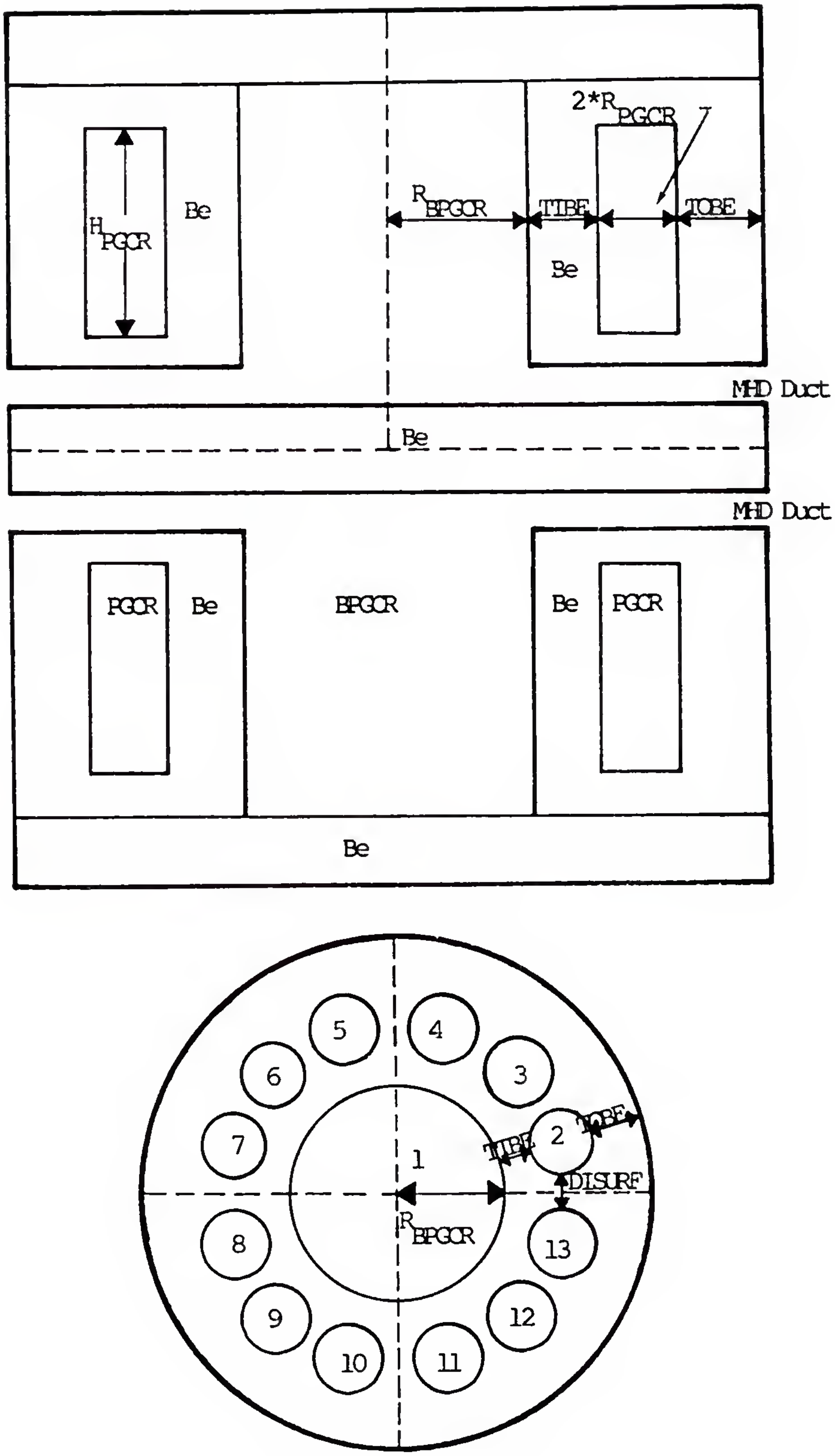

Figure 1-2. Top and Side View of Bimodal Gas Core Reactor.

is a mixture of uranium hexafluoride (UF_6) and helium gas. Highly enriched UF_6 is the reactor fuel. The helium gas is added to enhance the thermodynamic, transport, and heat transfer characteristics of the fluid. The identical upper and lower halves of the reactor system are separated by a common moderator slab at the mid plane. This moderator slab separates the magnetohydrodynamic (MHD) disk generator regions for the top and bottom central BPGCR chambers.

The annular ring of PGCR chambers is designed to provide low power for station keeping/surveillance purposes. In the PGCR chambers the fissile gaseous fuel (UF_6-He mixture) is cyclically injected into the power chambers, which are individually pulsed from far-subcritical to near-critical, critical, or a supercritical state and the heated gas is then discharged for energy conversion; each chamber is designed to produce a few MW(e) power.

With the multiple PGCR chamber design and proper timing of operation of the individual chambers among their intake, power, and exhaust (discharge) phases, the system is expected to provide a continuous source of high temperature pressurized gas for any suitable power conversion system. The multiple cavity design, therefore, should have a favorable impact on system reliability since power can be generated even if a few of the PGCR chambers fail. During low power operation of the system, the central BPGCR chamber will either be voided or have a constant, low pressure non-fuel gas flow.

The transition from station keeping to the high or burst power mode of operation can be achieved by circulating a gaseous uranium fuel through the central BPGCR cavity. The neutronic coupling effects of the PGCR chambers on the gaseous fuel bearing central chambers provide the necessary criticality/heating condition to generate a partially ionized plasma (≈ 2000-4000 K). The high pressure fuel gas mixture is driven into the disk MHD generator through a supersonic nozzle. The energy conversion occurs in the disk MHD generator. The fuel gas then passes through a diffuser and a radiator heat exchanger before being circulated back into the central BPGCR chamber by a compressor.

A more detailed description of the bimodal gaseous core reactor power system and its basic operational details are given in Chapter 4.

Aim and Scope of The Dissertation

The primary aim of this dissertation is to perform static (steady state) and dynamic neutronic design analysis of the bimodal multiple cavity pulsed gaseous core reactor system. The dynamic neutronic analysis of the system includes the effects of delayed neutrons and the neutronic coupling among the cavities separated by the moderator/reflector; effects of variation of inner and outer moderator thickness; and the effects of variation of core fuel gas loadings on the core neutron level of the system for various cycle times of operation.

The parameters required for the dynamic neutronic analysis of the system such as reactivity, neutron generation time, neutronic coupling coefficients among the various cores, core-to-core delay times etc., are obtained from static neutronic analysis of the system. Steady state neutronic analysis of the system includes examining the effects of variation of PGCR gas loading and inner and outer moderator/reflector thickness on the system neutron multiplication factor (k_{eff}), system neutron removal lifetime (ℓ), neutron generation time (Λ), and the neutronic coupling coefficients (α_{jk}) among the various chambers. Calculations have been performed for both equal and unequal gas loading among the PGCR chambers.

Organization of The Dissertation

Chapter 2 of the dissertation includes a brief survey of coupled core neutronics analysis methods that have been used in previous studies of various coupled core nuclear reactor systems. This chapter provides a comparative study of the different formulations for coupled core neutronic analysis which leads to a better understanding of the neutronic behavior of coupled core systems.

Chapter 3 discusses the highlights of previous gas core research efforts that have been performed at the University of Florida. This chapter includes a brief summary of methods used in the analyses and presents key results obtained from these previous studies. A basic understanding is provided of the single chamber pulsed gaseous core reactor system concept.

Chapters 4 and 5 deal with the static and dynamic neutronic studies,respectively, of the multiple cavity gaseous core reactor. The static neutronic analysis mainly includes the results from the general purpose, three-dimensional Monte Carlo transport code, MCNP (3), and the one-dimensional discrete ordinates transport code, XSDRNPM (4). The static neutronic analysis includes the effects of variation of inner and outer moderator thickness and the PGCR and BPGCR gas loading on the system neutron multiplication factor (k_{eff}), and the neutron removal lifetime (ℓ). Chapter 5, which contains the dynamic neutronic analysis of the system includes the effects of variation of inner and outer moderator thickness and gas loading on the core coupling coefficients, system reactivity, core power levels, and the delayed neutron precursor concentrations in the cores.

Chapter 6 draws conclusions from the results obtained in this study. This chapter also provides some recommendations in various areas for future research to be undertaken towards further development of multiple gaseous core nuclear reactor power systems.

The appendices that are given at the end of this dissertation include sections on the derivation and method of solution of coupled core point reactor kinetics equations as employed in this research, a discussion on the basic features and capabilities of the MCNP Monte Carlo code, benchmark neutronic calculations with XSDRNPM and MCNP codes on reference spherical and cylindrical gaseous core reactor systems, and comparative evaluation of results from the coupled core kinetics program, COUPKIN, for a single core and the point reactor kinetics code, ANCON (5), from the Los Alamos National Laboratory.

CHAPTER 2
PREVIOUS STUDIES ON COUPLED CORE NEUTRONICS

Introduction

The spatial and spectral coupling effects in reactor kinetics were treated by many authors (6-24) during the 1960s and 1970s. The coupled nuclear reactor systems subjected to kinetics studies included fast-thermal reactors, modular cores of large thermal power reactors, clustered rocket reactors, and Argonaut type reactors. From the point of view of coupling, that is, the amount of reactivity supplied by the mutual neutronic interactions among the subsystems, the above reactors range from very tightly coupled systems (as for instance, the fast-thermal reactors) to very loosely coupled systems (like the coupled rocket reactors). Except for the coupled core nuclear rocket engines, the other works on coupled core kinetics referenced in this chapter are directed towards reactors with solid fuel cores. In view of the existence of many apparently different formulations for coupled core neutronic analysis, it seems appropriate to compare various models for a better understanding of the neutronic behavior of coupled cores.

Coupled core reactor kinetics was initiated in 1958 by Robert Avery (6,7) with his investigation of dynamic characteristics of the coupled fast-thermal breeder reactors. The investigated fast-thermal reactor system that couples a fast and thermal assembly was designed to obtain a relatively long prompt neutron lifetime that is characteristic of a thermal assembly and a high breeding gain that is characteristic of a fast assembly (Figure 2-1). The coupled system considered by Avery consisted of a Pu-239 fueled cylindrical fast core surrounded by an annular blanket of natural uranium, coolant and structural material followed by an annular beryllium moderator surrounded by an outer blanket consisting primarily of depleted uranium. The inner blanket serves as the core for the thermal system, as a barrier for the low energy neutrons between the moderator and fast core, and as a "reflector" for the fast core.

In Avery's formulation, each core or system is divided into nodes and the point model kinetics equations are constructed for each node, taking into account the neutronic coupling effects among the nodes. The integral and coupling parameters in the coupled core point kinetics formulation are obtained from the steady state analysis of the corresponding system of cores or subsystem.

The multinode neutronic kinetic theory developed by Avery was applied to a time-dependent system composed of a multiplying media surrounded by a non-multiplying

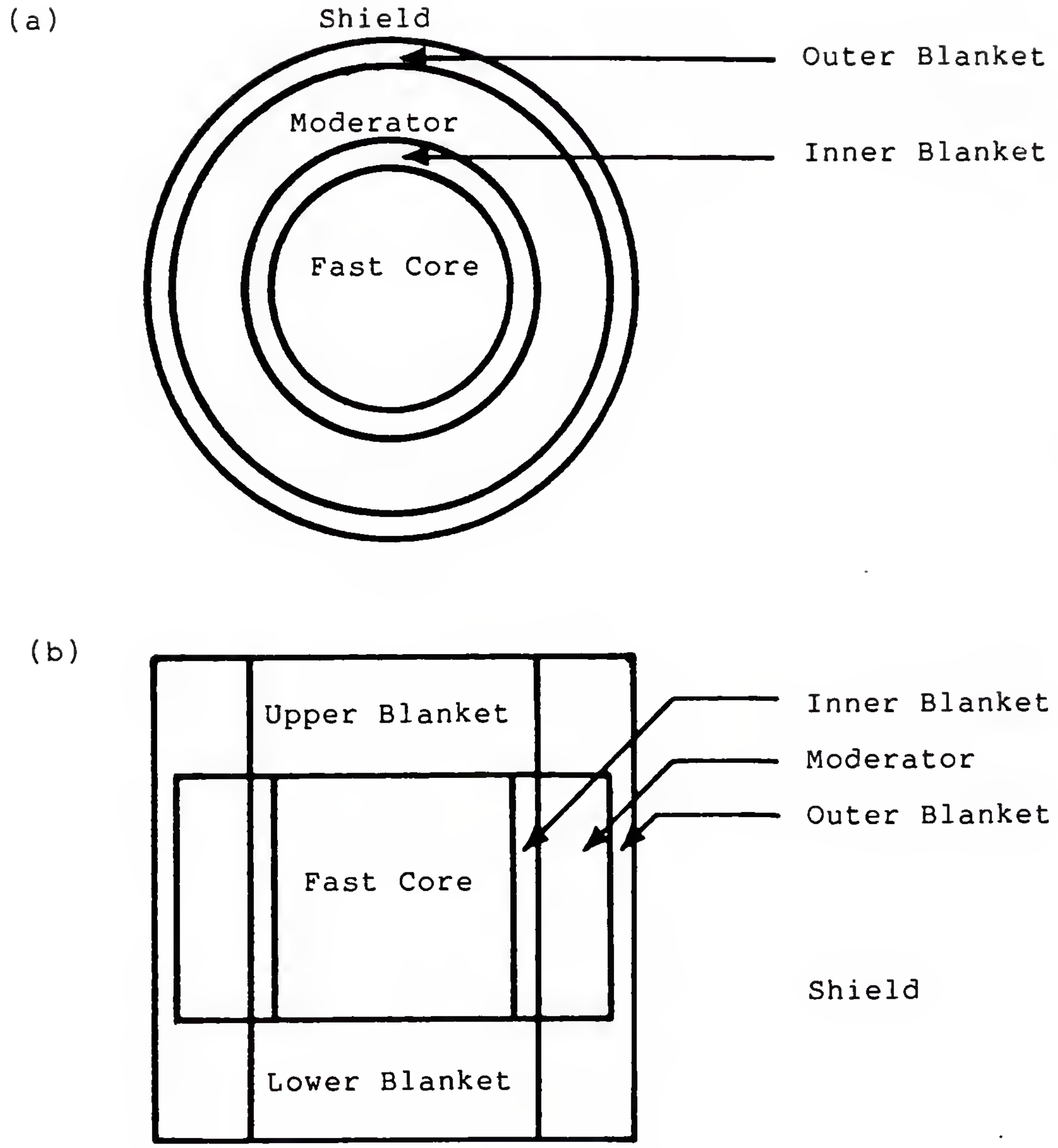

Figure 2-1. Schematic Representation of Coupled Fast - Thermal Power Breeder;
(a) Top View
(b) Side View.

moderator/reflector medium by Masaoki Komato (8). Komato developed two models; one multi-node kinetic theory model with time dependent coupling parameters and a time dependent multi-core diffusion theory model in which nuclear parameters, such as, the diffusion coefficient, microscopic cross section etc., are invariable with respect to space in each region but can vary with time. Modifications and alterations of the methods developed by Avery and Komato have been achieved by many authors and are referenced in this chapter (6-24). Except in Avery's approach and its modifications by others, all other formulations make use of the assumption that the neutron angular flux Φ can be factorized into a time dependent neutron angular flux Ψ and an amplitude (power level) function N. ,i.e.,

$$\Phi(\overline{r},E,\overline{\Omega},t) = N(t)\ \Psi\ (\overline{r},E,\overline{\Omega},t) \qquad (2\text{-}1)$$

with the restriction that

$$\frac{d}{dt}\int d^3r\int dE\int d^2\Omega\ w(\overline{r},\overline{\Omega},E)\ \psi(\overline{r},E,\overline{\Omega},t) = 0 \qquad (2\text{-}2)$$

where $w(\overline{r},\overline{\Omega},E)$ is an arbitrary weighting function.

The major differences in the various coupled core neutronic analyses that are examined in this work can be classified into three categories, namely, the choice of weighting function, $w(\overline{r},\overline{\Omega},E)$, the choice of suitable phase-space regions for the averaging process, and the selection of approach for the treatment of coupling effects among the various cores that include the coupling coefficients and core-to-core delay times.

Choice of Weighting Functions

Three procedures, namely, straight averaging of the neutron flux over individual cores or reactor regions, an importance weighting, and weighting by an average fission density can be distinguished.

In the straight averaging technique, as in the formulation of space-time reactor kinetics by S. Kaplan et al. (9) based on a one-group diffusion theory approximation, the averaging is done over the core volume

$$\Phi_j(t) = \frac{1}{v_j} \int_{v_j} d^3r \; \Phi(\bar{r},t) \qquad (2\text{-}3)$$

where, $\Phi(\bar{r},t)$ is the space-time dependent flux, and v_j is the core volume used as a basis for the averaging process leading to the nodal equations. The transport theory development of Bellani-Morante (10) introduces a space-angle averaged density, M_j as a basic variable

$$M_j(t) = \int_{R_j} d^3r \int_{\Omega} d^2\Omega \; F(\bar{x},\bar{\Omega},t) \qquad (2\text{-}4)$$

where $F(\bar{x},\bar{\Omega},t)$ is the neutron angular flux.

The transport theory approaches of Hansen (11), Cockrell and Perez (12), Gage et al. (13), and Schwalm (14,15) all use various forms of importance weighting. The choice of importance function depends on the nature of the coupled core array i.e., whether the cores are loosely or tightly coupled, whether or not a buffer zone exists between the regions, and whether the neutron exchange is primarily unidirectional or multi-directional. Another criterion in the selection of the importance function is whether the function describing the importance distribution should be valid over the entire reactor or the importance function be calculated separately for each core. If the reactor system can be analyzed by one-dimensional geometry the adoption of a single importance function for the entire reactor is most suitable. On the other hand, if the cores are nearly isolated (as, for example, the KIWI cores) weighting the neutron distribution with an importance function associated with each core is much more reasonable (16,17). In terms of the degree of coupling among the cores, a single importance function for the entire reactor is suitable for a tightly coupled system, whereas for a loosely coupled system the use of individual core weighting functions is required.

A comparison of the Cockrell and Perez (12) and Hansen (11) approaches illustrates the above criteria regarding the selection of the importance function. Cockrell in his treatment of the University of Florida Training Reactor (UFTR) which is an Argonaut type reactor with a thermal column between two cores, employed an one-dimensional slab geometry calculation that utilized an adjoint function for the entire reactor. On the other hand, Hansen's treatment (11) of the loosely coupled, clustered KIWI cores employed an importance function associated with each of the individual cores. Although each case must be considered separately, these examples from two extreme cases bear out the general guidelines suggested above.

Avery (6) in his formulation of coupled core kinetics introduced a fission source density as the weighting function in the determination of the integral parameters. In the application of Avery's method by Komato, a time dependent fission source density was used as the weighting function. Gyftopaulos (18) and Gage et al. (13) in their formulation of coupled core kinetics employed, in addition to the fundamental mode adjoint function, the fission source density $\Sigma_f(\bar{r},E,t)$ as the weighting function. The use of the fission density as a weighting function means that the dependent variables reflect the exact growth and decay tendencies in the average power of individual cores. Because this approach is exact in its treatment of neutron density within the boundaries of a particular core, the only assumption required are therefore for the source term that provides the coupling effects from the other cores in the array.

Selection of Phase Space Regions

Previous treatments of coupled core kinetics, except those of Cockrell and Perez (12) and Schwalm (15), have been based on the assumption that only spatial effects were significant in the coupling between spatial regions or nodes (cores) of the reactor system considered. In the case of the KIWI cores with a leakage spectrum characterized by an intermediate energy range or the Argonaut reactor with a largely thermal neutron interaction, energy independent kinetics equations are considered sufficient provided the parameters are properly weighted. In cases such as for large coupled core reactors, a better accounting of the spectral effects of leakage neutrons would be desirable, especially, in the study of short time transients because the spectrum in any of the cores is composed of two parts; one, a distribution i.e., fast, intermediate, and thermal which is characteristic of the material composition of the core, and two, a distribution characteristic of the coupling or leakage of neutrons from the other cores. In the dynamics of a single core, a common time dependency for all neutron energy groups is a good approximation since the neutron spectrum adjusts to any nuclear, mechanical, or thermal changes in the core within a few neutron generations after the changes are introduced. But in coupled cores, the assumption of a common time dependancy for all neutron groups is a bad approach because of the spectrum contribution from the leakage neutrons. Although the spectrum which is characteristic of the individual core adjusts within several prompt neutron generations, the contribution to the spectrum due to leakage neutrons may require a longer period to adjust. An example is for coupled thermal cores where the prompt neutron lifetime may be of the order of 10^{-5} second. For a short transient in which appreciable changes occur in the range of up to a few milliseconds, the assumption of a common time dependency for all neutron groups would ignore the important spectral coupling effects.

Cockrell and Perez (12), in their formulation, which they applied on the Argonaut type UFTR, accounted for the spectral effects of the leakage neutrons explicitly. In it the angular flux, $\psi_{k\beta}(\bar{r},\bar{\Omega},E)$ refers to the neutron flux which originated in region v_k and energy group E_β. Multiplication of the transport equation by the adjoint angular flux $\psi^*(\bar{r},\bar{\Omega},E)$ and integration over the j-th spatial region and over the α-th energy group leads to an ordinary differential equation in terms of the variable

$$N_{\substack{jk\\ \alpha\beta}} = \int_{R_j}\int_{\Omega}\int_{E_\beta} dE\, d^2\Omega\, d^3r\, \psi\, {}^*(\bar{r},\bar{\Omega},E)v^{-1}(E)\ \psi_{k\beta}(\bar{r},\bar{\Omega},E,t). \quad (2\text{-}5)$$

The quantity $N_{\substack{jk\\ \alpha\beta}}(t)$ represents the neutron number density in the j-th spatial region and α-th energy group due to neutrons born in the k-th spatial region and β-th energy group. Even though Cockrell's formulation has the advantage of full generality, the large number of basic equations introduced in his formulation presents a disadvantage. For example, for an m- group n- region problem, this formulation requires $(mn)^2$ basic equations, while the other approaches require a much smaller number of equations. This formulation may be classified as overly descriptive of the system; i.e. it provides more equations than are required to describe the neutronic behavior to a reasonable degree of accuracy.

Treatment of Coupling Effects

The reactivity contribution due to neutronic coupling effects among the cores is introduced in a manner consistent with the treatment of the time dependent variables, selection of phase space regions,and the selection of weighting functions. A particular technique for treating the coupling effect may be more compatible with the one formulation than with another.

Coupling Coefficients

Methods of introducing coupling effects can be classified as falling under either the "reactivity" approach or the "effective source" technique. For comparison of the various treatments of coupling effects that are examined in this chapter, we can classify the methods of Cockrell and Perez (12), Hansen (11), Kaplan et al. (9), Kohler and Plaza (19), and in a certain sense Avery (15) as the "reactivity" approach and those of Baldwin (20), Schwalm (15), Seale and

Hansen (21), Gage et al. (13), and Bellani-Morante (10) as the "effective source" technique.

In the reactivity approach, it is assumed that the generalized reactivity expression for a given core contains implicitly all the contribution due to coupling from the other cores. In this approach, to account for the coupling interaction with the transport theory formalism and importance weighting, the leakage term $\bar{\Omega}.\nabla\Phi(\bar{r},\bar{\Omega},E,t)$ is transformed into a surface integral. This concept of surface coupling accounts for the neutronic interaction between the cores.

The derivation of the coupled core kinetics equations is analogous to that of the generalized point reactor kinetics equations as developed by Henry (22) or Bell and Glasstone (23); the adjoint flux of an arbitrary stationary state of the unperturbed interacting reactor is used as a weighting function. Cockrell's coupled core kinetics formulation introduces both spatial and spectral coupling and arrives at generalized coupled point reactor kinetics equations for $N_{\substack{jk\\ \alpha\beta}}(t)$ which is the number of neutrons in region R_k and energy group E_β at time t that originated in region R_j and energy group E_α and $C_{ik}(t)$ is the precursor density for the i-th precursor group which emits neutrons into a region R_k and energy group E_β. Correspondingly all the integral parameters including the coupling terms account for both the spatial and spectral effects.

Cockrell's (12) formulation assumes that cores have common interfaces with one another and that the coupling neutrons travel only through interfaces. Cockrell's assumptions are too restrictive, and exclude many realistic physical situations in which coupling between isolated regions which do not share common interfaces is important. A second difficulty with Cockrell's approach is that the calculation of the source integral in the formulation in all but the simplest geometrical configurations may be impractical. Third, the partial lifetime $\sigma_{\substack{jk \\ \alpha\beta}}$ is a time dependent coefficient only under certain circumstances. Finally from a practical standpoint, the large number of equations introduced in Cockrell's formulation presents a significant disadvantage; for a m-group, n-region problem this formulation, as already indicated, requires $(mn)^2$ basic equations, while other approaches require a much smaller number of equations.

Plaza and Kohler (19), in their coupled core formulation consider a group of reactors or cores interacting with each other through a non-multiplying coupling medium. The point reactor kinetics equations for the coupled cores are derived using the weighting function (adjoint flux) from a source free adjoint equation and the coupling contribution is introduced as a reactivity contribution using the surface coupling technique (19).

Hansen's (11) one-group transport theory approach using importance weighting consists of dividing the total flux (F_s) in the j th core into two parts: F_j which refers to neutrons born in the j th core and remaining there until time t and F'_j which refers to all other neutrons in the j th core identified with neutron leakage into core j. Consequently he developed his theory starting from two transport equations and derived two sets of kinetics equations for N_j and N'_j.

Coupled core formulations by Baldwin (20), Seale and Hansen (21), and Gage et al. (12) include the contribution from coupling effects as an effective source; the fact that the reactivity requirement for each core is reduced by the coupling is recognized but not explicitly taken into account. The (tacit) assumption inherent in these derivations is that in calculating the reactivity associated with the j th core, the contributions due to "effective sources" on the surface of that core must be set to zero. In the Baldwin (20) formulation for the two core configuration of the Argonaut reactor, in which two slightly subcritical slabs about two feet apart are immersed in a large graphite reflector, the coupling effect is introduced into a one group diffusion equation for each of the two cores as an additional source component

$$\epsilon_j \Phi_k(t-\tau); \; ((j=1,2); \; k=1,2 \; j \neq k)$$

which accounts for the interaction between the two cores. In this expression for the additional source component, τ is the delay time due to the exchange of neutrons between the two cores and is characteristic of the graphite reflector, Φ_k represents the neutron flux in core k and ϵ_j is the interaction probability between the two cores. The interaction component of the source in core 1 is $\epsilon_1\Phi_2(t-\tau)$ and that in core 2 is $\epsilon_2\Phi_1(t-\tau)$, i.e., the interaction component is proportional to the average flux in the other core.

Seale and Hansen (21) uses Baldwin's (20) model, generalizing it to M cores but retaining a source component of the above form. Gage et al. (13), in their coupled core analysis introduced a source distribution function $S_j(\bar{r},E,t)$ that is composed of a series of terms representing the power coupling with the other cores in the reactor. Since there is a finite time lapse from the birth of a neutron in one core and its capture in another core causing fission, the coupling power growth is assigned a retarded argument in the form

$$S_j(\bar{r},E,t) = \sum_{\substack{k=1 \\ k\neq j}}^{M} \epsilon_{jk}(\bar{r},E,t)\ \Phi_{pj}(\bar{r},E,t)N_k(t-\tau_{jk}) \qquad (2\text{-}6)$$

where $\epsilon_{jk}(\bar{r},E,t)$ is the probability that a neutron escaping the boundaries of the k th core will cause fission at $\bar{r}$ and at energy E in the j th core. The term $\epsilon_{jk}(\bar{r},E,t)\Phi_{pj}(\bar{r},E,t)$ represents the new shape function that accounts for the power distribution arising from the effective surface source of coupling neutrons. In introducing such an effective source term, the contributions to the reactivity expression in each core due to the coupling neutrons from all other cores must be set to zero.

Avery's (6) formulation of coupled cores treats the system in terms of integral parameters which explicitly characterize the individual reactors and the coupling between them. The total fission source in the j th core S_j is set equal to the fission source contribution arising in that core and in the other (M-1) cores

$$S_j = \sum_{l=1}^{M} S_{jl}. \tag{2-7}$$

The coupling coefficient is defined as

$$k_{jk} = \frac{S_{jk}}{S_j} \tag{2-8}$$

where k_{jk} is the expectation value or probability that a fission neutron in core (reactor) k gives rise to a next generation of fission neutrons in j.

The equations describing the kinetic behavior of the coupled system are given by

$$l_{jk} \frac{dS_{jk}}{dt} = k_{jk}(1-\bar{\beta}) \sum_{l=1}^{M} S_{kl} - S_{jk} + k_{jk} \sum_{i=1}^{ND} \lambda_i C_{ki} \tag{2-9}$$

and $$\frac{dC_{ki}}{dt} = \bar{\beta}_i \sum_{l=1}^{M} S_{kl} - \lambda_i C_{ki}. \qquad (2\text{-}10)$$

In Equations (2-9) and (2-10) $\bar{\beta}_i$ and λ_i are the effective delayed neutron fraction and decay constant, respectively, for the i th group delayed neutron precursors, $\bar{\beta}$ is the total effective delayed neutron fraction, C_{ki} is a properly weighted measure of delayed neutron precursors of the i th group in core k, ND is the number of delayed neutron groups, M is the number of cores in the reactor, k_{jk} is the expectation value or probability that a fission neutron in core k gives rise to a next generation of fission neutrons in core j, and l_{jk} is the prompt neutron lifetime for the process. The term k_{jk} for $j \neq k$ is a measure of the cross coupling from core k to core j.

The Equations (2-9) and (2-10) can be rewritten in terms of the time rate of change of $N_{jk}(=l_{jk}S_{jk})$ neutrons as equal to the difference between the production (including delayed as well as prompt neutrons) and the loss of these neutrons

$$\frac{dN_{jk}}{dt} = k_{jk}\ (1-\bar{\beta}) \sum_{m=1}^{M} \frac{N_{km}}{l_{km}} - \frac{N_{jk}}{l_{jk}} + \sum_{i=1}^{ND} \lambda_i\ C_{ki} \qquad (2\text{-}11)$$

and $$\frac{dC_{ki}}{dt} = \beta_i \sum_{m=1}^{M} \frac{N_{km}}{l_{km}} - \lambda_i\ C_{km}. \qquad (2\text{-}12)$$

The quantity N_{jk} is similar to the neutron density. It is a measure of the number of neutrons, properly weighted, in the system which were born in core k that diffuse to core j and produce the next generation of neutrons in j. The term dN_{jk}/dt represents the difference in production and loss rate for N_{jk} type neutrons. The first term on the right hand side of Equation (2-11), $k_{jk}(1-\beta)S_k$, is the production rate of the N_{jk} type of neutrons by prompt emission. The term $\beta_i S_k$ represents the i th precursor type, so that this term represents the production rate term in Equation (2-12) for C_{ki}. The term $\lambda_i C_{ki}$ represents the loss rate for C_{ki}. The total number of delayed source neutrons in core k is $\Sigma\lambda_i C_{ki}$, so that the last term in equation (2-11) $k_{jk}\ \Sigma\lambda_i C_{ki}$ is the production rate of N_{jk} type of neutrons by delayed neutron emission. Finally N_{jk}/l_{jk} represents the loss rate of N_{jk} type neutrons in equation (2-11).

The power level P_j in each core j of the reactor system is proportional to the sum of the partial fission neutron sources:

$$P_j \ \alpha \sum_{k=1}^{M} S_{jk}, \qquad P_j \ \alpha \sum_{k=1}^{M} N_{jk} \ . \tag{2-13}$$

In applying this theory to the coupled fast-thermal breeder rector experiments, a spectral definition of the interacting thermal and fast cores in terms of thermal and fast sources was chosen. The definitions for these sources are given by

$$S_{th} = \int_{\text{system}} \int_0^{V} \Sigma_f \Phi_{th}(\bar{r},\bar{v})\ dv\ d^3r \tag{2-14}$$

and $$S_f = \int_{\text{system}} \int_{v_c}^{v_{max}} \Sigma_f \Phi_f(\bar{r},\bar{v})\, dv\, d^3r \qquad (2\text{-}15)$$

where v_c is the thermal cutoff speed and v_{max} is the speed at the maximum neutron energy considered.

Since the dependent variables in Avery's (6) kinetics equations are partial neutron densities (N_{jk}), this formulation requires M^2 equations where M is the number of cores in the system.

Delay Time Effects

In Avery's formulation, the delay times associated with the transfer of neutrons between cores are not introduced explicitly. When considering pulsed experiments with coupled cores or other aspects of the behavior of loosely coupled systems, it is desirable, and sometimes necessary to introduce the delay times explicitly into the coupled core kinetics formalism. One possible representation of the delay times can be in the probability $P^{\alpha}{}_{jk}(t-t')$ that a neutron born in the α th energy group in the k th core at time t' enters the j th core within dt at a time t. This probability should be chosen so as to represent the physical and nuclear characteristics of the system being considered.

In Baldwin's formulation (20) of two loosely coupled core loadings of the Argonaut type, the interaction term $\epsilon_j \Phi_k(t-\tau)$ is the source term that accounts for the contribution of neutrons to reactor j. The quantity τ in the interaction term is the delay time for the neutron transfer process between the cores.

Chezem and Helmick (24) developed a general theoretical model to analyze the Los Alamos Coupled core experiment in which two cores were separated by beryllium reflector. A pulse of neutrons was introduced into the core 1 at time t=0 and the neutron response in each of the core was obtained from neutron detectors located at the center of each core. The general model developed by Chezem and Helmick consists of a single neutron balance equation in terms of the neutron population $N_i(t)$ for the i th core of a loosely coupled array of M cores is given by

$$\frac{dN_i(t)}{dt} = \frac{\delta_{ki}^{p}}{\Lambda_i} N_i(t) + \frac{1}{\Lambda_i} \sum_{\substack{j=1 \\ j\neq i}}^{M} \alpha_{ij} \int_0^t N_j(t-T)\ P(T)dT + A\delta_{i1}(t) \qquad (2\text{-}16)$$

where δ_{ki}^{p} is the excess prompt reactivity of the i th core when isolated from the environment and Λ_i is the neutron lifetime. The source term $A\delta_{i1}(t)$ represents a delta pulse of neutrons in core 1 and at time t=0. The term $\alpha_{ij}N_j(t-T)P(T)dT$ is the source contribution to core i from fissions in core j at times t-T in dT. Quantity α_{ij} is the coupling coefficient for core i from fission neutrons in the j th core.

The "neutron distribution function" P(T) is defined as

$$P(T) = \frac{1}{\tau_{ij}} e^{-T/\tau_{ij}} \qquad (2\text{-}17)$$

where τ_{ij} is an "effective interaction time" for neutrons entering core i from core j. This expression for P(t) will lead to a simple form of transfer function and consequently a simple analytical form for the time dependent flux.

The interaction time τ_{ij} which may also be called the delay time does not really provide the function P(T) to represent the minimum time delay corresponding to the minimum neutron transit time. For example, in the case of an internally pulsed "driver" core coupled to a "passive" core, the response in the passive core would start at the time of the external pulse no matter how close or far apart the two cores are. This simple model would lead to a simple exponential behavior in the driver core while there are indications that a quasi-oscillatory response is possible and may have occurred in the KIWI-Transient Nuclear Test (KIWI-TNT) experiments (25,26).

For these reasons it is desirable to introduce a slightly more complicated representation for P(T) that will include a finite delay time. Hansen (11) in his neutronics studies of a cluster of reactors, gives the source term S_i for the i th core due to interaction of the other cores as

$$S_i = \epsilon_{ij} \sum_j \int \left(\frac{N_j}{l_j}\right) (t-\tau)\ P_{ij}(\tau)\ d\tau \qquad (2\text{-}18)$$

where $P_{ij}(\tau)d\tau$ is the probability that a fission neutron born in core j enters core i at a time τ in $d\tau$ later, N_j/l_j is the neutron loss rate from the core j, ϵ_{ij} represents the effectiveness of a fission neutron that moves from core j to core i in inducing fission and eventual neutron population in i, and $P_{ij}(\tau)$ is the time distribution function for this transfer. For the cluster array of coupled cores, Hansen (11) assumed that

$$P_{ij}(\tau) = \delta(t-\tau_{ij}) \qquad (2\text{-}19)$$

where τ_{ij} is the effective mean drift time of neutrons between the boundaries of cores j and i. It is to be noted that the first moment of the distribution function $P_{ij}(\tau)$ is the sum of three mean times; the time for a fission neutron to leak out of core j from birth, the drift time from the boundary of j to the boundary of i, and the time from its entrance in i to its absorption in i.

In Avery's (6) and Komato's (8) formulations of coupled core neutronics, the core-to-core delay time is introduced through a partial lifetime, $l_{jk}(t)$, the mean lifetime of neutrons for the process (j,k), i.e., of neutrons born in core k which diffuse in the system and ultimately cause fission in core j.

In the formulation of Gage et al. (13) of nonlinear stability of a coupled core reactor system, the coupling term that accounts for the contribution from remaining cores to a specific core is introduced with retarded time arguments $(t-\tau_{jk})$, where τ_{jk} is the core-to-core delay time, i.e., the transit time required for neutrons to diffuse from core k to core j through any intervening medium which separates the cores.

Comments

Salient features of the major formulations for coupled reactor kinetics are presented in this chapter. The various major formulations differ mainly in their treatment of the core-to-core coupling effects that include the coupling coefficients and delay times. Although the various approaches handling the coupling effects can be broadly classified into "effective source" and "reactivity" techniques, the various approaches differ in their actual implementation during the derivation of the coupled core kinetics equations. Based on the actual implementation of these approaches, three distinct categories can be identified for the introduction of the coupling effects in the coupled core kinetics equations: (i) introduction of these additional sources into the basic neutron balance equation (14,15,20); (ii) introduction of coupling sources during the derivation of the coupled point reactor kinetics equations from neutron balance equations to replace the contribution from the surface integral (11,19,24); and (iii) the partitioning of the neutron flux and hence the neutron source into partial sources that contain the contribution from other cores and form the dependent variables in the coupled core point reactor kinetics equations (6,7,12).

The method of introduction of time delay also differs among the various formulations. Delay time can be introduced as a probability distribution function in time or as finite time in a retarded time argument for the power levels of the remaining cores. The delay times can be neglected in a situation where the delay times are very short compared to the prompt neutron generation time. The expected influence of delay times in coupled core kinetics is a decrease in the systems stability (13). However, if the maximum delay time, τ_{max} is so short that

$$|N(t)-N(t-\tau_{max})| << N(t) \text{ or } N(t)\rightarrow N(t-\tau_{max})$$

for all times of practical interest, then the delay times can be expected to have very little or no practical effect on the time behavior of the system.

Most of the coupled core reactor kinetics formulations that have been previewed in this chapter are applied to solid systems in one-dimensional plane geometry with very restrictive conditions. If the system has a complex geometry, as in the case of the bimodal gaseous core reactor system, the calculation of precise coupling coefficients and delay times becomes complicated and hence should be obtained from Monte Carlo methods.

CHAPTER 3
PREVIOUS STUDIES ON PULSED GASEOUS CORE REACTOR AT THE UNIVERSITY OF FLORIDA

Introduction

Pulsed cyclic gaseous core reactors have undergone extensive theoretical and experimental investigation at the University of Florida. One of the earliest concepts that was proposed by Kylstra et al. (27) consists of a pulsed plasma core reactor enclosed by a cylinder and a piston and is analogous to a gasoline internal combustion engine (Figure 3-1). The fuel-working fluid is a UF_6-He mixture. The reactor is made critical during the compression stroke and the neutron flux is allowed to build up to a significant power level. The neutronic and energy calculations have shown that significant power (MWs) per cylinder with high efficiencies (40%-50%) can be achieved.

Kylstra's (27) feasibility studies on pulsed gas core reactors have indicated such good performance potential that Dugan et al. (28) were encouraged to undertake extensive theoretical and experimental neutronics and energetics studies on a variety of gas core reactor concepts. These concepts include the Pulsed Nuclear Piston (PNP) system with a gaseous core reactor enclosed by a moderating reflector

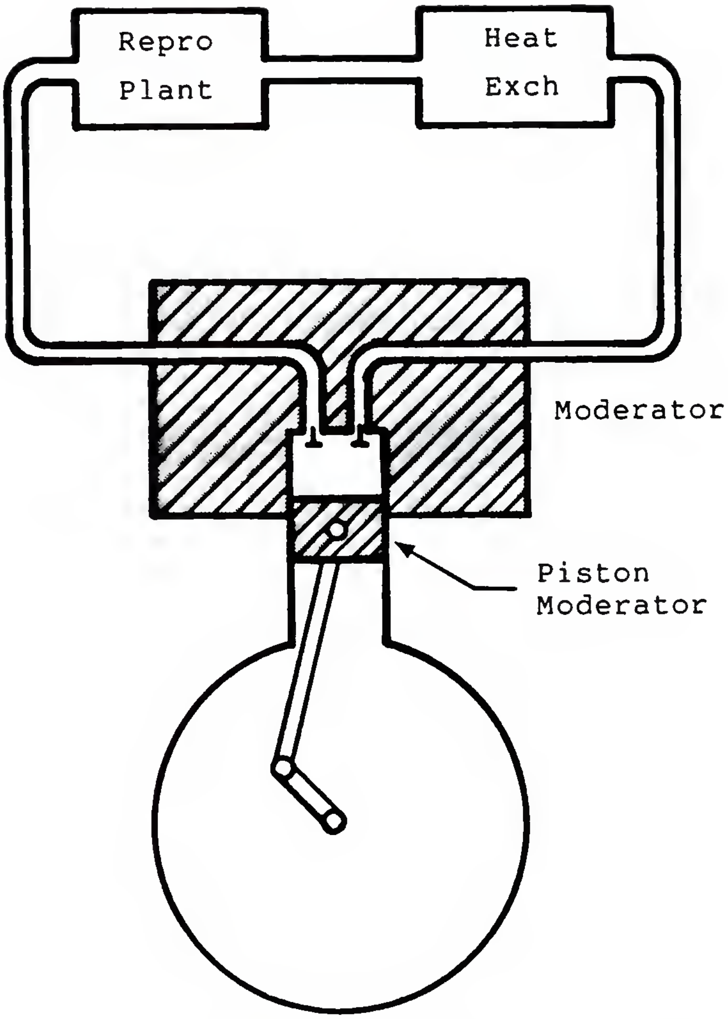

Figure 3-1. Schematic Representation of UF_6 Piston Engine.

piston assembly which operates on a thermodynamic cycle similar to the internal combustion engine and the Pulsed Gas Generator (PGG) that employs a core of fixed dimensions. These compact, cyclic, fission driven systems have been found to have unique power producing characteristics and are capable of generating 10 to 100 MW(e) power.

UF_6 Piston Engine of Kylstra et al.

The piston engine developed by Kylstra et al. (27) consists of a cylinder and a piston surrounded by graphite moderator with a nickel lining for protection from the fuel-working fluid, UF_6. During the intake stroke, the UF_6-He fuel-working fluid is drawn into the cylinder and during the exhaust stroke the gas and the fission products are ejected from the cylinder. The reactor is made critical during the compression stroke before the piston reaches the top dead center (TDC). To minimize the fission heat release after the piston has already passed the power stroke, the reactor is required to shut down rapidly.

The reflector surrounding the cylinder and piston is graphite. The graphite has an inner nickel lining because of its corrosion resistant properties in a UF_6 atmosphere. The graphite is chosen as the reflector for its low neutron absorption cross section and also for the desired high operating temperatures of 1000°-1200° F. Helium gas is added to UF_6 in order to enhance the heat transfer and thermodynamic properties of the working fluid. External equipment is to be used to remove the fission products, cool the gas, and recycle it back to the cylinder.

The reflector thickness is varied during the operation of the engine to simulate the desired time sequence of the subcritical-supercritical-subcritical state of the reactor. As the compression stroke starts, the reflector starts out as a thin reflector, then increases in thickness slowly until a step increase in reflector is removed going back to a thin reflector; the reflector continues to decrease in thickness until the piston bottoms.

The engine is designed to operate at a high graphite temperature of approximately 1000°-1200° F so as to minimize the heat loss from the core. The compression ratio for the engine is 10, with a clearance volume of 0.24 m^3. The engine shaft speed is 100 rpm and the UF_6 is 100% enriched.

Neutronic Analysis

For steady state, two-group, two region diffusion theory analysis, the following assumptions were made.

i) No fast neutron interaction in the core. The fast neutron core equation is replaced by a boundary condition for the net fast neutron current into the moderator.

ii) No absorption in the moderator. Any neutron absorptions in the moderator are considered to be included in the leakage.

iii) No delayed neutrons. It is assumed that the delayed neutron precursors are swept out of the cylinder before they exert any influence.

iv) No time dependence.

v) No angular dependence.

vi) For simplicity, the cylindrical geometry was replaced in the analysis by a spherical geometry with the core volume and reflector thickness conserved at all times; but they change in time simulating the motion of the piston within the cylinder.

The set of equations based on the above assumptions are solved for average thermal core and moderator flux and the neutron multiplication factor (k_{eff}) as a function of the position of the piston in the cylinder. As the multiplication factor approaches and exceeds unity, a one group, point reactor kinetics equation is used to solve for the time dependent thermal flux in the core. This time dependent solution method is adopted because of the slow variation in system configuration (due to piston motion) compared to the diffusion speed or neutron cycle time.

Energy Model

The conservation of energy equation for a non-flow system is used for the energy model of the system. It is assumed that the UF_6-He working fluid is a perfect gas and that it does not change its composition. It is assumed that the ionization and dissociation caused by high energy fission fragments is negligible and that the heat transferred to the walls is also negligible. The energy equation balances the rate of variation of the internal energy in the working fluid (UF_6+He) against the rate of fission heat release and the net work done by the gas on the piston. This equation is solved for the bulk temperature of the core.

Results

Figure (3-2) shows the multiplication factor, k_{eff} for a system with an infinite graphite reflector as a function of UF_6 partial pressure. It is seen that for a UF_6 partial pressure of greater than 1 atmosphere, the core becomes so black to the neutrons that additional uranium is ineffective. Figure (3-3) shows the relative thermal neutron flux distribution for a UF_6 partial pressure of 0.67 atmosphere and a core volume of 0.44 m^3. These two figures imply that a low UF_6 loading is required to minimize the nonuniform flux in the core so that the fission heat is not deposited in a thin shell next to the reflector.

The average core thermal flux and neutron multiplication factor (k_{eff}) as a function of percent time through the cycle in Figure 3-4 shows that the k_{eff} increases to a value greater than 1 when the thick reflector is superimposed on the thin reflector and then decreases as the core continues to decrease in size during the compression stroke. The fact that the k_{eff} value just

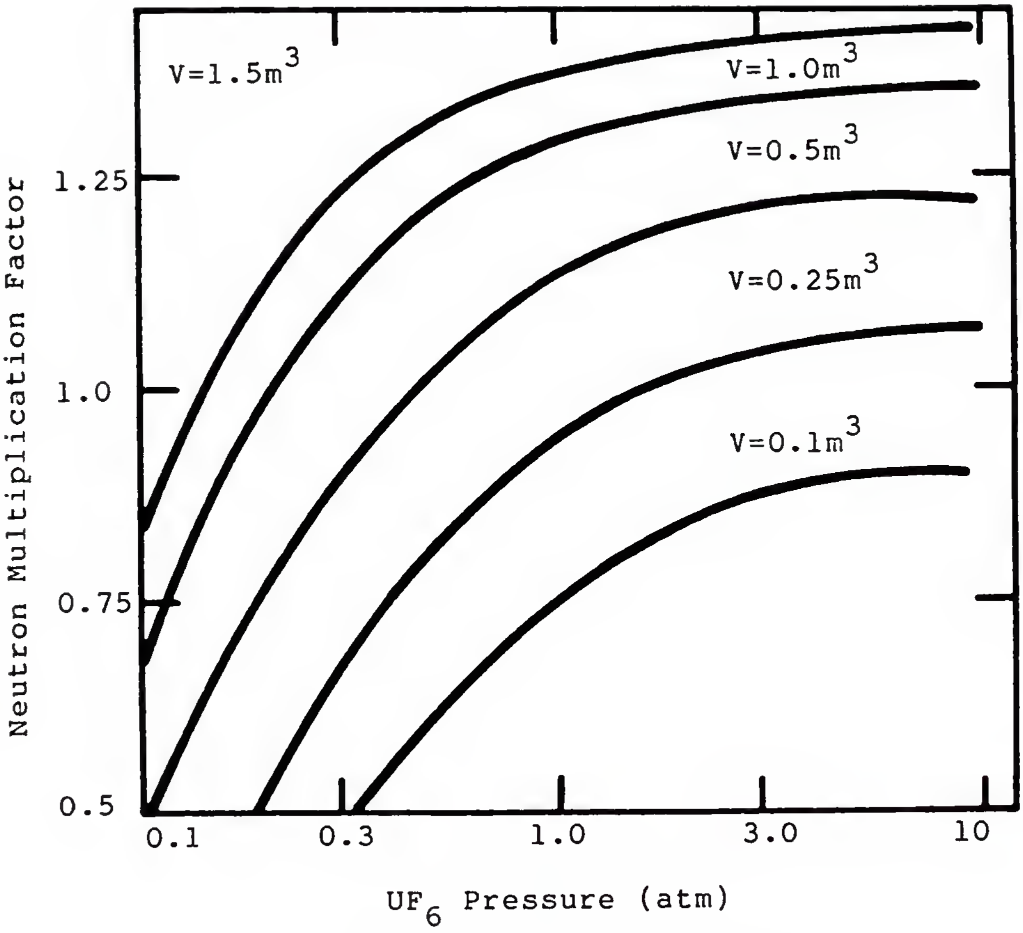

(Gas Temperature = 400°K)

Figure 3-2. Neutron Multiplication Factor Versus UF$_6$ Partial Pressure for an Infinite Graphite Reflector.

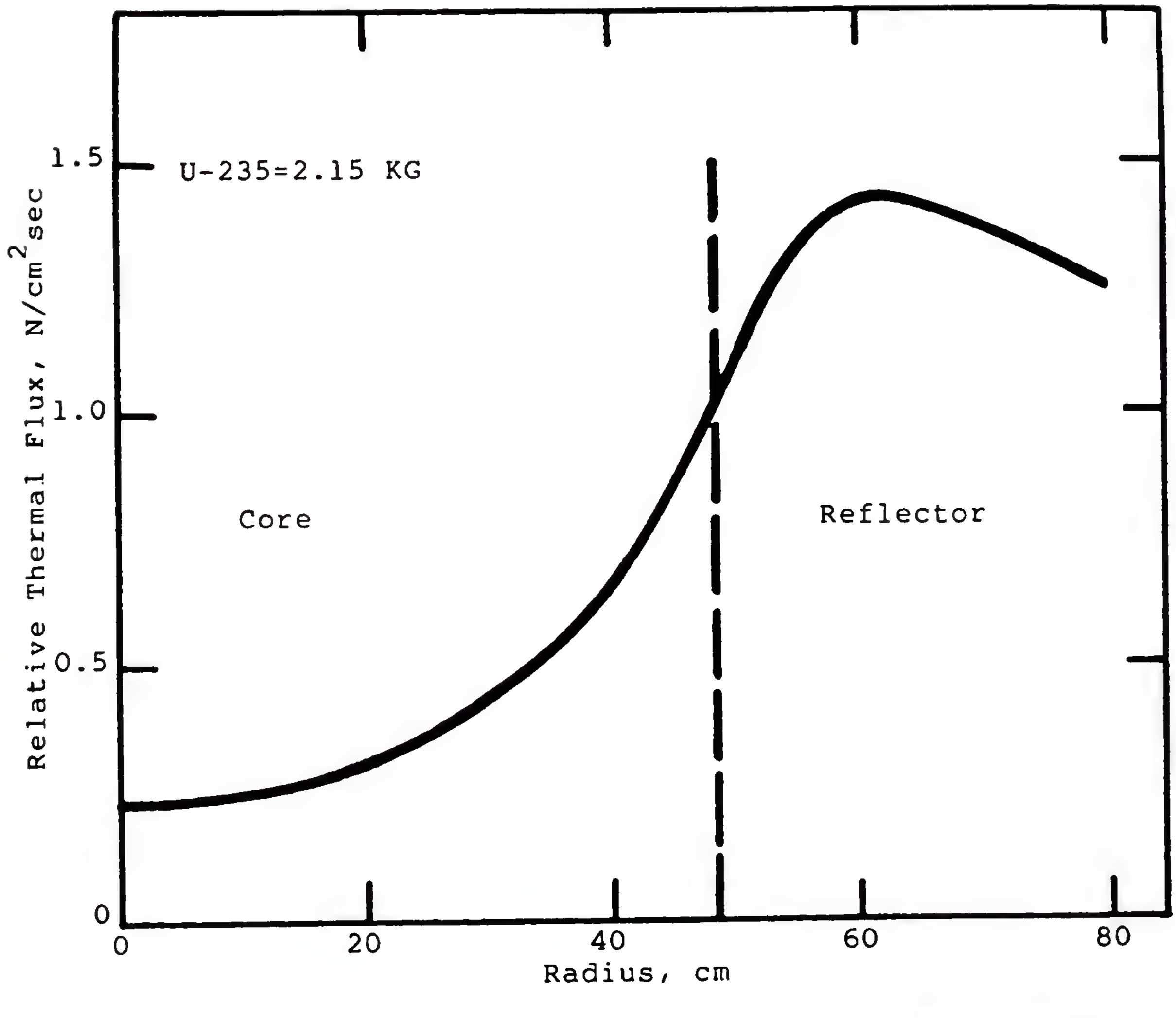

Figure 3-3 Relative Thermal Flux in Core and Graphite Reflector for the UF_6 Piston Engine

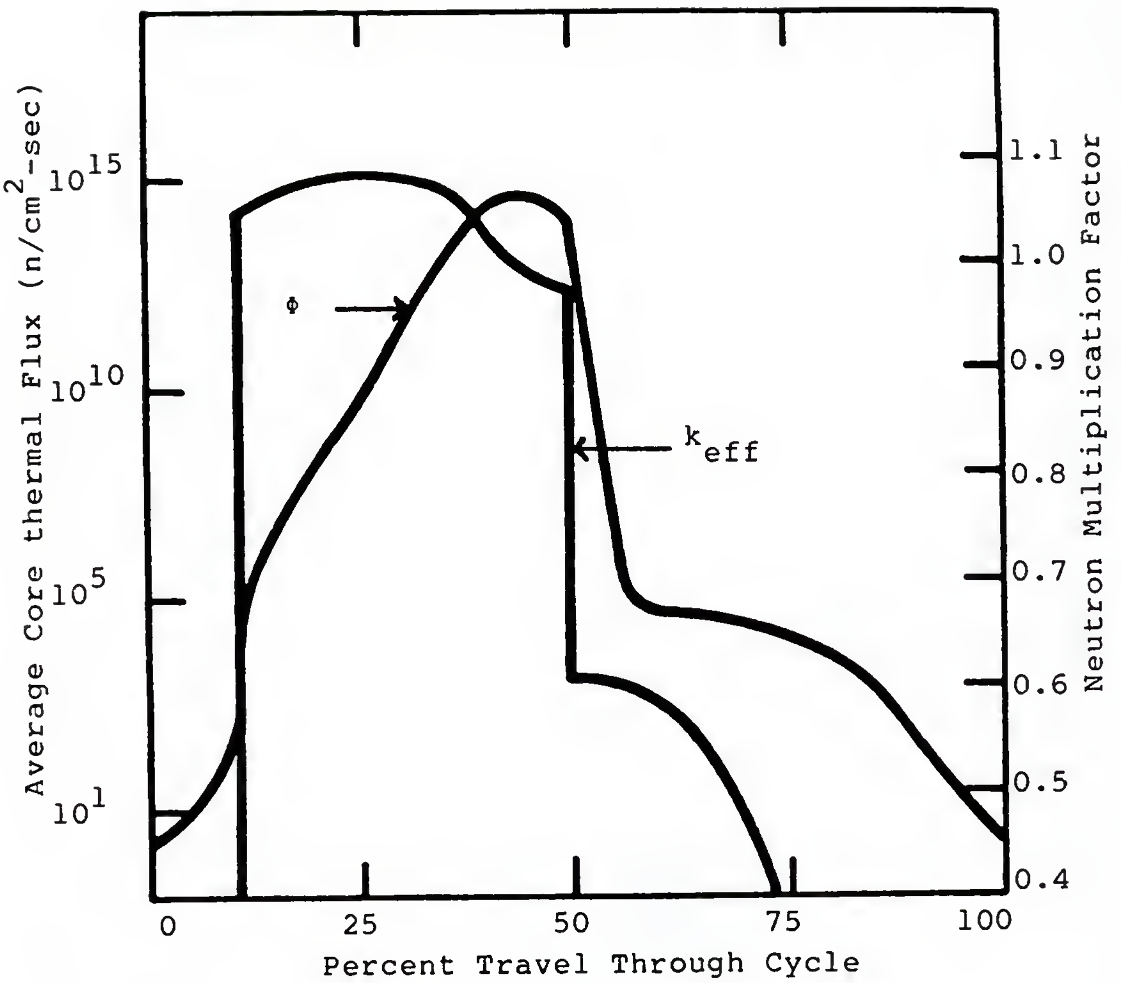

Initial Gas Pressure = 1 atm
Initial Gas Temperature = 400°K
U-235 Mass = 2.15 kg

Figure 3-4. Average Core Thermal Neutron Flux and Neutron Multiplication Factor as a Function of Percent Travel Through the Piston Cycle for a Graphite-Reflected Engine.

before the thick reflector is removed is slightly subcritical, causes the majority of heat to be added during the last 50 ms, i.e., 8% of the compression stroke. While this long cycle time permits easier control of the reactor, a little larger uranium loading yields a k_{eff} greater than 1 at this point; this results in the majority of the heat being added in a 15-25 ms period as the piston is passing the top dead center (TDC).

Figure (3-5) shows efficiency, power, and pressure versus U^{235} loading for an engine with the thick reflector imposed at the 10% cycle position and removed at the 50% position (40% of the cycle is available for buildup for neutron flux). A maximum k_{eff} of 1.07 to 1.10 is reached for these systems with the k_{eff} dropping to 0.99 from 1.01 as the TDC is approached. This behavior of k_{eff} greatly increases the control safety since the time constant is larger at higher pressure. Increasing the U^{235} loading leads to larger k_{eff}, but it also reduces the helium in the gas mixture, for the same initial pressure. Thus, the efficiency and the power curves are concave downward to reflect the lower average specific heat and hence the poorer thermodynamic properties of the gas mixture as more UF_6 is added at the expense of helium.

The preliminary feasibility studies conducted by Kylstra and his associates showed good performance potential for the pulsed gaseous core engines. This encouraged

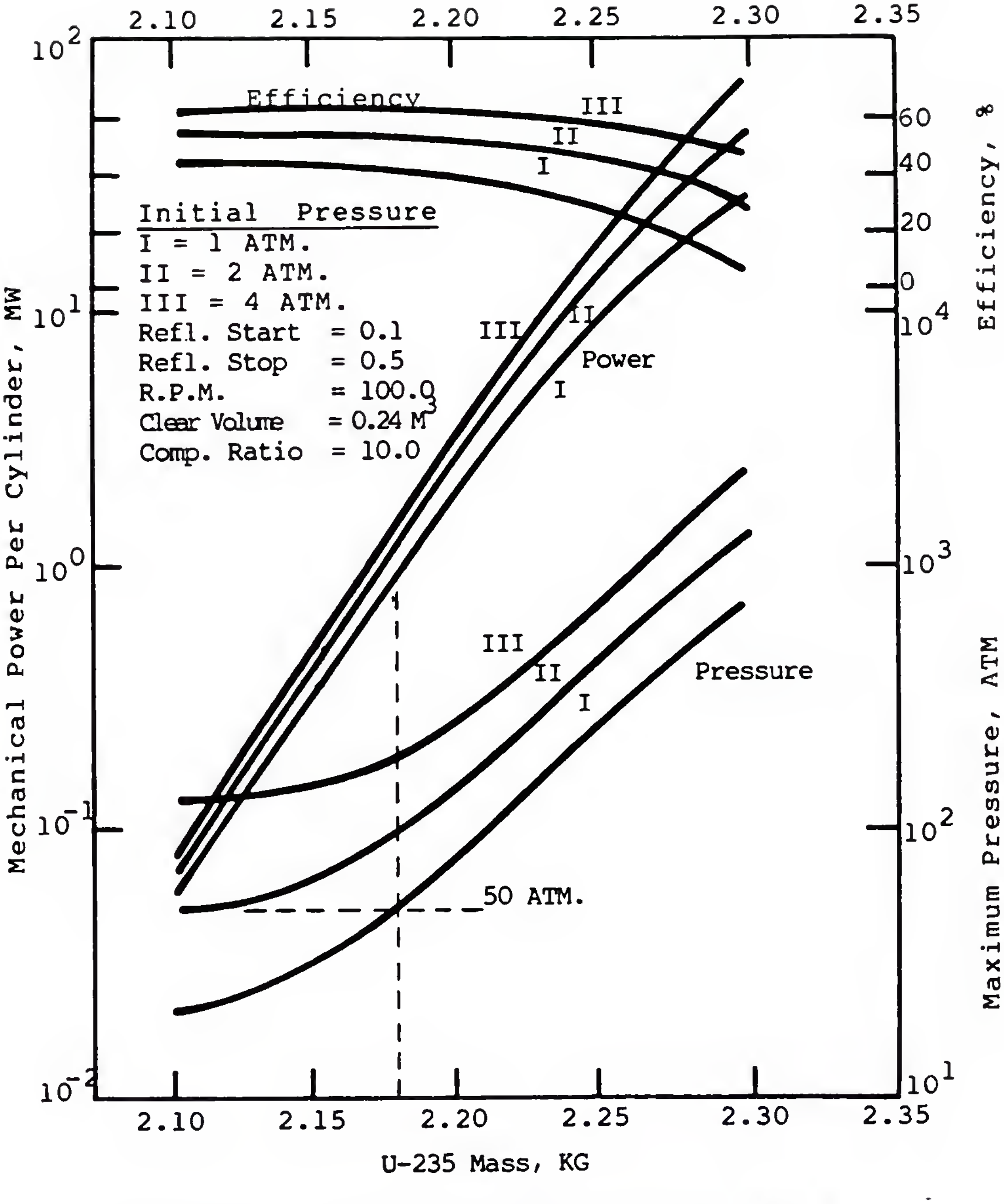

Figure 3-5. UF_6 Piston Engine Performance for Thick Reflector Imposed at 10 percent Cycle Position.

researchers at the University of Florida to embark on more refined and comprehensive studies on gaseous core reactor systems with and without movable pistons.

Pulsed Nuclear Piston and Pulsed Gas Generator Systems

Two basic alternative pulsed gaseous core reactor (PGCR) systems that have undergone extensive theoretical and experimental investigations since Kylstra's work are the Pulsed Nuclear Piston (PNP) and Pulsed Gas Generator (PGG) systems (29). These two reactors are based on a similar concept except that the PNP consists of a pulsed gaseous core reactor enclosed by a moderating reflector and a piston assembly while the PGG employs a core of fixed dimensions. These studies have established a basic scientific understanding of the physical phenomena associated with the conceptual operation of pulsed gaseous core systems and have resulted in a favorable response from the scientific and engineering community on their use for space applications. Results of detailed theoretical and experimental neutronic analyses and descriptions of processes used in the selection of optimum configuration for the PNP and PGG can be found in (28-31). This section presents a brief description of the two pulsed gaseous core reactor concepts, PNP and PGG, and a brief summary of the results from extensive neutronic and energetic studies of the system carried out by Dugan (30).

Pulsed Nuclear Piston System

The pulsed Nuclear Piston (PNP) system consists of a pulsed gaseous core reactor enclosed by a moderating-reflector cylinder and a piston assembly (Figure 3-6) which operates on a thermodynamic cycle similar to the internal combustion engine. The primary working fluid is a mixture of uranium hexafluoride (UF_6) and helium; highly enriched UF_6 is the reactor fuel and helium gas enhances the thermodynamic, transport, and heat transfer characteristics of the working fluid mixture.

The energy released by the fissioning gas can be extracted both as mechanical power and as heat from the circulating gas which recycles back to the core by the pressure differential established in the power chamber. Mechanical power can be derived from the engine by means of a conventional crankshaft operating at low speeds. In addition to the mechanical power, a significant amount of energy from the hot gas can be removed in an external heat removal loop. The high temperature (1000°-1300° F) UF_6/He exhaust gas can be cooled in an UF_6/He-to-He heat exchanger and the heated helium gas can be used in a suitable power conversion cycle to drive a turbine.

Summary of PNP Results

Selected neutronic/energetic analysis of both two-stroke and four-stroke PNP engines was accomplished by Dugan et al. (28) during the early years of gaseous core reactor

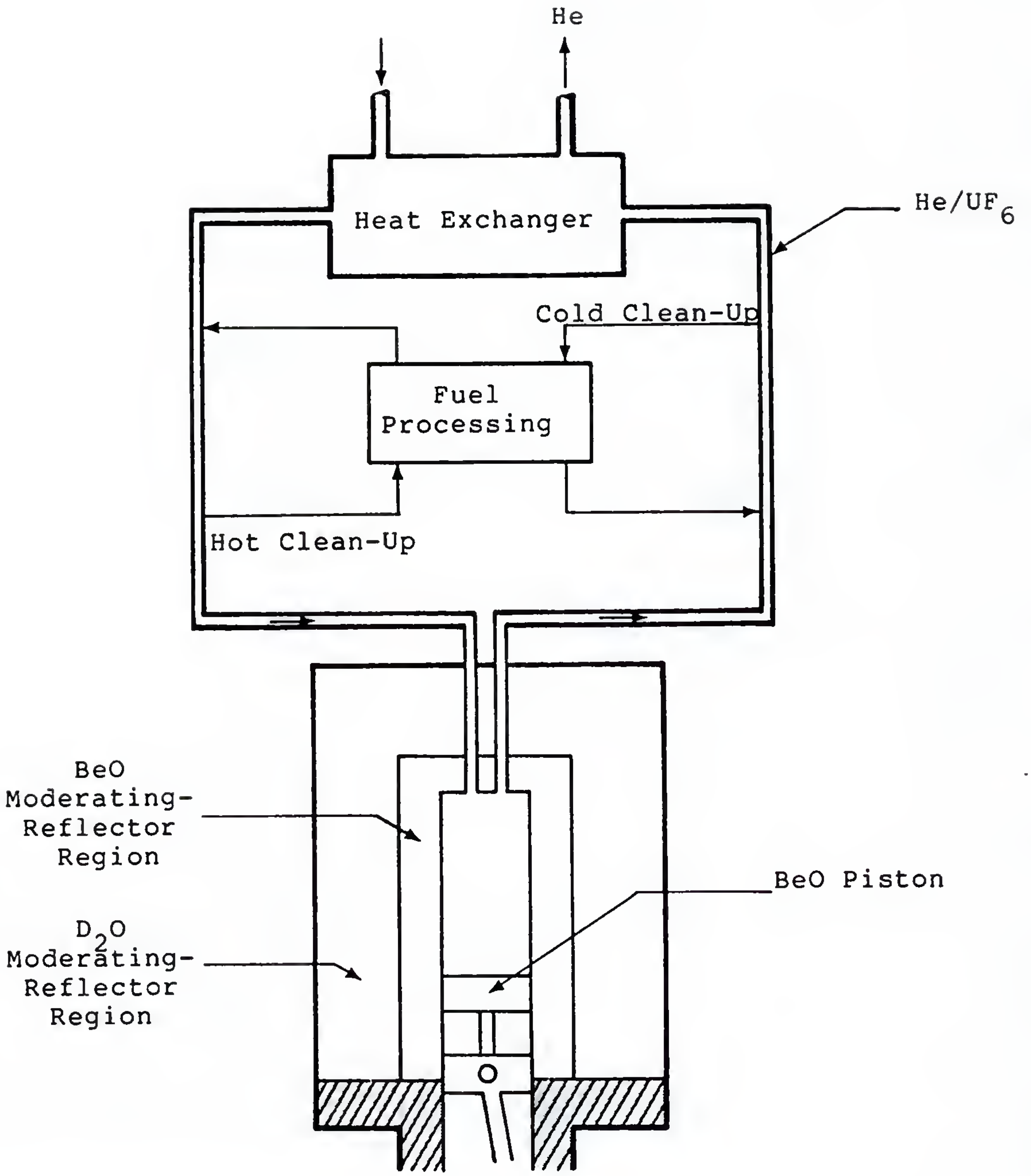

Figure 3-6. General Schematic for a Piston-Driven Pulsed Gas Core Nuclear Power System.

research at the University of Florida. Two-stroke engine analysis considered only the compression and power strokes while the four-stroke engine analysis explicitly examined the intake and exhaust phases of operation in addition to the compression and power strokes. While the earlier studies neglected delayed neutron and photoneutron effects, subsequent studies included first, the influence of delayed neutrons and then, the influence of both the delayed and photoneutrons on the PGCR's performance.

Graphite was found to be unacceptable as the moderating reflector since the dimensions of the system with graphite as a moderator were found to be too large to be practical. It was determined that Be (or BeO) and D_2O were the most desirable moderating-reflector materials from the standpoint of neutron economy and size of the system. The prompt neutron lifetimes for the beryllium moderated system were found to be half as great as for the D_2O reflected system. Although D_2O has a significantly lower thermal absorption cross section than beryllium, the Be reflected system has a smaller critical mass. This is due to the large (n,2n) production that occurs in beryllium. It has been estimated that the (n,2n) production leads to an effective increase of 6% in the average number of neutrons per fission (30).

The D_2O moderating-reflector temperature coefficient of reactivity over the temperature range of 300 to 1200 K was found to be large and negative ($-2.5x10^{-4}$ $\Delta k/k$ per K) whereas the moderator temperature coefficient of reactivity for Be reflected systems was found to be small and positive ($\approx 1x10^{-5}$ $\Delta k/k$ per K). Although this made Be or BeO undesirable as a moderator material it was suggested that a composite, with an inner Be or BeO region surrounded by D_2O would be an ideal moderator arrangement with an overall moderator temperature coefficient of reactivity large and negative ($\approx -2x10^{-4}$ $\Delta k/k$ per K). Moreover with the (n,2n) production in beryllium, this configuration will lead to a reduced critical mass.

Fuel temperature coefficients of reactivity for 100% enriched UF_6 were found to be small and positive ($\approx 5x10^{-7}$ $\Delta k/k$ per K). As the fuel enrichment was reduced the fuel temperature coefficient of reactivity was found to decrease and at 80% enrichment the coefficient was found to be small and negative ($\approx -1.2x10^{-7}$ $\Delta k/k$ per K).

The effects of delayed neutrons and photoneutrons on the system behavior were examined by different combinations of procedures. One procedure involved increasing the fuel loading to compensate for the absence of delayed neutrons and/or photoneutrons. For example, when both delayed neutrons and photoneutrons were neglected, the maximum neutron multiplication factor had to be increased from 1.055 (value of k_{eff} when both delayed neutrons and photoneutrons were present) to 1.091 in order to maintain the engine performance level. When photoneutrons were neglected, in order to maintain the system's performance level, the maximum neutron multiplication factor had to be increased to 1.061. When the delayed neutrons and photoneutrons were neglected in the analysis, the power output dropped by 70% relative to the case where only photoneutrons were ignored. Thus, the delayed neutrons and photoneutrons both exert a noticeable influence on system behavior with the delayed neutron influence being the stronger of the two.

The pulsed gaseous core system is capable of rapid startups in the presence of delayed neutrons. The startup procedures used in the referenced work (30) include variation in the inlet gas pressure and in the loop circulation time. Changes in the loop circulation time change the fraction of delayed neutrons which undergo decay while in the external circulation loop. Those precursors which do not decay in the loop, but decay upon reentering the core after passing through the loop, provide an extra neutron source and hence can be used to adjust the power level.

Figure 3-7 gives the delayed neutron and photoneutron precursor densities as a function of time during the PNP startup. Figure 3-8 illustrates the variation of output mechanical power and peak gas temperature during the startup. The time required to obtain a full power of 2.8 MW

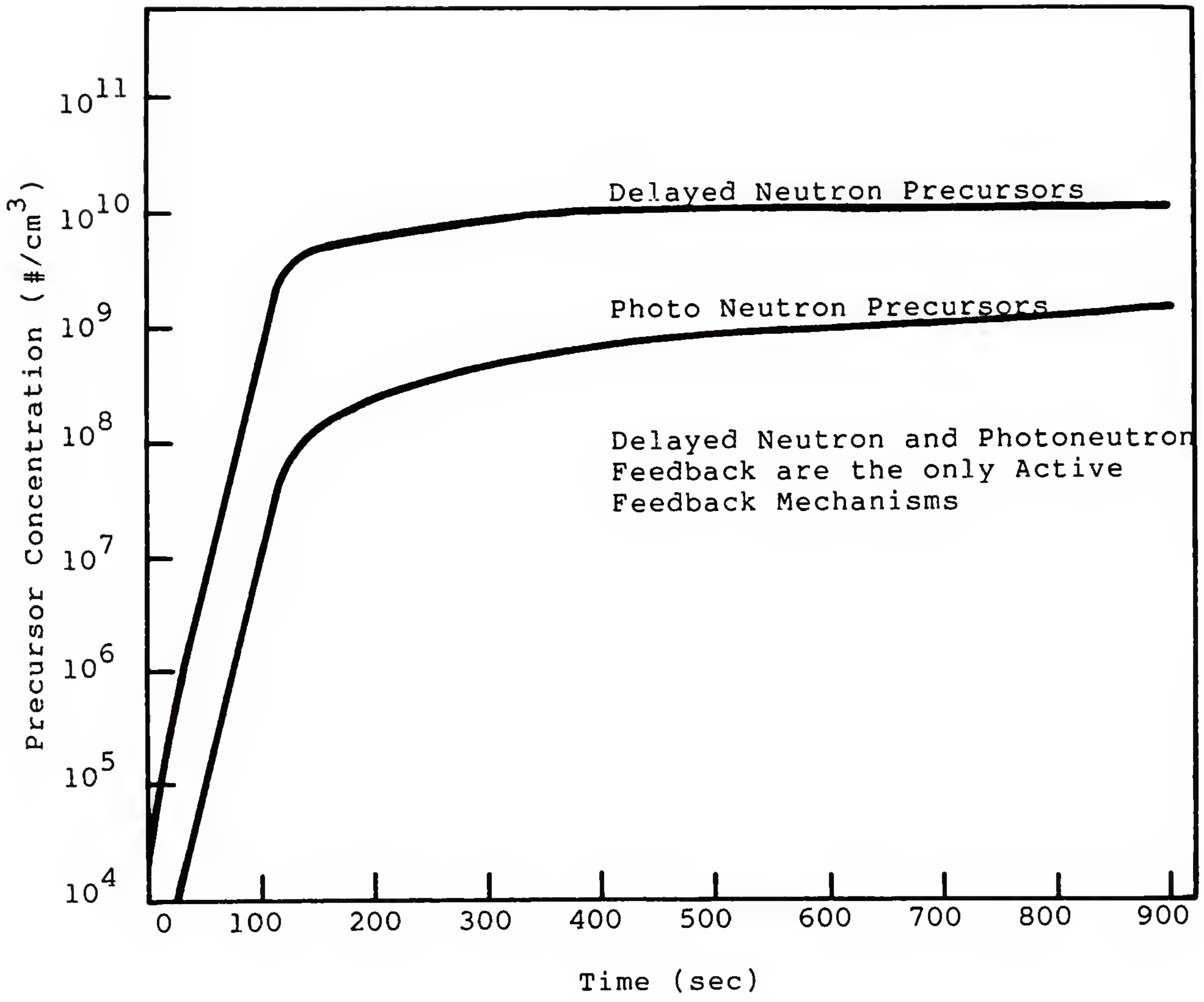

Figure 3-7. Delayed Neutron and Photoneutron Precursor Concentration Buildup During Startup from Shutdown for Pulsed Nuclear Piston Engine.

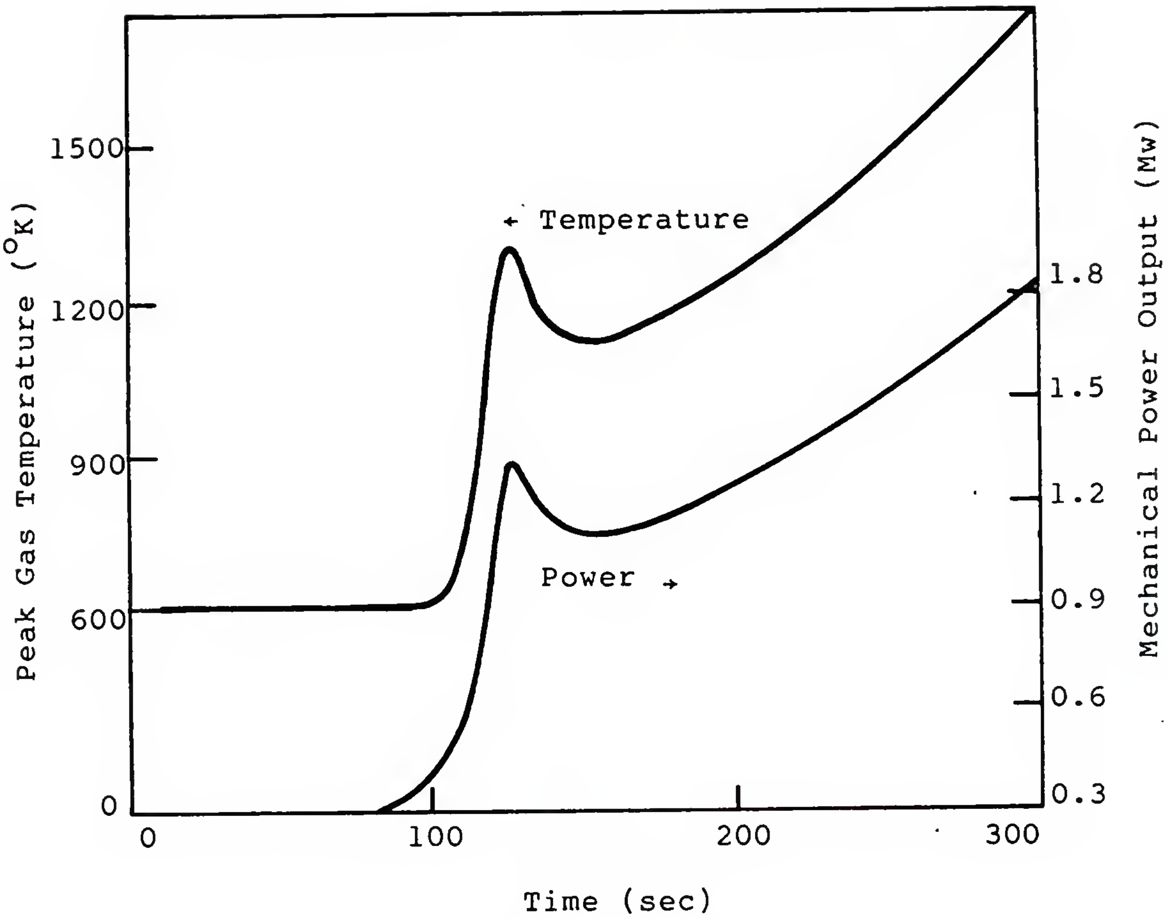

Figure 3-8. Peak Gas Temperature and Mechanical Power Versus Time During Startup from Shutdown for the Pulsed Neutron Piston Engine.

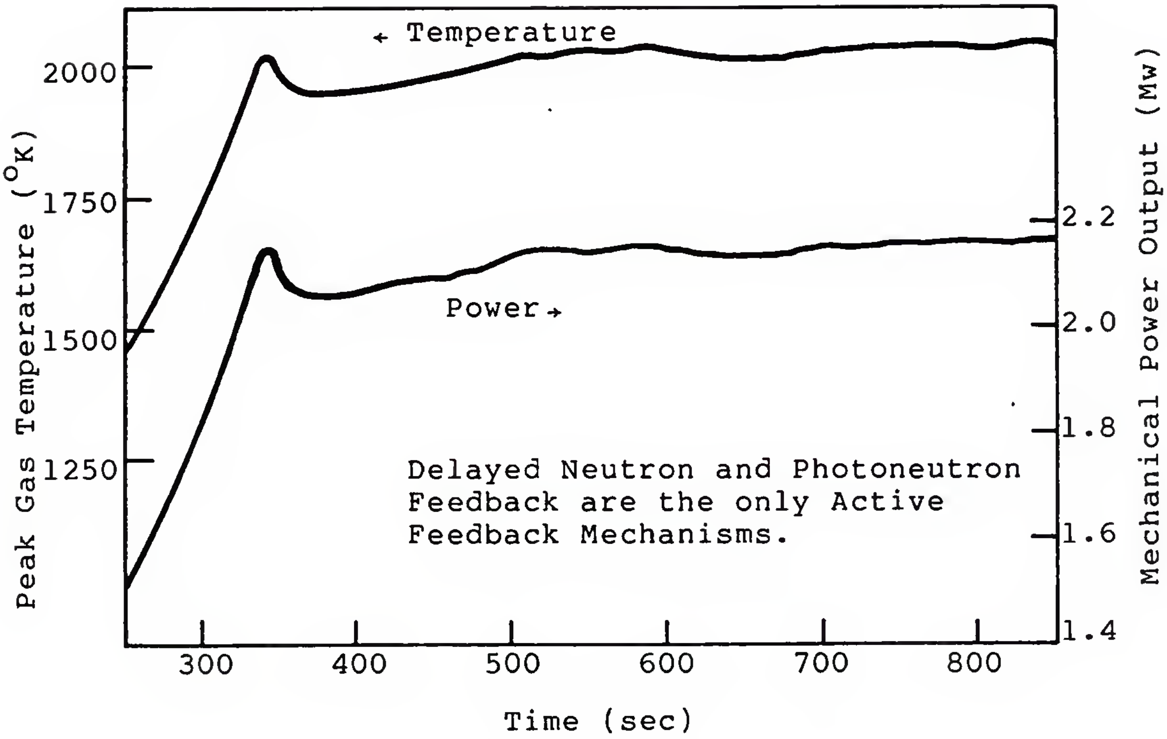

Figure 3-8. Peak Gas Temperature and Mechanical Power (continued) Versus Time During Startup from Shutdown for the PNP Engine.

with a loop circulation time of 11.3 seconds was found to be ≈ 13 minutes.

Dugan (30) in the PNP and PGG neutron kinetics analysis included both a simple point reactor kinetics model as well as a more sophisticated adiabatic kinetics model. Changes during the engine cycle, in the flux shape, and hence in the neutron lifetime and source weighting functions were thoroughly examined and found to be significant. The point reactor kinetics solution procedure was found inadequate to handle the significant variations in these parameters. To correct for the inadequacy of a simple point reactor kinetics model, a more complex adiabatic model was implemented. This method involves an iterative procedure between the point reactor kinetics program and other independent static neutronic analysis codes to obtain the integral parameters at various selected points throughout the cycle of operation of the system. Figures 3-9 and 3-10, which give the average core thermal neutron flux as a function of cycle time from the adiabatic model and the point reactor kinetics model, respectively, illustrate the inadequacy of the point reactor kinetics model in the neutronic analysis.

Results from the point reactor kinetics model were found to be equally poor whether prompt neutron lifetime and flux shape values that are representative of the system at the start of the cycle or cycle averaged values from the

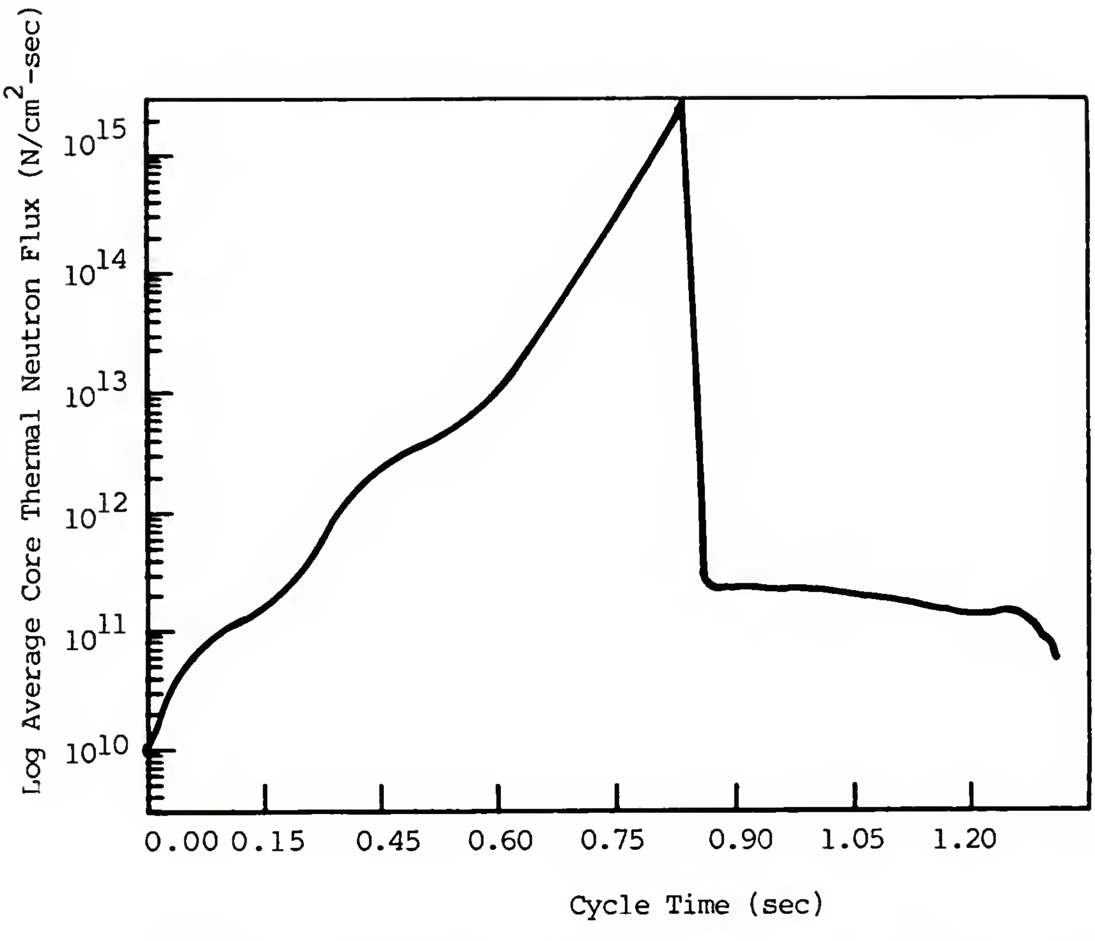

Figure 3-9. Average Thermal Neutron Flux in the Core Versus Cycle Time for the PNP Engine When the Adiabatic Kinetics Model is Used.

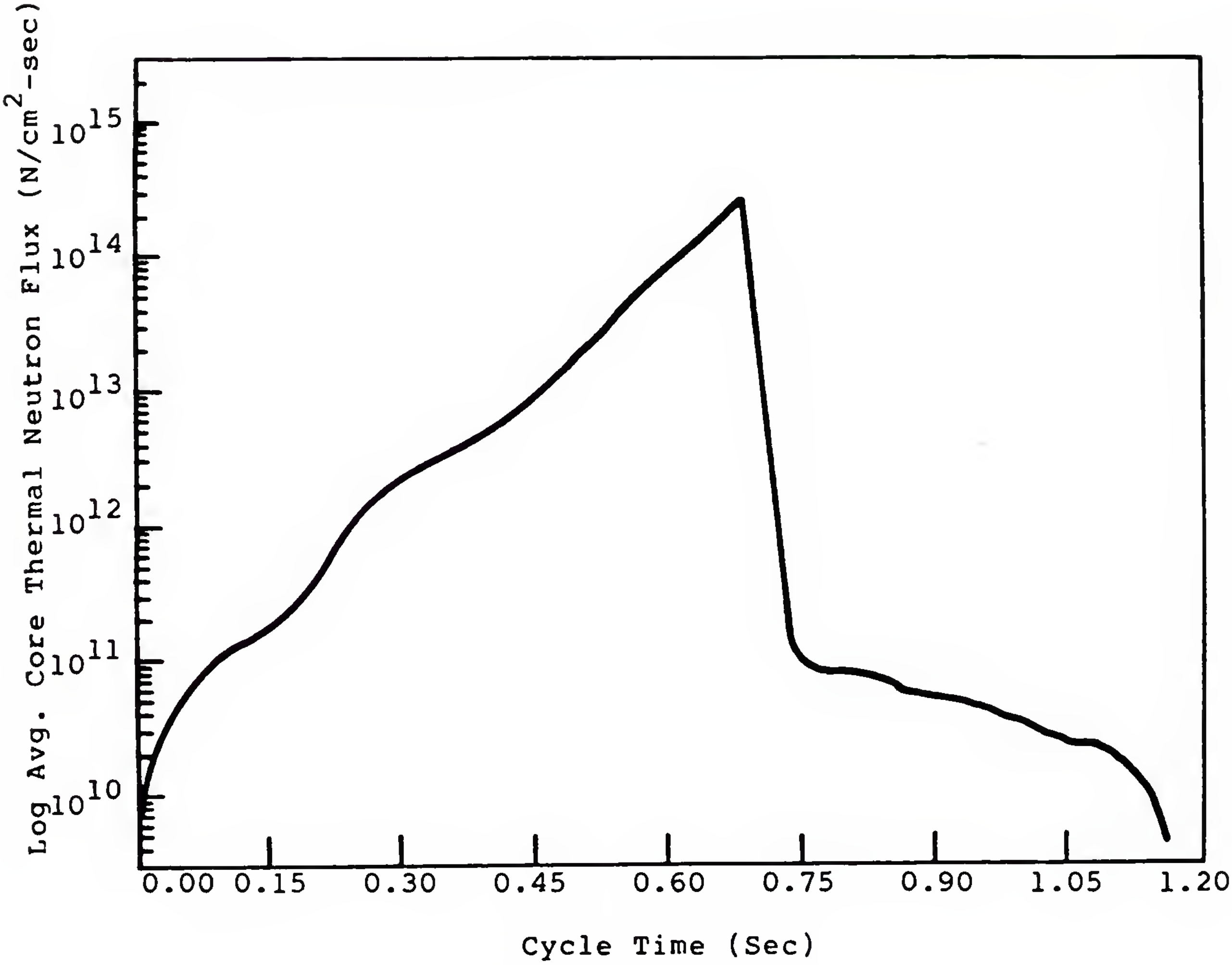

Figure 3-10. Average Thermal Neutron Flux in the Core Versus cycle Time for the PNP Engine when the Point Kinetics Model is used with ℓ=2.557 msec.

adiabatic analysis were used. However it was found to be possible to obtain an adjusted "equivalent" prompt neutron lifetime to be used in the point reactor kinetics calculations. The results from such a calculation were found to be very close to those obtained from the more complex adiabatic calculations. The variation of the average core thermal neutron flux with cycle time as obtained from a point reactor kinetics calculation with an "equivalent" prompt neutron lifetime of 1.718 milliseconds (ms) is shown in Figure 3-11. These results are much closer to the results from the adiabatic kinetics model (Figure 3-9) than those obtained from the point reactor kinetics model with a prompt neutron lifetime of 2.557 msec (Figure 3-10) which is the cycle-averaged prompt neutron lifetime value obtained from the adiabatic analysis. Results from these three different models for a specific configuration are given in Table 3-1.

Gas Generator Pulsed Gas Core Nuclear System

The pulsed gas generator (PGG) gas core nuclear concept is similar to the pulsed nuclear piston concept except that the gas generator employs a core of fixed dimensions (Figure 3-12). The gas generator system is simpler in operation and design than the nuclear piston concept and offers a more compact, self-contained nuclear energy generating package. Gas is cyclically injected into the core, the core is pulsed to supercriticality, and then the gas is exhausted. The

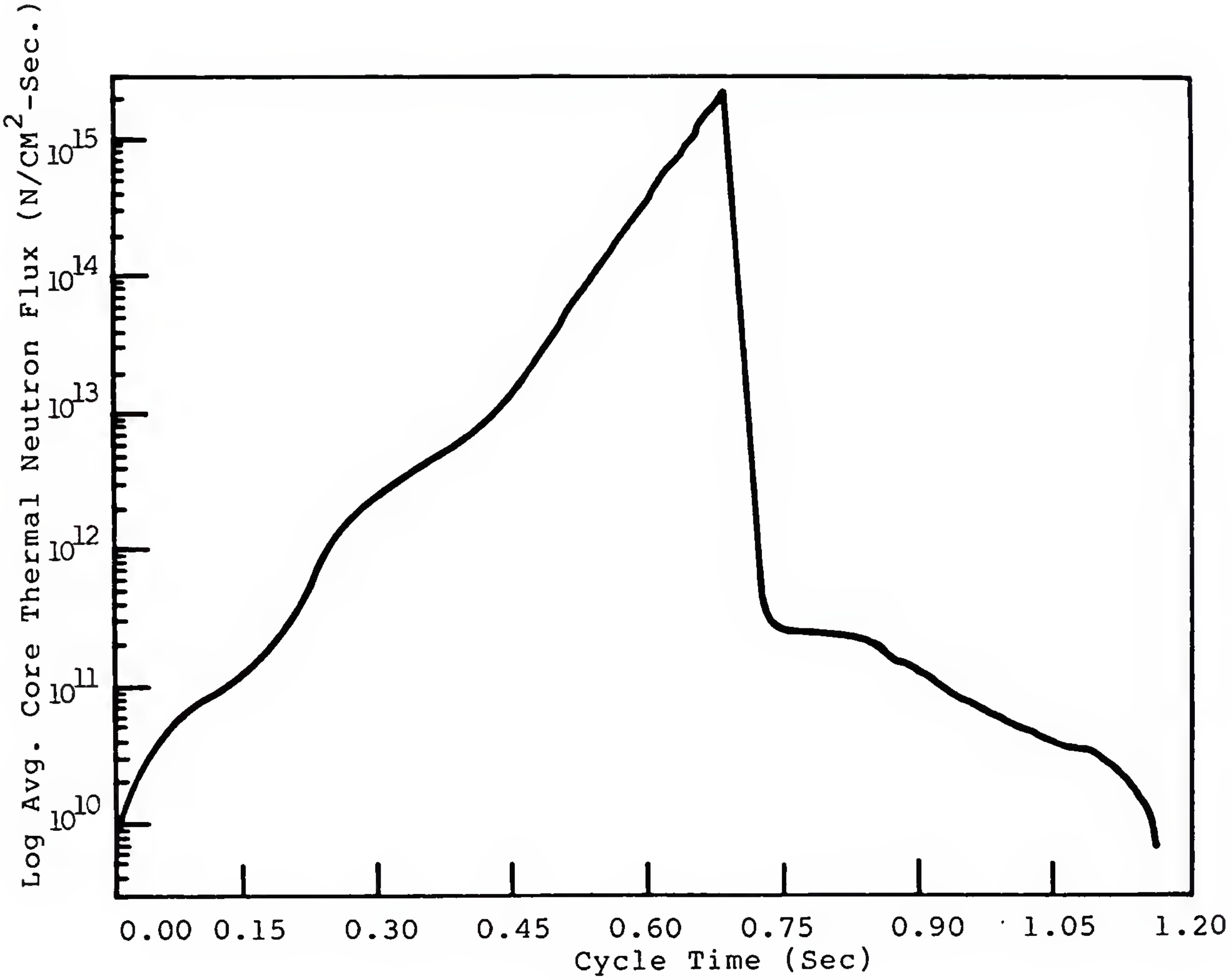

Figure 3-11. Average Thermal Neutron Flux in the Core Versus Cycle Time for the PNP Engine When the Point Kinetics Model Is Used with ℓ=1.718 msec.

Table 3-1. Summary of Results from the Different Neutron Kinetics Models for the PNP Configuration.

Neutron Kinetics Model Parameter	Adiabatic	Pt Kinetics* (ℓ=2.557 msec)	Pt Kinetics** (ℓ=1.718 msec)
Peak Gas Temperature (°K)	1938	710	1927
Exhaust Gas Temperature (°K)	1247	509	1260
Peak Gas Pressure (atm)	102.1	75.8	100.4
Mechanical Power (Mw)	2.054	0.633	2.095
Peak Average Thermal Neutron Flux In Core (n/cm^{2}sec)	2.961 X 10^{15}	2.688 X 10^{14}	2.256 X 10^{15}

* ℓ = 2.557 msec is the "cycle-averaged" prompt neutron lifetime obtained from the adiabatic analysis.

** ℓ = 1.718 msec is an adjusted "equivalent" prompt neutron lifetime which allows the point kinetics model to simulate the results obtained from the more complex adiabatic analysis.

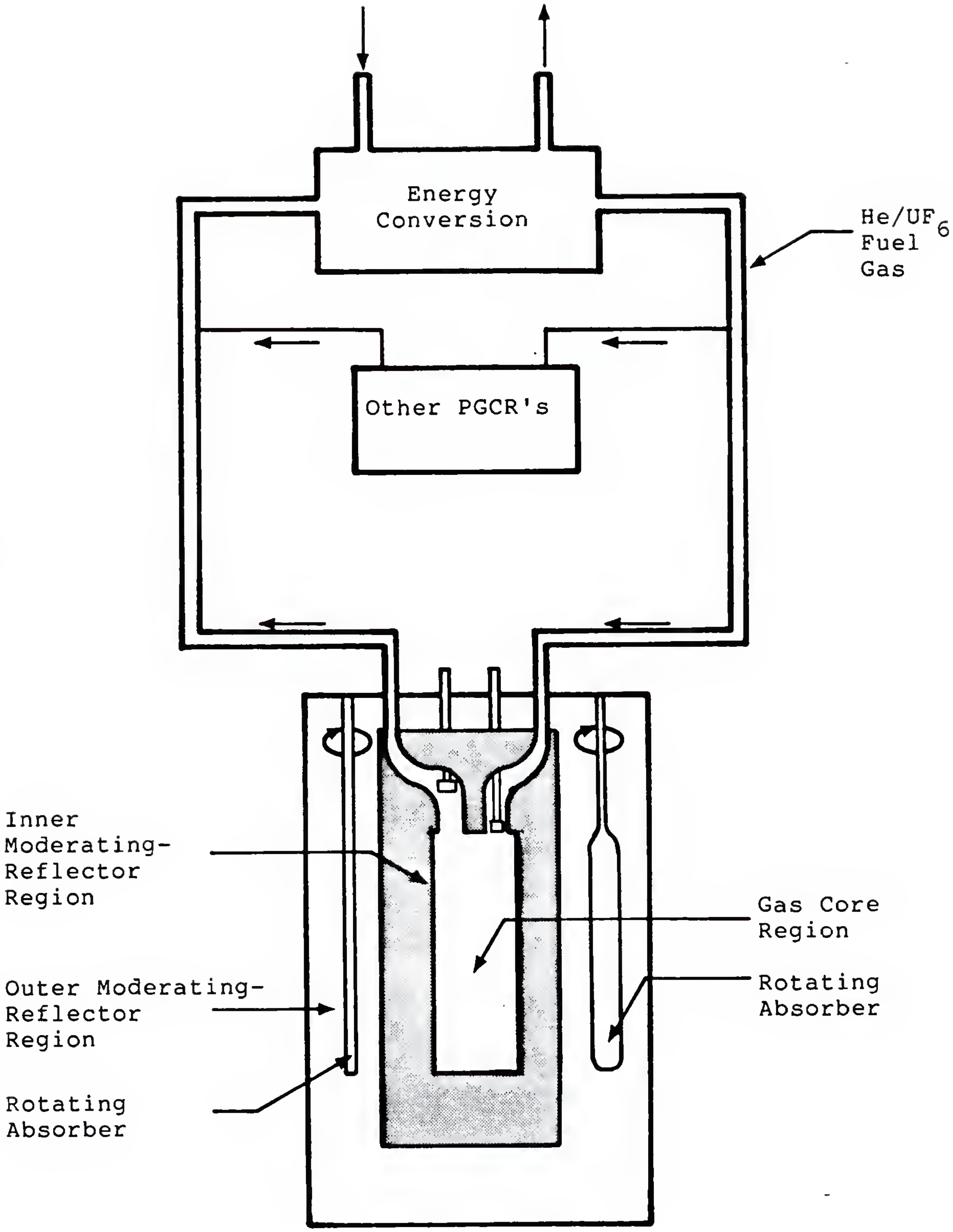

Figure 3-12. Pulsed Gas Generator Schematic

pulsing to supercriticality is achieved by means of a pile oscillator with a rotating absorber in the reflector surrounding the core. The system has the advantage of mechanical simplicity over the PNP concept while maintaining the advantages of a pulsed system mentioned elsewhere in this dissertation. These include the capacity for attaining high peak gas temperature (≈ 2000 K) and high neutron fluxes of 10^{15} neutrons/cm^2 sec while maintaining relatively low average gas temperatures (800-900 degree C).

Tables 3-2 and 3-3 compare typical operating conditions for the PGG and PNP systems, respectively, and reveal that the gas generator is capable of operating at lower enrichments than the nuclear piston system. Figures 3-13 and 3-14 which illustrate the variation of core average thermal neutron flux with cycle time for the PGG and PNP systems, respectively, reveal that the neutron flux for the gas generator peaks late in the cycle relative to the piston driven system. The PGG system can provide average exhaust gas temperatures that are closer to the peak gas temperature than can the PNP system. If UF_6 dissociation considerations limit the peak gas temperature to around 2000 K, then the piston driven system where gas temperature peaks earlier in the cycle can supply helium for gas turbines at temperatures of up to around 1200K as compared to 1400 K to 1500 K for the PGG system. For the PNP to provide higher temperature

Table 3-2. Typical Equilibrium Cycle Pulsed Gas Generator System Operating Conditions.

Core Volume (m^3)	0.80
Intake Line Gas Pressure (atm)	27.0
Intake Line Gas Temperature (°K)	400
Heated Gas Average Mass Flow Rate (kg/sec)	14.7
System Cycle Time (msec)	667
Loop Circulation Time (sec)	15.5
Average Prompt Neutron Lifetime (msec)	0.96
Core Height (cm)	95.6
Core Radius (cm)	51.7
Uranium Mass in Core (kg)	5.792
Helium Mass in Core (kg)	1.448
Helium Mole Fraction in Gas Mixture	0.9363
Uranium Enrichment (wt%)	85
Maximum Gas Temperature (°K)	1684
Maximum Gas Pressure (atm)	55.1
Maximum Core Thermal Neutron Flux ($n/cm^2 sec$)	1.8×10^{15}
Average Exhaust Gas Temperature (°K)	1405
Average Exhaust Gas Pressure (atm)	31.4
Cycle Average Gas Temperature (°K)	741
Cycle Average Gas Pressure (atm)	20.7
Cycle Average Core Thermal Neutron Flux ($n/cm^2 sec$)	2.0×10^{14}
Fission Energy Release Rate Per Chamber (Mw)	16.4
Net Turbine Power Output Per Chamber (Mw)	5.2
Efficiency (%)	32

The inner BeO region of the moderating-reflector regions is 30 cm thick and at an average temperature of 620°K.

The outer D_2O region of the moderating-reflector region is 70 cm thick and at an average temperature of 490°K.

Table 3-3. Typical Equilibrium Cycle Piston-Driven System Operating Conditions.

Compression Ratio	4-to-1
Clearance Volume (m^3)	0.180
Intake Line Gas Pressure (atm)	19.5
Intake Line Gas Temperature (°K)	650
Engine Speed (rpm)	100
Piston Cycle Time (sec)	1.2
Loop circulation Time (sec)	13.3
Average Prompt Neutron Lifetime (msec)	0.90
Core Height at TDC (cm)	58.1
Core Radius at TDC (cm)	31.4
Uranium Mass in Core (kg)	3.503
Helium Mass in Core (kg)	0.876
Uranium Enrichment (wt%)	93
Maximum Gas Temperature (°K)	2011
Maximum Gas Pressure (atm)	129.9
Maximum Core Thermal Neutron Flux (n/cm^2sec)	2.021×10^{15}
Average Exhaust Gas Temperature (°K)	1296
Average Exhause Gas Pressure (atm)	22.6
Cycle Average Gas Temperature (°K)	1100
Cycle Average Gas Pressure (atm)	43.6
Cycle Average Core Thermal Neutron Flux (n/cm^2sec)	1.065×10^{14}
Fission Energy Release Rate Per Chamber (Mw)	5.222
Mechanical (Shaft) Power Output Per Chamber (Mw)	1.670
Net Turbine Power Output Per Chamber (Mw)	1.446
Total Power Output Per Chamber (Mw)	3.116
Overall Efficiency (%)	59.7

Adiabatic Neutron Kientics Model Employed
Simple Harmonic Motion for Connecting Rod
D_2O Moderator-Reflector at 490°K and 100 cm thick

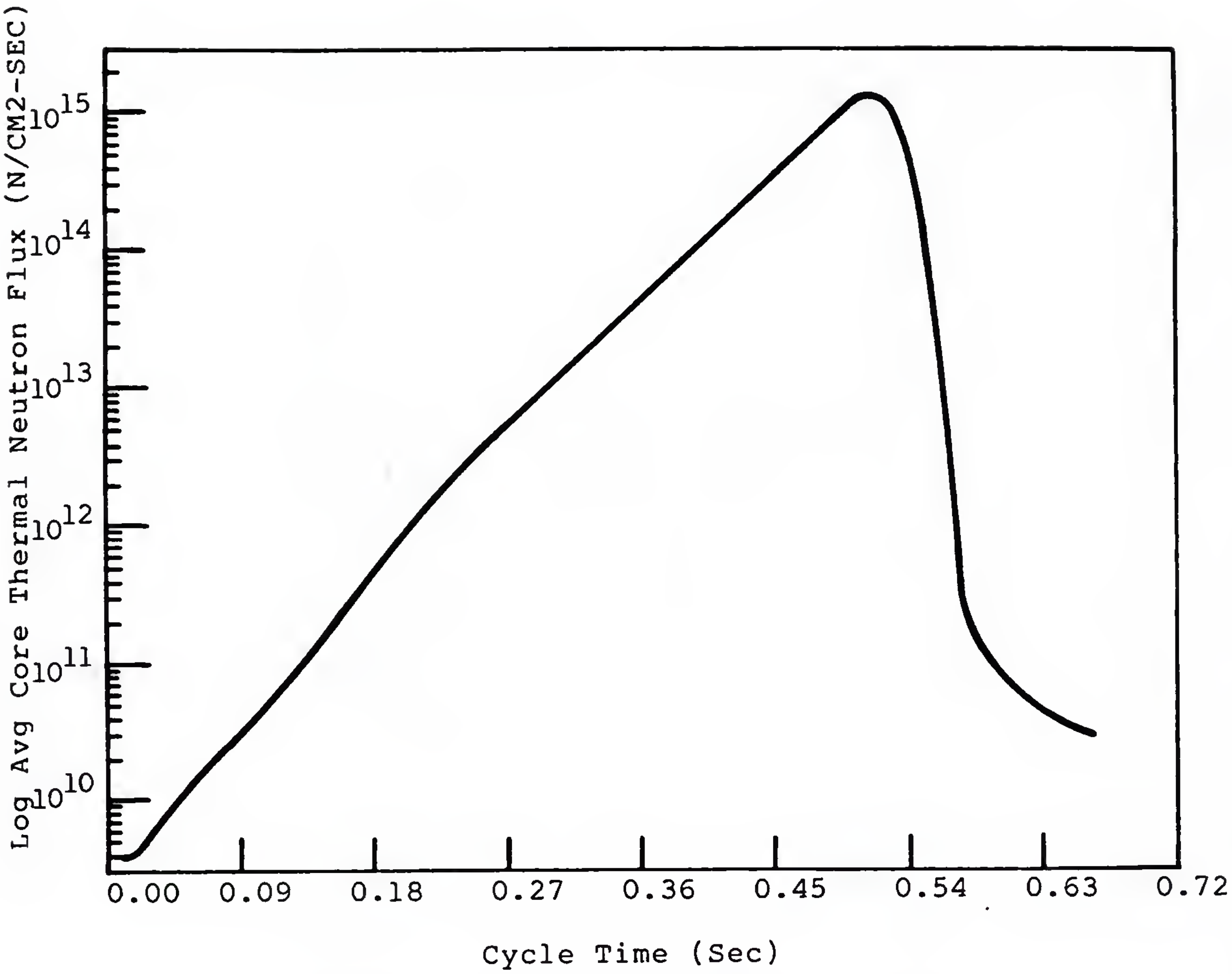

Figure 3-13. Average Core Thermal Neutron Flux Versus Cycle Time for a Typical Gas Generator Pulsed Gas Core Nuclear System.

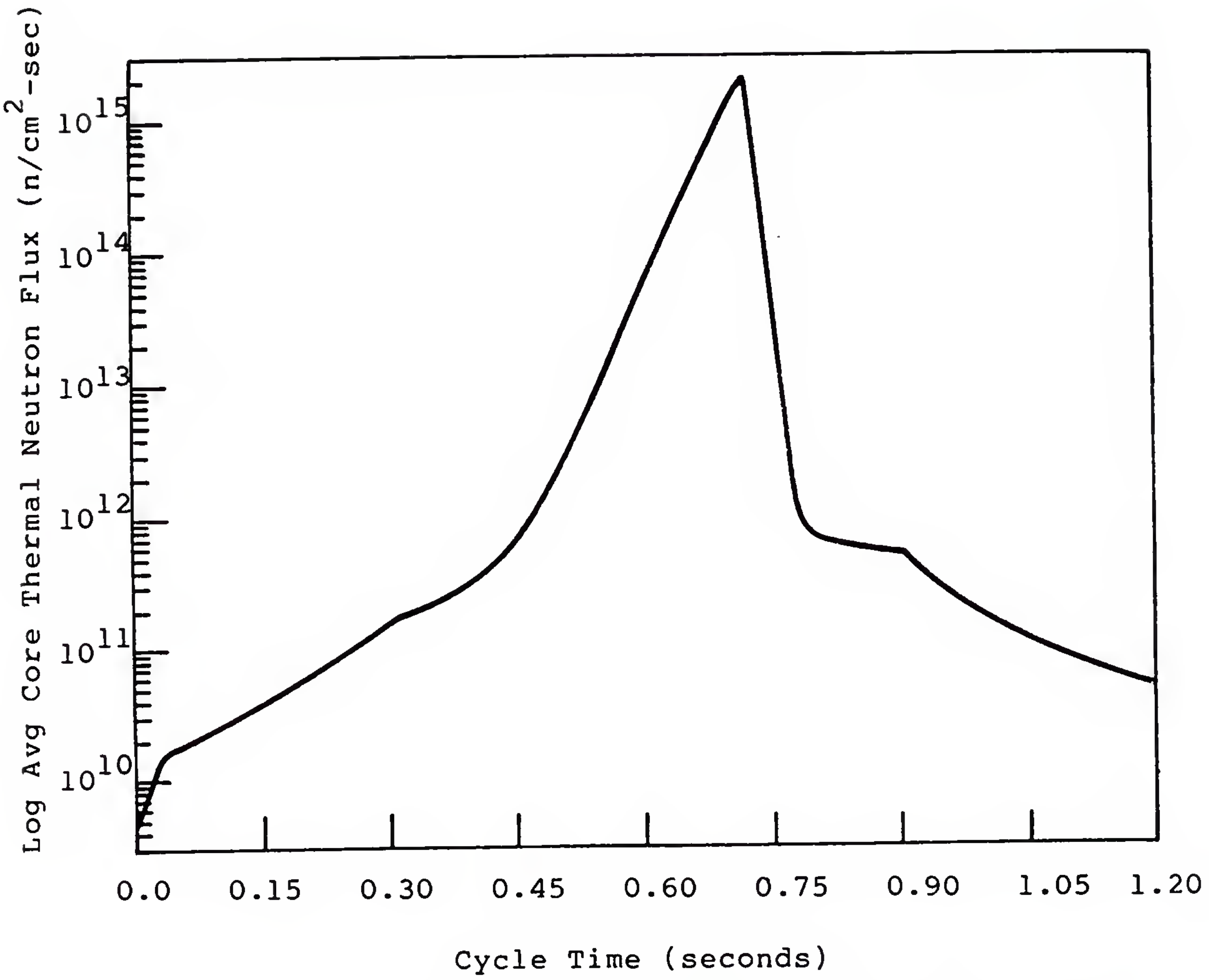

Figure 3-14. Average Core Thermal Neutron Flux Versus Cycle Time for a Typical Piston-Driven Pulsed Gas Core Nuclear System.

helium, would require it to exceed temperatures where a significant degree of UF_6 dissociation occurs.

Comparison between the PGG and PNP systems from Table 3-2 and 3-3 indicates that the PGG concept has the disadvantage of lower overall efficiency relative to the PNP concept due to the fact that only turbine power and no mechanical or shaft power is extracted from the system.

Comments

The promising results from the gaseous core reactor research efforts undertaken at the University of Florida by Dugan and others (28) have encouraged the engineering research community at the University of Florida to continue extensive research on various advanced gas core reactor concepts and different power conversion systems especially for space applications. The gas core reactor neutronics and energetics research have indicated that cyclic PGCR's are capable of attaining high peak gas temperatures (≈ 2000-2500 K) and high thermal neutron fluxes ($> 10^{15}$ neutrons/cm^2-sec) while maintaining relatively low cycle averaged gas temperatures (≈ 1000 K to 1200 K). The pulsed gaseous core systems are, thus, able to utilize a very high temperature and pressure working fluid while the structural stress and thermal shock are kept to a minimum.

One of the pulsed gas core systems that is being investigated is the bimodal gaseous core reactor system which is capable of both low power and high (burst) power mode of operation. The detailed description of the system and its static and dynamic neutronic characteristics are given in Chapters 4 and 5.

CHAPTER 4
STATIC NEUTRONIC STUDIES ON COUPLED MULTIPLE CAVITY GASEOUS CORE REACTOR SYSTEM

Introduction

This chapter examines the bimodal gaseous core reactor system in detail and predicts the results from the steady state neutronic analysis of the bimodal multiple cavity reactor system. Steady state neutronic analysis of the system includes examining the effects of variations in chamber dimensions, of inner and outer beryllium moderator/reflector thicknesses, of the BPGCR gas loading, and of equal and unequal gas loading among the PGCR chambers on the system neutron multiplication factor (k_{eff}), system neutron removal lifetime (ℓ), system neutron generation time (Λ), and the core-to-core neutronic coupling coefficients (α_{jk}).

The power requirements for space based systems under consideration range from 100's of KW(e) to about 10's of MW(e) for the station keeping or surveillance mode of operation and 100's of MW(e) to a few GW(e) for the burst mode of operation. The desired time durations for these modes range from 7 to 10 years for the station keeping mode to a few thousand seconds for the burst mode of operation.

If a low power pulsed gas core reactor system were to employ only one or two small chambers, compressor(s) would be needed to provide the necessary driving pressure not only during the system startup, but also during the steady state operation. With the multiple chamber design it is possible to arrange the chambers in the system so as to "optimize" the neutronic coupling and reduce the system critical mass requirement. Therefore, it is proposed to employ a PGCR system with multiple chambers surrounding the large central high power chamber; the multiple chamber design for the low power PGCR system would eliminate the need for compressor(s), except during system startup, and would reduce the fluid pulsation effects or flow discontinuities in the external loop (as compared to single chamber design). With the multiple cavities, the system can be designed to assure that at any given time, one or more chambers are in the exhaust phase to provide a relatively continuous source of pressurized gas for power generation. The multiple cavity design should have a favorable impact on system reliability since power can be generated even if a few of the reactor chambers fail.

The Bimodal Gas Core Reactor System Description

The bimodal gas core reactor system consists of two reactor systems, namely, the central high or burst power gaseous core reactor (BPGCR) system and the surrounding annular ring of low power pulsed gaseous core reactor (PGCR) chambers (Figures 1-1 and 1-2). The central cylindrical chamber and the annular ring of PGCR's are separated by an inner beryllium moderating/reflecting material. The ring of PGCR's is surrounded by an outer beryllium moderator/ reflector region. The identical upper and lower halves of the BPGCR are separated by a common moderator slab at the mid-plane and the MHD disk generator regions for the top and bottom central, high power chambers. The bimodal reactor system is also provided with top and bottom moderator/ reflectors of appropriate thickness.

The PGCR chambers are intended to provide low power for station keeping/surveillance purposes. The primary working fluid is a mixture of highly enriched uranium hexafluoride (UF_6) which is the reactor fuel and helium gas which is added to enhance the thermodynamic, transport, and heat transfer characteristics of the primary working fluid. The fissile gaseous fuel (UF_6-He) mixture is cyclically injected into the PGCR chambers, which are individually pulsed to near-critical, critical, or supercritical state and the heated gas is then discharged for energy conversion; each chamber is capable of providing a few MW(e) power. Neutronically the PGCR cores go from a far-subcritical state to near-critical, critical, or supercritical state during the final fraction of the intake and power phases of operation. Just before the exhaust phase of operation, the core will have achieved an adequate neutron flux level for a sufficient duration to generate a hot gas for the energy conversion system.

The fissionable gaseous fuel whose nuclei undergo fission primarily by thermal neutrons neither moderates nor absorbs fast and epithermal neutrons to any significant degree. Fast neutrons released by fission leave the chamber, slow down to thermal energies in the beryllium moderator, and diffuse as thermal neutrons thereafter until they leak or are absorbed either in the chambers or in the reflector. With multiple PGCR chambers and proper timing of operation of the individual chambers among their intake, power, and exhaust (discharge) phases the system is expected to provide a relatively continuous source of pressurized gas for any suitable power conversion system. During low power PGCR operation of the system, the central cavity will either be voided, have a constant non-fuel gas flow, or have a low density fuel gas mixture flow.

The transition from station keeping to burst power operation can be achieved by circulating a uranium bearing fuel gas through the central BPGCR cavity. The neutronic coupling effects of the PGCR chambers on the gas fuel bearing central cavity provide the necessary initial heating/reactivity conditions to generate a partially ionized plasma (≈ 2000 to 4000 K). For the burst power mode of operation, which may last for a few thousand seconds, the power is provided by the central BPGCR chamber; the surrounding PGCR's continue to provide low or station keeping power. The energy conversion for the BPGCR chamber occurs in the disk MHD generator. The fuel gas then passes through a radiator heat exchanger before being circulated back into the central chamber by a compressor.

In addition to providing station keeping power, the PGCR's support burst power operation of the central chamber for the following reasons:

i) The neutronically coupled PGCR chambers surrounding the central chamber are near-critical, critical, or supercritical during a significant portion of their power cycle. They relax the reactivity requirements for the central BPGCR. This provides greater flexibility in selecting the BPGCR/MHD system working fluid composition.

ii) The PGCR's provide a base level neutron flux in the system and maintain the system "hot" so that a more rapid transition to burst power mode is possible than if the PGCR's were absent.

The pulsed nature of the system greatly minimizes the thermal stresses as compared to those typically experienced by comparable performance steady state systems. Also the pulsed operation reduces the thermal energy losses from the core (due to the short time duration of the pulse).

Steady State Neutronic Analysis

Steady state neutronic analysis of the multiple cavity bimodal gaseous core reactor system has been performed primarily by using the Monte Carlo Neutron Photon (MCNP) transport code (3) and the discrete ordinates (S_N) transport code, XSDRNPM (4). The complex geometry of the bimodal system and the tenuous nature of the fuel-gas mixture in the core require multidimensional S_N or Monte Carlo transport type calculations for the static neutronic analysis. One-dimensional static neutronic analysis of the system is performed by using an "equivalent" sphere in which the volume of the core and thickness of the moderator are preserved. As the later results show, this can lead to considerable errors in the values of parameters such as the system neutron multiplication factor, neutron removal lifetime, etc. Even though a two-dimensional S_N transport calculation can be expected to yield good results for the system neutron multiplication factor and neutron removal lifetime, it cannot be expected to provide an accurate estimate of the coupling coefficients among the PGCR cores themselves and between the central chamber and the PGCR cores. The complex geometry of the bimodal system requires a full three-dimensional Monte Carlo calculation to obtain a reliable estimate of the core-to-core coupling coefficients. The fact that the exact geometry of the system and probabilities of interaction can be simulated in the MCNP code provides the capability to estimate the integral kinetics parameters, especially the coupling coefficients, with a high degree of confidence.

MCNP is a general purpose, continuous energy, generalized three-dimensional geometry, time-dependent, coupled neutron-photon Monte Carlo transport code which has the capability of calculating the k_{eff} eigenvalues for fissile systems. It has an elaborate tally structure and user interface that allow a user to calculate almost anything conceivable and has elaborate and complete cross section data. It has a rich collection of variance reduction techniques. The tally structure in MCNP is capable of producing cell-averaged particle flux, surface neutron current and flux, and neutron, photon and fission heating in a cell. The cell flagging and surface flagging capabilities of MCNP allow one to determine the tally contribution of particle tracks from a flagged cell or surface to any other specified cell or surface of the system. This capability of MCNP is used to determine the neutronic coupling coefficients (α_{jk}) which are a measure of the degree of influence of the k-th core neutron flux on the j-th core neutron flux. Both free gas thermal and $S(\alpha,\beta)$ cross section data for materials in which significant neutron thermalization occurs have been provided in the MCNP cross section data files. The delayed neutrons are implicitly included in the MCNP treatment by considering the total ν, the average number of neutrons generated per fission. A more detailed description of the MCNP code, the associated nuclear cross section data library, its capabilities and features, and sample inputs for a single chamber PGCR and multiple chamber bimodal system are given in Appendix A.

Neutronic studies of the bimodal reactor system have utilized the generalized three dimensional geometry capability of the MCNP code. However, because of the gaseous nature of the cores, the convergence of the source from its initial guess to a distribution fluctuating around the eigenmode solution has been found to be too slow. Therefore, in order to get a reasonably converged value for the eigenvalue (k_{eff}) and the neutron removal lifetime it has been necessary to run MCNP for many more cycles or generations with a larger source distribution per cycle than would have been required with a denser, solid fueled core.

XSDRNPM is a one-dimensional, time independent, discrete ordinates transport code that is capable of calculating neutron multiplication factor and angular and spatial neutron flux (4). XSDRNPM is used for the "equivalent" one dimensional spherical mock-ups of the three dimensional multi-region bimodal gaseous core reactor. The cylindrical bimodal gaseous core reactor is replaced by a four region (Figure 4-1) spherical configuration with equivalent volume core and equivalent thickness moderator. The spherical mock-up has a central spherical chamber (BPGCR) surrounded by an annular ring of beryllium, followed by an annular ring of gaseous fuel (PGCR's), and then finally by an outer moderator ring. The k_{eff} values from XSDRNPM have mainly been used as the required initial k_{eff} guesses for the respective MCNP runs in order to have the MCNP eigenvalue and neutron flux converge faster. XSDRNPM k_{eff} values have also been used to explain trends in the neutronic behavior of different configurations of the BGCR system.

Steady State Calculations Procedure

A series of preliminary calculations were made with the MCNP code for various configurations of the bimodal gas core reactor system (Figure 1-2). These initial steady state calculations were done for system configurations with inner beryllium thicknesses (TIBE) of 10 cm, 20 cm, 25 cm, 30 cm, and 40 cm during which the outer beryllium thickness (TOBE) was maintained at 50 cm. For each value of the inner beryllium thickness the PGCR gas fuel (UF_6-He) mixture pressure was varied from 20 atmospheres to 60 atmospheres. The PGCR chambers were equally loaded with the UF_6-He

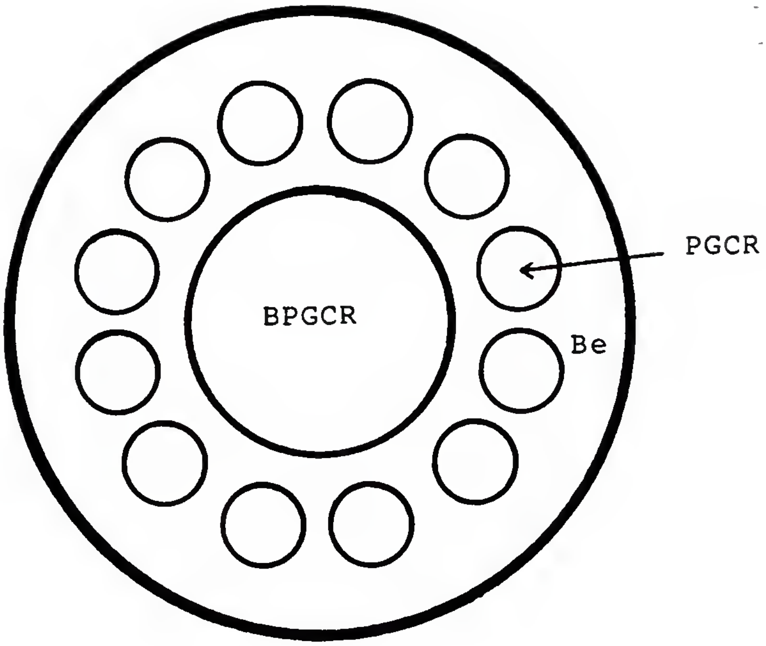

Cylindrical Geometry for MCNP Calculation

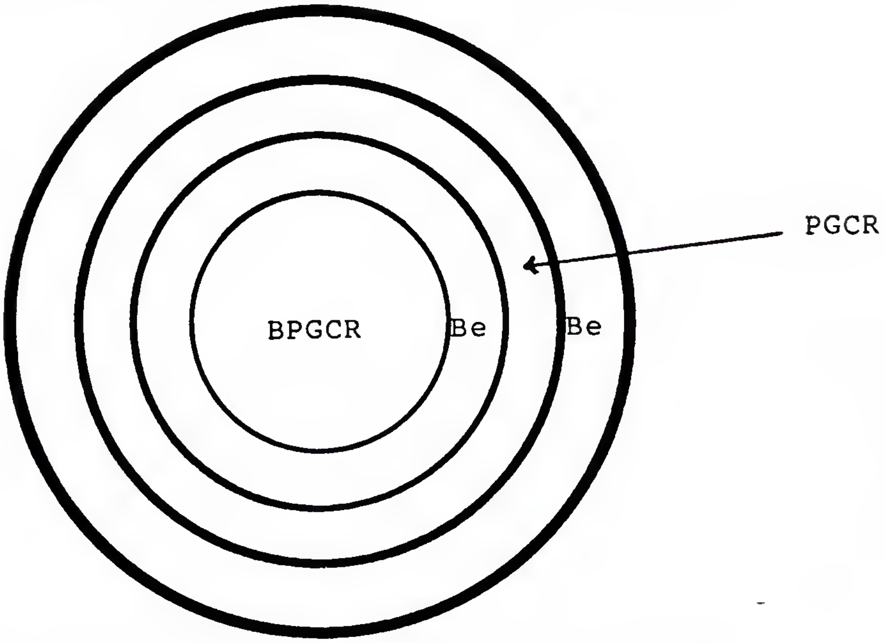

Spherical Mock-up for XSDRNPM Calculation

Figure 4-1. Cross-Sectional View of Cylindrical Bimodal Gas Core Reactor for MCNP and Spherical Mock-up of BGCR for XSDRNPM Calculation.

mixture and the central BPGCR cavity was maintained at a pressure of 20 atmospheres helium gas. For each fuel gas loading and system geometry configuration the MCNP code provides the system neutron multiplication factor (k_{eff}), the system neutron removal lifetime (ℓ), system neutron generation time (Λ), and the track length averaged neutron flux in each of the PGCR chambers and cells of the system. The cell flagging capability of the MCNP code in which the particle contribution from a flagged cell to any other individual cell or a group of cells can be tallied is used to compute the neutronic coupling coefficients among the PGCR cells.

To study the variation of the system neutron multiplication factor with the outer beryllium moderator thickness, calculations were done with the MCNP code in which the outer beryllium thickness was changed from 20 cm to 70 cm for two cases of inner beryllium thicknesses of 20 cm and 30 cm. The gaseous fuel mixture was maintained at a constant pressure of 50 atmospheres in each of the PGCR chambers.

MCNP calculations were then repeated for two configurations of the system with inner beryllium thicknesses of 20 cm and 30 cm but with unequal fuel-gas mixture pressures among the PGCR chambers. This staggered loading pattern of the PGCR chambers was used to simulate the situation in which a fraction of the total number of the PGCR chambers will always be in intake, power, or exhaust (discharge) phases of operation so that the reactor will be capable of delivering a continuous supply of pressurized gas to the PGCR power conversion system.

Steady state calculations were also done with the central burst power chamber fueled. In this case the central chamber fuel-gas mixture pressure was varied from 25 atmospheres to 100 atmospheres. This series of steady state calculations examined system configurations with inner beryllium thicknesses of 10 cm, 20 cm, 30 cm, and 40 cm. The outer beryllium thickness was maintained at 50 cm. The fuel-gas pressure was maintained at 10 atmospheres in each of the individual PGCR chambers, for this series of calculations. For these calculations, in addition to the system neutron multiplication factors, neutron removal lifetimes, and the fluxes at various BPGCR fuel-gas mixture pressures, the neutronic coupling effect of the central chamber on the PGCR chambers, the neutronic coupling effects of the individual PGCR chambers on the central BPGCR chamber, and the coupling effects among the PGCR chambers themselves were calculated separately.

Static neutronic calculations were also performed on various configurations of the bimodal reactor system with nominal central BPGCR chamber fuel-gas loading and various PGCR core fuel-gas loadings. This set of static neutronic calculations examined bimodal system configurations with inner beryllium thicknesses of 20 cm and 30 cm and an outer beryllium thickness of 50 cm. The fuel-gas loading in the central BPGCR chamber was maintained at 25 atmospheres while the fuel-gas loadings in the PGCR chamber were varied equally from 10 atmospheres to 50 atmospheres in both cases. The quantities calculated were the system neutron multiplication factor, neutron removal lifetime, the coupling coefficients among the BPGCR chamber and the PGCR cores, and the coupling coefficients among the PGCR cores themselves.

Steady state calculations for each geometric configuration of the system and for the different PGCR and BPGCR fuel-gas loadings were also done with the one dimensional, multi-group, discrete ordinates transport code, XSDRNPM. XSDRNPM calculations were done with a four-group cross section library processed from ENDF/B-IV files using the AMPX package from Oak Ridge National Laboratory. These calculations were done with an "equivalent" spherical mock-up of the three dimensional multi-region bimodal gas core reactor. The cylindrical bimodal gas core reactor is replaced by a four region spherical configuration with an equivalent volume core region and equivalent thickness reflector-moderator regions (see Figure 4-1). The k_{eff} values obtained from XSDRNPM have been used as initial k_{eff} guesses for the respective MCNP runs. XSDRNPM k_{eff} values for different system configurations have also been used for a comparative study of the static neutronics of the system.

Discussion of Results

Atom densities of the isotopes in the fuel-gas (UF_6-He) mixture, the corresponding gas pressures and temperatures, and typical dimensions of the BPGCR and PGCR chambers used in this study are given in Table 4-1. The fuel enrichment used in this study is 85% and the helium mole fraction in the UF_6-He mixture is 93%.

Effect of PGCR Core Loading and Inner Beryllium Thickness Variations When the BPGCR Core Is Unfueled

Results from a series of MCNP and XSDRNPM calculations for various configurations of the bimodal gaseous core reactor system with inner beryllium thicknesses, TIBE, of 10 cm, 20 cm, 25 cm, 30 cm, and 40 cm are given in Tables 4-2, 4-3, 4-4, 4-5, and 4-6, respectively. In each case (except in the case of TIBE of 10 cm) the total gas loading (UF_6+He) in the PGCR cores is varied from 20 atmospheres to 60 atmospheres in steps of 10 atmospheres while maintaining the inner BPGCR chamber at a constant pressure of 20 atmospheres of helium gas; the helium gas serves as an auxiliary coolant and flows through the central BPGCR chamber while the PGCR's are loaded with fuel during the low power operation of the bimodal system. The outer beryllium thickness is maintained at 50 cm. The gas loading for the case of 10 cm inner

Table 4-1. Core Physics Parameters for the Bimodal Gaseous Core Reactor System

	BPGCR*	PGCR*
Number Densities (atoms/cm^3)		
U-235	1.454 E+19	3.357 E+18
U-238	2.565 E+18	5.920 E+17
F-19	1.027 E+20	2.369 E+19
He-4	2.273 E+20	5.246 E+19
Pressure (atm)	100	10
Gas Temperature (k)	3000	1300
Volume (cm^3)	1.571 E+6	9.425 E+4
U-235 Enrichment	85%	85%
He-Mole Fraction	93%	93%
Radius (cm)	50	20
Height (cm)	200	75

*Each BPGCR and PGCR Chamber

Table 4-2. System Neutron Multiplication Factor (k_{eff}) and Neutron Removal Lifetime (ℓ) as a Function of PGCR Gas Loading for the Bimodal Gas Core Reactor System with Inner Beryllium Thickness of 10 cm.

TIBE=10cm
DISURF=1.88cm

PGCR Core Pressure (atm)	UF_6-He Number Density (atoms/ b-cm)	Uranium Mass per Core (kg)	k_{eff}^{**} -MCNP	ℓ^{**} -MCNP	k_{eff}^{*} -XSDRNPM
10	8.0115-05	0.145	0.4860(3.3)	3.594(3.0)	0.5779
20	1.6023-04	0.291	0.7675(3.0)	3.002(3.0)	0.8574
30	2.4056-04	0.437	0.9058(2.7)	2.728(2.4)	1.0219
40	3.2067-04	0.583	0.9846(3.0)	2.486(2.9)	1.1314
50	4.0058-04	0.728	1.0719(3.0)	2.312(2.6)	1.2060

**Relative Error or Uncertainty in Percentage Given in Parenthesis.
*k_{eff} Convergence Level in XSDRNPM Calculation is 10^{-5}.

Table 4-3. System Neutron Multiplication Factor (k_{eff}) and Neutron Removal Lifetime (ℓ) as a Function of PGCR Gas Loading for the BGCR System with TIBE of 20 cm.

TIBE=20cm
DISURF=7.14cm

PGCR Core Pressure (atm)	UF_6-He Number Density (atoms/ b-cm)	Uranium Mass per Core (kg)	k_{eff}^{**} -MCNP	ℓ^{**} -MCNP	k_{eff}^{*} -XSDRNPM
20	1.6023-04	0.291	0.7136(2.1)	3.027(1.6)	0.7468
30	2.4056-04	0.437	0.8881(2.5)	2.696(2.8)	0.9124
40	3.2067-04	0.583	0.9891(2.6)	2.465(2.7)	1.0241
50	4.0058-04	0.728	1.0429(1.6)	2.291(1.9)	1.1060
60	4.8069-04	0.873	1.1530(2.4)	2.142(2.4)	1.1682

**Relative Error or Uncertainty in Percentage Given in Parenthesis.
*k_{eff} Convergence Level in XSDRNPM Calculation is 10^{-5}.

Table 4-4. System Neutron Multiplication Factor (k_{eff}) and Neutron Removal Lifetime (ℓ) as a Function of PGCR Gas Loading for the BGCR System with TIBE of 25 cm.

TIBE=25cm
DISURF=9.74cm

PGCR Core Pressure (atm)	UF_6-He Number Density (atoms/b-cm)	Uranium Mass per Core (kg)	k_{eff}^{**} -MCNP	ℓ^{**} -MCNP	k_{eff}^{*} XSDRNPM
20	1.6023-04	0.291	0.7188(2.1)	3.032(1.9)	0.6989
30	2.4056-04	0.437	0.8743(1.9)	2.769(1.8)	0.8616
40	3.2067-04	0.583	0.9384(2.2)	2.443(2.1)	0.9749
50	4.0058-04	0.728	1.0321(2.5)	2.294(2.2)	1.0584
60	4.8069-04	0.873	1.1205(1.8)	2.216(1.7)	0.1225

**Relative Error or Uncertainty in Percentage Given in Parenthesis.
*k_{eff} Convergence Level in XSDRNPM Calculation is 10^{-5}.

Table 4-5. System Neutron Multiplication Factor (k_{eff}) and Neutron Removal Lifetime (ℓ) as a Function of PGCR Gas Loading for the BGCR System with TIBE of 30 cm.

TIBE=30cm
DISURF=12.36cm

PGCR Core Pressure (atm)	UF_6-He Number Density (atoms/ b-cm)	Uranium Mass per Core (kg)	k_{eff}** -MCNP	ℓ** -MCNP	k_{eff}* -XSDRNPM
20	1.6023-04	0.291	0.6941(2.7)	3.033(2.5)	0.6567
30	2.4056-04	0.437	0.8529(2.7)	2.715(2.2)	0.8173
40	3.2067-04	0.583	0.9387(1.8)	2.449(1.6)	0.9309
50	4.0058-04	0.728	0.9885(2.5)	2.292(2.1)	1.0155
60	4.8069-04	0.873	1.0991(2.5)	2.185(2.8)	1.0818

**Relative Error or Uncertainty in Percentage Given in Parenthesis.
*k_{eff} Convergence Level in XSDRNPM Calculation is 10^{-5}.

Table 4-6. System Neutron Multiplication Factor (k_{eff}) and Neutron Removal Lifetime (ℓ) as a Function of PGCR Gas Loading for the BGCR System with TIBE of 40 cm.

TIBE=40cm
DISURF=17.60cm

PGCR Core Pressure (atm)	UF_6-He Number Density (atoms/ b-cm)	Uranium Mass per Core (kg)	k_{eff}^{**} -MCNP	ℓ^{**} -MCNP	k_{eff}^{*} -XSDRNPM
20	1.6023-04	0.291	0.6377(2.5)	2.997(2.6)	0.5846
30	2.4056-04	0.437	0.7595(1.8)	2.652(1.6)	0.7407
40	3.2067-04	0.583	0.8899(2.0)	2.493(1.6)	0.8535
50	4.0058-04	0.728	0.9419(2.2)	2.259(1.9)	0.9394
60	4.8069-04	0.873	1.0423(2.0)	2.191(2.0)	1.0069

**Relative Error or Uncertainty in Percentage Given in Parenthesis.

*k_{eff} Convergence Level in XSDRNPM Calculation is 10^{-5}.

beryllium thickness is varied from 10 atmospheres to 50 atmospheres. The Tables 4-2 through 4-6 give the gas density, uranium mass in each PGCR core, the system neutron multiplication factor (k_{eff}) from both MCNP and XSDRNPM, and system neutron removal lifetime (ℓ) from MCNP at each PGCR gas loading. The relative percentage error in the system k_{eff} and neutron removal lifetime for the MCNP calculations are given in parenthesis following the respective quantities. The k_{eff} values from XSDRNPM have a convergence level of 10^{-5}. The parameter DISURF given in these tables is the perpendicular distance between the outer surfaces of any two adjacent PGCR cores.

Figures 4-2, 4-3, 4-4, 4-5, and 4-6 illustrate the variation of system neutron multiplication factor (k_{eff}) from both MCNP and XSDRNPM and the system neutron removal lifetime (ℓ) with the total PGCR gas loading per chamber for the bimodal gaseous core reactor configurations with inner beryllium thicknesses of 10 cm, 20 cm, 25 cm, 30 cm, and 40 cm. respectively.

It can be seen that for both MCNP and the one-dimensional spherical mock-up XSDRNPM calculations, the system neutron multiplication factor increases with an increase in the PGCR gas loading. The results indicate that the system k_{eff} values obtained from XSDRNPM for the bimodal systems with an inner beryllium thickness of 10 cm and 20 cm

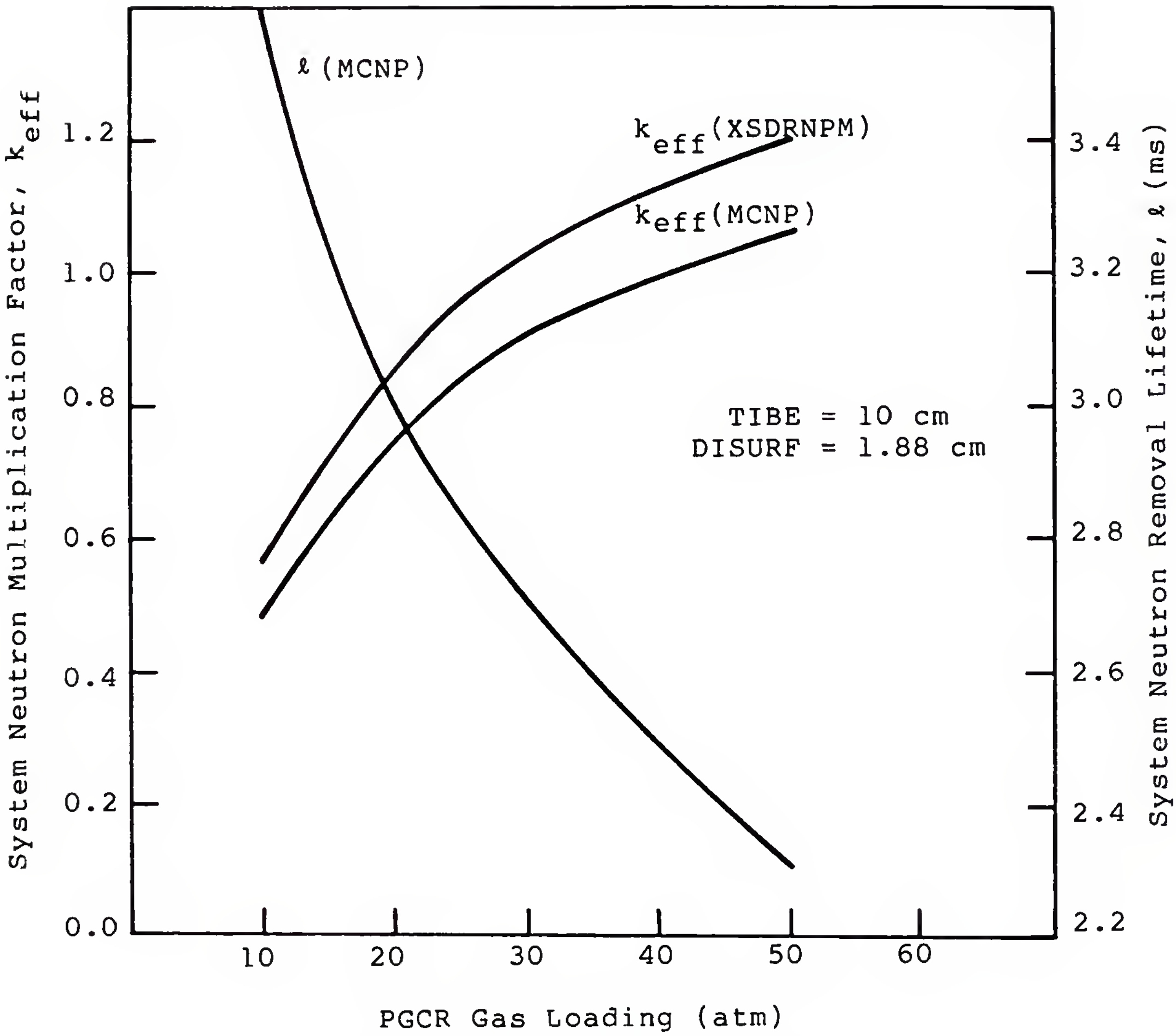

Figure 4-2. k_{eff} and ℓ as a Function of PGCR Gas Loading for TIBE of 10 cm.

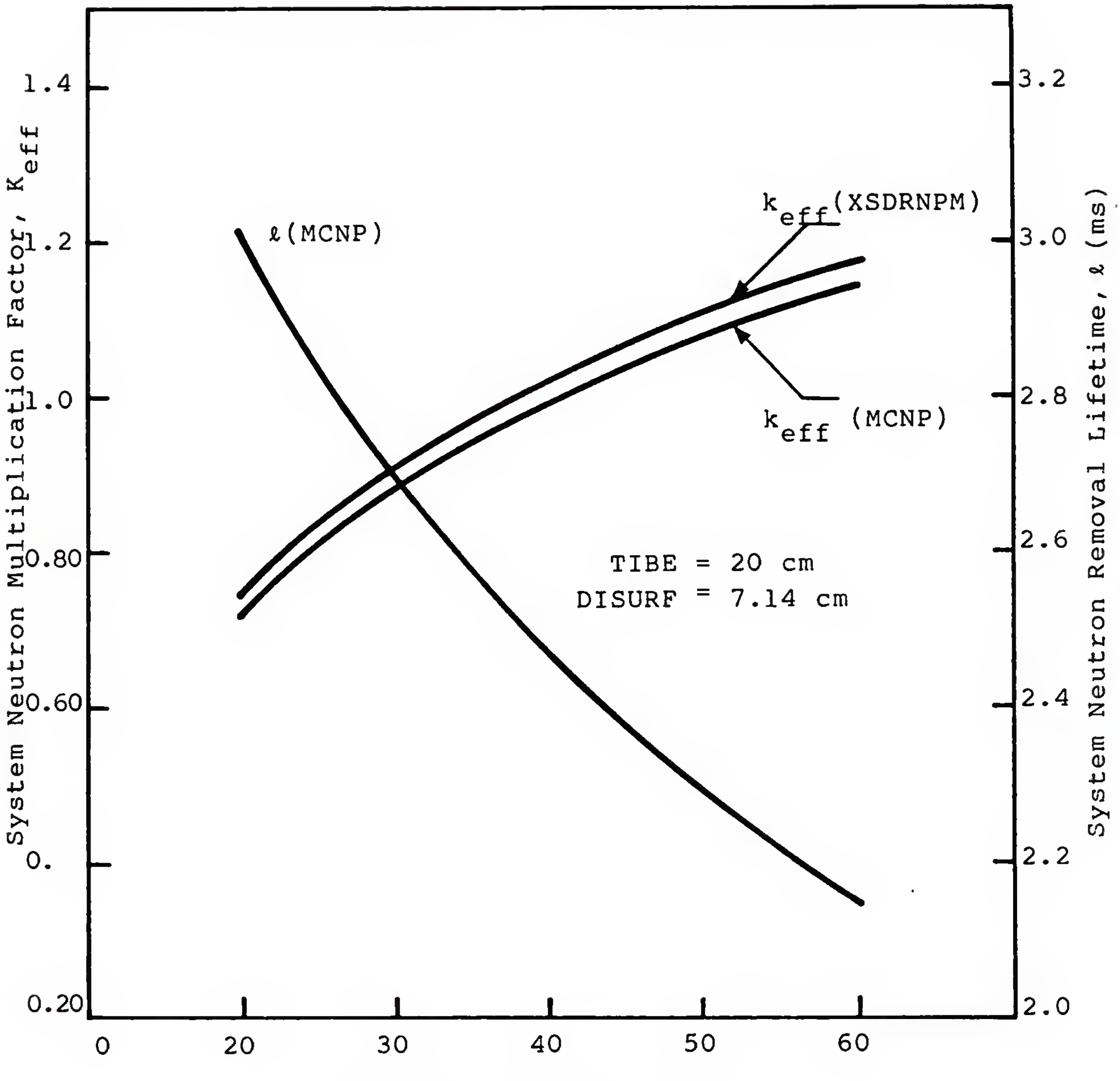

Figure 4-3. K_{eff} and ℓ as a Function of PGCR Gas Loading for TIBE of 20 cm.

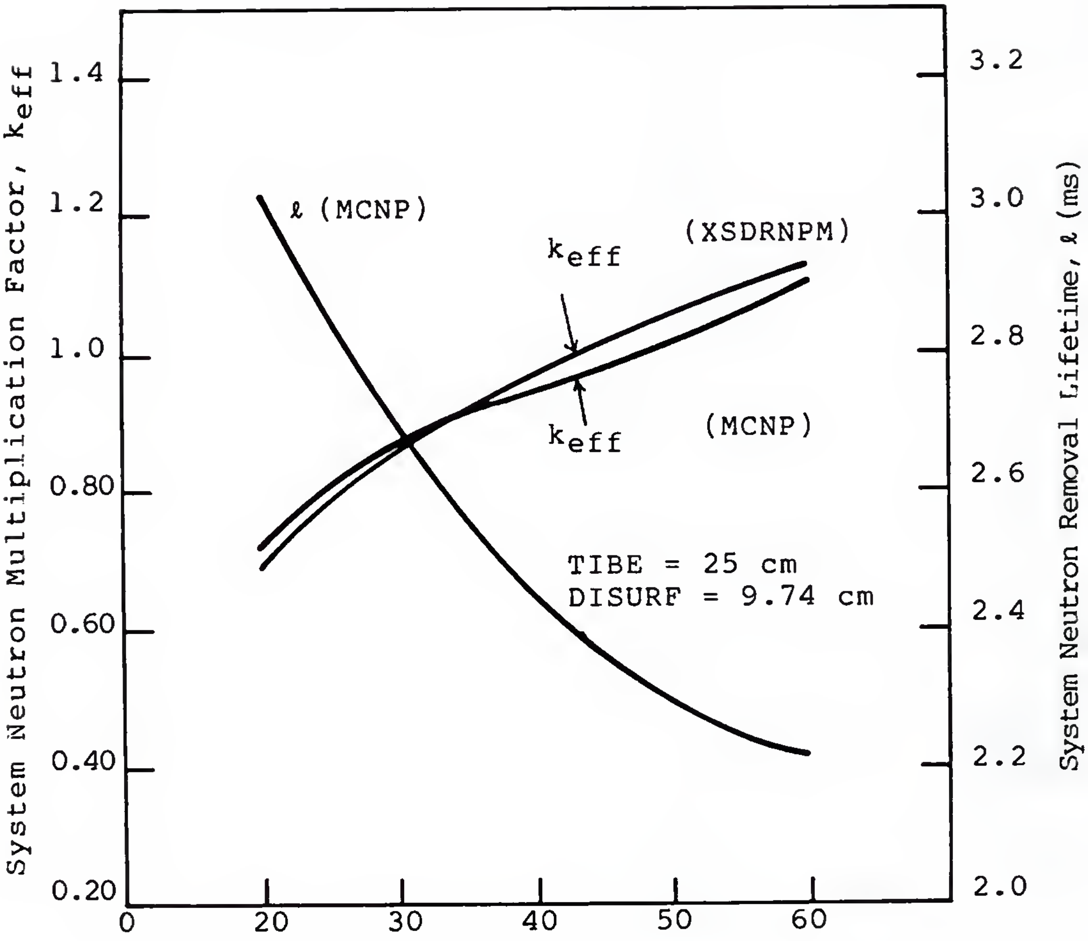

Figure 4-4. k_{eff} and ℓ as a Function of PGCR Gas Loading for TIBE of 25 cm.

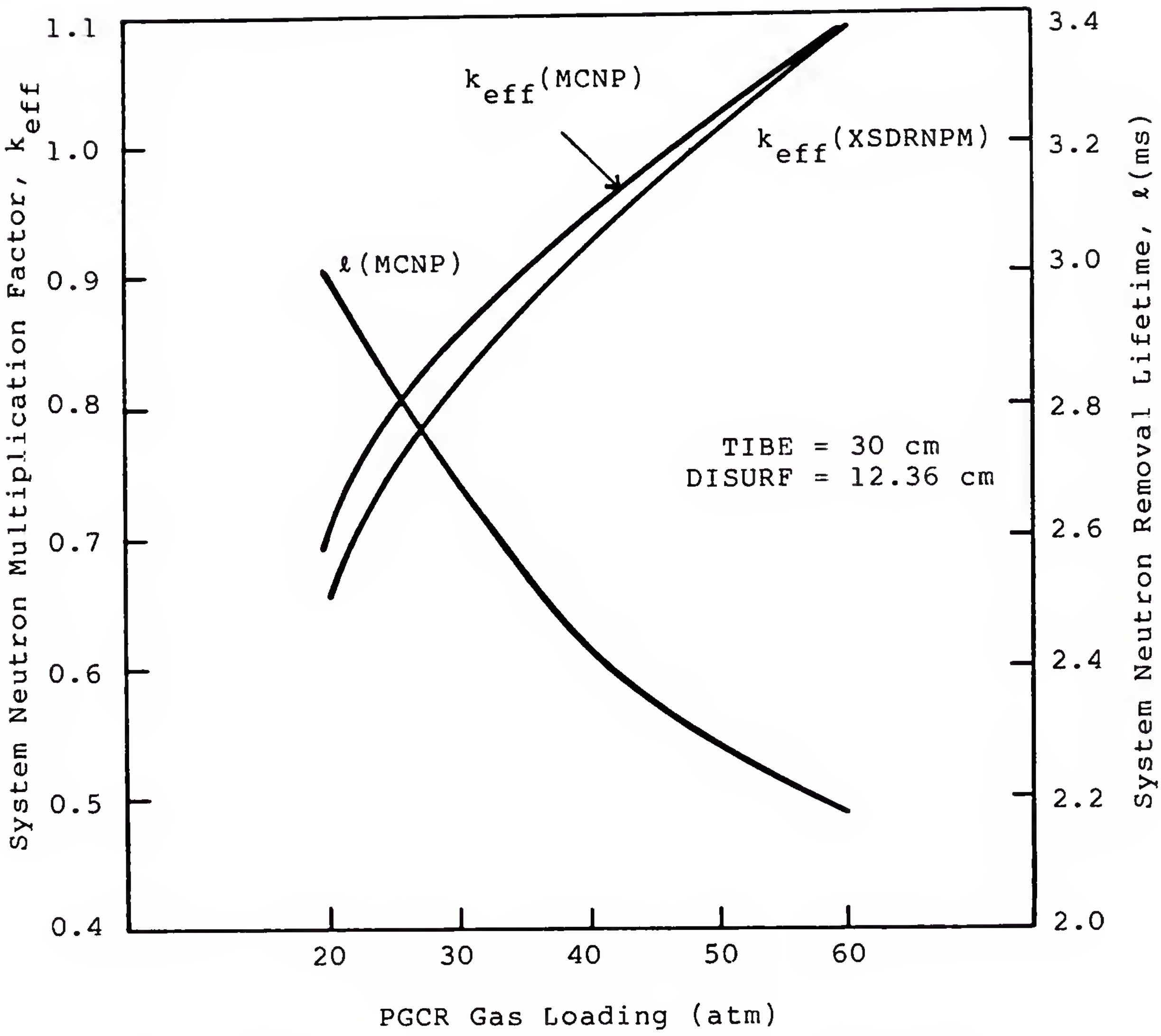

Figure 4-5. k_{eff} and ℓ as a Function of PGCR Gas Loading for TIBE of 30 cm.

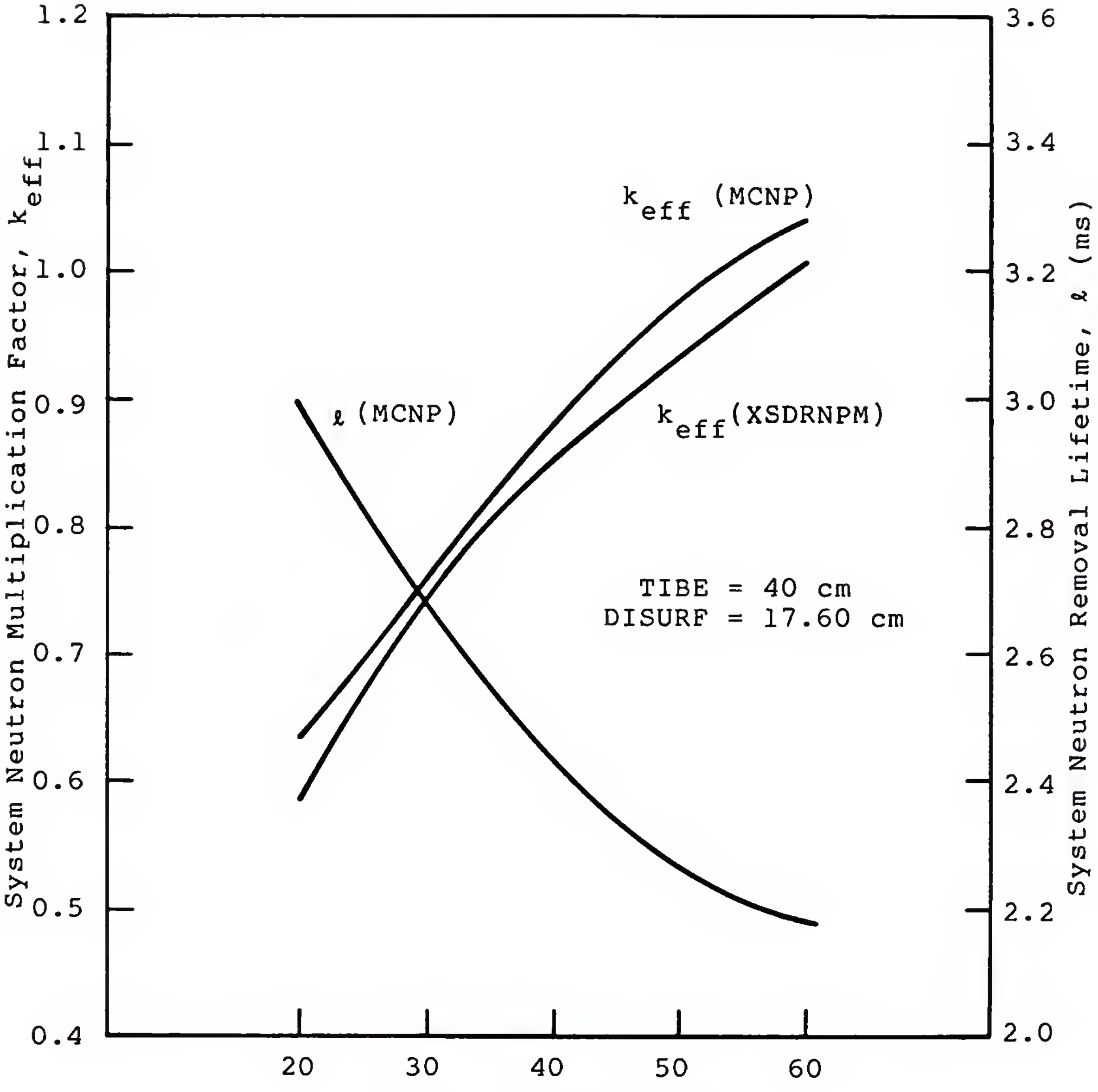

Figure 4-6. k_{eff} and ℓ as a Function of PGCR Gas Loading for TIBE of 40 cm.

are clearly higher than those values obtained from the MCNP code. The system k_{eff} values from XSDRNPM for a TIBE of 10 cm are about 12%-19% higher than the corresponding k_{eff} values from MCNP. For a TIBE of 20 cm, the XSDRNPM k_{eff} values are about 1%-5% greater than the corresponding k_{eff} values from MCNP. For systems with inner beryllium thickness of 30 cm and 40 cm, the system k_{eff} values from XSDRNPM are about 0.3%-8% lower than the corresponding k_{eff} values from MCNP. For a system with an inner beryllium thickness of 25 cm, the system k_{eff} values given by XSDRNPM are about 1.5% - 2.5% lower for PGCR core pressure of 20 atm and 30 atm and 0.2% - 3.5% higher for PGCR core pressures of 40 atm, 50 atm and 60 atm than the k_{eff} values obtained from MCNP.

The main reason for this inconsistency in the k_{eff} results from MCNP and XSDRNPM for various TIBE values is the inability of XSDRNPM to accurately account for the coupling effect among the individual PGCR cores especially when the inner beryllium thickness increases. The inability of XSDRNPM to accurately account for the neutronic coupling among the PGCR cores is due to the one-dimensional nature of the XSDRNPM calculations. In contrast, the exact geometry of the system is represented in the MCNP calculations.

With the core volume being conserved in the spherical mock-up of the system in XSDRNPM, the thickness of the "equivalent" PGCR annular ring decreases as the inner beryllium thickness of the BGCR increases. As the inner beryllium thickness increases from 10 cm to 40 cm, the thickness of the "equivalent" PGCR ring region of the spherical mock-up decreases from 15.3 cm to 9.8 cm. In contrast, the diameter of the PGCR core as represented in MCNP is always 40 cm. As the inner beryllium thickness increases from 10 to 40 cm, the perpendicular distance between the adjacent PGCR core surfaces increases from 1.88 cm to 17.6 cm. When the inner beryllium thickness is small, say, 10 cm and 20 cm, the neutronic coupling effect is over estimated in XSDRNPM. As a result, the system neutron multiplication factor for lower values of TIBE (10 cm and 20 cm) are higher from XSDRNPM calculations than those values from MCNP calculations. For higher inner beryllium thicknesses of 30 cm and 40 cm, since the thickness of the "equivalent" PGCR ring region is small compared to the thermal neutron mean free path in the PGCR core, thermal neutrons will have more chance of passing through the ring into the reflector region and they will thus have less interaction in the core region. This causes XSDRNPM to underestimate the system k_{eff} for inner beryllium thicknesses of 30 cm and 40 cm. Therefore, rather than having a stringent conservations of core volume and reflector thickness in the XSDRNPM spherical mock-up of the BGCR system, a compromise between these two have to be implemented.

Tables 4-2 through 4-6 and Figures 4-2 through 4-6 indicate that the system k_{eff} increases with an increase in the PGCR gas loading and the system neutron removal lifetime decreases with an increase in the PGCR gas loading for all the inner beryllium thicknesses considered. The decrease in the neutron removal lifetime with increasing fuel-gas density is due to the fact that as the fuel-gas density increases, the neutrons disappear from the system at a faster rate by absorption. That is, as the fuel-gas density increases, the average time required for a fission neutron to be removed from the system by either absorption or leakage decreases.

Figure 4-7 shows the variation of system neutron multiplication factor from the one-dimensional spherical mock-up XSDRNPM calculations with PGCR gas loading for different inner beryllium thicknesses of the bimodal gaseous core reactor. It can be seen that the slopes of the curves decrease considerably as the PGCR gas loading increases. This behavior indicates that the PGCR cores tend to become black at higher fuel loading.

Figure 4-8 illustrates the variation of the system k_{eff} from MCNP with the inner beryllium thickness, TIBE, for PGCR gas pressures of 20, 30, 40, 50, and 60 atmospheres. Figure 4-9 illustrates the variation of the system k_{eff} from the spherical mock-up XSDRNPM calculation with inner beryllium thickness for fuel-gas mixture pressures of 10, 20, 30, 40,

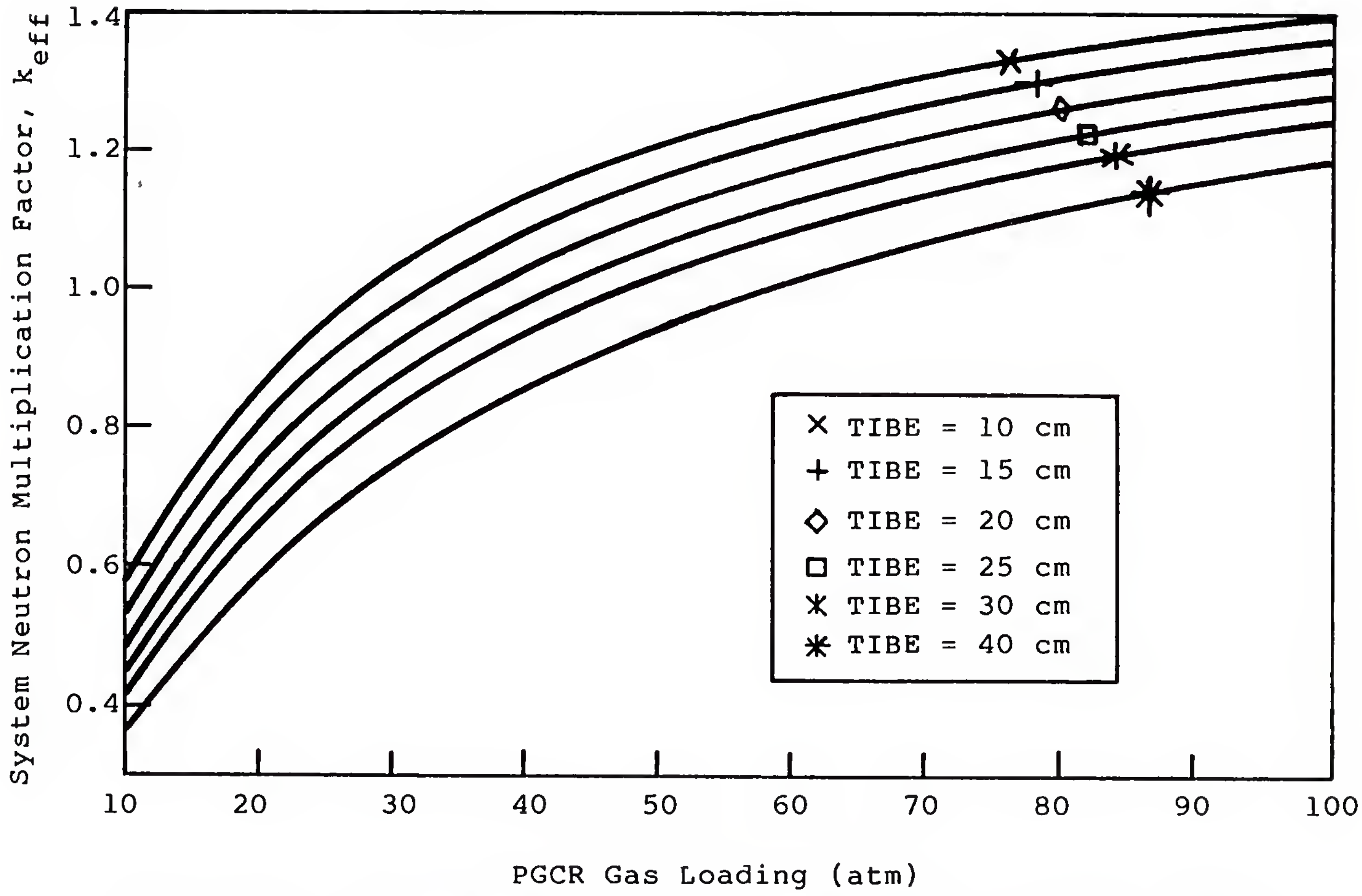

Figure 4-7. System Neutron Multiplication Factor from XSDRNPM as a Function of PGCR Gas Loading.

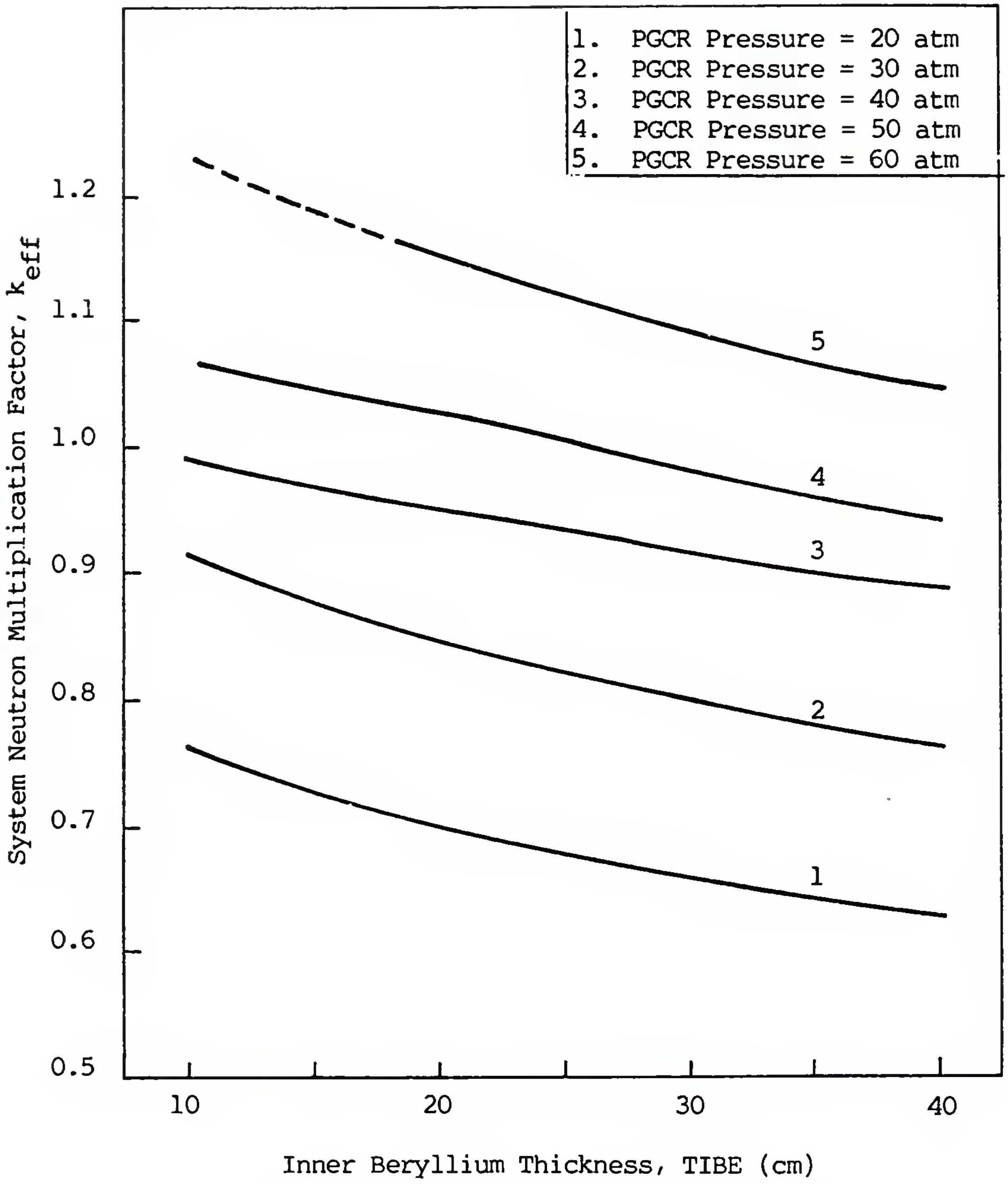

Figure 4-8. System Neutron Multiplication Factor (k_{eff}) from MCNP as a Function of Inner Beryllium Thickness.

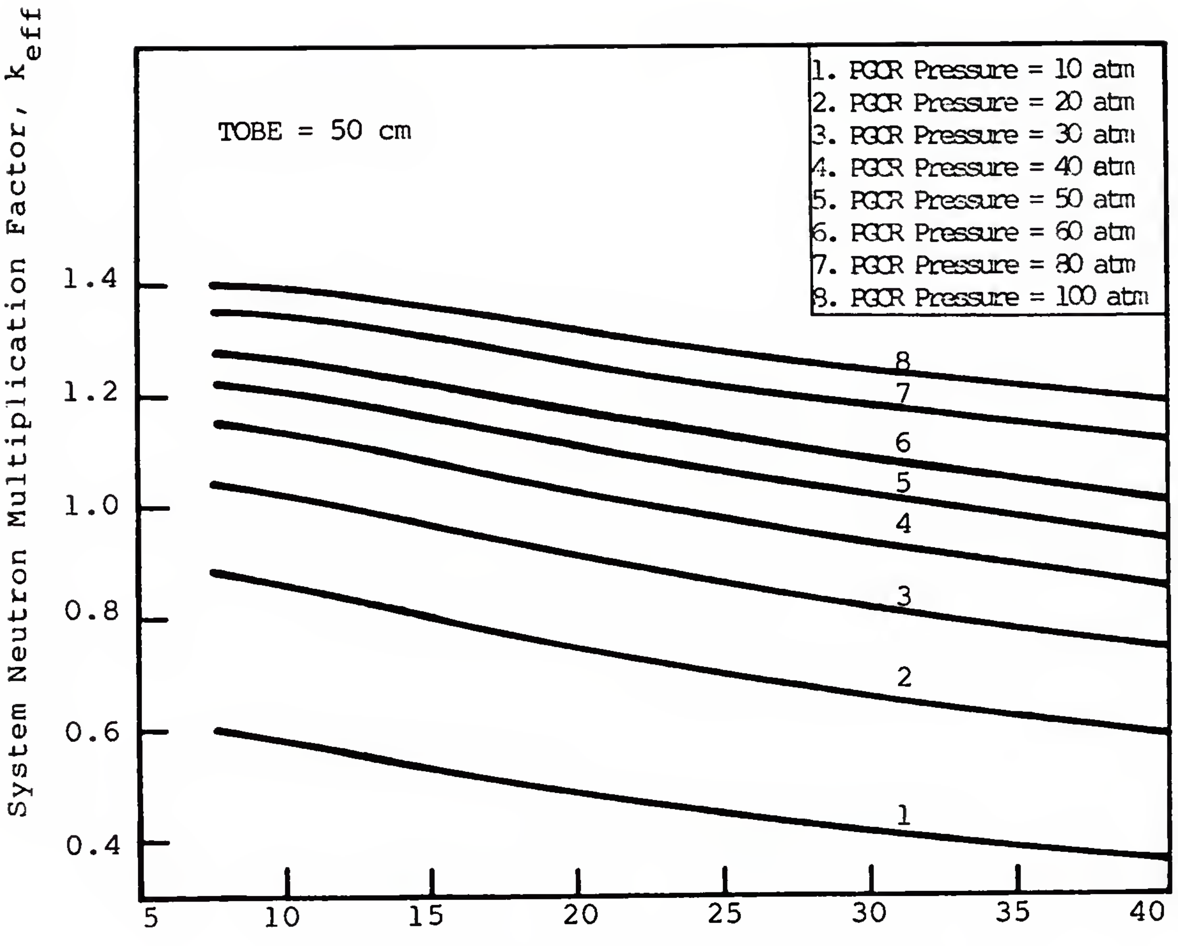

Figure 4-9. System Neutron Multiplication Factor from XSDRNPM as a Function of Inner Beryllium Thickness.

50, 60, 80, and 100 atmospheres. Tables 4-7 and 4-8 present the system k_{eff} values from MCNP and XSDRNPM, respectively, for various inner beryllium moderator thicknesses.

It can be seen from the Figures 4-8 and 4-9 that the system k_{eff} decreases with increases in the inner beryllium thickness. This means that as the inner beryllium thickness increases the system achieves criticality at higher PGCR gas-fuel loading. For example, MCNP predicts that the system attains criticality (k_{eff} = 1) at PGCR gas loadings of about 41, 41.5, 45, 47.5, and 53 atmospheres for inner beryllium thicknesses of 10 cm, 20 cm, 25 cm, 30 cm, and 40 cm, respectively. Critical gas loading as predicted by both MCNP and XSDRNPM calculations as well as the respective system neutron removal lifetimes from MCNP are given in Table 4-9. As we shall see in Chapter 5 on the dynamic behavior of the bimodal gaseous core reactor system, the neutronic coupling influence among the PGCR cores decreases as the inner beryllium thickness increases for any specific core gas-fuel loading. The fact that the system k_{eff} decreases with an increase in the inner beryllium thickness is due to this decrease in neutronic coupling among the PGCR cores with an increase in TIBE.

Table 4-10 and Figure 4-10 show the variation of the system neutron removal lifetime as predicted by MCNP with the inner beryllium thickness for a number of equal PGCR core gas loadings ranging from 20 atmospheres to 60

Table 4-7. System Neutron Multiplication Factor (k_{eff}) from MCNP as a Function of Inner Beryllium Thickness (TIBE) for Various PGCR Core Gas Loadings.

TIBE = 10 cm - 40 cm
TOBE = 50 cm
P_{BPGCR} = 20 atm He

PGCR Gas Pressure (atm) →	System Neutron Multiplication Factor, k_{eff}					
	10	20	30	40	50	60
TIBE						
10	0.4860	0.7675	0.9058	0.9846	1.0719	-
20	-	0.7136	0.8881	0.9891	1.0429	1.1530
25	-	0.7188	0.8743	0.9384	1.0321	1.1205
30	-	0.6941	0.8529	0.9387	0.9885	1.0991
40	-	0.6377	0.7595	0.8899	0.9419	1.0423

Table 4-8. System Neutron Multiplication Factor (k_{eff}) from XSDRNPM as a Function of Inner Beryllium Thickness (TIBE) for various PGCR Core Gas Loadings.

TIBE = 7.5 cm - 40cm
TOBE = 50cm
P_{BPGCR} = 20 atm He

PGCR Gas Pressure (atm) →	System Neutron Multiplication Factor, k_{eff}							
	10	20	30	40	50	60	80	100
TIBE								
7.5	0.5999	0.8813	1.0413	1.1481	1.2205	1.2747	1.3488	1.3967
10	0.5779	0.8574	1.0219	1.1314	1.2060	1.2631	1.3422	1.3921
15	0.5287	0.8010	0.9605	1.0777	1.1575	1.2170	1.3022	1.3577
20	0.4842	0.7468	0.9124	1.0241	1.1060	1.1682	1.2561	1.3150
25	0.4459	0.6989	0.8616	0.9749	1.0584	1.1225	1.2138	1.2757
30	0.4132	0.6567	0.8173	0.9309	1.0155	1.0818	1.1760	1.2406
40	0.3620	0.5856	0.7407	0.8535	0.9394	1.0069	1.1129	1.1823

Table 4-9. Total PGCR Gas Loading and Neutron Removal Lifetime at Criticality for Various Inner Beryllium Thicknesses of the BGCR System.

Inner Beryllium Thickness TIBE (cm)	Total PGCR Gas Loading for Criticality (atm)		System Neutron Removal Lifetime (ℓ) from MCNP (ms)
	MCNP	XSDRNPM	
10	41.0	28.0	2.46
20	41.5	38.5	2.43
25	45.0	42.5	2.36
30	47.5	49.0	2.28
40	53.0	59.5	2.21

Table 4-10. Neutron Removal Lifetime (ℓ) as a Function of Inner Beryllium Thickness for Various PGCR Gas Loading as Predicted by MCNP.

TOBE=50 cm

PGCR Loading atm →	Neutron Removal Lifetime, ℓ (ms)				
	20	30	40	50	60
TIBE (cm)					
10	3.002	2.728	2.486	2.312	2.140
20	3.027	2.696	2.465	2.291	2.142
25	3.032	2.769	2.443	2.289	2.216
30	3.033	2.715	2.449	2.292	2.185
40	2.997	2.652	2.493	2.259	2.191

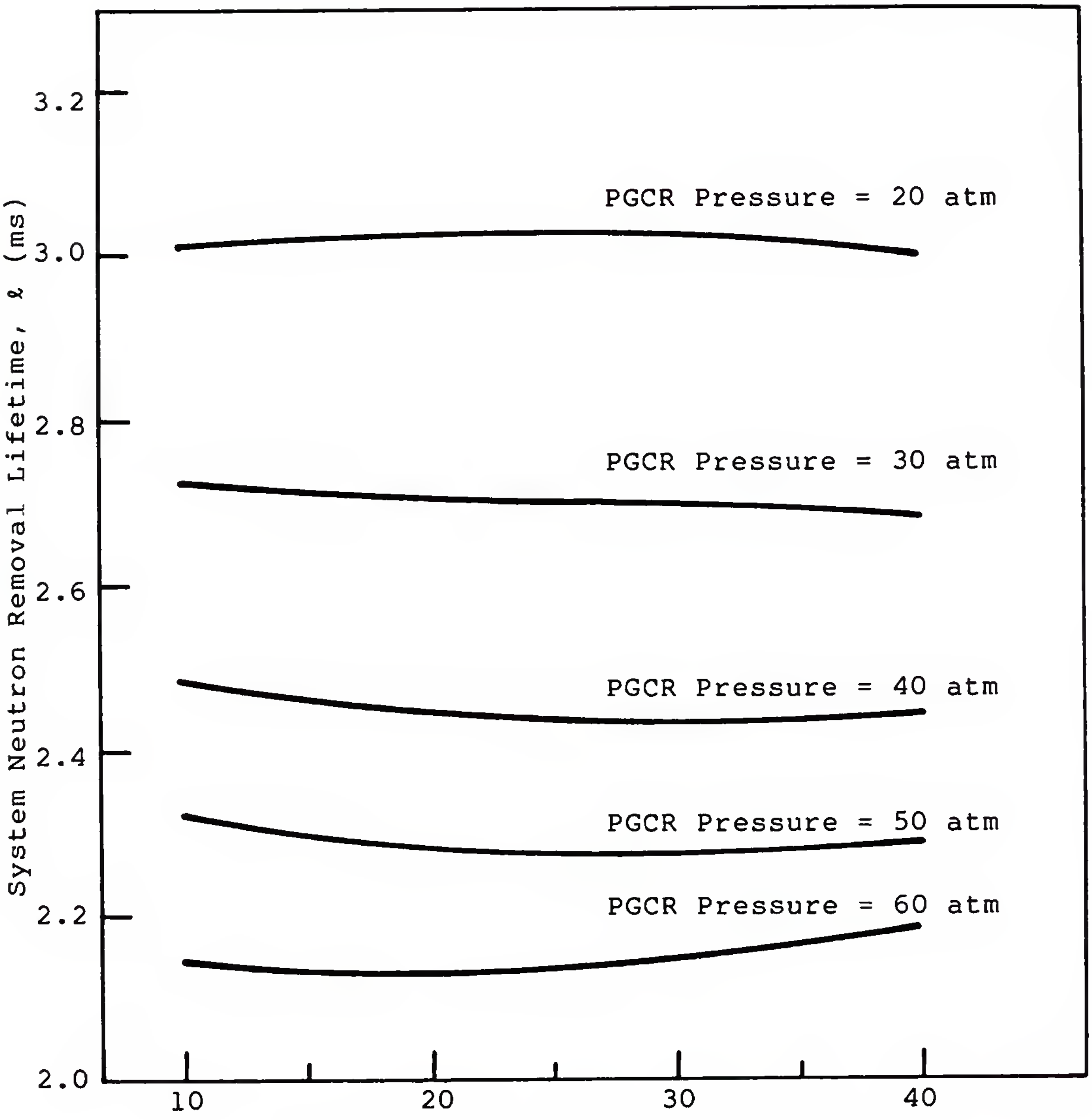

Figure 4-10. Neutron Removal Lifetime (ℓ) from MCNP as a Function of Inner Beryllium Thickness (TIBE) for Various PGCR Gas Loading.

atmospheres. The outer beryllium reflector thickness is fixed at 50 cm. It can be seen that for any specific PGCR gas loading the neutron removal lifetime is essentially independent of the inner beryllium thickness for the range of inner beryllium thickness examined.

Effect of Outer Beryllium Thickness Variation

Tables 4-11 and 4-12 give the system neutron multiplication factor from both MCNP and the one-dimensional spherical mock-up XSDRNPM calculation as well as the MCNP neutron removal lifetime for the bimodal gaseous core reactor system. These parameters are given for various values of the outer beryllium thickness, TOBE, ranging from 20 cm to 70 cm for an inner beryllium thickness of 20 cm (Table 4-11) and 30 cm (Table 4-12). The variation of system k_{eff} and the neutron removal lifetime, ℓ, with the outer beryllium thickness is illustrated in Figures 4-11 and 4-12. In both cases the PGCR cores are loaded equally with the fuel-gas (UF_6-He) mixture at a pressure of 50 atmospheres and the central BPGCR chamber is maintained at a pressure of 20 atmospheres of helium gas.

For both values of TIBE, the system k_{eff} rises sharply with an increase in the outer beryllium thickness for a range of TOBE from 20 cm to about 50 cm. This is due to increase in moderation of neutrons from the cores in the outer beryllium region. It can be seen from Figures 4-11 and

Table 4-11. System Neutron Multiplication Factor (k_{eff}) and Neutron Removal Lifetime (ℓ) as a Function of Outer Beryllium Thickness (TOBE) for TIBE of 20 cm.

PGCR Pressure = 50 atm fuel
BPGCR Pressure = 20 atm He

TIBE = 20 cm
DISURF = 7.14 cm

TOBE (cm)	k_{eff}** -MCNP	ℓ (ms)** -MCNP	k_{eff}* -XSDRNPM
20	0.9449(1.9)	1.639(1.9)	0.8920
30	1.0043(1.4)	1.927(1.3)	1.0239
40	1.0218(1.8)	2.104(1.8)	1.0808
50	1.0273(1.8)	2.291(1.8)	1.1060
60	1.0507(1.6)	2.393(1.7)	1.1186
70	1.0371(1.9)	2.451(1.9)	1.1242

**Relative error or uncertainty in percentage given in parenthesis.

*k_{eff} convergence level in XSDRNPM calculations is 10^{-5}.

Table 4-12. System Neutron Multiplication Factor (k_{eff}) and Neutron Removal Lifetime (ℓ) as a Function of Outer Beryllium Thickness (TOBE) for TIBE of 30 cm.

PGCR Pressure = 50 atm fuel
BPGCR Pressure = 20 atm Helium

TIBE = 30 cm
DISURF = 7.14 cm

TOBE (cm)	k_{eff} -MCNP**	ℓ(ms) -MCNP**	k_{eff} -XSDRNPM*
20	0.9325(1.9)	1.655(1.9)	0.8200
30	0.9776(2.5)	1.931(2.2)	0.9402
40	1.0175(2.0)	2.137(1.9)	0.9923
50	1.0228(1.6)	2.134(1.5)	1.0155
60	1.0206(2.0)	2.413(1.6)	1.0263
70	1.0208(1.8)	2.469(1.6)	1.0311

**Relative error or uncertainty in percentage given in parenthesis.

*k_{eff} convergence level in XSDRNPM calculations is 10^{-5}.

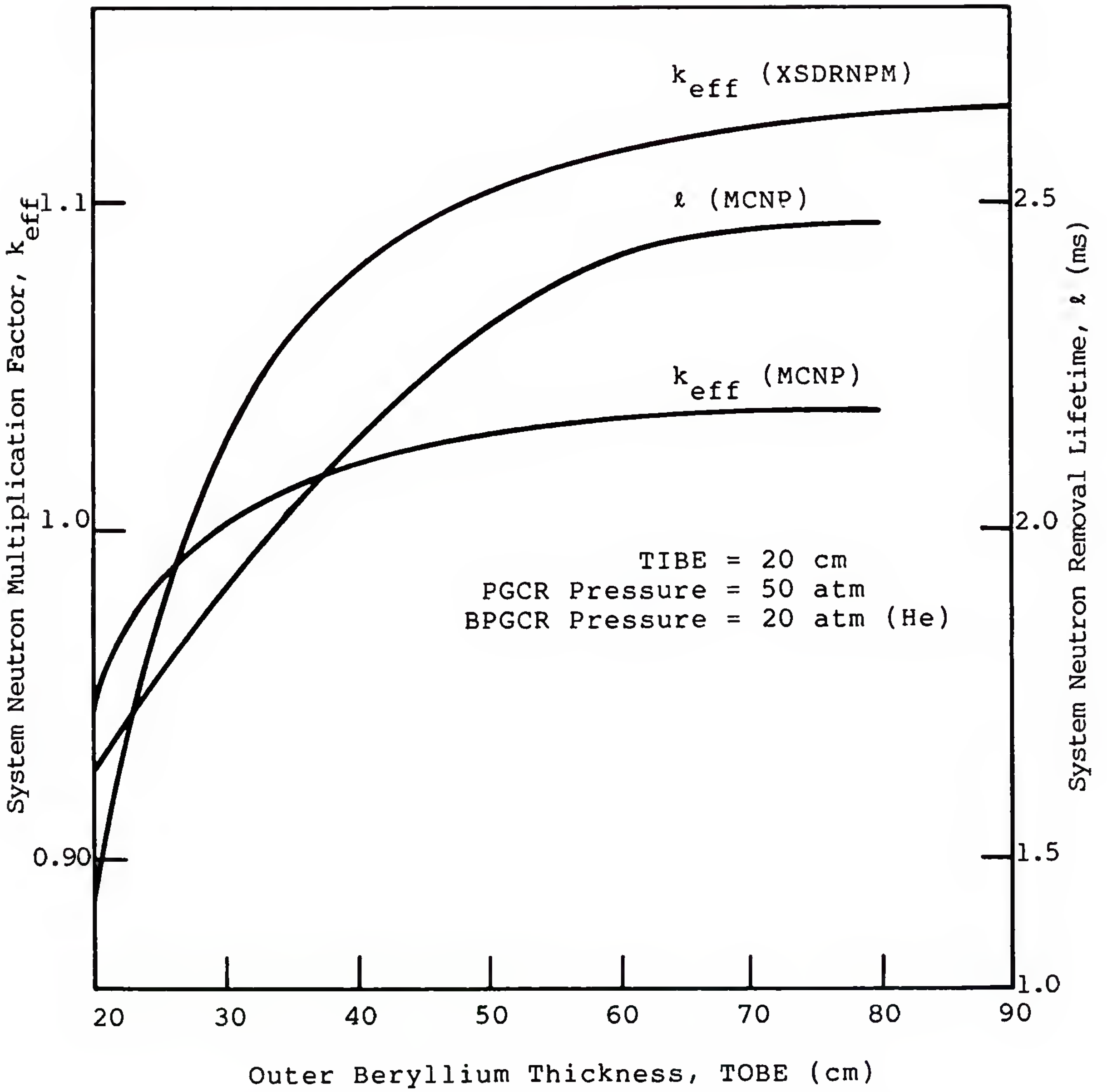

Figure 4-11. System Neutron Multiplication Factor (k_{eff}) and Neutron Removal Lifetime (ℓ) as a Function of Outer Beryllium Thickness (TOBE) for TIBE of 20 cm.

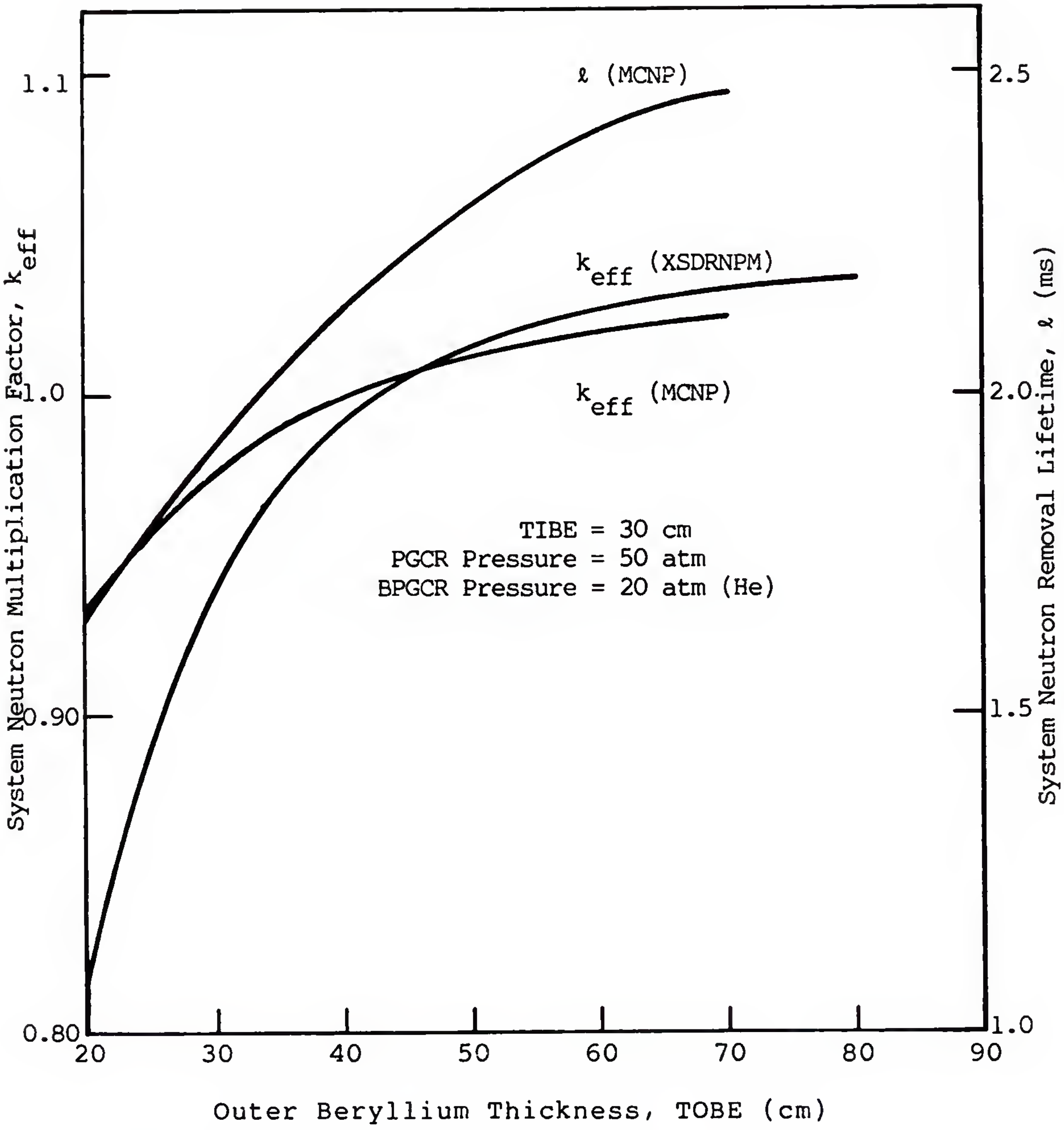

Figure 4-12. System Neutron Multilication Factor (k_{eff}) and Neutron Removal Lifetime (ℓ) as a Function of Outer Beryllium Thickness (TOBE) for TIBE of 30 cm.

4-12 that increases in outer beryllium thickness beyond about 50 cm do not result in any significant gain in the neutron multiplication factor. Any further increase in TOBE will only result in an increase in the overall weight of the reactor system which is undesirable for any space based reactor system.

Figures 4-11 and 4-12 show that in both cases, the system neutron removal lifetime follows the same trend as that of system k_{eff} values. The neutron removal lifetime increases sharply with outer beryllium thickness for the range of 20 cm to about 50 cm TOBE. The neutron removal lifetime is found to be essentially independent of the outer beryllium thickness beyond around 55 cm. Comparing the two sets of ℓ values in Tables 4-11 and 4-12, it can also be seen that the neutron removal lifetime is essentially independent of the inner beryllium thickness.

Effect of BPGCR Core Fuel Loading and Inner Beryllium Thickness Variations When the PGCR Core Fuel Loading Is Fixed

Static neutronic calculations have been carried out on the bimodal gaseous core reactor system for cases in which the central chamber is fueled with a UF_6-He gas mixture. In this case the PGCR cores are maintained at a total UF_6-He gas pressure of 10 atmospheres each while the central BPGCR chamber fuel-gas pressure is increased from 25 atmospheres to 100 atmospheres. Tables 4-13 through 4-16 give the

Table 4-13. System Neutron Multiplication Factor (k_{eff}) and Neutron Removal Lifetime (ℓ) as a Function of BPGCR Gas Loading for TIBE of 10 cm.

TIBE = 10cm
PGCR Loading= 10 atm (UF_6-He)

BPGCR Chamber Pressure (atm)	UF_6-He Number Density (atoms/ b-cm)	Uranium Mass in BPGCR Chamber (kg)	k_{eff}^{**} -MCNP	ℓ^{**} -MCNP	k_{eff}^{*} -XSDRNPM
25	8.6766-05	2.628	0.8246(.56)	2.706(.52)	1.0052
50	1.7353-04	5.254	0.9898(.56)	2.248(.62)	1.1458
60	2.0824-04	6.305	1.0411(.54)	2.121(.40)	1.1779
75	2.6029-04	7.882	1.0836(.56)	1.992(.45)	1.2133
90	3.1235-04	9.458	1.1262(.53)	1.873(.79)	1.2389
100	3.4706-04	10.509	1.1494(.61)	1.819(.41)	1.2522

**Relative Error or Uncertainty in Percentage Given in Parenthesis.
*k_{eff} Convergence Level in XSDRNPM Calculation is 10^{-5}.

Table 4-14. System Neutron Multiplication Factor (k_{eff}) and Neutron Removal Lifetime (ℓ) as a Function of BPGCR Gas Loading for TIBE of 20 cm.

TIBE = 20 cm
PGCR Pressure = 10 atm (UF_6-He)

BPGCR Chamber Pressure (atm)	UF_6-He Number Density (atoms/b-cm)	Uranium Mass in BPGCR Chamber (kg)	k_{eff}-MCNP**	ℓ**-MCNP	k_{eff}-XSDRNPM*
25	8.6766-05	2.628	0.8222(2.5)	2.892(3.0)	0.9891
50	1.7353-04	5.254	1.0301(2.5)	2.385(3.0)	1.1568
60	2.0824-04	6.305	1.0305(2.2)	2.202(3.1)	1.1961
75	2.6029-04	7.882	1.0845(1.8)	1.983(2.5)	1.2349
90	3.1235-04	9.458	1.1529(1.6)	1.917(2.2)	1.2657
100	3.4706-04	10.509	1.1472(1.3)	1.833(1.9)	1.2793

**Relative Error or Uncertainty in Percentage Given in Parenthesis.
*k_{eff} Convergence Level in XSDRNPM Calculation is 10^{-5}.

Table 4-15. System Neutron Multiplication Factor (k_{eff}) and Neutron Removal Lifetime (ℓ) as a Function of BPGCR Gas Loading for TIBE of 30 cm.

TIBE = 30 cm
PGCR Pressure = 10 atm (UF_6-He)

BPGCR Chamber Pressure (atm)	UF_6-He Number Density (atoms/ b-cm)	Uranium Mass in BPGCR Chamber (kg)	k_{eff}** -MCNP	ℓ** -MCNP	k_{eff}* -XSDRNPM
25	8.6766-05	2.628	0.7477(1.8)	2.894(2.1)	0.9461
50	1.7353-04	5.254	0.9604(2.4)	2.421(2.6)	1.1368
60	2.0824-04	6.305	1.0262(1.6)	2.198(1.8)	1.1803
75	2.6029-04	7.882	1.0630(1.7)	2.040(2.2)	1.2235
90	3.1235-04	9.458	1.1395(2.0)	1.961(2.3)	1.2555
100	3.4706-04	10.509	1.1636(1.8)	1.907(2.7)	1.2734

**Relative Error or Uncertainty in Percentage Given in Parenthesis.

*k_{eff} Convergence Level in XSDRNPM Calculation is 10^{-5}.

Table 4-16. System Neutron Multiplication Factor (k_{eff}) and Neutron Removal Lifetime (ℓ) as a Function of BPGCR Gas Loading for TIBE of 40 cm.

TIBE = 40 cm
PGCR Pressure = 10 atm (UF_6-He)

BPGCR Chamber Pressure (atm)	UF_6-He Number Density (atoms/b-cm)	Uranium Mass in BPGCR Chamber (kg)	k_{eff}^{**} -MCNP	ℓ^{**} -MCNP	k_{eff}^{*} -XSDRNPM
25	8.6766-05	2.628	0.7352(2.3)	2.896(2.0)	0.9119
50	1.7353-04	5.254	0.9280(2.2)	2.378(2.6)	1.1164
60	2.0824-04	6.305	1.0147(2.2)	2.184(1.9)	1.1605
75	2.6029-04	7.882	1.0609(1.6)	2.005(2.0)	1.2080
90	3.1235-04	9.458	1.1171(1.9)	1.974(2.3)	1.2416
100	3.4706-04	10.509	1.1411(1.1)	1.854(1.8)	1.2589

** Relative Error or Uncertainty in Percentage Given in Parenthesis.
* k_{eff} Convergence Level in XSDRNPM Calculation is 10^{-5}.

system neutron multiplication factor (k_{eff}) from both 3-dimensional MCNP and one-dimensional spherical mock-up XSDRNPM calculations and the system neutron removal lifetime (ℓ) from MCNP for the bimodal gaseous core reactor as a function of central BPGCR chamber gas loading for inner beryllium thicknesses of 10 cm, 20 cm, 30 cm,and 40 cm, respectively. Figures 4-13 through 4-16 graphically illustrate these same variations. These Figures and Tables show that the system k_{eff} increases with an increase in the central BPGCR chamber gas loading while the neutron removal lifetime decreases with an increase in the central chamber gas loading.

Unlike in the previous cases where the central BPGCR chamber is unfueled, the present cases show large differences between the system k_{eff} values as obtained from the three-dimensional MCNP and the one-dimensional spherical mock-up XSDRNPM calculations. The discrepancy between the MCNP and XSDRNPM k_{eff} values seems to be independent of the variation in the inner beryllium thickness. It can be seen that for a low central BPGCR chamber fuel-gas mixture loading of 25 atmospheres, the XSDRNPM k_{eff} values are about 20%-27% higher than the corresponding MCNP k_{eff} values and for a high central chamber fuel-gas loading of 100 atmospheres the XSDRNPM k_{eff} values are about 9%-11% higher than the corresponding system k_{eff} values from MCNP for the

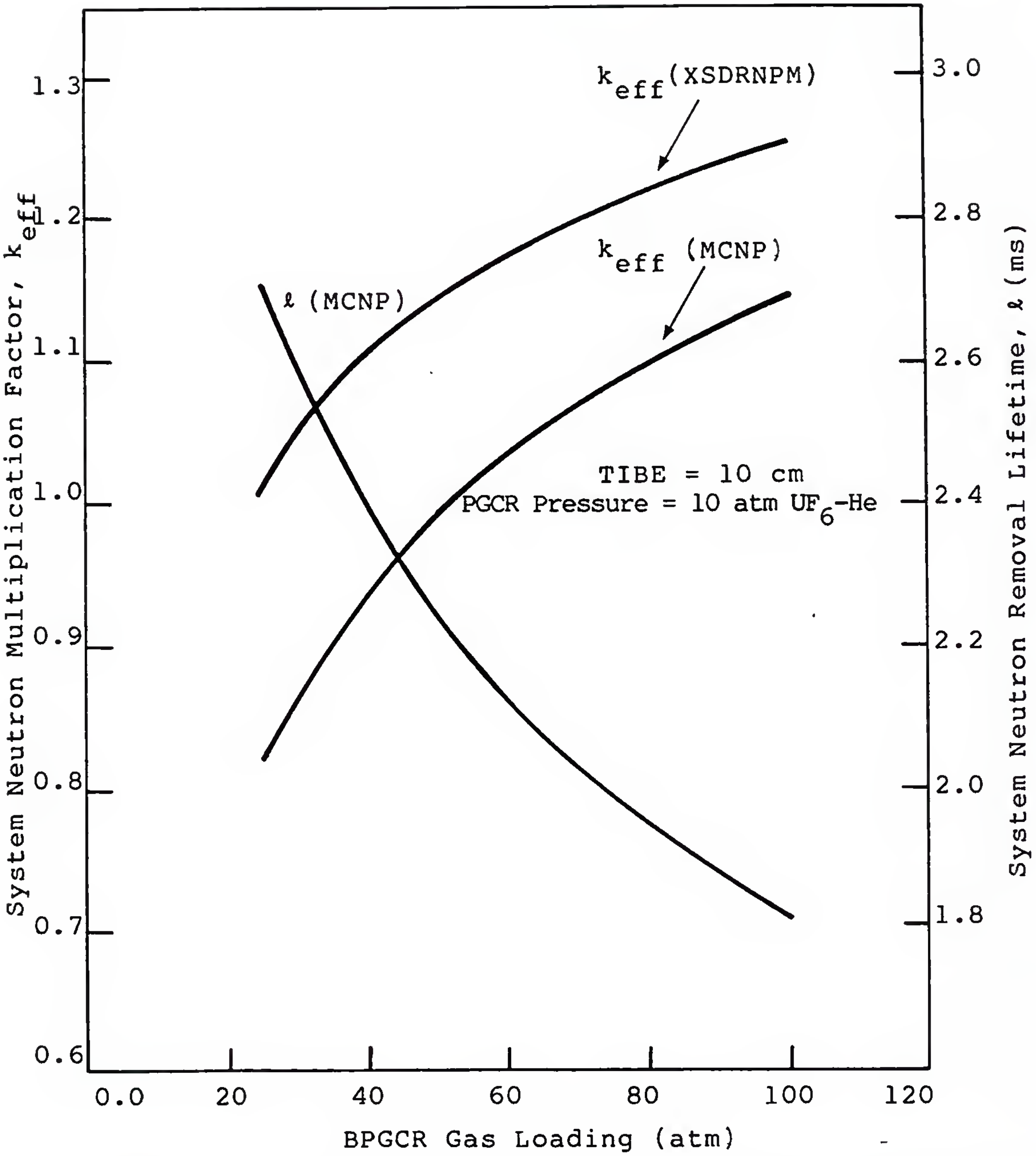

Figure 4-13. System k_{eff} and ℓ as a Function of BPGCR Gas Loading for TIBE of 10 cm.

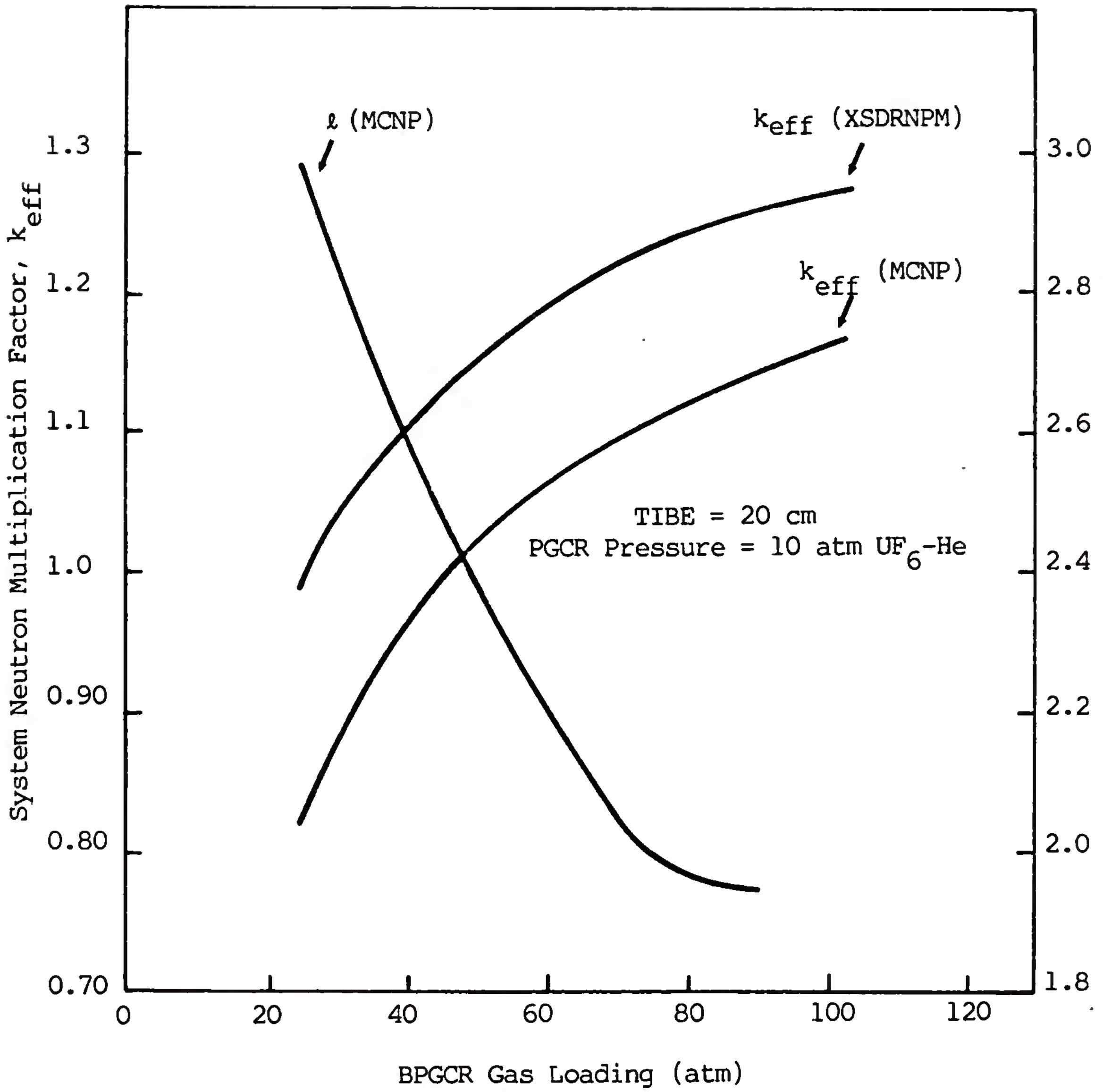

Figure 4-14. System k_{eff} and ℓ as a Function of BPGCR Gas Loading for TIBE of 20 cm.

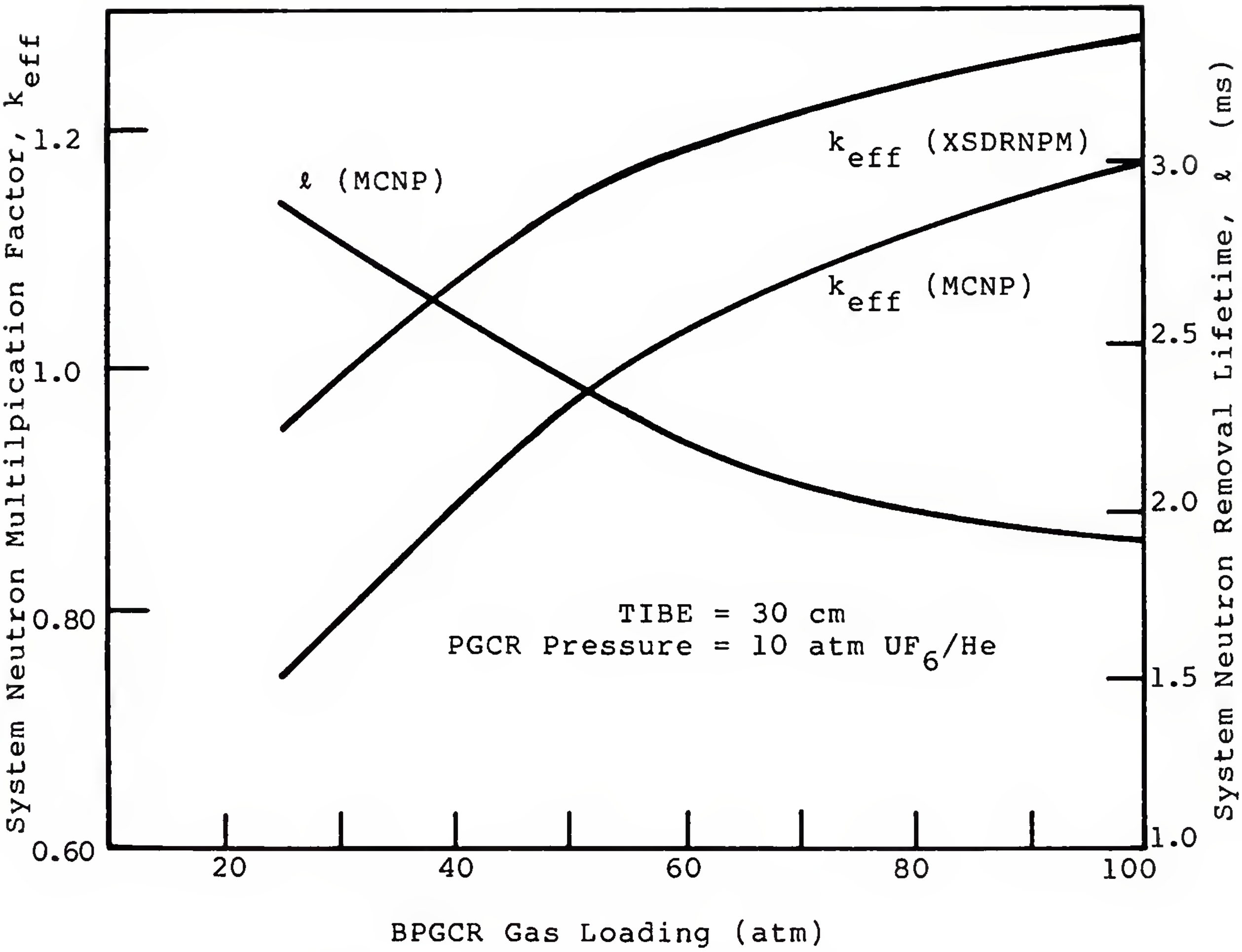

Figure 4-15. System k_{eff} and ℓ as a Function of BPGCR Gas Loading for TIBE of 30 cm.

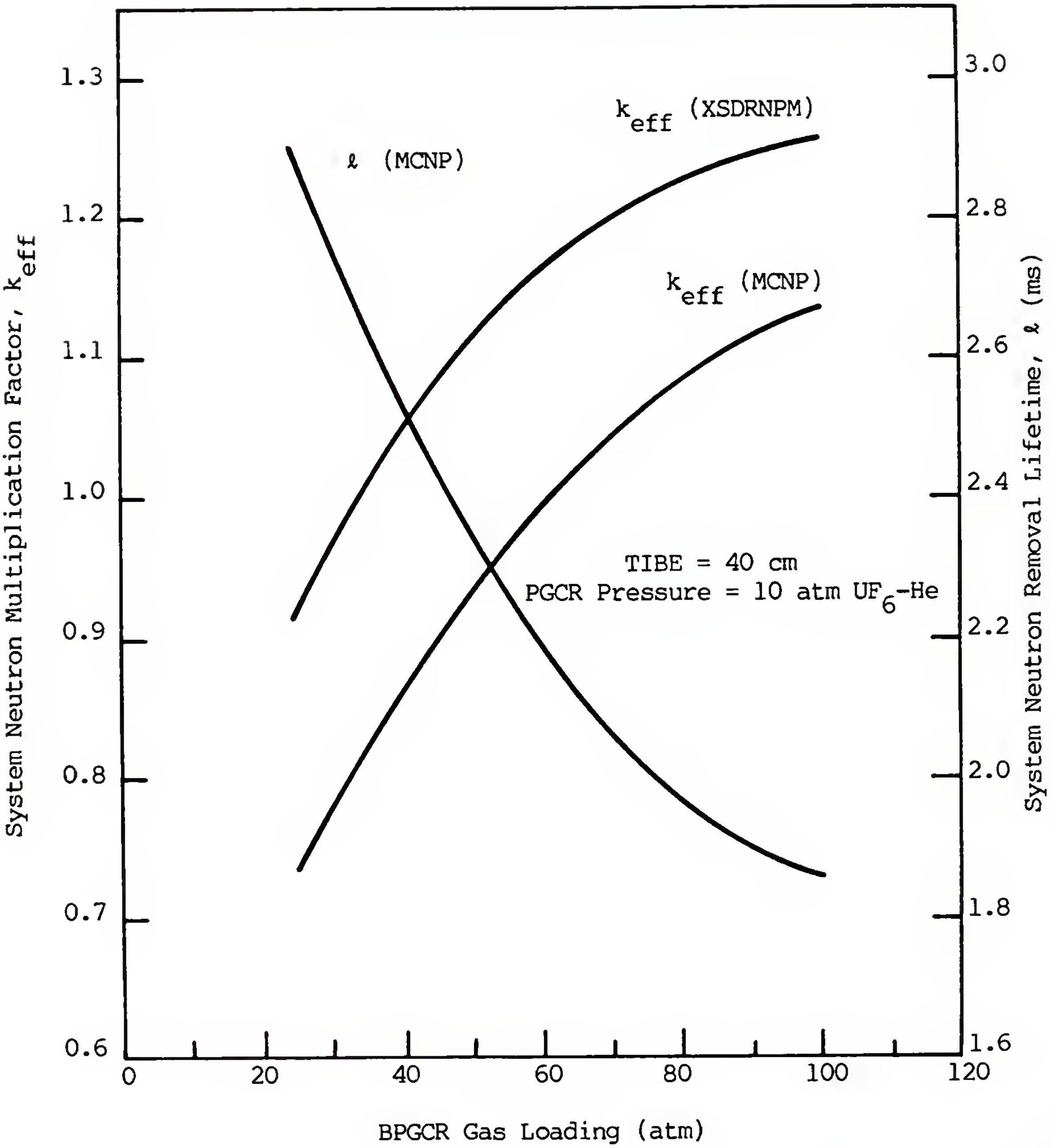

Figure 4-16. System k_{eff} and ℓ as a Function of BPGCR Gas Loading for TIBE of 40 cm.

range of inner beryllium thicknesses examined. These results suggest that the discrepancy between the XSDRNPM and MCNP system k_{eff} decreases as the central chamber gas loading increases. As the density of the fissile material in the BPGCR core increases with the increase in fuel-gas loading, XSDRNPM k_{eff} and flux values converge faster to the required tolerance criteria for the higher central chamber loading than for the lower central chamber gas loading.

The deviation of the system k_{eff} values given by XSDRNPM from k_{eff} values from MCNP is due to a combination of reasons. As shown in Appendix C, one of the reasons for this discrepancy is due to the MCNP Monte Carlo transport theory calculation versus XSDRNPM discrete ordinate calculation and the MCNP continuous energy cross section library versus the AMPX multi-group (four groups) cross section library for XSDRNPM calculations. Another reason for the discrepancy is due to the inability of XSDRNPM code to accurately account for the neutronic coupling among the BGCR cores because of its one-dimensional limitation.

Since in the XSDRNPM spherical mockup of the BGCR the annular ring of PGCR cores is replaced by an annular ring region, the neutronic coupling influence between the BPGCR chamber and the PGCR core and between the PGCR cores themselves have been over estimated. This has also resulted in the overestimation of k_{eff} values in XSDRNPM.

Figures 4-13 through 4-16 show that the slopes of the k_{eff} curves decrease as the central BPGCR chamber fuel-gas mixture loading increases. These figures indicate that the system k_{eff} values for the given configuration begin to level off at around a central BPGCR chamber loading of about 100 atmospheres. This implies that increasing the fuel-gas mixture pressure beyond about 100 atmospheres do not significantly increase the system k_{eff} values. At central BPGCR cavity fuel-gas loadings beyond 100 atmospheres the core becomes increasingly black to thermal neutrons.

Tables 4-17 and 4-18 give the system k_{eff}, from MCNP and XSDRNPM, respectively, as a function of inner beryllium thickness for the bimodal gaseous core reactor system for various values of the central BPGCR chamber gas loading. Figures 4-17 and 4-18 graphically illustrate these same data. The uncertainty in the system k_{eff} values from MCNP is too large for these values to be able to reflect the trend exhibited by the system k_{eff} values from XSDRNPM. It can be seen that, for any specific central BPGCR gas loading, the system k_{eff} increases to a maximum value and then decreases with the increasing inner beryllium thickness. When the inner beryllium moderator thickness is small, the fission neutrons from the central chamber have more chance of escaping to the outer beryllium moderator region and causing fission in the PGCR cores. As the inner beryllium thickness is increased, the fast neutrons from the central BPGCR

Table 4-17. System Neutron Multiplication Factor (k_{eff}) from MCNP as a Function of Inner Beryllium Thickness (TIBE) for the Bimodal Gas Core Reactor for Various BPGCR Gas Loadings.

PGCR Pressure = 10 atm He/UF_6
TOBE = 50 cm

BPGCR Loading (atm)→	System Neutron Multiplication Factor, k_{eff} (from MCNP)					
	25	50	60	75	90	100
TIBE (cm)						
10	0.8246	0.9898	1.0411	1.0836	1.1262	1.1494
20	0.8222	1.0301	1.0305	1.0845	1.1529	1.1472
30	0.7477	0.9664	1.0262	1.0630	1.1395	1.1686
40	0.7352	0.9280	1.0147	1.0609	1.1171	1.1411

Table 4-18. System Neutron Multiplication Factor (k_{eff}) from XSDRNPM as a Function of Inner Beryllium Thickness (TIBE) for the Spherical Mockup of the BGCR System for Various BPGCR Gas Loadings.

PGCR Pressure = 10 atm He/UF_6
TOBE=50 cm

BPGCR Gas Loading (atm)→	System Neutron Multiplication Factor, k_{eff} (from XSDRNPM)						
	25	40	50	60	75	90	100
TIBE							
7.5	0.9960	1.0887	1.1295	1.1604	1.1957	1.2198	1.2329
10	1.0052	1.1032	1.1458	1.1779	1.2133	1.2389	1.2522
15	1.0034	1.1121	1.1589	1.1938	1.2320	1.2595	1.2737
20	0.9891	1.1063	1.1568	1.1961	1.2349	1.2657	1.2793
30	0.9461	1.0804	1.1368	1.1803	1.2235	1.2555	1.2734
40	0.9119	1.0562	1.1164	1.1605	1.2080	1.2416	1.2589

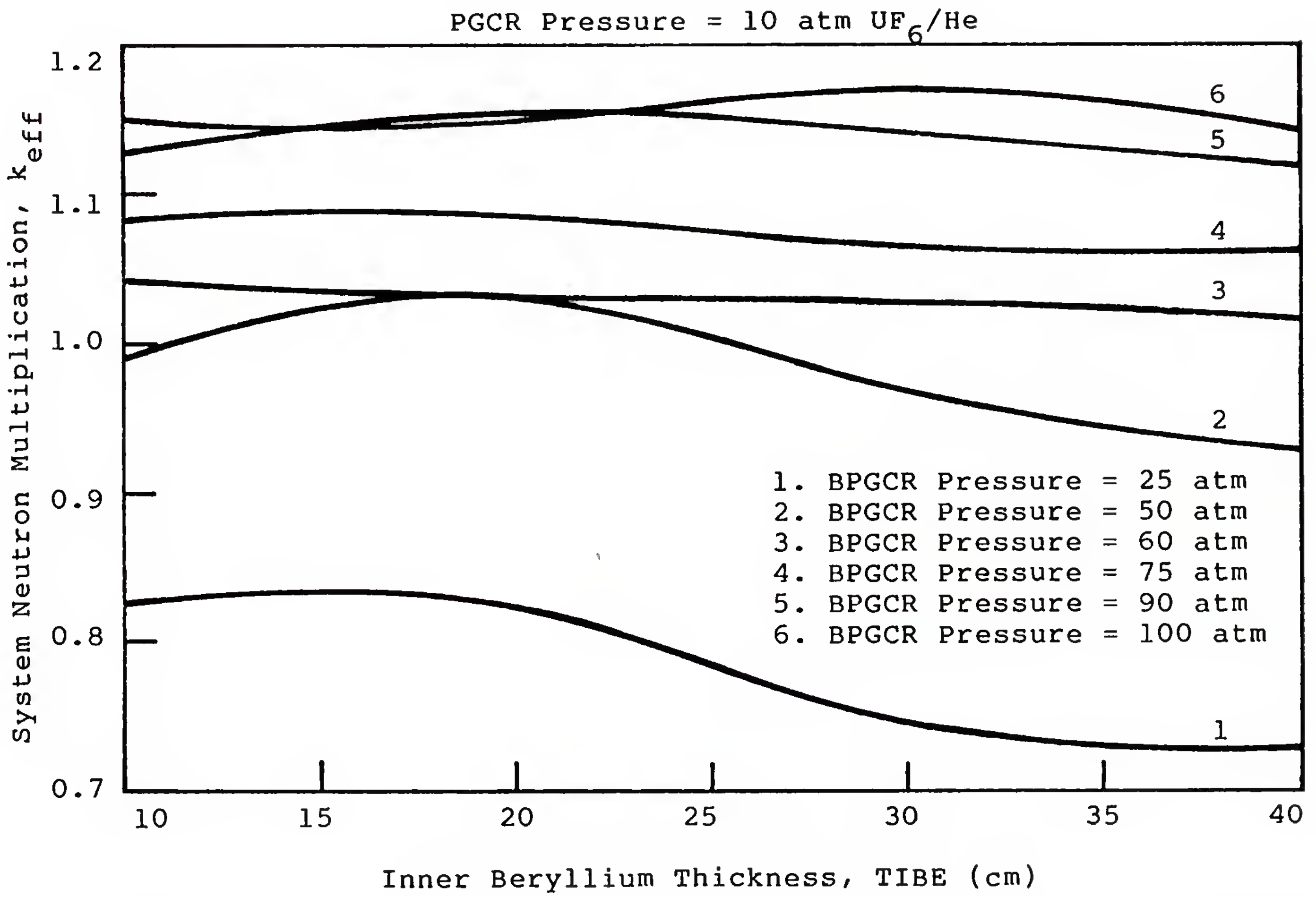

Figure 4-17. System Neutron Multiplication Factor (k_{eff}) from MCNP as a Function of Inner Beryllium Thickness for Various BPGCR Chamber Fuel-Gas Loadings.

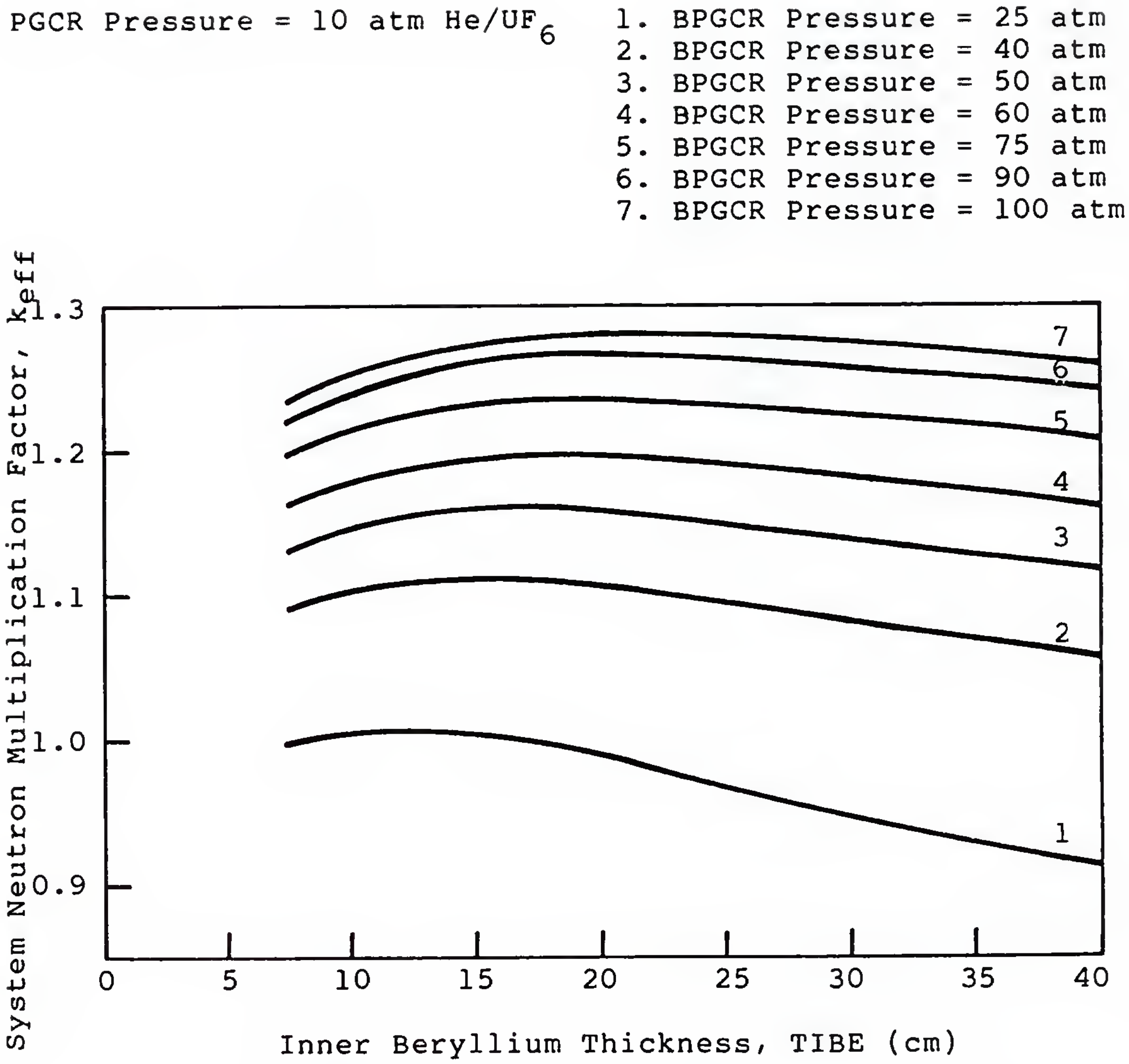

Figure 4-18. System k_{eff} from XSDRNPM as a Function of Inner Beryllium Thickness for Various BPGCR Chamber Gas-Fuel Loadings

chamber will have more chance of getting thermalized in the inner beryllium moderator region and return to the central chamber causing fission there and further increasing the system k_{eff}. The increase in reactivity due to any increase in fission in the large heavily fueled central BPGCR chamber exceeds the increase in reactivity due to a corresponding change in fission in the small lightly fueled PGCR cores. As the inner beryllium thickness is increased further, the neutronic coupling between the central BPGCR chamber and the PGCR core region decreases, (as we shall see in Chapter 5) and as a result, the k_{eff} of the system decreases.

The behavior of the bimodal gaseous core reactor system as predicted by the set of curves in Figure 4-18 is analogous to the undermoderated and overmoderated behavior of conventional light water reactors.

From the set of curves in Figure 4-18 for various central BPGCR fuel-gas loadings, it can be seen that as the central chamber gas loading is increased the optimum inner beryllium thickness (at which the system k_{eff} is a maximum) shifts towards higher values. This is due to the fact that as the central BPGCR chamber fuel-gas density increases, the necessary moderation of fast neutrons required for maintaining higher k_{eff} and higher fission rate is achieved only by a thicker beryllium moderator region. As a result, the optimum moderator thickness at which the maximum system k_{eff} occurs shifts towards higher inner beryllium thickness.

Table 4-19 and Figure 4-19 illustrate the variation of the system neutron removal lifetime with the inner beryllium thickness for various central BPGCR fuel-gas loadings with PGCR chambers maintained at a gas loading of 10 atmospheres. It can be seen that the system neutron removal lifetime decreases with an increase in the central BPGCR chamber loading for any specific inner beryllium thickness. The set of curves in Figure 4-19 indicate that for a specific BPGCR core fuel loading, the system neutron removal lifetime is essentially independent of the inner beryllium thickness for the range of TIBE examined. This conforms with the results of Figure 4-10 in which the neutron removal lifetime was also found to be essentially independent of the inner beryllium thickness when the central BPGCR chamber was unfueled. The effect of the fuel-gas loading in the central chamber is a decrease of about 15% in the neutron removal lifetime relative to the case where the central chamber is unfueled.

Effect of PGCR Core Fuel Loading and Inner Beryllium Thickness variations When the BPGCR Core Fuel Loading Is Fixed

The effect of varying the PGCR chamber fuel-gas loading with constant central BPGCR chamber fuel-gas loading on the system neutron multiplication factor has been investigated. In this case, MCNP has been used to study two system configurations with inner beryllium thicknesses of 20 cm and 30 cm. XSDRNPM is used to study the spherical mock-up

Table 4-19. System Neutron Removal Lifetime (ℓ) as a Function of Inner Beryllium Thickness (TIBE) for the BGCR System at Various BPGCR Gas-Fuel Loadings.

PGCR Pressure = 10 atm He/UF_6
TOBE = 50 cm

BPGCR Gas Loading (atm)→	System Neutron Multiplication Factor, k_{eff} (from MCNP)					
	25	50	60	75	90	100
TIBE (cm)						
10	2.7061	2.2475	2.1209	1.9919	1.8726	1.8187
20	2.8919	2.3850	2.2022	1.9830	1.9166	1.8333
30	2.8940	2.4210	2.1980	2.0400	1.9610	1.9070
40	2.8960	2.3780	2.1840	2.0049	1.9744	1.8544

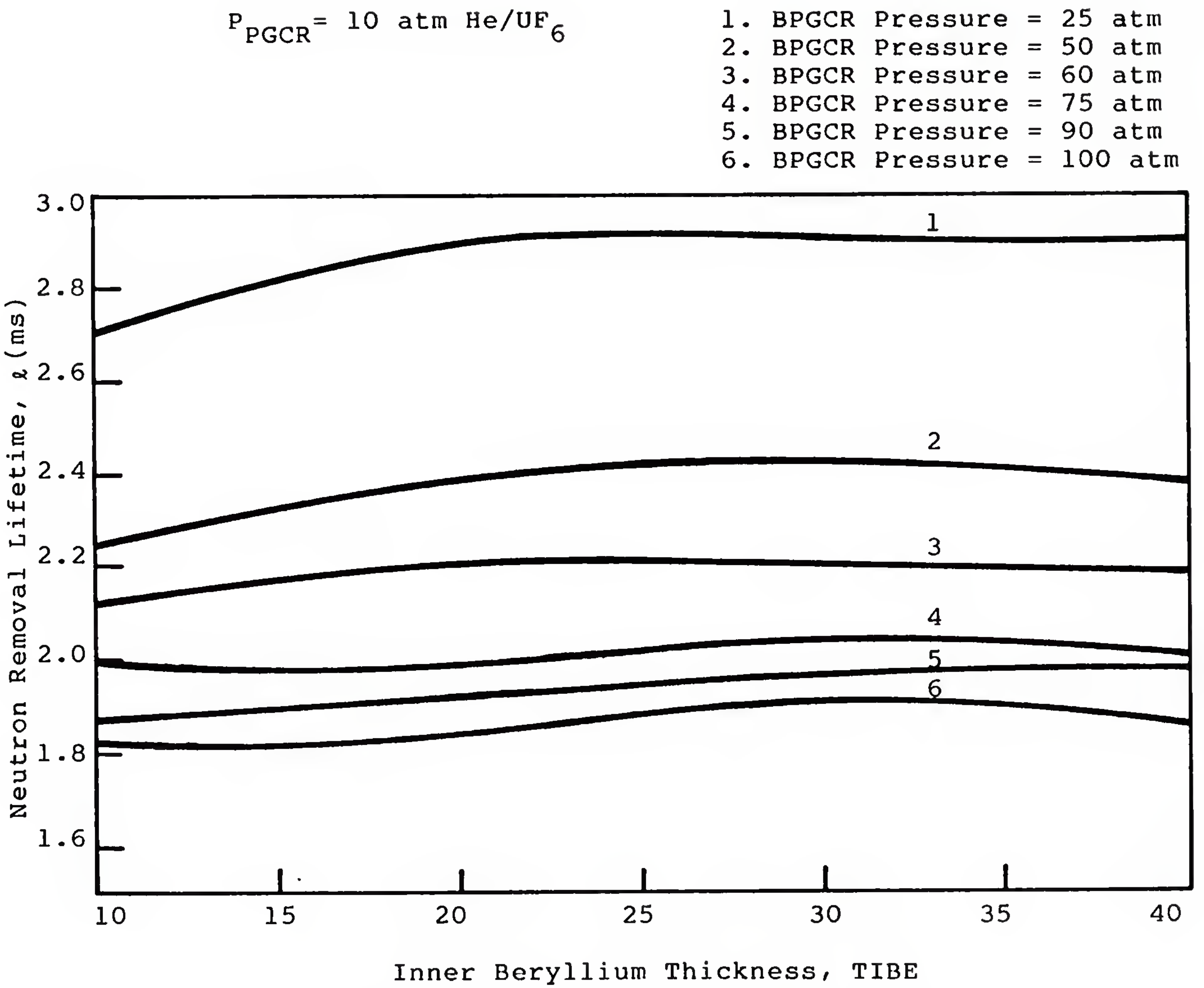

Figure 4-19. System Neutron Removal Lifetime (ℓ) as a Function of Inner Beryllium Thickness as Predicted by MCNP for BPGCR Gas Loadings.

system configurations for inner beryllium thicknesses of 7.5 cm, 10 cm, 15 cm, 20 cm, 30 cm, and 40 cm. In all of these cases the central BPGCR chamber is maintained at 25 atmospheres of fuel-gas mixture while the PGCR core fuel-gas loadings are varied from 10 atmospheres to 60 atmospheres in steps of 10 atmospheres.

Figures 4-20 and 4-21 present the variation of the system k_{eff} and neutron removal lifetime for inner beryllium thicknesses of 20 cm and 30 cm, respectively. These figures indicate that the system k_{eff} increases with an increase in the PGCR core fuel-gas loading. The system k_{eff} values are higher than those obtained in the case where the central chamber is filled with just helium gas.

Table 4-20 gives the system k_{eff} from XSDRNPM as a function of inner beryllium thickness for various values of equal PGCR core fuel-gas loading. The inner beryllium thickness ranges from 7.5 cm to 40 cm while the outer beryllium thickness is 50 cm. Figure 4-22 graphically illustrates these same data. Figure 4-22 shows that the system k_{eff} increases with an increase in PGCR gas loading. In order to study the effect of central BPGCR chamber gas loading on system k_{eff}, the results from Table 4-8 are compared with the results from Table 4-20. Table 4-8 gives the system k_{eff} as a function of inner beryllium thickness for various PGCR fuel-gas loadings with 20 atmospheres of helium in the central BPGCR chamber. The percentage

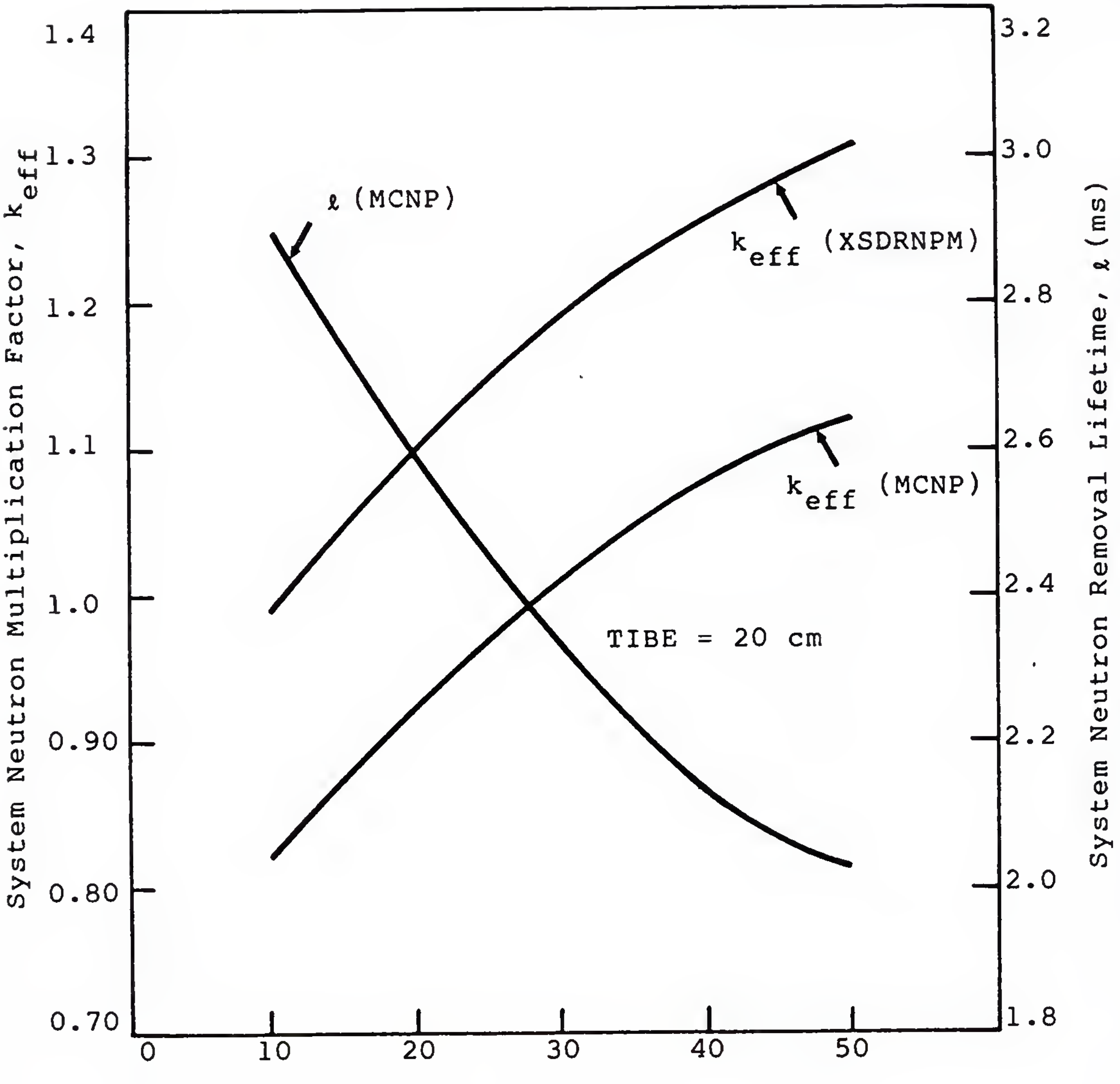

Figure 4-20. System k_{eff} and ℓ as a Function of PGCR Gas Loading with 25 Atmospheres of Fuel-Gas in BPGCR Chamber for TIBE of 20 cm.

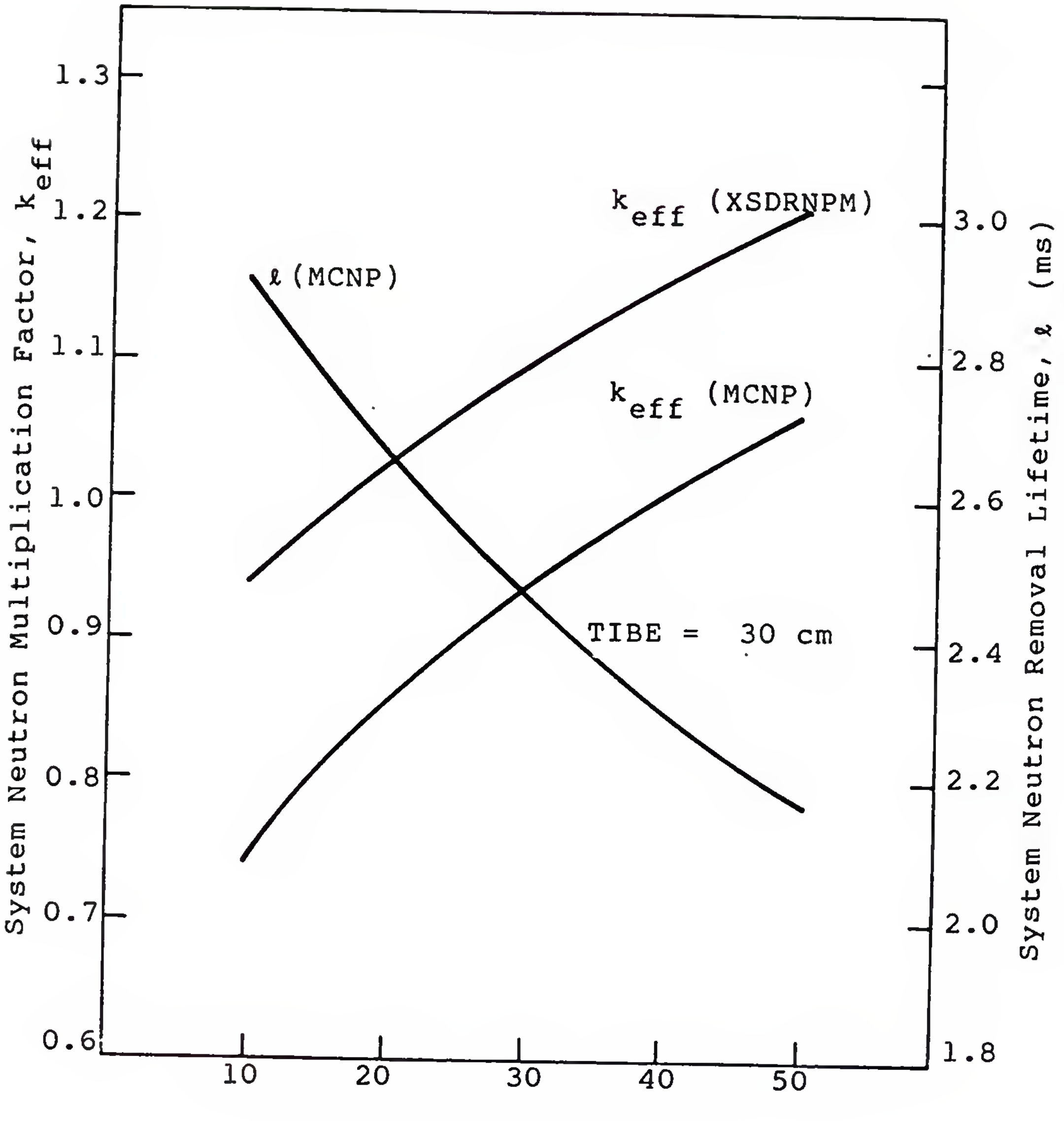

Figure 4-21. System k_{eff} and ℓ as a Function of PGCR Gas Loading with 25 Atmospheres of Fuel-Gas in BPGCR Chamber for TIBE of 30 cm.

Table 4-20. System Neutron Multiplication Factor (k_{eff}) from XSDRNPM as a Function of Inner Beryllium Thickness (TIBE) for the Spherical Mockup of BGCR System for Various BPGCR Gas Loadings.

BPGCR Pressure = 25 atm He/UF_6
TOBE = 50 cm
TIBE = 7.5 cm - 40 cm

PGCR Gas Loading (atm)→	System Neutron Multiplication Factor, k_{eff} (from XSDRNPM)					
	10	20	30	40	50	60
TIBE (cm)						
7.5	0.9960	1.1361	1.2275	1.2929	1.3382	1.3740
10	1.0052	1.1448	1.2372	1.3022	1.3514	1.3872
15	1.0034	1.1333	1.2242	1.2903	1.3399	1.3784
20	0.9891	1.1039	1.1902	1.2559	1.3066	1.3464
30	0.9461	1.0214	1.0934	1.1546	1.2053	1.2473
40	0.9119	0.9559	1.0067	1.0583	1.1061	1.1486

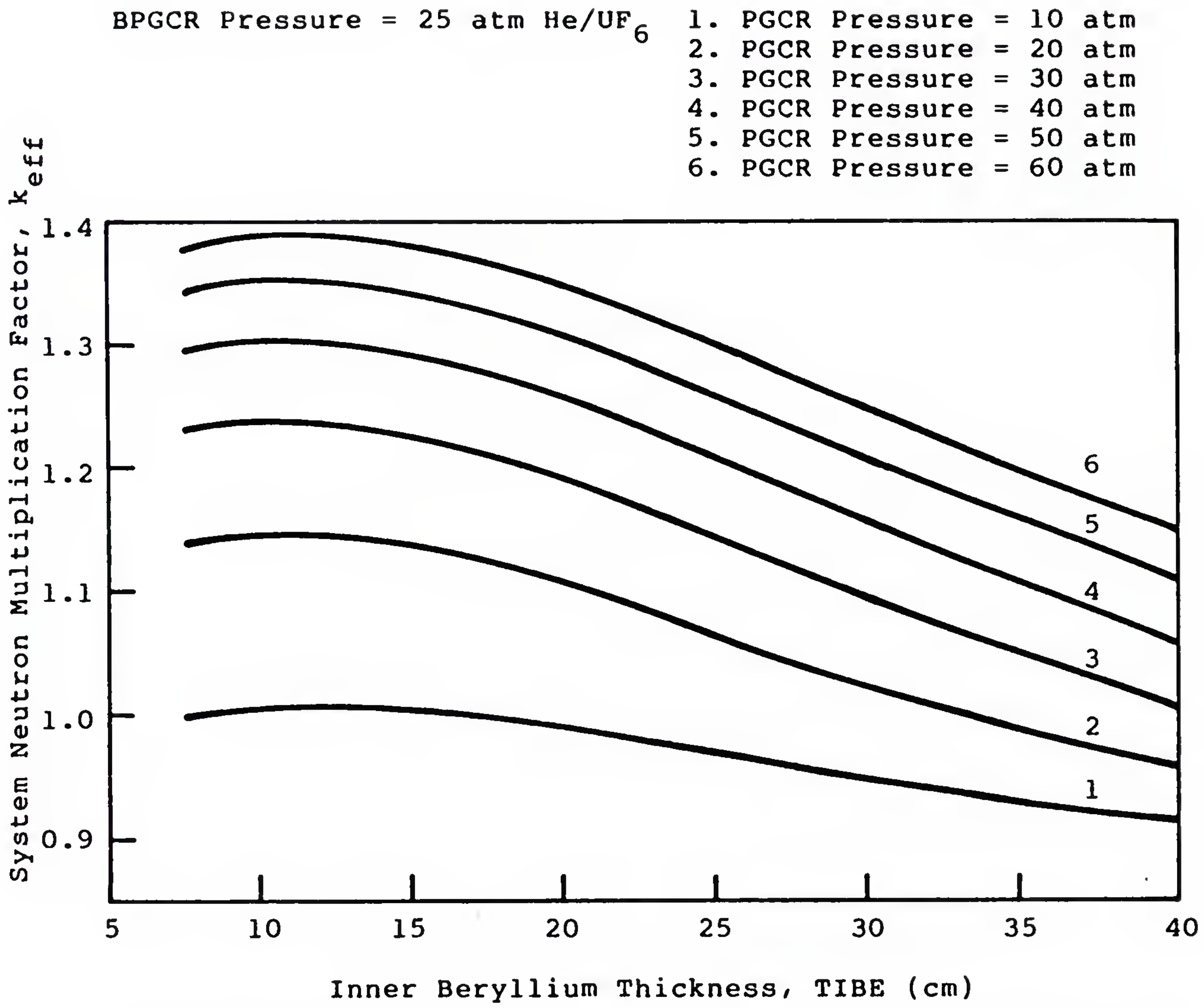

Figure 4-22. System k_{eff} as a Function of Inner Beryllium Thickness Predicted by XSDRNPM for Various PGCR Gas Loadings.

increase in the k_{eff} for a TIBE of 7.5 cm with fueled central chamber (Table 4-20) over the respective system k_{eff} for the configuration with unfueled central chamber (Table 4-8) ranges from about 66% for a PGCR gas loading of 10 atmospheres to about 8% for a PGCR gas loading of 60 atmospheres. This percentage increase for a TIBE of 40 cm ranges from about 152% for a PGCR gas loading of 10 atmospheres to 14% for a PGCR gas loading of 60 atmospheres. For an intermediate TIBE of 20 cm, this percentage increase in system k_{eff} ranges from 104% for a PGCR gas loading of 10 atmospheres to about 14% for a PGCR gas loading of 60 atmospheres. This increase is due to the fuelling of the central chamber. It can also be seen that for any given value of TIBE, as the PGCR pressure increases from 10 to 60 atmospheres, the ratio of the increase in system k_{eff} to the corresponding increase in pressure ($\Delta k_{eff}/\Delta P$) is 1.3% for the unfueled BPGCR (Table 4-8). For the system with the fueled BPGCR (Table 4-20) this ratio ($\Delta k_{eff}/\Delta P$) decreases from a value of 0.76% for a TIBE of 7.5 cm to 0.47% for a TIBE of 40 cm.

Figure 4-22 indicates that when the BPGCR chamber is loaded with 25 atmospheres of He/UF_6, the optimum inner beryllium thickness at which the system attains the maximum system k_{eff} is around 10 cm irrespective of the various PGCR core gas loadings examined. In contrast, when the central chamber fuel-gas loading is increased with a constant PGCR gas loading, the optimum inner beryllium thickness is found to increase slightly with an increase in central chamber gas loading (see Figure 4-18). Recall that when the central chamber is unfueled it is found that the system k_{eff} continues to decrease for the entire range of inner beryllium thickness examined (see for example, Figure 4-9). That is, there is no optimum inner beryllium thickness in this case.

Figures 4-23 and 4-24 illustrate the relative radial thermal neutron flux profile in the bimodal gaseous core reactor configuration for an inner beryllium thickness of 20 cm. Figure 4-23 gives the relative radial thermal flux distribution in the bimodal gaseous core reactor with the central BPGCR chamber at a total fuel-gas mixture loading of 75 atm and the PGCR cores at a fuel-gas loading of 30 atm. Figure 4-24 shows the relative radial thermal flux distribution when the central BPGCR chamber is loaded with fuel-gas mixture at 100 atm and the PGCR core with fuel gas mixture at 10 atm. The flux profiles are obtained from MCNP by calculating the surface averaged neutron flux over a large number of concentric cylindrical pseudo surfaces around the centerline of the bimodal gas core reactor system.

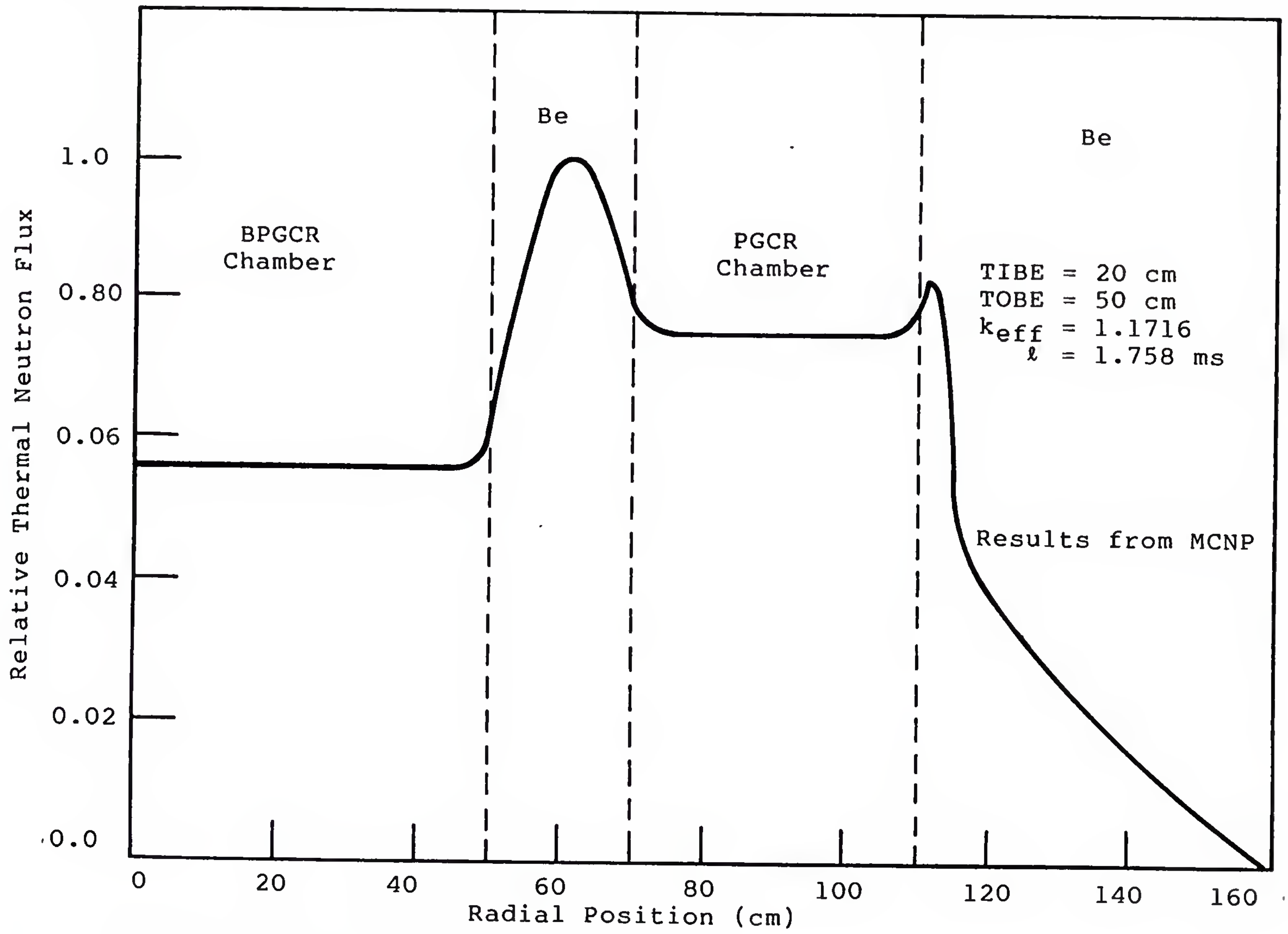

Figure 4-23. Relative Radial Thermal Neutron Flux Distribution in the BGCR System with BPGCR Chamber at 75 Atmospheres and PGCR core at 30 Atmospheres Fuel-Gas Loading.

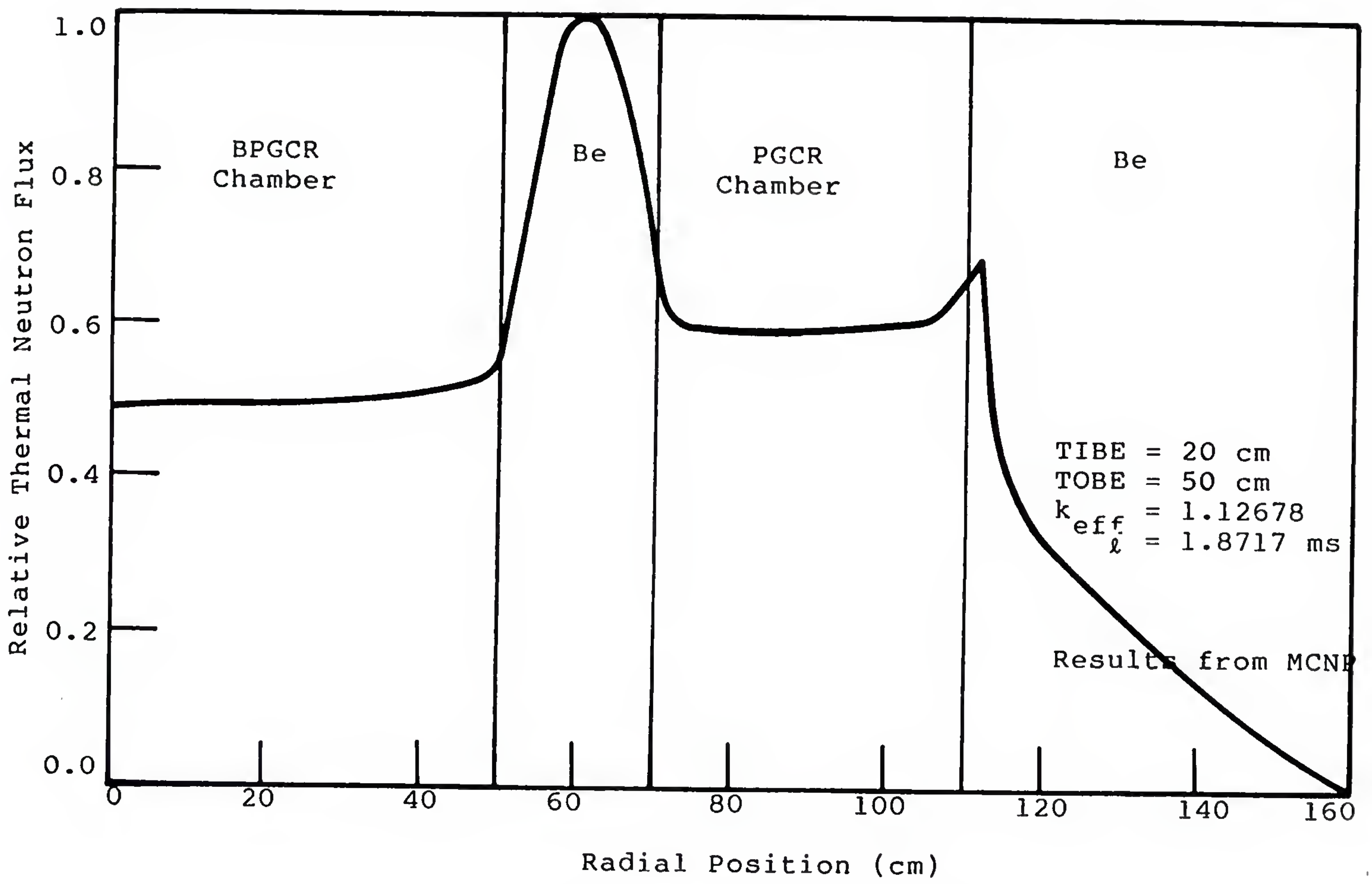

Figure 4-24. Relative Radial Thermal Neutron Flux Distribution in the BGCR System with the BPGCR Chamber at 100 Atmospheres and PGCR Cores at 10 Atmospheres Fuel-Gas Loading.

Effect of Unequal PGCR Core Fuel Loading When the BPGCR Core Is Unfueled

Criticality calculations are repeated with MCNP for the bimodal gaseous core reactor system with the PGCR cores loaded unequally among themselves in order to simulate the situation in which there is always a fraction of the total number of PGCR cores in the intake, power and exhaust phases of operation so that the reactor system will be capable of delivering a continuous supply of hot, pressurized gas to the power conversion unit. Table 4-21 gives the system neutron multiplication factor (k_{eff}) and system neutron removal lifetime from MCNP for various loading patterns of the bimodal system. XSDRNPM calculations are not performed in this case since the unequal PGCR core loading pattern cannot be mocked-up in an equivalent spherical geometry. The numbers in parenthesis denote the total number of PGCR cores which are maintained at the given total fuel-gas mixture pressure. The loading pattern of the PGCR cores is in such a way that the adjacent cores are at different fuel-gas loading. For example, in the Figure A-3, the loading pattern for the first case [60(4) 20(4) 10(4)] in Table 4-21 will be such that the PGCR core number 2 will be at 60 atm, core number 3 will be at 20 atm and core number 4 will be at 10 atm. This loading pattern is repeated for all the 12 PGCR cores in both the upper and lower halves of the bimodal reactor system. In this case 4 of the 12 PGCR cores will be

Table 4-21. System Neutron Multiplication Factor (k_{eff}) and System Neutron Removal Lifetime (ℓ) of the BGCR System as Predicted by MCNP for Various Unequal PGCR Gas Loadings.

Inner Beryllium Thickness, TIBE (cm)	Core Loading Pattern (atm)		System k_{eff}	System Neutron Removal Lifetime (ms)
	PGCR's	BPGCR's		
20	60(4), 20(4), 10(4)	20-He	0.8521	2.778
20	50(4), 30(4), 20(4)	20-He	0.8602	2.533
20	70(4), 30(4), 20(4)	20-He	0.9260	2.456
20	70(6), 10(6)	20-He	0.9068	2.581
20	80(4), 40(4), 30(4)	20-He	1.0206	2.307
20	80(4), 40(4), 30(4)	20-Fuel	1.2363	1.899
30	80(4), 40(4), 30(4)	20-He	1.0103	2.295

at 60 atm pressure, another 4 will be at 20 atm and the remaining 4 will be loaded with 10 atm of fuel-gas mixture.

The discussion on integral parameters such as reactivity, neutron generation time, core-to-core coupling coefficients etc., and their dependence on the geometry and core fuel-gas loading pattern is given in Chapter 5 on the dynamic neutronic studies of the bimodal reactor system.

Summary

Criticality studies of the bimodal gaseous core reactor system with UF_6-He mixture as the reactor fuel and beryllium as the moderating material has been the main focus of the discussion in this chapter. In this chapter we have examined the effects on system neutron multiplication factor and system neutron removal lifetime of variations in inner and outer beryllium moderator thickness; variation of PGCR core gas loading with and without fuel-gas in the central BPGCR chamber; and variation of the central BPGCR chamber gas loading with constant PGCR core gas loading.

The three-dimensional Monte Carlo transport code, MCNP and the one-dimensional S_N transport code, XSDRNPM have been used in the static neutronic analysis of the bimodal gaseous core reactor system. System neutron multiplication factors from XSDRNPM for various configurations of the bimodal reactor system have been used as the required initial guesses for system k_{eff} in the criticality calculations with

MCNP for improving the speed of convergence. XSDRNPM system k_{eff} values have also been used for comparative study of the variation of the system k_{eff} for a large number of bimodal gas core reactor configurations with different inner and outer beryllium thicknesses. This is done to minimize the number of expensive MCNP calculations for various system configurations.

For MCNP runs, variance reduction techniques such as geometry splitting and Russian roulette, weight cutoff, and time and energy cutoff have been used in order to reduce the relative error in the system k_{eff} and system neutron removal lifetime to about 0.55 to 2%. The coupling contributions among the cores of the system have been calculated with relative errors of better than 8%. MCNP running time depends on the input importance ratio of the core region to the beryllium reflector region, the fuel-gas loading in the cores, inner and outer beryllium thickness of the bimodal reactor system and the different variance reduction techniques used. If MCNP were required to achieve a relative error or uncertainty equal to the XSDRNPM convergence level of 10^{-5}, a prohibitively expensive MCNP run would be required on the Cray X-MP/48 machine.

Even though the system k_{eff} values from MCNP involve a relatively high statistical error, the fact that the exact geometry of the system and probabilities of interactions can be simulated in the MCNP code provides the capability to make the estimations for the kinetics parameters, especially for the coupling coefficients, with a high degree of confidence. The motivation behind the extensive use of MCNP in the static neutronic analysis of the bimodal gas core reactor system has been the need for calculation of the coupling coefficients with a relatively high degree of accuracy without compromising the accuracy in the system k_{eff} to an unacceptable level.

For any bimodal gaseous core reactor configuration, the system neutron multiplication factor increases with an increase in the PGCR core or the central BPGCR chamber gas loading. For the bimodal system with the PGCR chambers loaded with fuel-gas mixture and the central BPGCR chamber unfueled, the system k_{eff} is found to decrease with an increase in the inner beryllium thickness for the range of TIBE examined. When the large central BPGCR chamber is loaded, the system k_{eff} is found to increase initially with an increase in inner beryllium thickness up to an optimum value of TIBE (at which maximum system k_{eff} occurs) and thereafter the system k_{eff} decreases with an increase in inner beryllium thickness. As the BPGCR chamber fuel-gas loading increases, the optimum inner beryllium thickness is found to increase. This is due to the increase in neutronic coupling between the central BPGCR chamber and the PGCR cores up to the optimum TIBE and the decrease in the neutronic coupling between the BPGCR and PGCR cores when the inner beryllium thickness increases beyond the optimum TIBE value. This optimum inner beryllium thickness is found to be in the range of 10 cm to about 30 cm for a range of central BPGCR loadings of 25 atm to 100 atm of fuel-gas mixture. When the PGCR core fuel-gas mixture loading is varied with constant central BPGCR fuel-gas loading, this optimum inner beryllium thickness is found to be around 10 cm irrespective of the PGCR core fuel-gas loading.

The system neutron removal lifetime is found to be essentially independent of the inner beryllium thickness for all examined fuel-gas loadings of the central BPGCR chamber and the PGCR cores. The neutron removal lifetime is found to be a strong function of the outer beryllium thickness. As the outer beryllium thickness increases, the neutron removal lifetime increases for a range of TOBE values from 20 cm to about 55 cm; thereafter the neutron removal lifetime is independent of the outer beryllium thickness.

The effects of the BPGCR/PGCR chamber gas loading and the inner and outer beryllium thicknesses on other system kinetics parameters such as reactivity, system neutron generation time, and the core coupling coefficients are discussed in detail in the next chapter on the dynamic neutronics of the coupled core bimodal gaseous core reactor system.

CHAPTER 5
DYNAMIC NEUTRONIC STUDIES ON COUPLED MULTIPLE CAVITY GASEOUS CORE REACTOR SYSTEM

Introduction

Results from the static neutronic analysis of the bimodal gaseous core reactor (BGCR) system have been used in the dynamic neutronic analysis of the system. The dynamic neutronic analysis of the coupled core BGCR system is done by using the computer program, COUPKIN, which is developed as part of this work and is described in detail in Appendix B. Parameters obtained from the static neutronic calculations with the MCNP and XSDRNPM codes have been used in the coupled core point reactor kinetics (COUPKIN) program. The integral parameters which are calculated from MCNP results include the system reactivity, neutron generation time, and the core-to-core neutronic coupling coefficients. Definitions of these and other integral parameters required for the solution of coupled core point reactor kinetics equations and their interpretations based on the MCNP results are given in Appendix B.

This Chapter examines the effects of variations in PGCR and BPGCR core gas loadings and the inner and outer beryllium thicknesses on the system integral kinetics parameters such as system reactivity, system neutron generation time, and the core-to-core coupling coefficients. The effects of various PGCR and BPGCR core gas loadings on the integral parameters are examined for all the different configurations of the BGCR system investigated in Chapter 4; namely, for various PGCR core gas loadings with and without fuel in the central BPGCR chamber, and for various BPGCR chamber gas loadings with a nominal amount of fuel in the PGCR cores. This study for each range of variation in core fuel-gas loading is repeated for different inner and outer beryllium thicknesses.

Core neutron level changes during each cycle of operation for various configurations with different fuel loadings and different inner and outer beryllium thicknesses are examined in this Chapter. This is done by using the coupled core point reactor kinetics equations which are described in detail in Appendix B. The integral kinetics parameters such as reactivity, neutron generation time, and average coupling coefficients which are required in the COUPKIN program are calculated from the results obtained from the MCNP code. The influence of the coupling coefficients and delay times on the core power level is studied parametrically by varying these parameters in the coupled core point reactor kinetics equations. The effect of variation of the cycle time on the power level is also studied.

The effect of delayed neutrons is included in the study of the dynamic behavior of the bimodal system. The coupled core point reactor kinetics program, COUPKIN, has the capability of handling either six groups of delayed neutrons or one effective group of delayed neutrons. The effect of photoneutrons is not included in this study. It was determined by Dugan (30) in his extensive investigation of gaseous core reactors that even though both delayed neutrons and photoneutrons exert an influence on the dynamic (kinetic) behavior of the beryllium reflected gaseous core reactor systems, the photoneutron influence was much smaller than the delayed neutron influence. The delayed neutron parameters such as effective delayed neutron fractions and initial effective delayed neutron precursor concentrations are user inputs into the COUPKIN program.

The bimodal gaseous core reactor is a circulating fuel reactor. During the operation of the reactor for any given cycle time delayed neutron precursors are produced and a fraction also decays while they are in the reactor core. The gas is exhausted into the external loop. Changes in the external loop circulation time change the number or fraction of the delayed neutron precursors which undergo decay in the external loop. The precursors which do not decay in the external loop, but decay upon reentering the core after passing through the loop act as an additional or extra neutron source and, hence, can be used to adjust the core power level. The coupled core point reactor kinetics algorithm is capable of handling this effect due to the fuel circulation in the external loop. This is accomplished by including residence times of the delayed neutrons in the cores and the circulation time of the fuel in the external loop in the time dependent equation for the delayed neutron precursor concentration (Equation B-25 in Appendix B) of the coupled core point reactor kinetics equations.

The results from the coupled core point reactor kinetics (COUPKIN) program for a few reference single core systems have been compared with the results from the ANCON code from the Los Alamos National Laboratory (5) (see Appendix D). The ANCON code solves the point reactor kinetics equations for a single core by a method known as continuous analytic continuation. In order to compare the results from the COUPKIN program directly with the results from the ANCON code, the coupled core kinetics equations in COUPKIN are reduced to one set of equations for a single core.

Method of Solution of Coupled Core Point Reactor Kinetics Equations in COUPKIN

The coupled core point reactor kinetics equations which consist of time dependent equations for core neutron level and delayed neutron precursor concentrations are given in Appendix B. The procedure used to solve the coupled core point reactor kinetics equations is highlighted below.

The coupled source term for any specific core, that accounts for the neutronic coupling from the remaining cores on the specific core, has been introduced as an "effective source" in the coupled core kinetics Equation (B-1). The coupled source term appears as the third term on the right hand side of the coupled core kinetics Equation (B-1). The core neutron level in the coupled source term with the retarded time argument, i.e. $N_k(t-\tau_{jk})$, is approximated by a truncated Taylor series expansion. The time derivatives in the coupled point reactor kinetics equations are approximated by forward finite differences. The terms involving time dependent parameters such as reactivity, core neutron levels, and delayed neutron precursor concentrations are approximated by the "theta differencing" technique as described in Appendix B. The "theta differencing" technique (see Equations (B-20a) through (B-20e)) makes it possible to solve the coupled core kinetics equations either by a fully implicit method, a fully explicit method, or by an averaged implicit method (similar to the Crank-Nicolson method). The resulting coupled equations are simultaneously and iteratively solved for core neutron levels and delayed neutron precursor concentrations at each time step during the operation of the reactor system. The reactivity, neutron generation time, and the coupling coefficients are updated in the coupled equations at each time step during the solution of the Equation (B-21) for core neutron level.

Discussion of Results

Analysis of results from dynamic neutronic studies of the coupled BGCR system is given in the two sections which follow. The first section examines the effects of variations of PGCR and BPGCR core fuel-gas loading and of inner and outer beryllium thicknesses on the integral kinetics parameters such as coupling coefficients, neutron generation time, and reactivity. The second part includes the effects of variations in PGCR and BPGCR fuel-gas loading, variations of the inner and outer beryllium thickness, variation in cycle time, and variations in the coupling effects on both core neutron level and delayed neutron precursor concentration for both low power PGCR and high power BPGCR short term operational transients.

Integral Parameters: Coupling Coefficients, Neutron Generation Time, and Reactivity

Conventional expressions for the integral parameters such as coupling coefficients, neutron generation time, and reactivity and their appropriate interpretations and derivations in terms of the quantities that are calculated from the MCNP code are given in Appendix B.

Coupling coefficients (α_{jk}) which appear in the coupled point reactor kinetics Equations (B-1) are interpreted as the fraction of neutrons in core j that diffuse from any core k and enter core j and cause fission in core j. In terms of the quantities that are obtained from the MCNP code, α_{jk} is expressed in the form (Equation B-16)

$$\alpha_{jk}(t) = \frac{(SO_{jk})_{th}(t)}{(SO_j)_{tot}(t)} \left(\frac{\Sigma_f}{\Sigma_a}\right)$$

where $(SO_{jk})_{th}$ is the thermal neutron contribution from core k that is absorbed in core j, $(SO_j)_{tot}$ is the total neutron source in core j, Σ_f is the total macroscopic fission cross section of all fissionable isotopes in the core j, and Σ_a is the total macroscopic absorption cross section of all isotopes in core j. For the gas core reactor in which the gaseous fuel-gas mixture is highly enriched UF_6-He, the macroscopic fission and absorption cross sections in equation (B-16) can be replaced by the respective microscopic cross sections for the uranium fuel since neutrons are primarily absorbed by uranium-235 of the UF_6-He mixture.

The cell flagging capability of MCNP is used to determine the thermal neutron contribution from any specific cell or core to any other cell or core of the bimodal gaseous core reactor system. The use of the cell flagging capability of MCNP is explained in Appendix A. The neutron contribution from each of the cells or cores of the BGCR to each of the other remaining cells or cores as well as to the same cell or core can be tallied. The core-to-core contribution can also be tallied according to the neutron energy by specifying the desired energy bin. For a 13 core system the total number of tallies which give the core-to-core neutronic contribution is 169.

Effect of PGCR core fuel loading and inner beryllium thickness variations when the BPGCR chamber is unfueled

Tables 5-1 through 5-5 give the average coupling coefficients (α_{2k}), system neutron multiplication factors (k_{eff}), neutron generation time (Λ), and the reactivity (ρ) for various PGCR fuel-gas loadings for inner beryllium thicknesses of 10 cm, 20 cm, 25 cm, 30 cm, and 40 cm, respectively. The central BPGCR chamber is maintained at a pressure of 20 atmospheres of helium gas. The coupling coefficients (α_{2k}) given in Tables 5-1 through 5-5 have been obtained by averaging twice; first by averaging the coupling coefficients, α_{jk}, for any specific core j and for cores k where k varies from the adjacent core on one side to the adjacent core on the other side in either the clockwise or the counter clockwise direction (see Figure A-3). This is repeated for all cores j. The second averaging is done for the coupling coefficients for azimuthally symmetric pairs of cores about any specific core. For example, the symmetric pairs of cores about core 2 are cores 3 and 13, 4 and 12, 5 and 11, 6 and 10, 7 and 9, and the single core 8.

Figures 5-1 through 5-5 illustrate the variation of coupling coefficients, for the three most strongly coupled pairs of PGCR cores with respect to core 2, with the PGCR

Table 5-1. Integral Kinetics Parameters as a Function of PGCR Core Fuel-Gas Loading for the BGCR System with Inner Beryllium Thickness of 10 cm.

BPGCR Pressure = 20 atm He
TOBE = 50 cm

Cores	Average Coupling Coefficients (α_{2k})						k_{eff}	Λ (ms)	ρ
k →	3,13	4,12	5,11	6,10	7,9	8			
PGCR Loading (atm)									
10	0.2411	0.1096	0.0561	0.0341	0.0309	0.0290	0.4860	7.3951	-1.0576
20	0.2142	0.0956	0.0450	0.0266	0.0206	0.0188	0.7675	3.9114	-0.3029
30	0.1864	0.0768	0.0382	0.0221	0.0186	0.0178	0.9058	3.0117	-0.1039
40	0.1610	0.0619	0.0246	0.0163	0.0145	0.0144	0.9846	2.5248	-0.0156
50	0.1474	0.0557	0.0238	0.0135	0.0115	0.0119	1.0719	2.1569	0.0671

Results from MCNP

Table 5-2. Integral Kinetics Parameters as a Function of PGCR Core Fuel-Gas Loading for the BGCR System with Inner Beryllium Thickness of 20 cm.

BPGCR Pressure = 20 atm He
TOBE = 50 cm

Cores k→	Average Coupling Coefficients (α_{2k})						k_{eff}	Λ (ms)	ρ
	3,13	4,12	5,11	6,10	7,9	8			
PGCR Loading (atm)									
20	0.1654	0.0446	0.0157	0.0082	0.0073	0.0068	0.7136	4.242	-0.4013
30	0.1486	0.0356	0.0106	0.0058	0.0050	0.0049	0.8881	3.036	-0.1259
40	0.1319	0.0321	0.0096	0.0055	0.0047	0.0050	0.9891	2.492	-0.0110
50	0.1175	0.0252	0.0065	0.0042	0.0045	0.0044	1.0429	2.197	0.0411
60	0.1111	0.0247	0.0075	0.0046	0.0040	0.0040	1.1530	1.858	0.1327

Results from MCNP

Table 5-3. Integral Kinetics Parameters as a Function of PGCR Core Fuel-Gas Loading for the BGCR System with Inner Beryllium Thickness of 25 cm.

BPGCR Pressure = 20 atm He
TOBE = 50 cm

Cores k →	Average Coupling Coefficients (α_{2k})						k_{eff}	Λ (ms)	ρ
	3,13	4,12	5,11	6,10	7,9	8			
PGCR Loading (atm)									
20	0.1547	0.0337	0.0129	0.0055	0.0061	0.0054	0.7188	4.2181	-0.3912
30	0.1343	0.0293	0.0083	0.0039	0.0041	0.0040	0.8743	3.1671	-0.1438
40	0.1134	0.0213	0.0052	0.0027	0.0036	0.0029	0.9384	2.6034	-0.0656
50	0.1098	0.0178	0.0039	0.0027	0.0028	0.0037	1.0321	2.2226	0.0311
60	0.1011	0.0171	0.0042	0.0029	0.0027	0.0032	1.1205	1.9776	0.1075

Results from MCNP

Table 5-4. Integral Kinetics Parameters as a Function of PGCR Core Fuel-Gas Loading for the BGCR System with Inner Beryllium Thickness of 30 cm.

BPGCR Pressure = 20 atm He
TOBE = 50 cm

Cores k →	Average Coupling Coefficients (α_{2k})						k_{eff}	Λ (ms)	ρ
	3,13	4,12	5,11	6,10	7,9	8			
PGCR Loading (atm)									
20	0.1379	0.0282	0.0057	0.0029	0.0033	0.0031	0.6941	4.3696	-0.4407
30	0.1272	0.0219	0.0046	0.0031	0.0026	0.0027	0.8529	3.1833	-0.1725
40	0.1164	0.0188	0.0044	0.0020	0.0016	0.0019	0.9387	2.6089	-0.0653
50	0.0981	0.0145	0.0033	0.0024	0.0017	0.0014	0.9885	2.3186	-0.0116
60	0.0972	0.0129	0.0027	0.0013	0.0016	0.0015	1.0991	1.9879	0.0902

Results from MCNP

Table 5-5. Integral Kinetics Parameters as a Function of PGCR Core Fuel-Gas Loading for the BGCR System with Inner Beryllium Thickness of 40 cm.

BPGCR Pressure = 20 atm He
TOBE = 50 cm

Cores k →	Average Coupling Coefficients (α_{2k})						k_{eff}	Λ (ms)	ρ
	3,13	4,12	5,11	6,10	7,9	8			
PGCR Loading (atm)									
20	0.1154	0.0161	0.0042	0.0019	0.0018	0.0014	0.6377	4.6997	-0.5681
30	0.0957	0.0119	0.0023	0.0013	0.0011	0.0010	0.7595	3.4917	-0.3167
40	0.0900	0.0089	0.0014	0.0007	0.0006	0.0007	0.8899	2.8014	-0.1237
50	0.0796	0.0086	0.0014	0.0007	0.0007	0.0007	0.9419	2.3983	-0.0616
60	0.0761	0.0070	0.0010	0.0006	0.0006	0.0006	1.0423	2.1021	0.0406

Results from MCNP

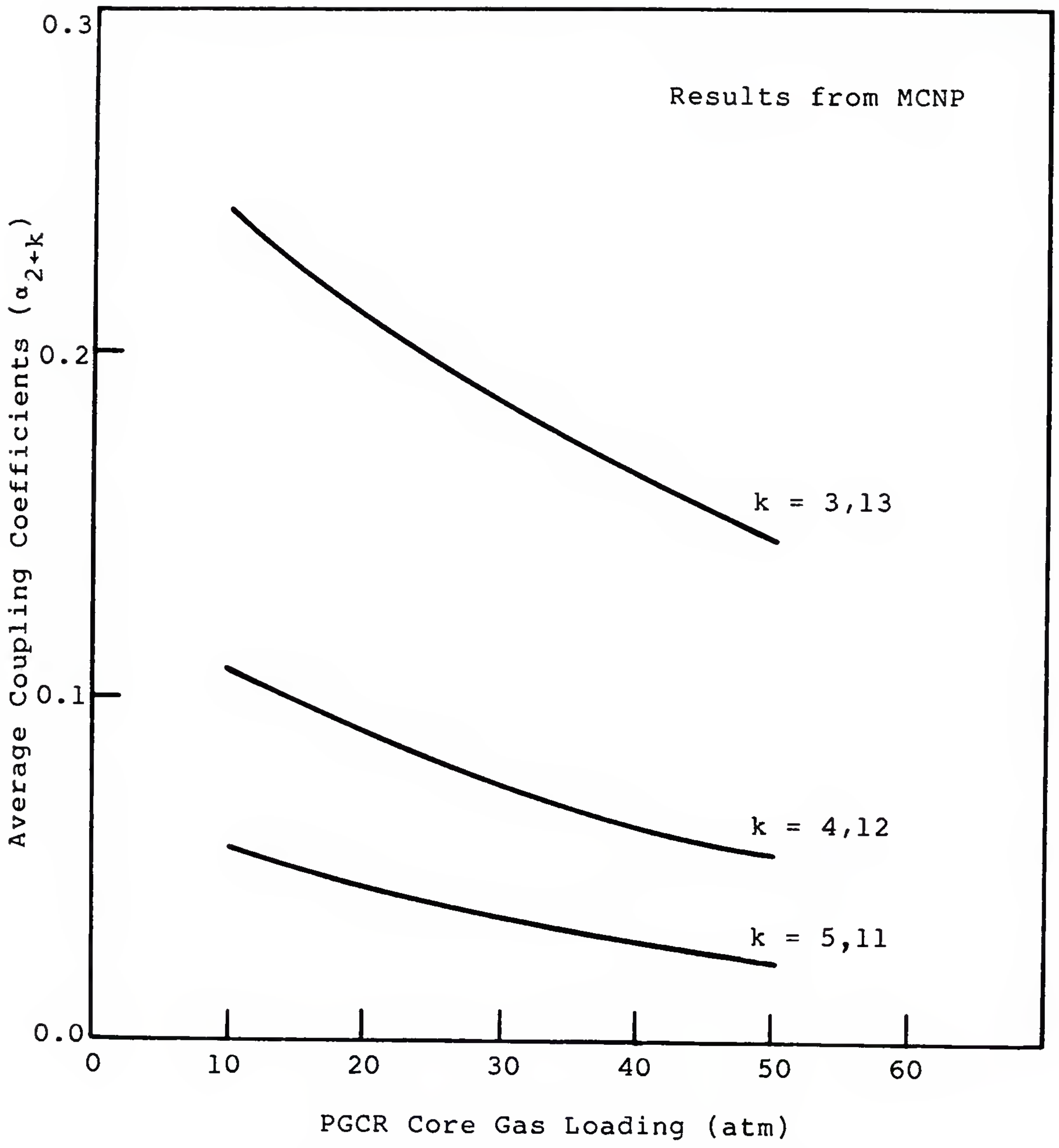

Figure 5-1. Average Coupling Coefficients ($\alpha_{2 \leftarrow k}$) as a Function of PGCR Gas Loading for a BGCR with TIBE of 10 cm.

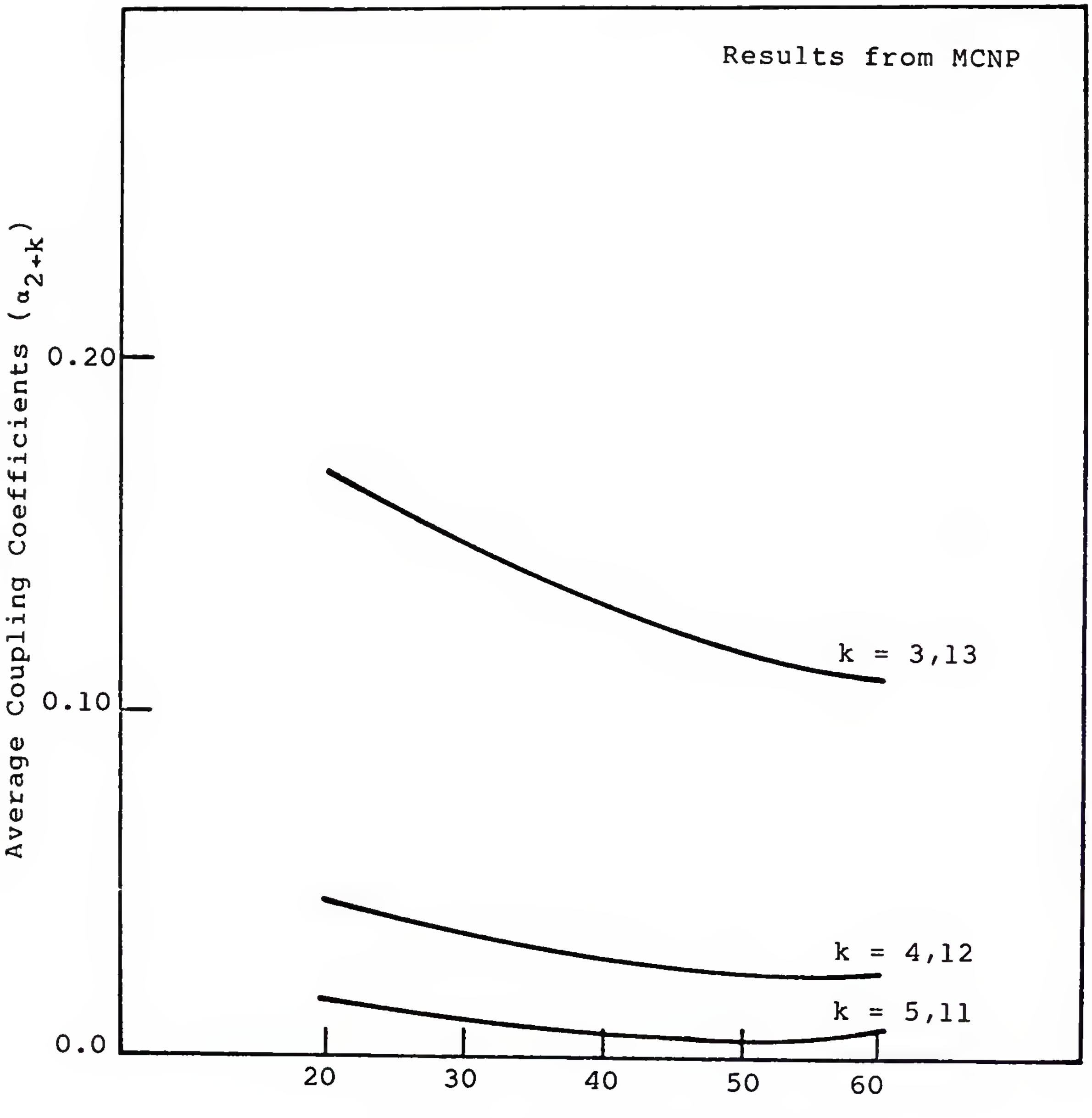

Figure 5-2. Average Coupling Coefficients ($\alpha_{2\to k}$) as a Function of PGCR Gas Loading for a BGCR with TIBE of 20 cm.

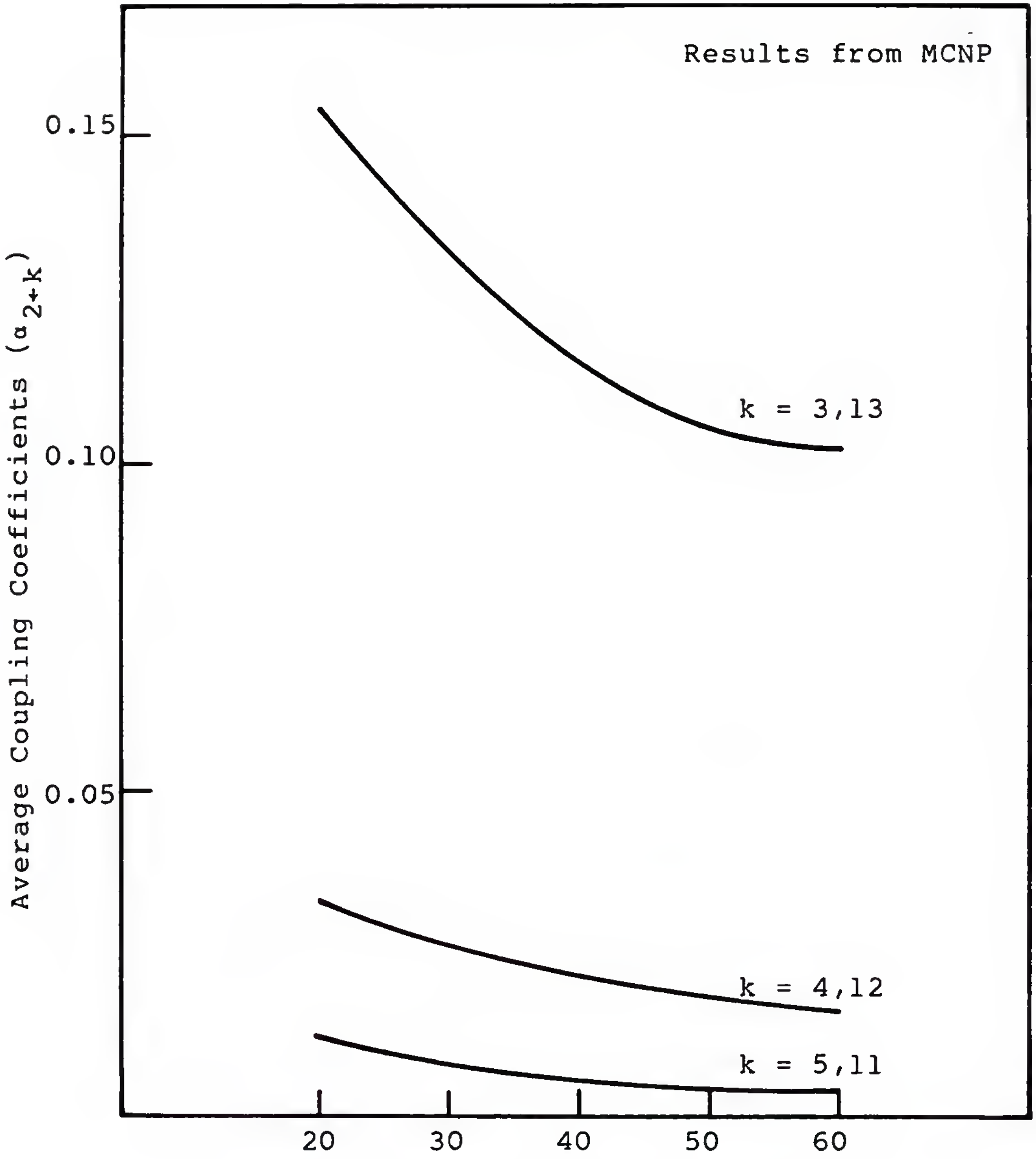

Figure 5-3. Average Coupling coefficients ($\alpha_{2 \leftarrow k}$) as a Function of PGCR Gas Loading for a BGCR with TIBE of 25 cm.

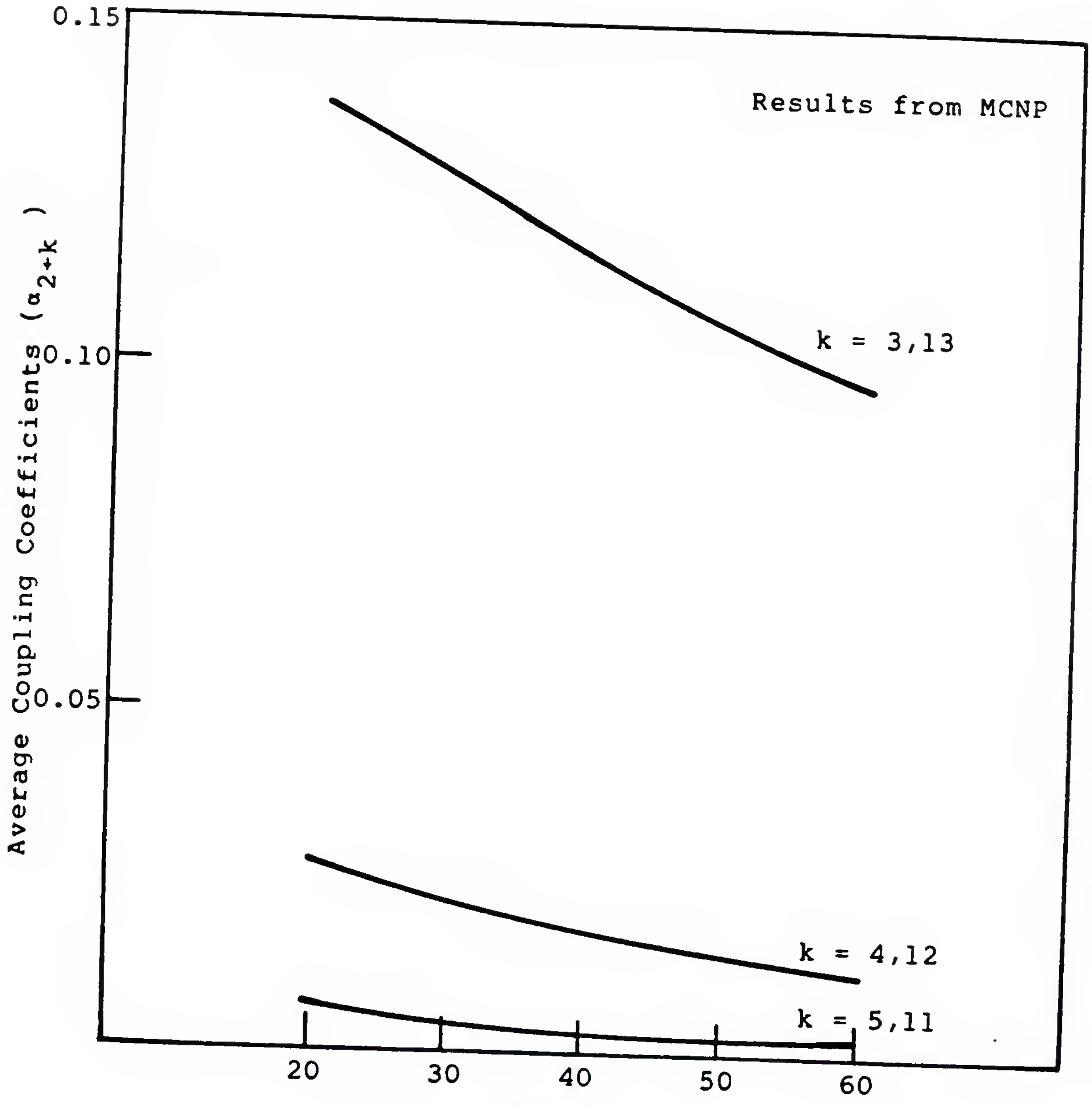

Figure 5-4. Average Coupling Coefficients (α_{2+k}) as a Function of PGCR Gas Loading for a BGCR with TIBE of 30 cm.

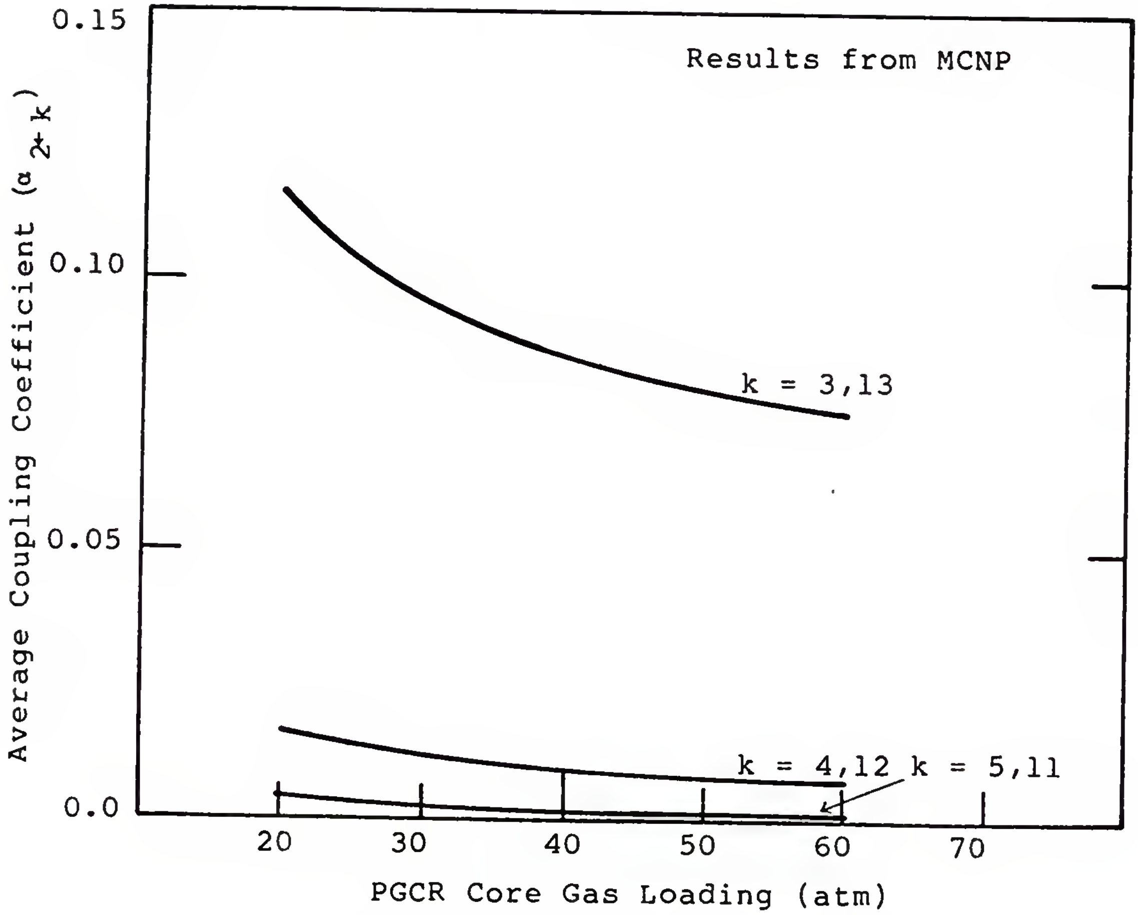

Figure 5-5. Average Coupling Coefficients (α_{2+k}) as a Function of PGCR Gas Loading for a BGCR with TIBE of 40 cm.

core fuel-gas loading. These figures illustrate coupling coefficient variations for BGCR configurations with inner beryllium thicknesses of 10 cm, 20 cm, 25 cm, 30 cm, and 40 cm, respectively. It can be seen that the coupling coefficients decrease as the PGCR core fuel-gas loading increases for any specific inner beryllium thickness. This is due to the fact that as the fissile gas density in the PGCR core increases the neutron absorption in the individual cores increases and consequently the coupling contribution among the cores decreases. It can be seen from these Figures and Tables that for any specific PGCR core fuel-gas loading, the coupling coefficients are a maximum for any pair of adjacent cores. The coupling coefficients decrease as the distance between the cores increases.

Figure 5-6 illustrates the variation of average coupling coefficients ($\alpha_{2\leftarrow3}$) between adjacent cores with the PGCR fuel-gas loading for various values of inner beryllium thickness. It can be seen that for any specific inner beryllium thickness, the coupling coefficients for adjacent PGCR cores decrease as the core fuel-gas loading increases. Figure 5-7 illustrates the variation of coupling coefficients for adjacent PGCR cores with the inner beryllium thickness for various PGCR core fuel-gas loadings. Figure 5-7 shows that the neutronic coupling among the cores decreases as the inner beryllium thickness increases. Tables 5-1 through 5-5 indicate that the coupling

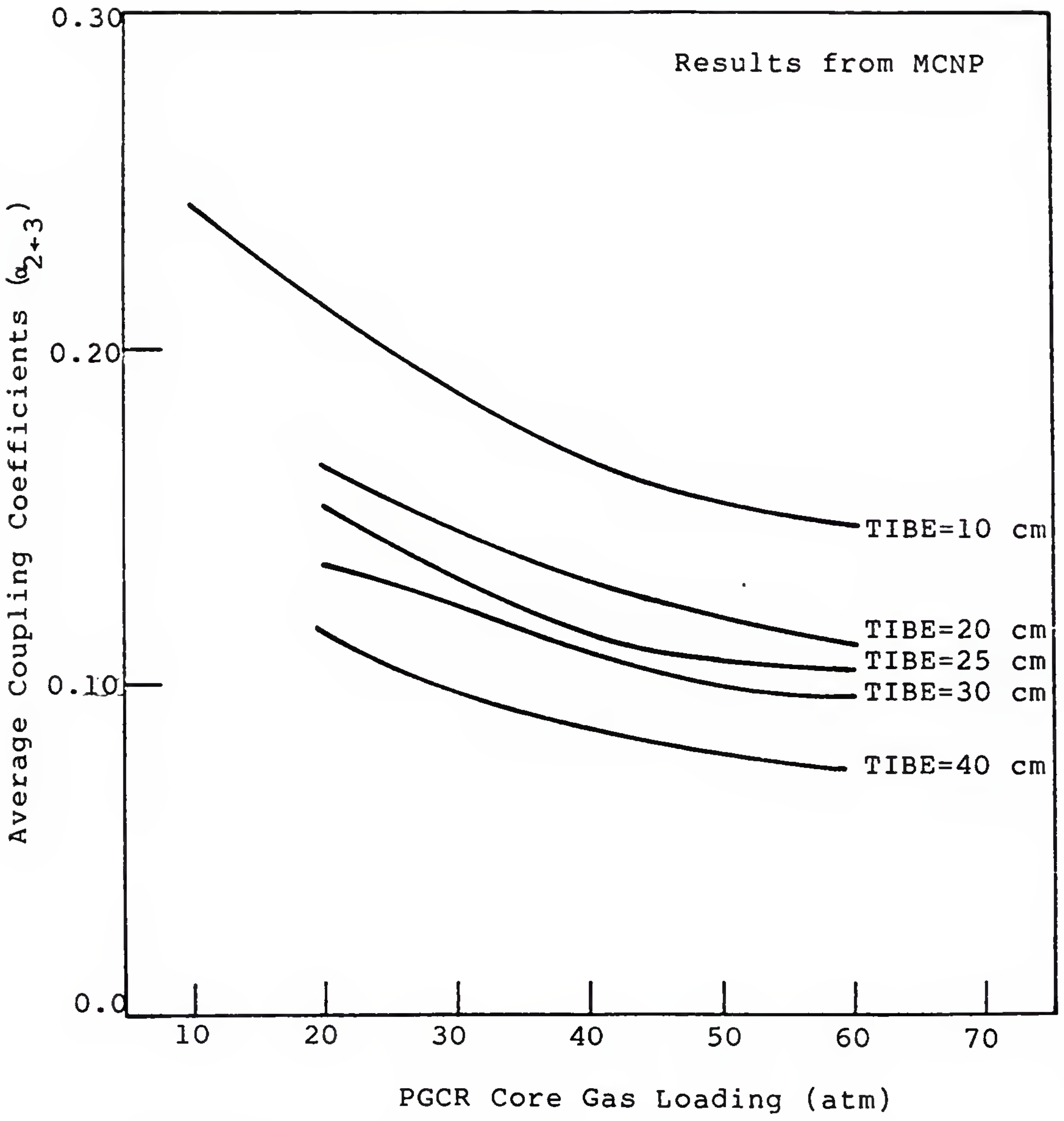

Figure 5-6. Average Coupling Coefficients ($\alpha_{2\to3}$) as a Function of PGCR Gas Loading for Various Inner Beryllium Thickness.

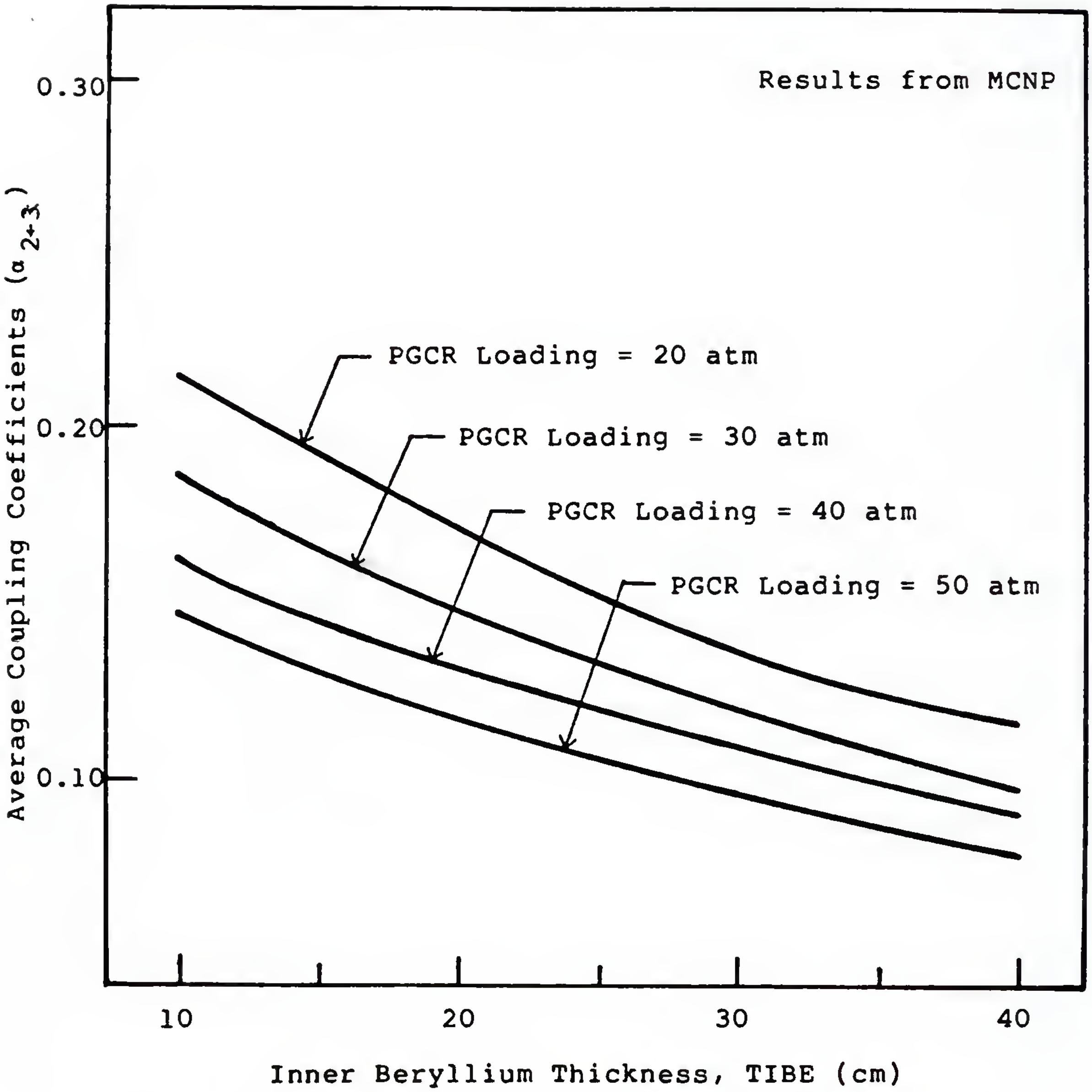

Figure 5-7. Average Coupling Coefficients ($\alpha_{2\to3}$) as a Function of Inner Beryllium Thickness for Various PGCR Gas Loadings.

coefficients for other pairs of cores that are not adjacent to each other also follow the same trend as exhibited by Figures 5-6 and 5-7.

The fact that the neutronic coupling contribution among the PGCR cores decreases as the inner beryllium thickness increases is the main reason for the decrease in the system neutron multiplication factor with an increase in the inner beryllium thickness for any specific PGCR gas loading when the BPGCR is unfueled. The variation in system k_{eff} with an increase in the inner beryllium thickness when the BPGCR is unfueled is graphically illustrated in Figures 4-8 and 4-9 of Chapter 4 on the static neutronic studies of the BGCR.

Figure 5-8 shows the variation of the system reactivity (in terms of the departure from criticality as $\Delta k/k$) with the PGCR gas loading for the BGCR configurations with inner beryllium thicknesses of 10 cm, 20 cm, 30 cm, and 40 cm. These curves illustrate the need for higher fuel-gas loading for larger systems in order to maintain the system critical.

Figure 5-9 illustrates the variation of neutron generation time as a function of inner beryllium thickness of the bimodal gaseous core reactor system with an unfueled central BPGCR chamber. For the lower PGCR core loadings of 20 and 30 atmospheres, the neutron generation time is found to undergo a modest increase with an increase in the inner

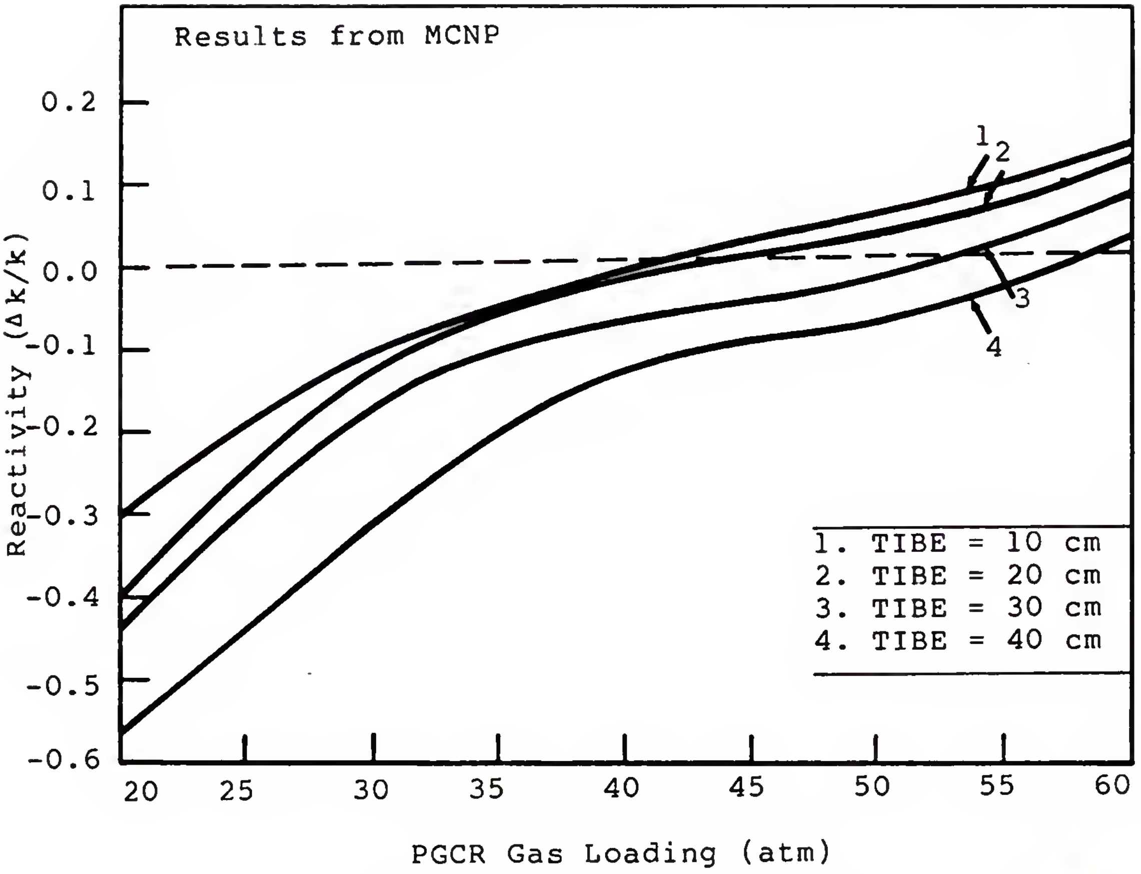

Figure 5-8. Reactivity of BGCR System as a Function of PGCR Core Gas Loading for Various Inner Beryllium Thickness.

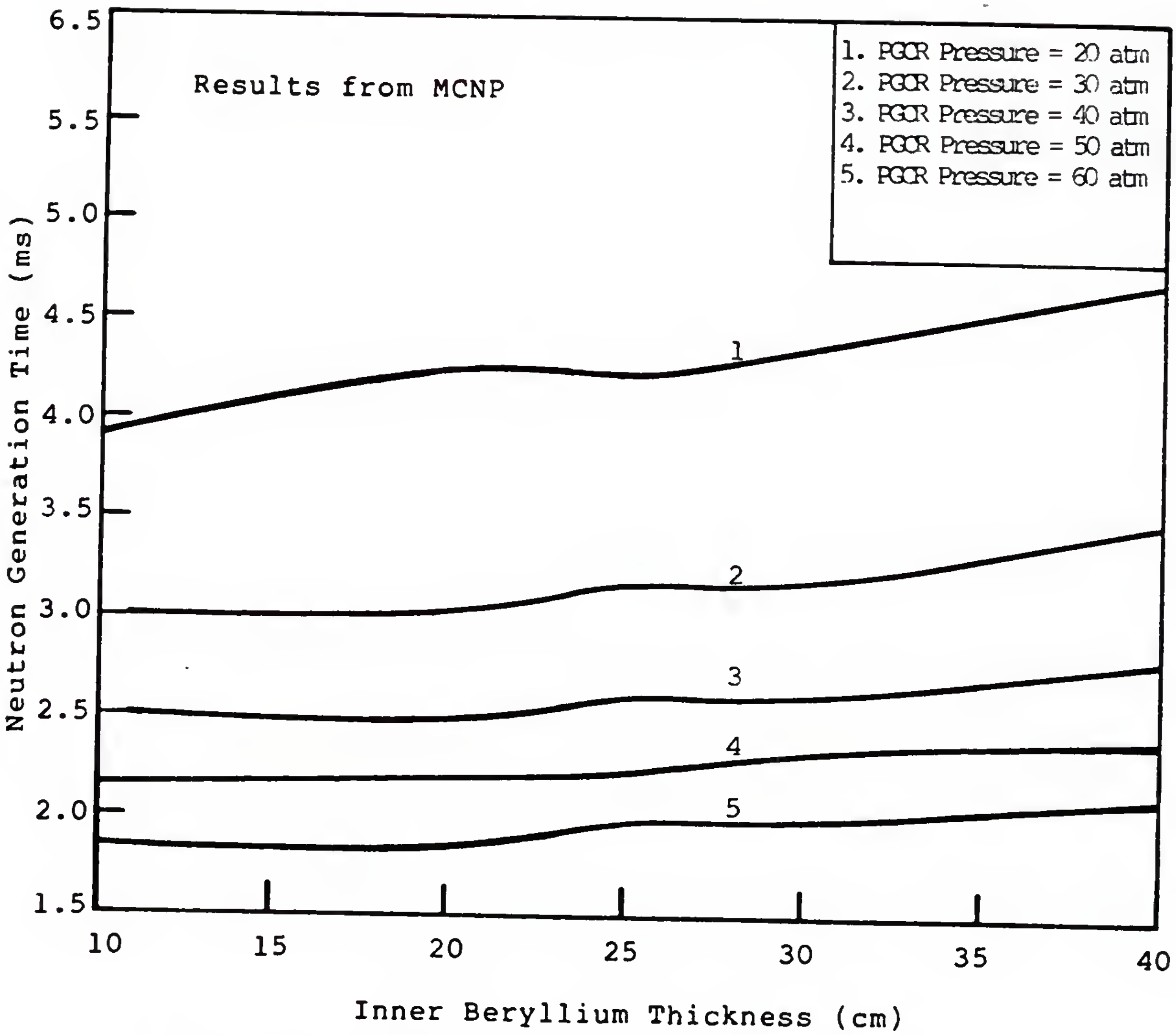

Figure 5-9. Neutron Generation Time as a Function of Inner Beryllium Thickness for a BGCR with a BPGCR Chamber Loading of 20 atm Helium Gas.

beryllium thickness. For higher PGCR gas loadings, above 30 atmospheres, the neutron generation time of the BGCR is essentially independent of the inner beryllium thickness. This behavior of neutron generation time with the inner beryllium thickness is similar to the behavior of neutron removal lifetime with inner beryllium thickness (Table 4-10, Figure 4-10) that is discussed in Chapter 4.

Effect of outer beryllium thickness variations

Tables 5-6 and 5-7 give the average coupling coefficients (α_{2k}), system neutron multiplication factor (k_{eff}), neutron generation time (Λ), and the reactivity (ρ) of the bimodal gaseous core reactor system as a function of outer beryllium thickness for inner beryllium thickness of 20 cm and 30 cm, respectively. The outer beryllium thickness for each case is varied from 20 cm to 70 cm. The PGCR core fuel-gas loading is maintained at 50 atmospheres while the central BPGCR chamber is maintained at a constant pressure of 20 atmospheres of helium gas.

Figure 5-10 illustrates the variation of the coupling coefficients, $\alpha_{2\leftarrow 3,13}$ and $\alpha_{2\leftarrow 4,12}$, (see Figure A-3 of Appendix A) with the outer beryllium thickness, TOBE, for two BGCR configurations with inner beryllium thicknesses of 20 cm and 30 cm. It can be seen from Tables 5-6 and 5-7 and Figure 5-10 that the coupling coefficients increase moderately with an increase in the outer beryllium thickness

Table 5-6. Integral Kinetics Parameters as a Function of Outer Beryllium Thickness (TOBE) for the BGCR System with TIBE of 20 cm.

PGCR Pressure = 50 atm UF_6/He
BPGCR Pressure = 20 atm He

Cores k →	Average Coupling Coefficients (α_{2k})						k_{eff}	Λ (ms)	ρ
	3,13	4,12	5,11	6,10	7,9	8			
Outer Be Thickness (cm)									
20	0.1096	0.0234	0.0068	0.0041	0.0038	0.0039	0.9449	1.7346	-0.0583
30	0.1165	0.0258	0.0074	0.0043	0.0033	0.0030	1.0043	1.9187	0.0043
40	0.1188	0.0267	0.0071	0.0040	0.0036	0.0038	1.0218	2.0591	0.0213
50	0.1175	0.0252	0.0065	0.0042	0.0046	0.0046	1.0273	2.2301	0.0266
60	0.1153	0.0262	0.0073	0.0048	0.0038	0.0039	1.0507	2.2775	0.0483
70	0.1186	0.0256	0.0070	0.0043	0.0038	0.0023	1.0315	2.3760	0.0305

Results from MCNP

Table 5-7. Integral Kinetics Parameters as a Function of Outer Beryllium Thickness (TOBE) for the BGCR System with TIBE of 30 cm.

PGCR Pressure = 50 atm UF_6/He
BPGCR Pressure = 20 atm He

Cores k →	Average Coupling Coefficients (α_{2k})						k_{eff}	Λ (ms)	ρ
	3,13	4,12	5,11	6,10	7,9	8			
Outer Be Thickness cm									
20	0.0925	0.0137	0.0033	0.0019	0.0021	0.0017	0.9235	1.7748	-0.0724
30	0.0996	0.0140	0.0033	0.0019	0.0015	0.0014	0.9775	1.9753	-0.0029
40	0.0989	0.0136	0.0039	0.0021	0.0022	0.0016	1.0175	2.1002	0.0172
50	0.0981	0.0145	0.0033	0.0021	0.0017	0.0014	1.0228	2.0864	-0.0096
60	0.0974	0.0134	0.0031	0.0019	0.0019	0.0020	1.0206	2.3643	0.0202
70	0.0998	0.0150	0.0034	0.0019	0.0018	0.0019	1.0208	2.4187	0.0204

Results from MCNP

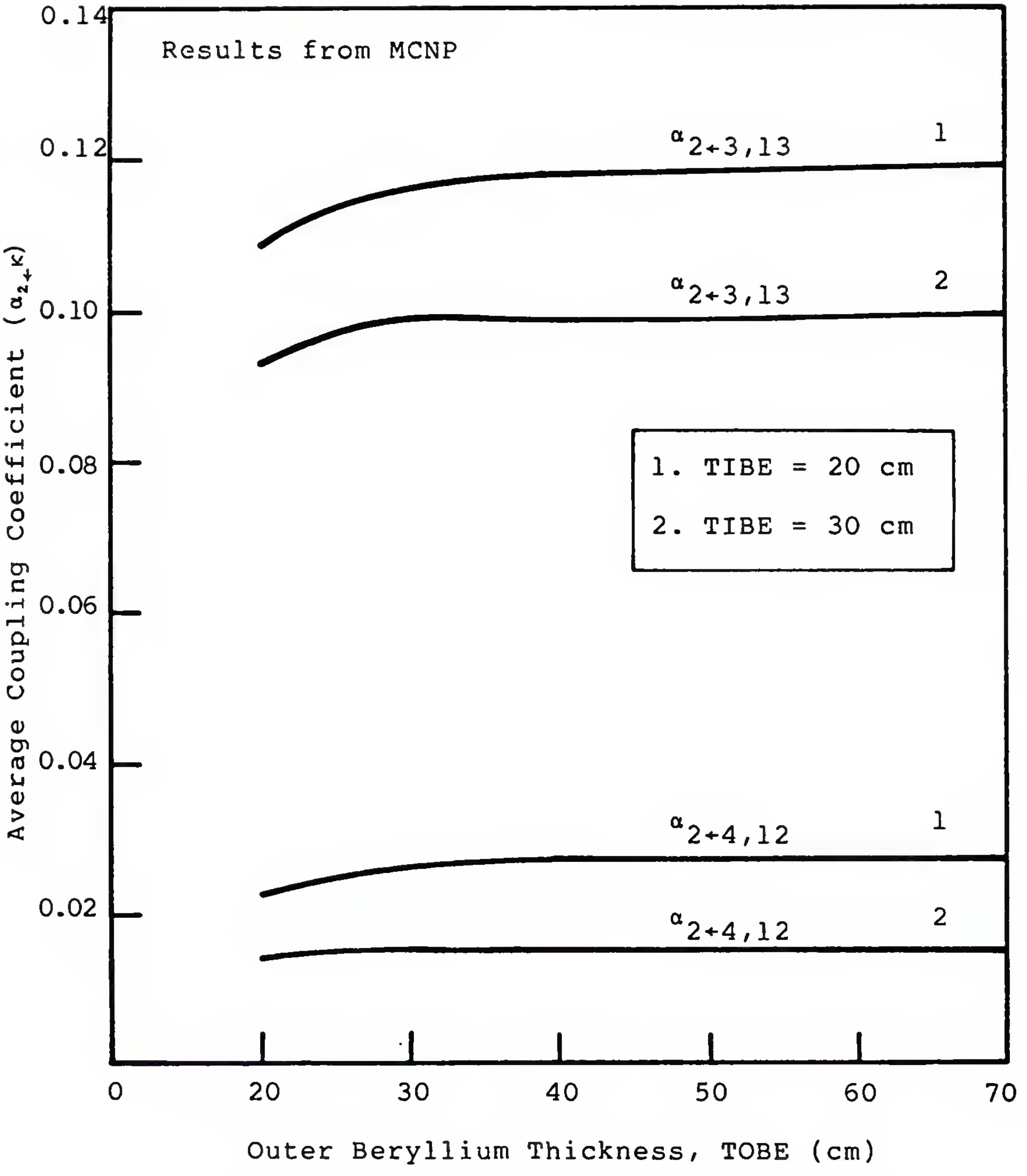

Figure 5-10. Average Coupling Coefficient ($\alpha_{2\to K}$) as a Function of Outer Beryllium Thickness For TIBE of 20 cm and 30 cm.

for up to about 30 cm. An increase in outer beryllium thickness beyond about 30 cm does not result in any significant increase in the coupling coefficients. The small fluctuation in the average coupling coefficients for outer beryllium thickness greater than 40 cm is mainly due to the relatively large uncertainty in the MCNP calculations of the quantity $S_{j \leftarrow k}$ which appears in the expression for the coupling coefficients (Equation B-16). Comparing the results for the two sets of coupling coefficients for TIBE of 20 cm and 30 cm, the coupling coefficients for the adjacent PGCR cores, $\alpha_{2 \leftarrow 3,13}$, are about 15% lower for a TIBE of 30 cm than the corresponding coupling coefficients for a TIBE of 20 cm. Further, the coupling coefficients, $\alpha_{2 \leftarrow 4,12}$, for a TIBE of 30 cm are about 40% lower than the corresponding coupling coefficients for a TIBE of 20 cm. For the distant pairs of cores, 5 and 11, 6 and 10, 7 and 9, and the single core 8, the coupling coefficients with core 2 are on the average 50% less for a TIBE of 30 cm than the corresponding coupling coefficients for a TIBE of 20 cm.

Figure 5-11 illustrates the variation of system reactivity in terms of departure from criticality ($\Delta k/k$) with the outer beryllium thickness for the two BGCR configurations with TIBE values of 20 cm and 30 cm.

Tables 5-6 and 5-7 indicate that for a specific inner beryllium thickness the neutron generation time increases

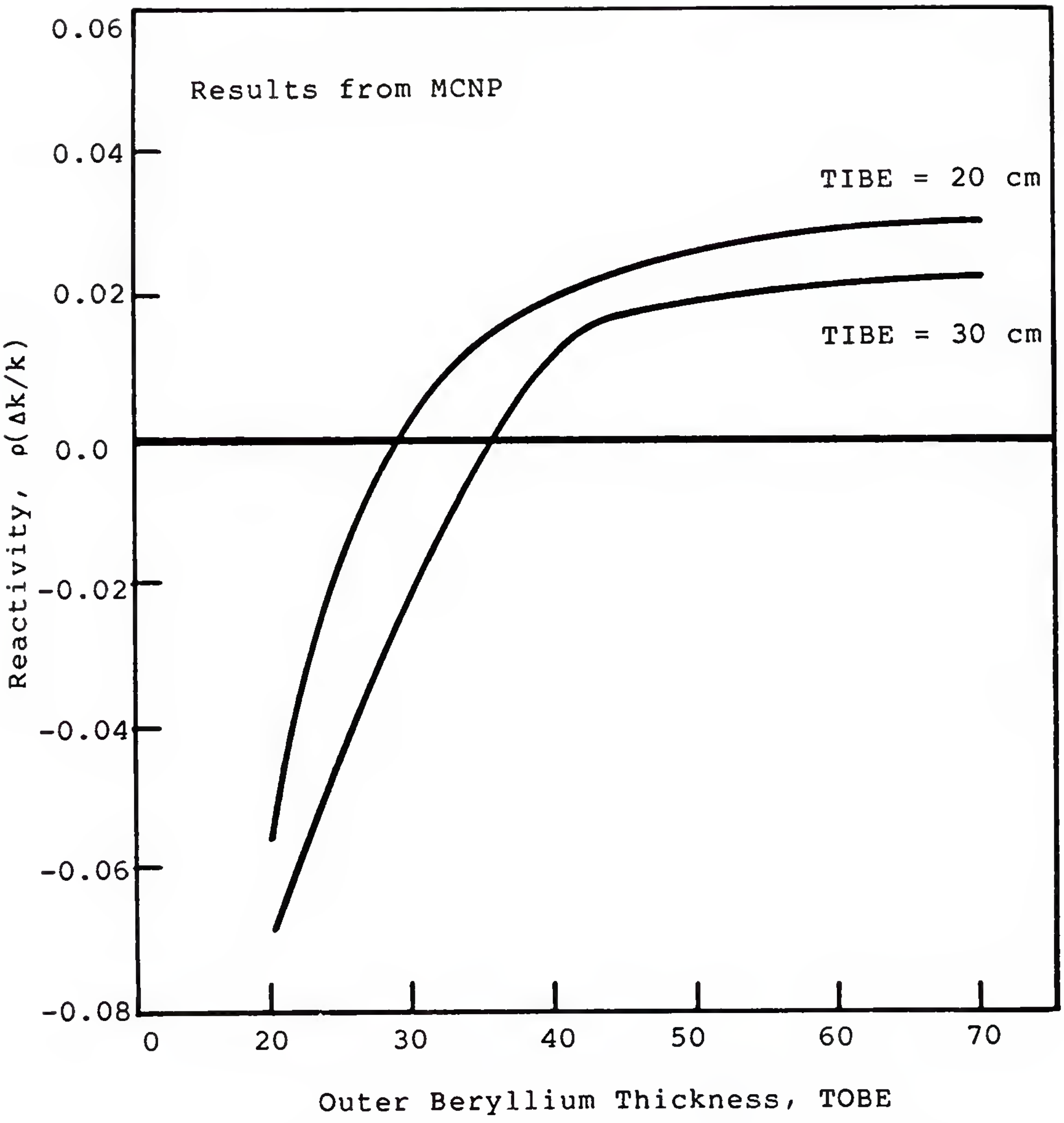

Figure 5-11. System Reactivity as a Function of Outer Beryllium Thickness.

with an increase in the outer beryllium thickness. Comparing the results for TIBE of 20 cm (Table 5-6) and those for TIBE of 30 cm (Table 5-7), the neutron generation times for a TIBE of 30 cm are 2% to 3% higher than the corresponding neutron generation times for a TIBE of 20 cm.

Effect of BPGCR core fuel loading and inner beryllium thickness variations when PGCR gas loading is fixed

Tables 5-8 through 5-11 give the average coupling coefficients among the cores, system neutron multiplication factor, neutron generation time, and reactivity of the BGCR system as a function of the central BPGCR fuel-gas loading for system configurations of inner beryllium thickness of 10 cm, 20 cm, 30 cm, and 40 cm, respectively. For this set of calculations, the PGCR cores are maintained at an equal fuel-gas loading of 10 atmospheres and the BPGCR chamber fuel-gas loading is varied from 25 atmospheres to 100 atmospheres.

The coupling coefficients listed in these Tables include the average coefficients corresponding to the neutronic contributions from the BPGCR chamber to the PGCR cores, from the PGCR cores to the central BPGCR chamber, and among the PGCR cores themselves. The coupling coefficients between the BPGCR chamber and the PGCR cores have been averaged over the number of PGCR cores for each case of BPGCR chamber fuel-gas loading. The core-to-core coupling coefficients for the PGCR cores are averaged in the manner described earlier in this chapter.

Table 5-8. Integral Kinetics Parameters as a Function of BPGCR Core Fuel-Gas Loading for the BGCR System with TIBE of 10 cm.

TOBE = 50 cm
PGCR Pressure = 10 atm UF_6/He

BPGCR Core Loading (atm)	Average Coupling Coefficient $(\alpha_{j \leftarrow k})$						k_{eff}	Λ (ms)	ρ
	BPGCR ↓ PGCR	PGCR ↓ BPGCR	2←3,13	2←4,12	2←5,11	2←6,10			
25	0.331	0.0348	0.239	0.0987	0.0438	0.0246	0.8246	3.2816	-0.2127
50	0.383	0.0216	0.225	0.0899	0.0357	0.0179	0.9898	2.2712	-0.0103
60	0.394	0.0186	0.232	0.0921	0.0368	0.0183	1.0411	2.0373	0.0395
75	0.393	0.0166	0.236	0.0891	0.0364	0.0179	1.0836	1.8383	0.0772
90	0.402	0.0145	0.234	0.0913	0.0375	0.0182	1.1262	1.6631	0.1121
100	0.404	0.0136	0.238	0.0939	0.0378	0.0174	1.1494	1.5826	0.1299

Results from MCNP

Table 5-9. Integral Kinetics Parameters as a Function of BPGCR Core Fuel-Gas Loading for the BGCR System with TIBE of 20 cm.

TOBE = 50 cm
PGCR Pressure = 10 atm UF_6/He

BPGCR Core Loading (atm)	Average Coupling Coefficient ($\alpha_{j \leftarrow k}$)						k_{eff}	Λ (ms)	ρ
	BPGCR ↓ PGCR	PGCR ↓ BPGCR	2←3,13	2←4,12	2←5,11	2←6,10			
25	0.334	0.0119	0.189	0.0514	0.0147	0.0061	0.8222	3.5174	-0.2162
50	0.366	0.0079	0.181	0.0465	0.0134	0.0057	1.0301	2.3153	0.0292
60	0.365	0.0077	0.190	0.0487	0.0130	0.0041	1.0305	2.1368	0.0296
75	0.412	0.0064	0.187	0.0488	0.0128	0.0037	1.0845	1.8285	0.0779
90	0.404	0.0049	0.183	0.0485	0.0137	0.0042	1.1529	1.6628	0.1326
100	0.432	0.0043	0.182	0.0457	0.0125	0.0040	1.1472	1.5978	0.1283

Results from MCNP

Table 5-10. Integral Kinetics Parameters as a Function of BPGCR Core Fuel-Gas Loading for the BGCR System with TIBE of 30 cm.

TOBE = 50 cm
PGCR Pressure = 10 atm UF_6/He

BPGCR Core Loading (atm)	Average Coupling Coefficient ($\alpha_{j \leftarrow k}$)						k_{eff}	Λ (ms)	ρ
	BPGCR ↓ PGCR	PGCR ↓ BPGCR	2←3,13	2←4,12	2←5,11	2←6,10			
25	0.246	0.0070	0.1540	0.0313	0.0072	0.0026	0.7477	3.8700	-0.3374
50	0.343	0.0038	0.1600	0.0291	0.0042	0.0011	0.9664	2.5050	-0.0348
60	0.417	0.0029	0.1500	0.0299	0.0060	0.0010	1.0262	2.1418	0.0255
75	0.408	0.0031	0.1530	0.0311	0.0053	0.0015	1.0630	1.9190	0.0593
90	0.406	0.0022	0.1470	0.0267	0.0062	0.0017	1.1395	1.7209	0.1224
100	0.415	0.0021	0.1540	0.0327	0.0069	0.0019	1.1636	1.6388	0.1406

Results from MCNP

Table 5-11. Integral Kinetics Parameters as a Function of BPGCR Core Fuel-Gas Loading for the BGCR System with TIBE of 40 cm.

TOBE = 50 cm
PGCR Pressure = 10 atm UF_6/He

BPGCR Core Loading (atm)	Average Coupling Coefficient ($\alpha_{j \leftarrow k}$)						k_{eff}	Λ (ms)	ρ
	BPGCR ↓ PGCR	PGCR ↓ BPGCR	2←3,13	2←4,12	2←5,11	2←6,10			
25	0.326	0.0026	0.1160	0.0184	0.0034	0.0012	0.7352	3.9391	-0.3602
50	0.391	0.0014	0.1210	0.0171	0.0029	0.0008	0.9280	2.5625	-0.0776
60	0.394	0.0012	0.1140	0.0183	0.0024	0.0005	1.0147	2.1524	0.0145
75	0.352	0.0010	0.1160	0.0153	0.0022	0.0008	1.0609	1.8890	0.0574
90	0.358	0.0011	0.1220	0.0201	0.0034	0.0006	1.1171	1.7671	0.1048
100	0.419	0.0008	0.1150	0.0192	0.0020	0.0004	1.1411	1.6247	0.1236

Results from MCNP

Tables 5-8 through 5-11 indicate that the average coupling coefficients $\alpha_{PGCR \leftarrow BPGCR}$ due to the neutronic contribution from the central BPGCR chamber to the PGCR cores increase with an increase in the BPGCR chamber fuel loading over the pressure range from 25 atmospheres to 60 atmospheres. For BPGCR chamber fuel loadings beyond 60 atmospheres the coupling coefficients $\alpha_{PGCR \leftarrow BPGCR}$ remain essentially unchanged. The fluctuations exhibited by the BPGCR-to-PGCR coupling coefficients can be attributed to the relatively large uncertainties in the quantities $S_{j \leftarrow k}$ and S_j which are obtained from MCNP.

Figure 5-12 illustrates the variation of average coupling coefficients due to neutronic contribution from the PGCR cores to the central BPGCR chamber, $\alpha_{BPGCR \leftarrow PGCR}$, as a function of the BPGCR chamber fuel-gas loading for inner beryllium thicknesses of 10 cm, 20 cm, 30 cm, and 40 cm. It can be seen from Figure 5-12 that the coupling coefficients, $\alpha_{BPGCR \leftarrow PGCR}$, generally decrease as the central chamber fuel loading increases. This decrease in the coupling coefficients with the increase in BPGCR chamber gas loading is larger for low BPGCR gas loading and low values of inner beryllium thickness. As the inner beryllium thickness increases, the neutronic coupling influence of the PGCR cores on the large central BPGCR chamber becomes less dependent on the BPGCR chamber fuel loading. Figure 5-13 illustrates the variation of the coupling coefficients,

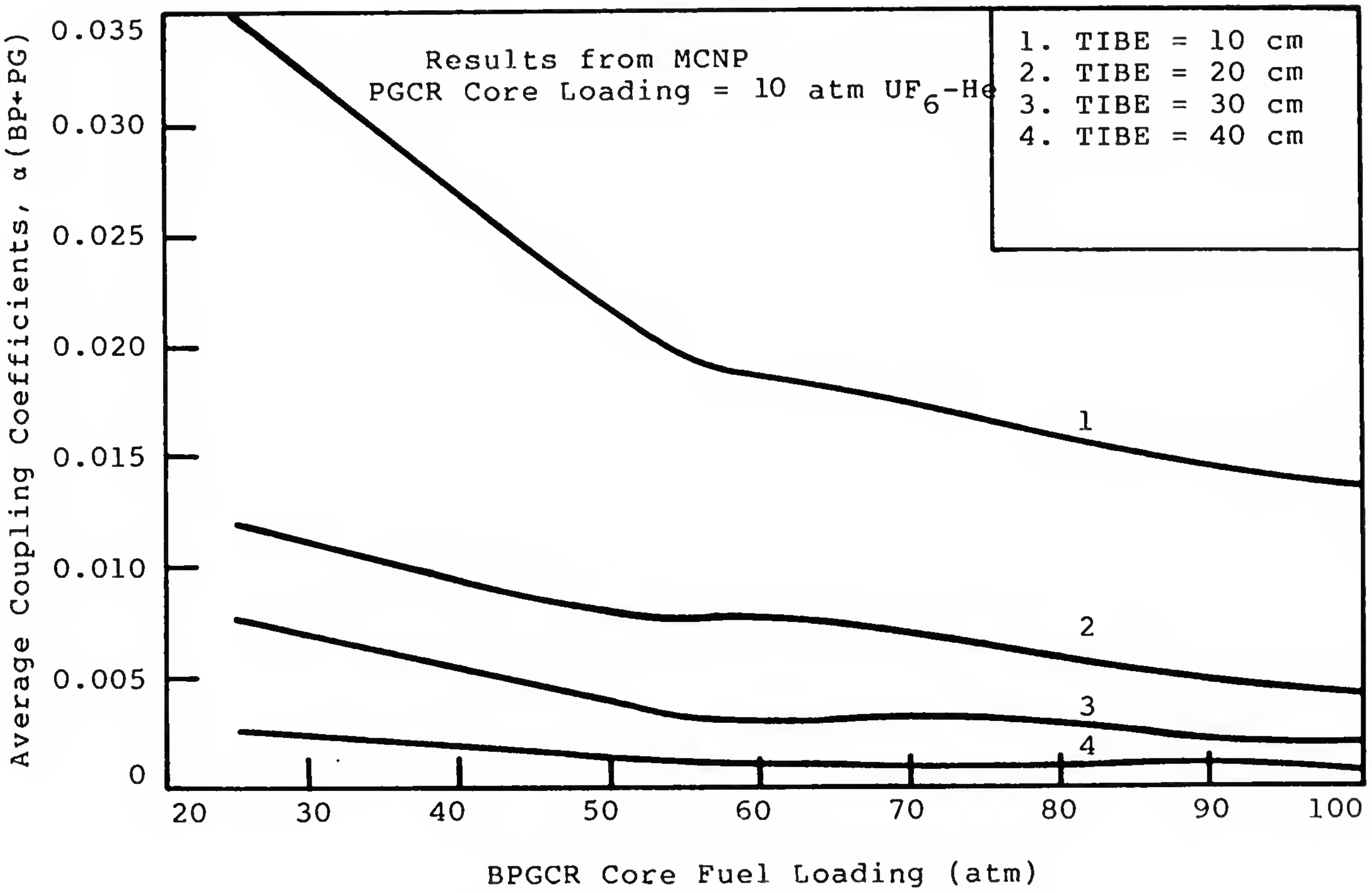

Figure 5-12. Average Coupling Coefficients (α_{jk}) due to Neutronic Contribution from PGCR Cores to BPGCR Chamber as a Function of BPGCR Core Fuel-Gas Loading.

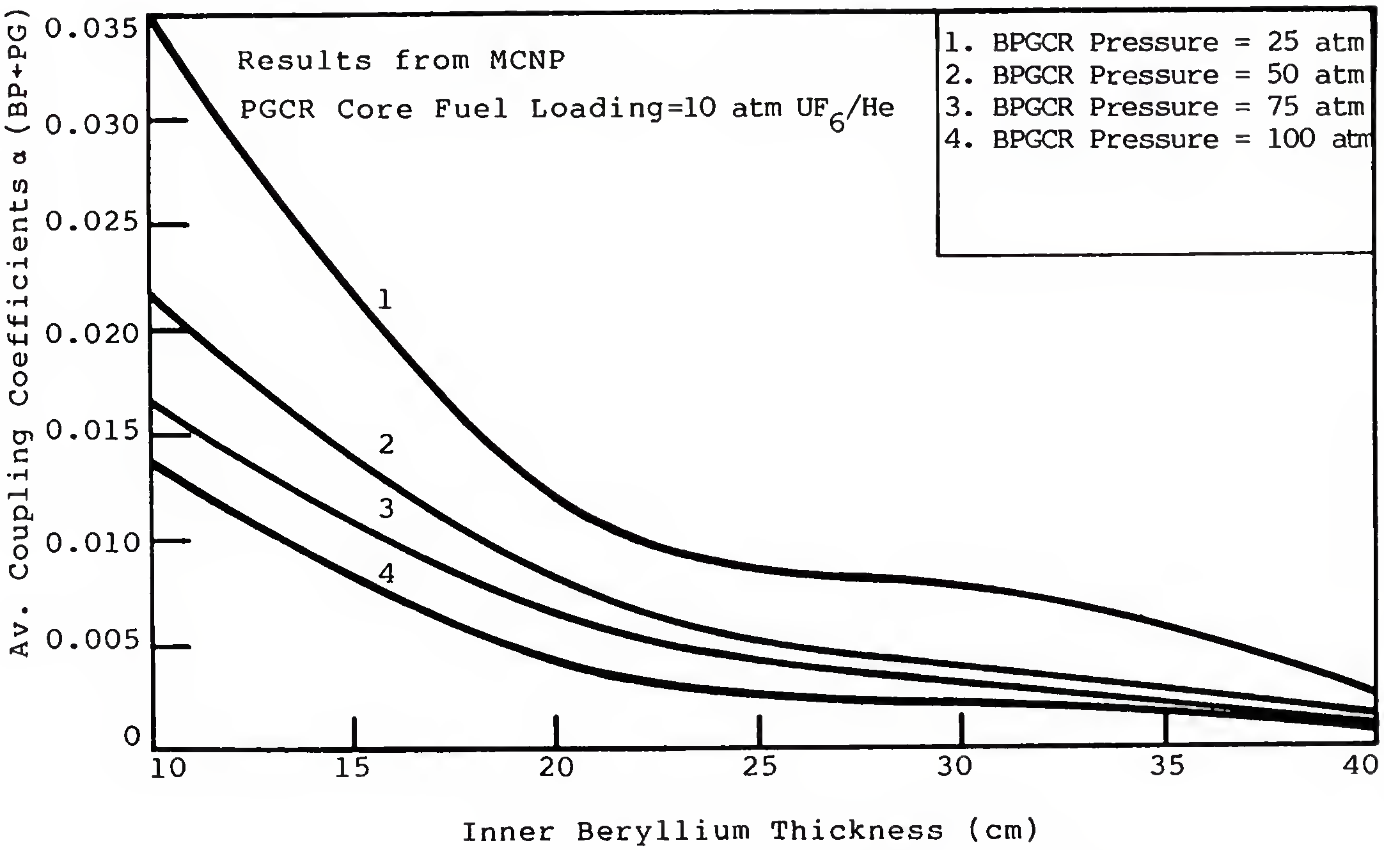

Figure 5-13. Average Coupling Coefficients (α_{jk}) due to Neutronic Contribution from PGCR Cores to BPGCR Chamber as a Function of Inner Beryllium Thickness.

$\alpha_{BPGCR \leftarrow PGCR}$, with the inner beryllium thickness for various BPGCR chamber fuel loadings. It can be seen that for any specific BPGCR chamber fuel loading, the coupling coefficients, $\alpha_{BPGCR \leftarrow PGCR}$, decrease with an increase in the inner beryllium thickness. The decrease in the neutronic coupling effect of the PGCR cores on the large central chamber with an increase in the BPGCR chamber fuel loading is mainly due to the fact that the PGCR cores are maintained at a constant low fuel loading of 10 atmospheres of UF_6-He mixture. The higher BPGCR loading means a greater reactivity worth for the central core and reduced relative worth for the PGCR cores and, hence, reduced coupling coefficients due to reduced neutronic influence of the smaller PGCR cores on the larger central BPGCR chamber. Figures 5-12 and 5-13 also show that for higher inner beryllium thicknesses the neutronic influence of the PGCR cores on the large central BPGCR chamber becomes less dependent on the BPGCR gas loading.

Tables 5-8 through 5-11 also give the coupling coefficients due to the neutronic interaction among the PGCR cores as a function of BPGCR chamber fuel loading. Figure 5-14 illustrates the typical variation of the average coupling coefficients among adjacent PGCR cores as a function of the inner beryllium thickness for BPGCR chamber loadings of 25 atmospheres and 100 atmospheres. The coupling coefficients for all other intermediate BPGCR

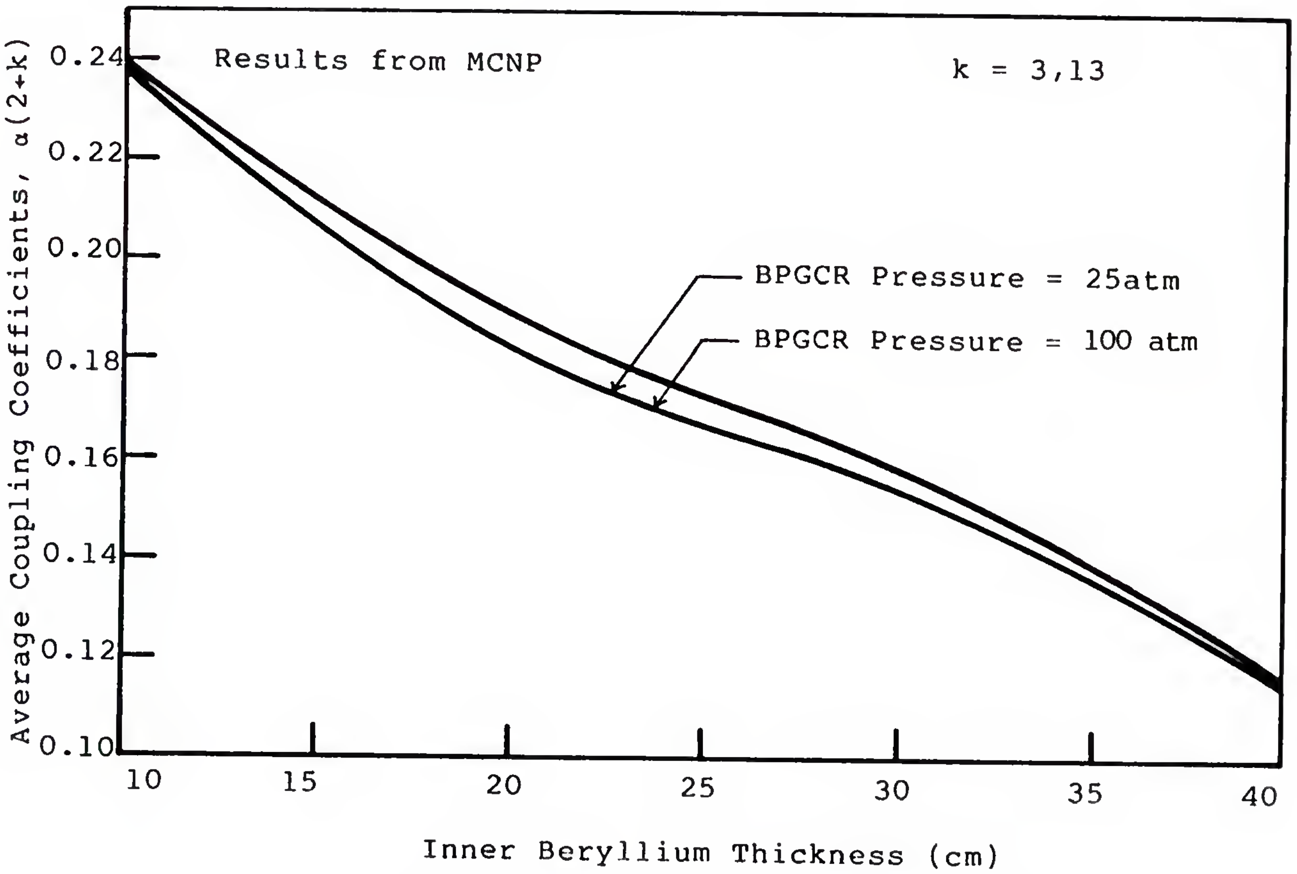

Figure 5-14. Average Coupling coefficients Between Adjacent PGCR Cores ($\alpha_{2\to3,13}$) as a Function of Inner Beryllium Thickness for a BGCR with a PGCR Gas Loading of 10 atmonspheres UF_6-He Mixture.

chamber gas loadings are very close to the values that are plotted in Figure 5-14 for 25 and 100 atmospheres. It can be seen that for any specific inner beryllium thickness, the coupling coefficients for the adjacent pair of PGCR cores are essentially independent of the BPGCR chamber fuel loading. This is due to the fact that the PGCR cores are maintained at a constant and relatively low fuel-gas loading of 10 atmospheres and that the strong neutronic coupling influence of the BPGCR chamber on the PGCR cores dominates the coupling among the PGCR cores as can be seen in the values for the α's listed in these tables. It can also be seen from Tables 5-8 through 5-11 and Figure 5-14 that for any specific central chamber fuel loading, the coupling coefficients decrease as the inner beryllium thickness increases.

Figure 5-15 shows the variation of neutron generation time as a function of inner beryllium thickness for the BPGCR system for the various BPGCR chamber fuel-gas loadings considered. It can be seen that for low BPGCR chamber fuel loadings of 25 and 50 atmospheres, the neutron generation time increases moderately with the increase in the inner beryllium thickness. For BPGCR gas loadings of 60 atmospheres and above, the neutron generation time is found to be essentially independent of the inner beryllium thickness for the range of TIBE examined in this section. Figure 5-16 illustrates the variation of neutron generation

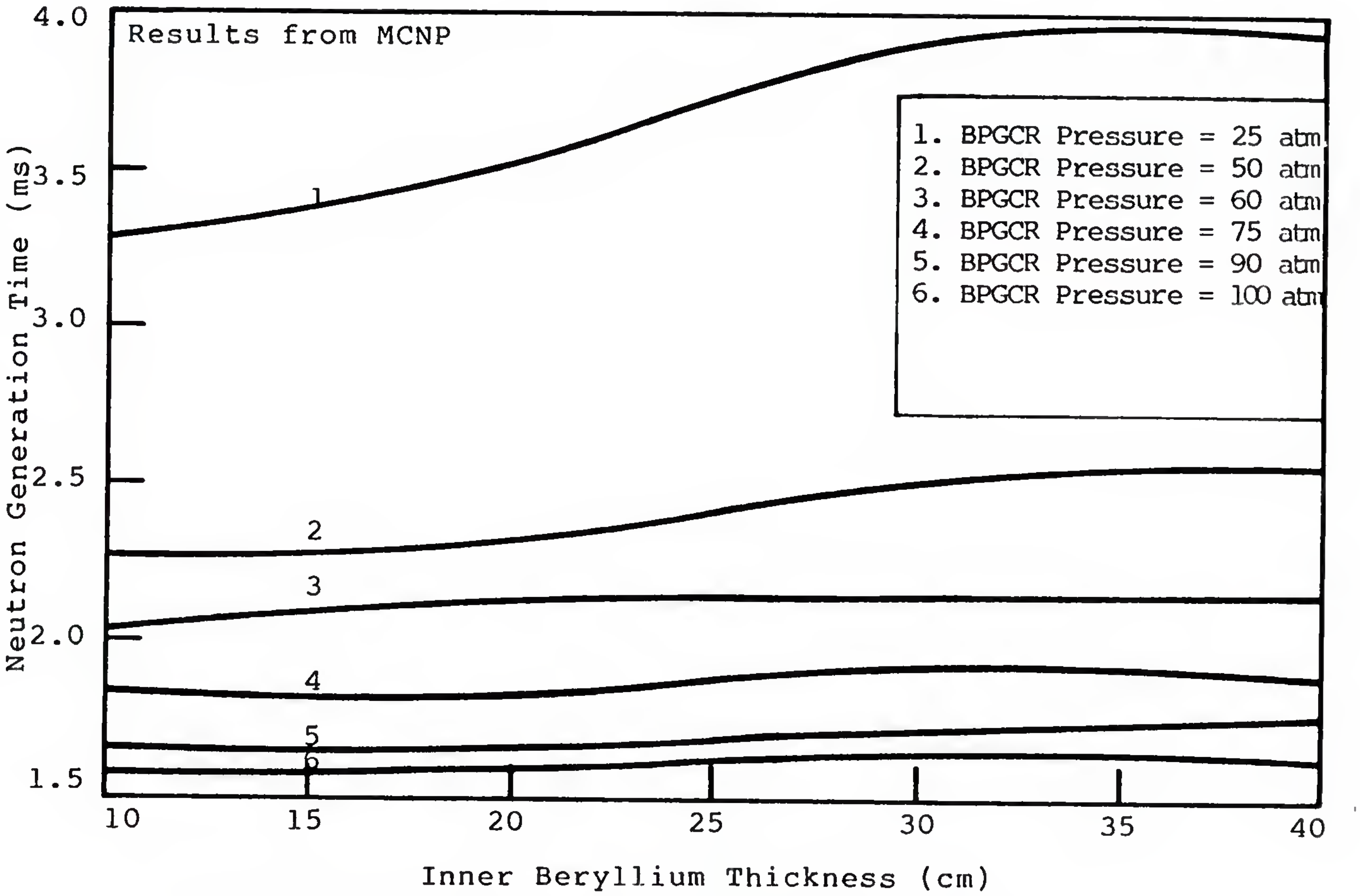

Figure 5-15. Neutron Generation Time (Λ) as a Function of Inner Beryllium Thickness of a BGCR System With PGCR Core Gas Loading of 10 Atmospheres UF_6-He Mixture.

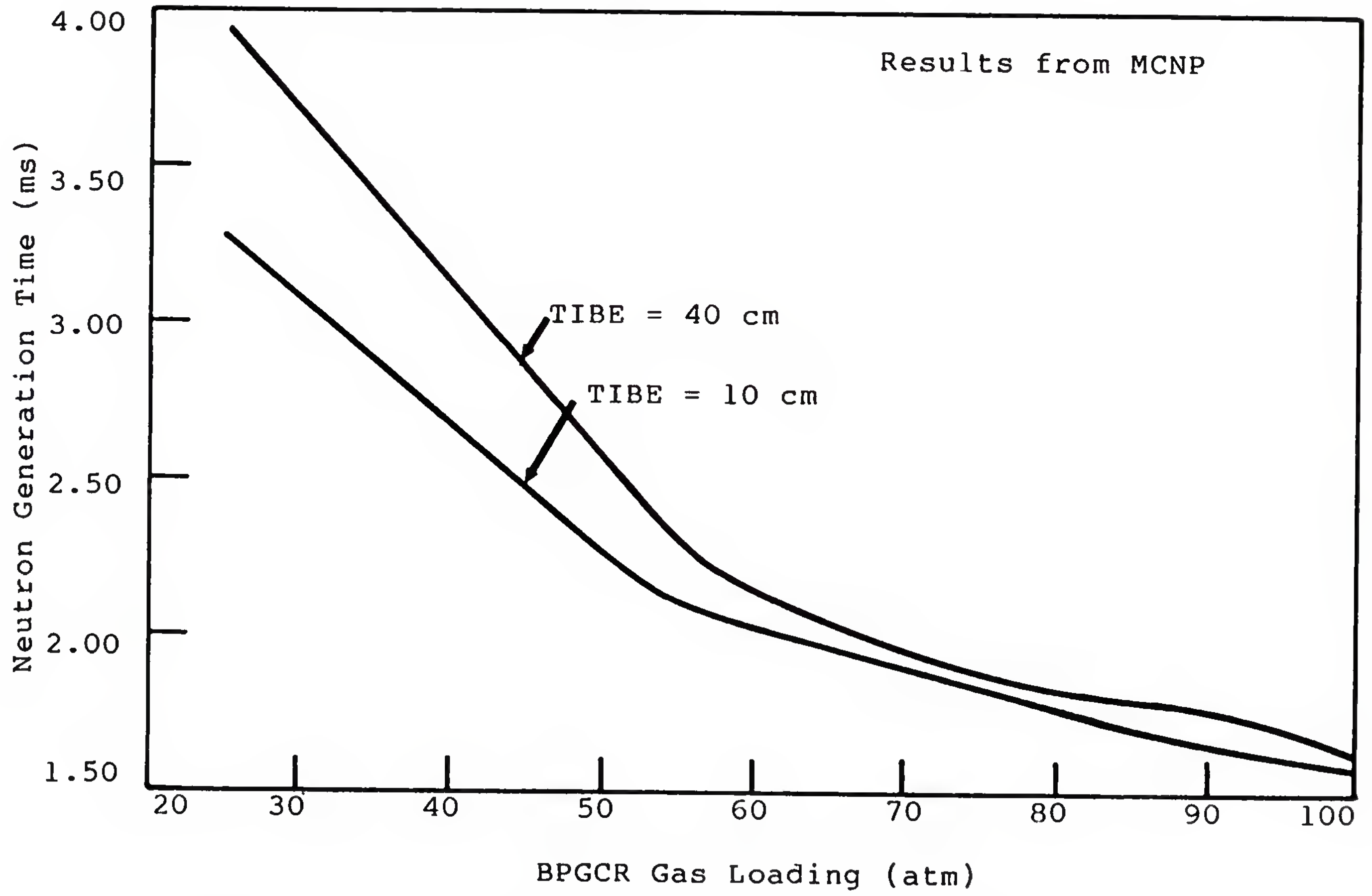

Figure 5-16. Neutron Generation Time (Λ) as a Function of BPGCR Chamber Gas Loading for a BGCR System for Inner Beryllium thickness of 10 cm and 40 cm.

time with the BPGCR gas loading for inner beryllium thicknesses of 10 cm and 40 cm. The neutron generation times for inner beryllium thickness of 20 and 30 cm lie within the range of values given by the two curves in Figure 5-16. For all the inner beryllium thicknesses considered, the neutron generation times decrease sharply with the BPGCR chamber gas loading for the range of BPGCR loading from 25 atmospheres to 55 atmospheres. For BPGCR gas loading above 55 atmospheres, the neutron generation time shows only a moderate decrease with increase in the BPGCR gas loading. This moderate decrease in neutron generation time for higher BPGCR gas loadings is due to the fact that beyond around 55 atmospheres the BPGCR core becomes black to neutrons as the fissile material density in the core increases.

Figure 5-17 illustrates the typical variation of the BGCR system reactivity with the central chamber gas-fuel loading for inner beryllium thicknesses of 10 cm and 40 cm. System reactivity for TIBE values of 20 and 30 cm for various BPGCR core loadings are very close to the values plotted in Figure 5-17 and they show the same trend. Figure 5-17 shows a sharp increase in system reactivity with an increase in BPGCR gas loading for the range of BPGCR gas loadings from 25 to 55 atmospheres; this is followed by a moderate increase in the system reactivity for BPGCR loadings above 55 atmospheres of fuel-gas mixture. The moderate increase in reactivity for higher BPGCR loadings is

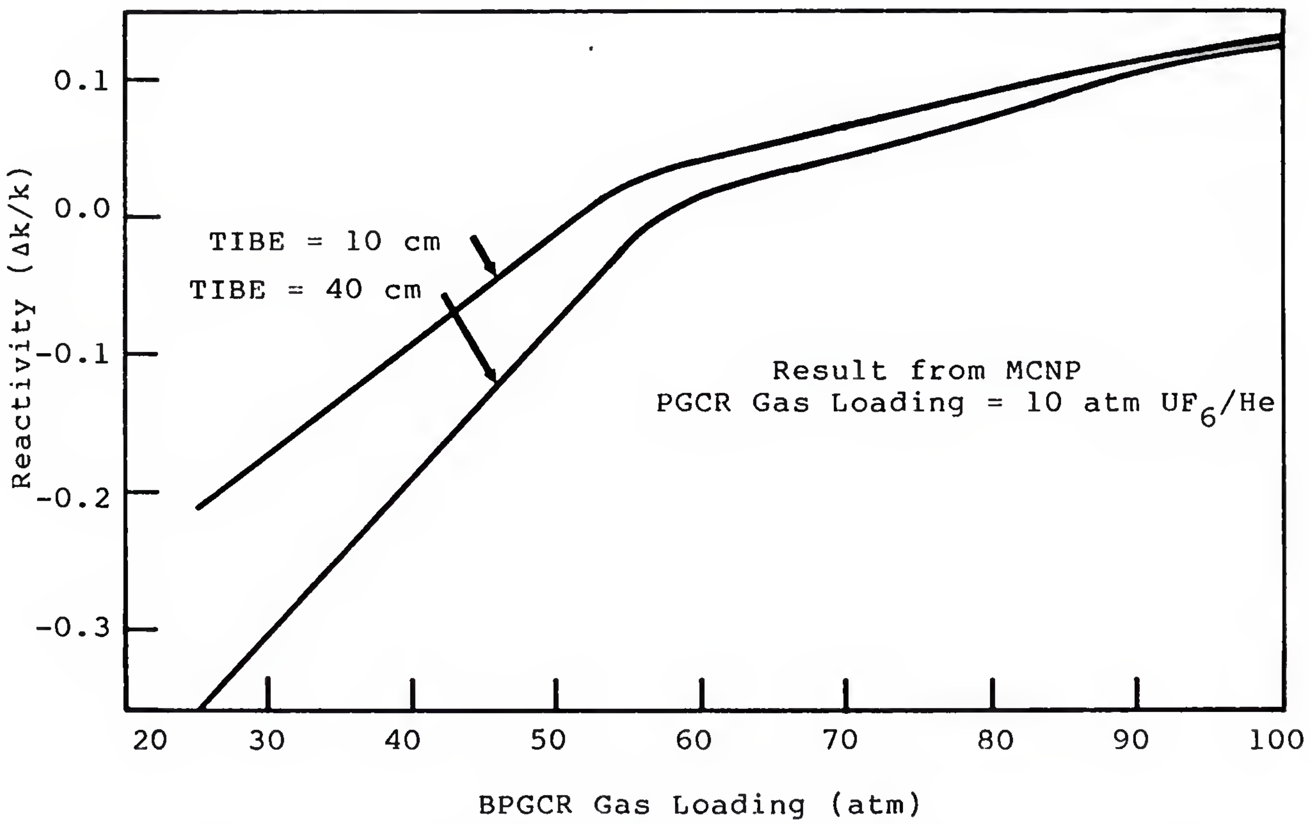

Figure 5-17. System Reactivity as a Function of BPGCR Gas Loading.

due to the fact that at around 55 to 60 atmospheres the BPGCR core becomes black to neutrons and undergoes a decreasing gain in k_{eff} as the fissile material density in the core increases.

Effect of PGCR core fuel loading and inner beryllium thickness variations when the BPGCR core has a nominal fuel loading

Tables 5-12 and 5-13 give the average coupling coefficients between the BPGCR chamber and the PGCR cores, the average coupling coefficients among the PGCR cores themselves, the system neutron multiplication factor (k_{eff}), neutron generation time, and the reactivity of the bimodal gaseous core reactor system as a function of PGCR core fuel-gas loading for inner beryllium thicknesses of 20 cm and 30 cm, respectively. The central chamber is maintained at a nominal fuel-gas loading of 25 atmospheres. The PGCR cores are loaded equally with fuel-gas mixture. The outer beryllium thickness is maintained at 50 cm.

It can be seen from Tables 5-12 and 5-13 that the average coupling coefficients, $\alpha_{PGCR \leftarrow BPGCR}$, due to the neutronic contribution from the central BPGCR chamber on the PGCR cores decrease as the PGCR core fuel gas loading increases. Figure 5-18 illustrates the variation of the average coupling coefficients due to the neutronic influence of the BPGCR chamber on the smaller PGCR cores with the PGCR core gas loading. In the previous section, for constant PGCR core fuel loading and increasing central chamber fuel

Table 5-12. Integral Kinetics Parameters as a Function of PGCR Core Fuel-Gas Loading for the BGCR System with TIBE of 20 cm.

TOBE = 50 cm
PGCR Pressure = 25 atm UF_6/He

PGCR Core Loading (atm)	Average Coupling Coefficient ($\alpha_{j \leftarrow k}$)						k_{eff}	Λ (ms)	ρ
	BPGCR ↓ PGCR	PGCR ↓ BPGCR	$2 \leftarrow 3,13$	$2 \leftarrow 4,12$	$2 \leftarrow 5,11$	$2 \leftarrow 6,10$			
10	0.334	0.0119	0.189	0.0144	0.0147	0.0061	0.8222	3.517	-0.2163
20	0.161	0.0200	0.155	0.0397	0.0109	0.0047	0.9127	2.796	-0.0956
30	0.112	0.0232	0.146	0.0324	0.0079	0.0033	1.0138	2.311	0.0136
40	0.084	0.0255	0.129	0.0267	0.0057	0.0028	1.0830	1.961	0.0766
50	0.070	0.0262	0.133	0.0220	0.0047	0.0022	1.1245	1.808	0.1107

Results from MCNP

Table 5-13. Integral Kinetics Parameters as a Function of PGCR Core Fuel-Gas Loading for the BGCR System with TIBE of 30 cm.

TOBE = 50 cm
PGCR Pressure = 25 atm UF_6/He

PGCR Core Loading (atm)	Average Coupling Coefficient $(\alpha_{j \leftarrow k})$						k_{eff}	Λ (ms)	ρ
	BPGCR $\downarrow$ PGCR	PGCR $\downarrow$ BPGCR	$2 \leftarrow 3,13$	$2 \leftarrow 4,12$	$2 \leftarrow 5,11$	$2 \leftarrow 6,10$			
10	0.246	0.0070	0.154	0.0313	0.0072	0.0026	0.7477	3.8700	-0.3374
20	0.144	0.0101	0.133	0.0226	0.0051	0.0021	0.8599	3.1182	-0.1629
30	0.089	0.0129	0.117	0.0181	0.0033	0.0013	0.9419	2.6138	-0.0617
40	0.066	0.0151	0.106	0.0144	0.0021	0.0013	1.0085	2.2877	0.0084
50	0.053	0.0167	0.095	0.0128	0.0019	0.0008	1.0683	2.0212	0.0639

Results from MCNP

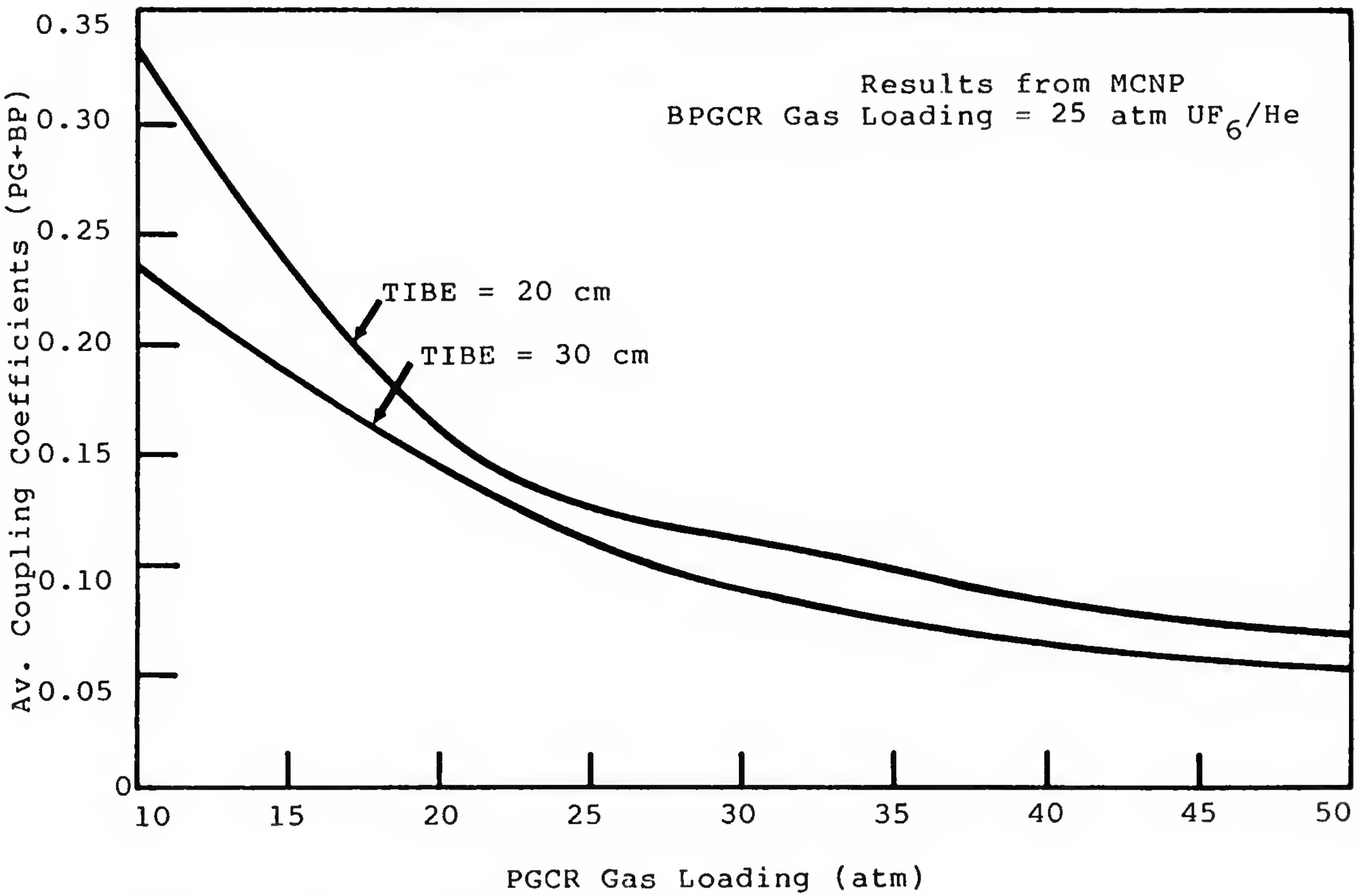

Figure 5-18. Average Coupling Coefficients due to Neutronic Contribution from BPGCR chamber to PGCR Cores as a Function of PGCR Gas Loading.

loading the neutronic coupling from the BPGCR chamber to the PGCR cores was found to increase initially for loadings up to about 60 atmospheres and then remaining essentially unchanged (see Tables 5-8 through 5-11). The decrease in the neutronic coupling influence of the BPGCR chamber on the PGCR cores with an increase in the PGCR core fuel loading (Table 5-12 and 5-13) is due to the decreased relative reactivity worth of the BPGCR chamber. Comparing the results from Tables 5-12 and 5-13 the neutronic coupling influence of the BPGCR chamber on the PGCR cores is about 20-30% less for the case of inner beryllium thickness of 30 cm than for the case of TIBE of 20 cm.

Tables 5-12 and 5-13 also give the neutronic coupling influence of the PGCR cores on the central BPGCR chamber as a function of PGCR gas loading for inner beryllium thicknesses of 20 cm and 30 cm, respectively. Figure 5-19 illustrates the variation of the average coupling coefficients due to the neutronic contribution from the PGCR cores to the central BPGCR chamber as a function of the PGCR gas loading. Tables 5-12 and 5-13 and Figure 5-19 show that the neutronic influence of the PGCR cores on the central chamber increases with an increase in the PGCR core loading. This is to be contrasted with the results of the previous section where the PGCR cores were maintained at constant fuel loading while the central chamber fuel loading was increased (Tables 5-1 through 5-5). The increase in the

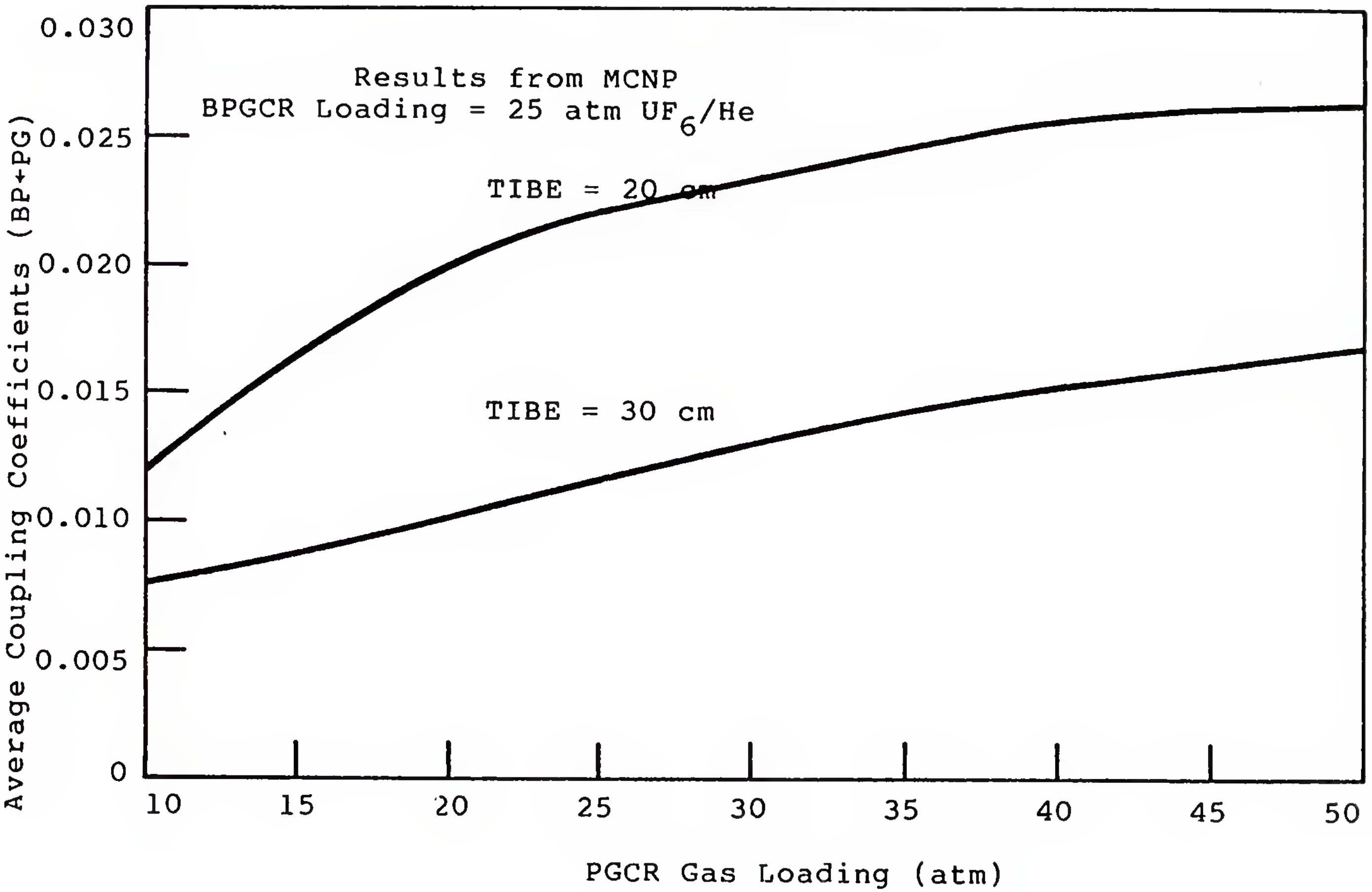

Figure 5-19. Average Coupling Coefficients due to Neutronic Contribution from PGCR Cores to BPGCR Chamber of the BGCR As a Function of PGCR Core Gas Loading.

coupling influence of PGCR cores on the central chamber is due to the increase in the PGCR core fuel loading. Comparing Table 5-12 with Table 5-13, it can be seen that the coupling coefficients decrease as the inner beryllium thickness increases.

The average coupling coefficients among the PGCR cores themselves as a function of PGCR gas loading are also given in Tables 5-12 and 5-13. Figure 5-20 illustrates the variation of the average coupling coefficients ($\alpha_{2\leftarrow3,12}$) between adjacent PGCR cores as a function of PGCR gas loading for inner beryllium thicknesses of 20 cm and 30 cm. Figure 5-20 also illustrates the variation of the coefficients for the case in which the central chamber is unfueled (Tables 5-2 and 5-4). For a specific inner beryllium thickness, the coupling coefficients among the PGCR cores decrease as the PGCR core fuel loading increases. It can be seen from the two sets of curves in Figure 5-20 and from Tables 5-2 and 5-4, 5-12, and 5-13 that the coupling coefficients among the PGCR cores when the central BPGCR chamber is unfueled are 3 to 4% higher than the corresponding coupling coefficients when the central chamber is fueled. The main reason for the lower PGCR core-to-core coupling when the central chamber is fueled is due to the overall (net) loss of neutrons from the PGCR cores to the central BPGCR chamber. When the central chamber is unfueled neutrons emerging from any PGCR core will be able traverse

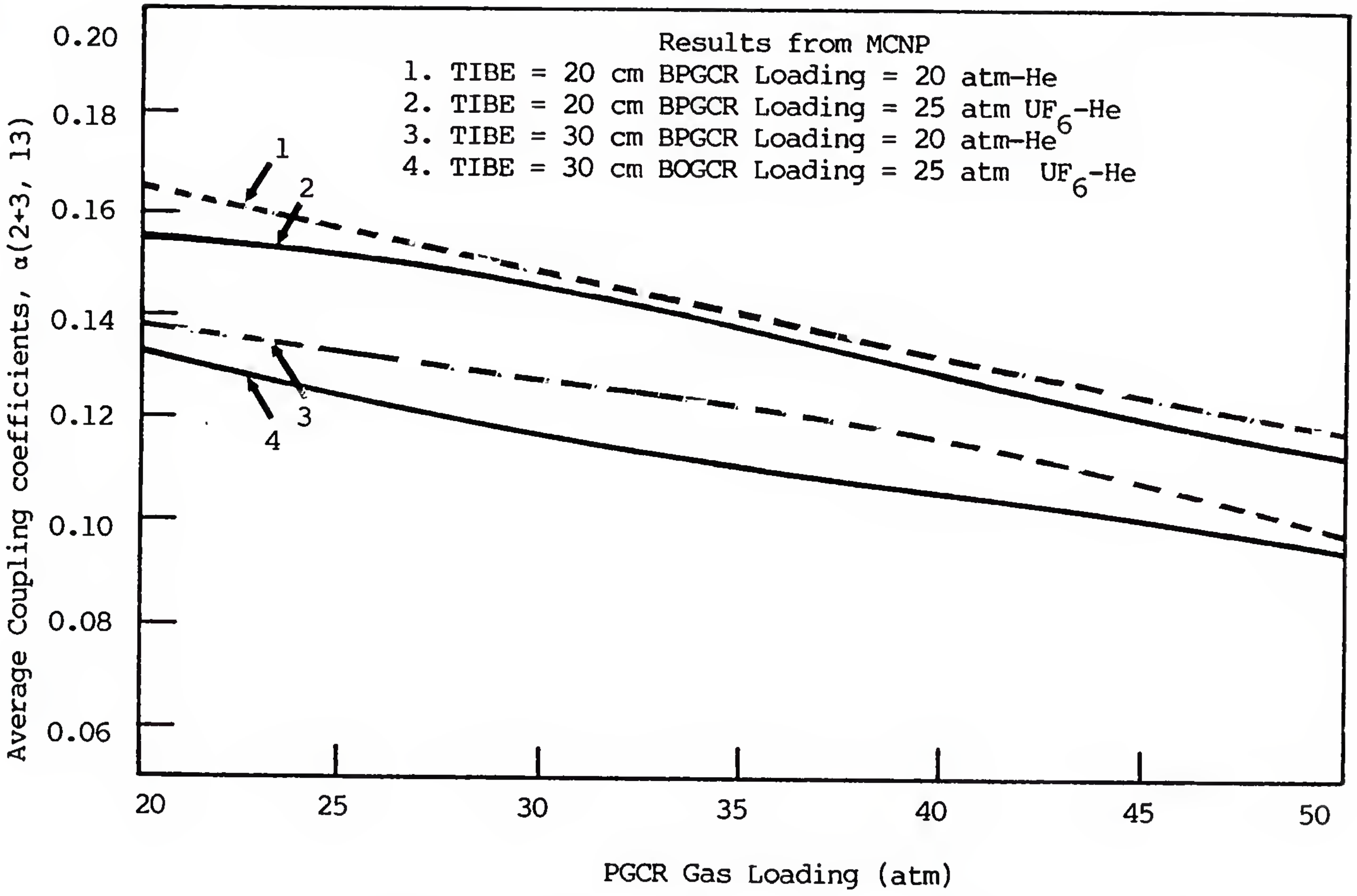

Figure 5-20. Average Coupling Coefficients Between Adjacent PGCR Cores as a Function of PGCR Gas Loading for the BGCR for both Unfueled and Fueled BPGCR Chamber.

the central chamber without any interaction there and enter another PGCR core. In contrast, when the central chamber is fueled the neutrons emerging from a PGCR core have a probability of being absorbed in the central chamber rather than in another PGCR core.

Figure 5-21 illustrates the variation of neutron generation time as a function of PGCR gas loading for inner beryllium thicknesses of 20 cm and 30 cm. Figure 5-21 also presents the variation of neutron generation time with PGCR gas loading for the case in which the central chamber is unfueled (Tables 5-2 and 5-4). It can be seen that for a specific PGCR gas loading, the neutron generation time of the BGCR system with unfueled central chamber is much higher (21% to 52% for TIBE of 20 cm and 14% to 40 % for TIBE of 30 cm) than the respective neutron generation time with fueled central chamber. The reason for the shorter neutron generation time with fueled central chamber is due to the fact that the fueled central chamber increases the absorption and thereby reduces the generation time of neutrons.

Figure 5-22 illustrates the variation of reactivity of the BGCR system with the PGCR gas loading for inner beryllium thicknesses of 20 cm and 30 cm. Figure 5-22 also presents the variation of reactivity with PGCR gas loading for the case when the central BPGCR chamber is unfueled. It can be seen that when the BPGCR chamber is unfueled, the

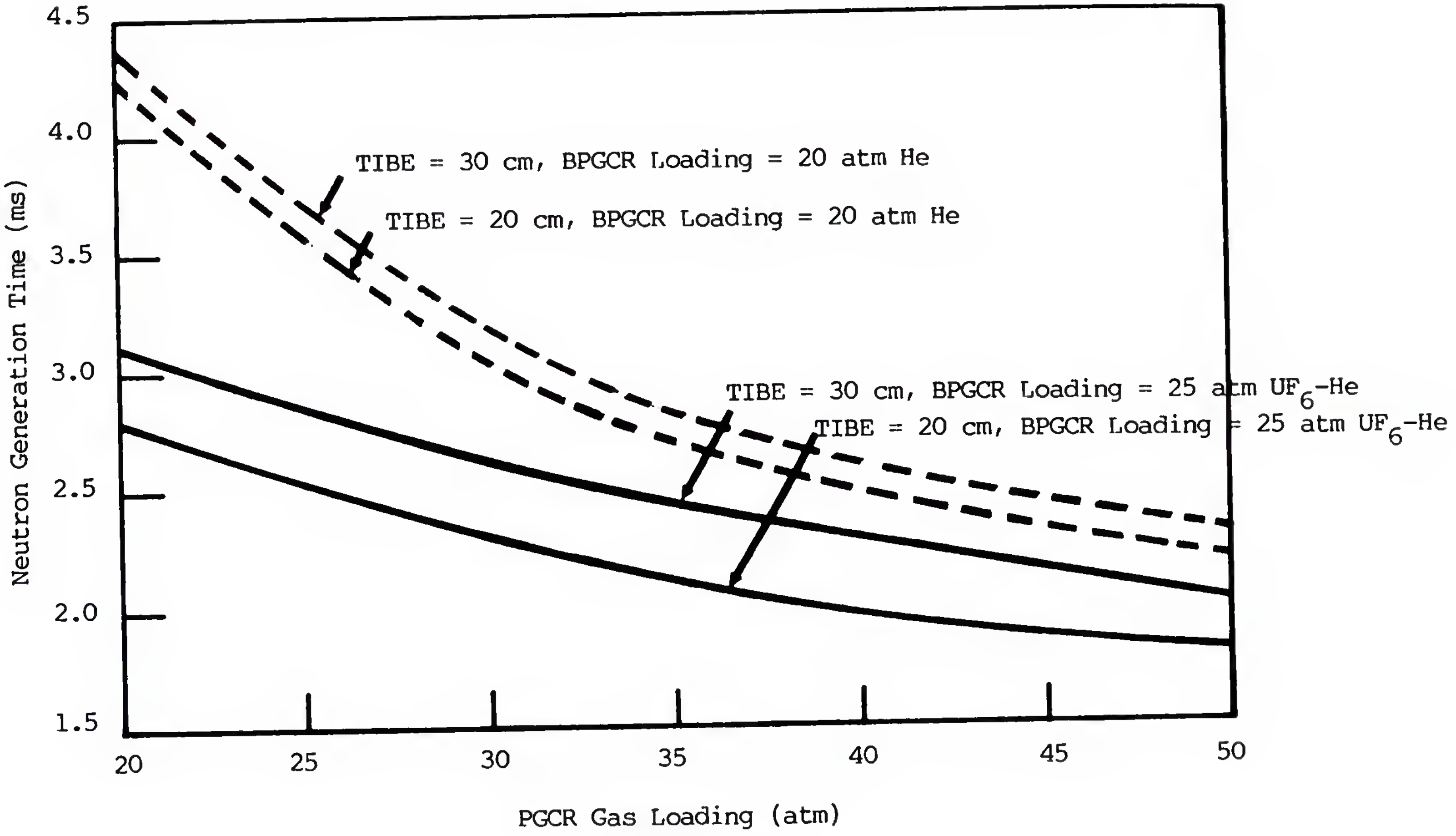

Figure 5-21. Neutron Generation Time as a Function of PGCR Core Gas Loading for the BGCR with Fueled and Unfueled BPGCR Chamber.

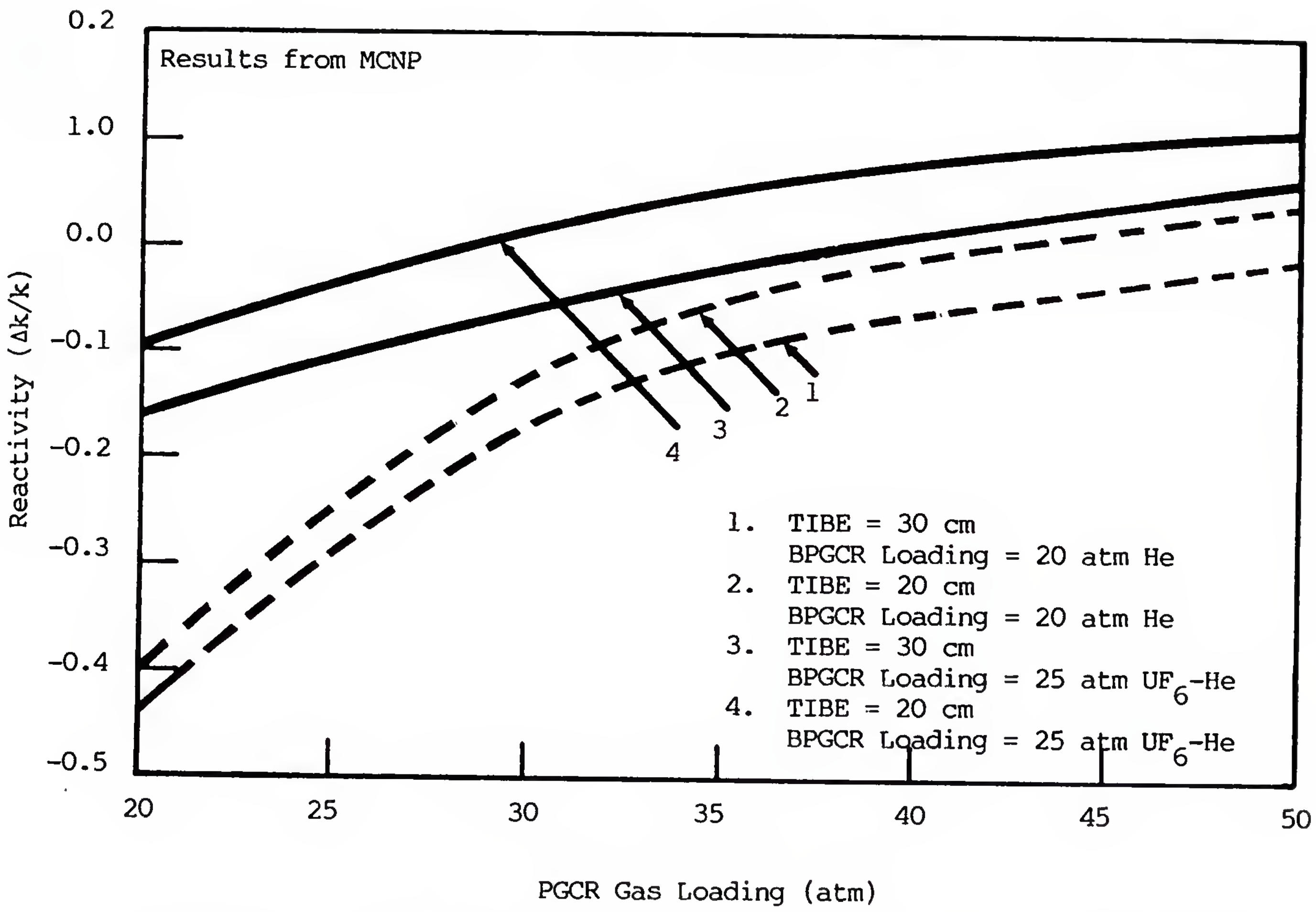

Figure 5-22. System Reactivity as a Function of PGCR Core Gas Loading for the BGCR with Unfueled and Fueled BPGCR Chamber.

reactivity increases sharply with PGCR gas loading up to about 35 atmospheres and thereafter increases moderately with an increase in the PGCR gas loading. In contrast, when the BPGCR is fueled, the increase of reactivity with PGCR loading is gradual throughout the range of examined gas loadings. The fueled central chamber is responsible for the larger reactivity and more gradual increase in the system reactivity throughout the range of PGCR gas loadings.

Effect of unequal PGCR core loading when the BPGCR core is unfueled

This section examines the coupling coefficients among the PGCR cores for a few selected cases in which the PGCR cores are loaded unequally among themselves with UF_6-He mixture. The effect of unequal PGCR core fuel-gas loading on the neutron removal lifetime and neutron generation time is also examined in this section. Tables 5-14 through 5-18 give the average coupling coefficients among the PGCR cores of the BGCR system when the PGCR cores are loaded unequally with UF_6-He mixture for various indicated loading patterns; the central BPGCR chamber is filled with helium at 20 atmospheres. The inner beryllium thickness for these cases is 20 cm and the outer beryllium thickness is maintained at 50 cm. Each table also gives the system neutron multiplication factor, neutron removal lifetime, and neutron generation time.

Table 5-14. Average Coupling Coefficients Among the PGCR Cores of the BGCR System with a TIBE of 20 cm When the PGCR Core Loading Pattern Is [60(4), 20(4), 10(4)]*.

BPGCR Pressure = 20 atmospheres He
System Neutron
Multiplication Factor = 0.8521
Neutron Removal Lifetime = 2.778 ms
Neutron Generation Time = 3.200 ms

	Average Coupling Coefficients ($\alpha_{j\leftarrow k}$)				
Core k→	2	3	4	5	6
Core j					
2	0.3357	0.0938	0.0247	0.0133	0.0047
3	0.2062	0.4730	0.1605	0.0797	0.0067
4	0.0866	0.2258	0.5375	0.2779	0.0393
5	0.0112	0.0242	0.0699	0.3357	0.0438
6	0.0084	0.0116	0.0342	0.2062	0.4730

*PGCR Core Fuel Loading Pattern:
Core # 2, 5, 8, 11 at 60 atmospheres
Core # 3, 6, 9, 12 at 20 atmospheres
Core # 4, 7, 10, 13 at 10 atmospheres

Table 5-15. Average Coupling Coefficients Among the PGCR Cores for the BGCR System with a TIBE of 20 cm When the PGCR Core Loading Pattern Is [50(4), 30(4), 20(4)]*.

BPGCR Pressure = 20 atmospheres He
System Neutron
Multiplication Factor= 0.8602
Neutron Removal Lifetime = 2.533 ms
Neutron Generation Time = 2.945 ms

	Average Coupling Coefficients ($\alpha_{j \leftarrow k}$)				
Core k→	2	3	4	5	6
Core j					
2	0.3595	0.1034	0.0214	0.0108	0.0039
3	0.1548	0.4258	0.1415	0.0432	0.0093
4	0.0432	0.1916	0.4713	0.1803	0.0319
5	0.0084	0.0357	0.1011	0.3595	0.1034
6	0.0058	0.0120	0.0235	0.1548	0.4258

*PGCR Core Fuel Loading Pattern:
Core # 2, 5, 8, 11 at 50 atmospheres
Core # 3, 6, 9, 12 at 30 atmospheres
Core # 4, 7, 10, 13 at 20 atmospheres

Table 5-16. Average Coupling Coefficients Among the PGCR Cores for the BGCR System with a TIBE of 20 cm When the PGCR Core Loading Pattern Is [70(4), 30(4), 20(4)]*.

BPGCR Pressure = 20 atmospheres He
System Neutron
Multiplication Factor= 0.9256
Neutron Removal Lifetime = 2.456 ms
Neutron Generation Time = 2.653 ms

	Average Coupling Coefficients ($\alpha_{j \leftarrow k}$)				
Core k→	2	3	4	5	6
Core j					
2	0.3113	0.0723	0.0203	0.0119	0.0028
3	0.1183	0.4328	0.1416	0.0579	0.0038
4	0.0469	0.1981	0.4878	0.1743	0.0258
5	0.0108	0.0263	0.0811	0.3113	0.0723
6	0.0009	0.0070	0.0229	0.1183	0.4328

*PGCR Core Fuel Loading Pattern:
Core # 2, 5, 8, 11 at 70 atmospheres
Core # 3, 6, 9, 12 at 30 atmospheres
Core # 4, 7, 10, 13 at 20 atmospheres

Table 5-17. Average Coupling Coefficients Among the PGCR Cores for the BGCR System with a TIBE of 20 cm When the PGCR Core Loading Pattern Is [80(4), 40(4), 30(4)]*.

BPGCR Pressure = 20 atmospheres He
System Neutron
Multiplication Factor= 1.0206
Neutron Removal Lifetime = 2.307 ms
Neutron Generation Time = 2.260 ms

	Average Coupling Coefficients ($\alpha_{j\leftarrow k}$)				
Core k→	2	3	4	5	6
Core j					
2	0.2906	0.0700	0.0265	0.0156	0.0077
3	0.1529	0.3912	0.0629	0.0438	0.0089
4	0.0413	0.1466	0.4296	0.1629	0.0220
5	0.0369	0.0203	0.0883	0.2906	0.0700
6	0.0057	0.0049	0.0199	0.1529	0.3912

*PGCR Core Fuel Loading Pattern:
Core # 2, 5, 8, 11 at 80 atmospheres
Core # 3, 6, 9, 12 at 40 atmospheres
Core # 4, 7, 10, 13 at 30 atmospheres

Table 5-18. Average Coupling Coefficients Among the PGCR Cores for the BGCR System with a TIBE of 20 cm When the PGCR Core Loading Pattern Is [70(6), 10(6)]*.

BPGCR Pressure = 20 atmospheres He
System Neutron
Multiplication Factor= 0.9068
Neutron Removal Lifetime = 2.581 ms
Neutron Generation Time = 2.846 ms

	Average Coupling Coefficients ($\alpha_{j \leftarrow k}$)			
Core k→	2	3	4	5
Core j				
2	0.3216	0.0760	0.0335	0.0049
3	0.2527	0.5315	0.2475	0.0277
4	0.0356	0.0759	0.3216	0.0761
5	0.0148	0.0269	0.2527	0.5315

*PGCR Core Fuel Loading Pattern:
Core # 2, 4, 6, 8, 10, 12 at 70 atmospheres
Core # 3, 5, 7, 9, 11, 13 at 10 atmospheres

Table 5-14 gives the average coupling coefficients among the PGCR cores when the core loading pattern is [60(4),20(4),10(4)]. This core loading pattern can be explained with the aid of Figure A-3 of Appendix A. PGCR cores 2, 3, and 4 are loaded with UF_6-He mixture at pressures of 60, 20, and 10 atmospheres, respectively. This loading pattern is repeated for the rest of the PGCR cores. The averaging of the coupling coefficients for the unequal PGCR core loading pattern is done in a manner different from the case where the PGCR cores are loaded equally. Since the PGCR core loading pattern is repeated over the four quarters of the BGCR system as represented in the top view of Figure A-3, the coupling coefficients for a given pair of cores are averaged for the four quarters of the reactor system. For example, the coupling coefficient α_{32} in Table 5-14 is the average of α_{32}, α_{65}, α_{98}, and α_{1211} and the coupling coefficient α_{23} is the average of α_{23}, α_{56}, α_{89}, and α_{1112}. It can be seen from the Tables 5-14 through 5-18 that since the fuel-gas loadings of any given adjacent pairs of the cores are different, the coupling contributions between the adjacent pairs of the cores are different in the two directions, i.e., the neutronic coupling contribution from any specific core to an adjacent core is different from the contribution from the latter to the former core. The coupling contribution from any core of higher fuel loading to a core of lower fuel loading is larger than the contribution from the core of lower fuel loading to the core of higher fuel loading. For example, the coupling coefficient, α_{32} is 0.2062 while α_{23} is 0.0938. The reason for this is due to the fact that the reactivity worth of the core with larger fuel loading is greater than the reactivity worth of the core with smaller fuel loading.

Table 5-15 gives the average coupling coefficients among the PGCR cores for the BGCR system when the PGCR core loading pattern is [50(4),30(4),20(4)]. Tables 5-16 and 5-17 give the coupling coefficients among the PGCR cores when the PGCR core loading pattern are [70(4),30(4),20(4)] and [80(4),40(4),30(4)], respectively. Table 5-18 gives the average coupling coefficients among the PGCR cores when the PGCR core loading pattern is [70(6),10(6)] in which alternate cores are loaded with UF_6-He mixture at pressures of 70 and 10 atmospheres.

Table 5-19 gives the average coupling coefficients among the PGCR cores of the BGCR system when the PGCR core loading pattern is [80(4),40(4),30(4)] and the inner beryllium thickness is 30 cm. Comparing the respective results of Table 5-19 and 5-17, it can be seen that the coefficients representing "self" coupling (core-to-itself) are about 7-8% higher for system with a TIBE of 30 cm than those for the system with a TIBE of 20 cm. This is due to the fact that the larger beryllium moderator region around any core for the system with a TIBE of 30 cm is capable of

Table 5-19. Average Coupling Coefficients Among the PGCR Cores for the BGCR System with a TIBE of 30 cm When the PGCR Core Loading Pattern Is [80(4), 40(4), 30(4)]*.

BPGCR Pressure = 20 atmospheres He
System Neutron
Multiplication Factor= 1.0103
Neutron Removal Lifetime = 2.295 ms
Neutron Generation Time = 2.272 ms

	Average Coupling Coefficients ($\alpha_{j \leftarrow k}$)				
Core k→	2	3	4	5	6
Core j					
2	0.3143	0.0684	0.0081	0.0039	0.0014
3	0.1231	0.4119	0.1054	0.0292	0.0033
4	0.0287	0.1253	0.4655	0.1515	0.0123
5	0.0029	0.0269	0.0678	0.3143	0.0684
6	0.0036	0.0118	0.0082	0.1231	0.4199

*PGCR Core Fuel Loading Pattern:
Core # 2, 5, 8, 11 at 80 atmospheres
Core # 3, 6, 9, 12 at 40 atmospheres
Core # 4, 7, 10, 13 at 30 atmospheres

returning a higher fraction of thermalized neutrons back to the same core. Comparison of Tables 5-19 and 5-17, indicates that the core-to-core coupling coefficients (excluding self coupling) for the system with a TIBE of 30 cm are less than the corresponding coefficients for the system with a TIBE of 20 cm except for $\alpha_{5\leftarrow 3}$ and $\alpha_{3\leftarrow 4}$. The isolated reverse trend in these two values is due to the relatively large uncertainty in the respective coupling contributions calculated by MCNP.

Examination of the BGCR system with unequal PGCR fuel-gas loading is done to simulate the situation in which there are always fractions of the total number of PGCR cores in the intake, power and exhaust phases of operation so that the reactor will be capable of delivering a continuous supply of hot, pressurized gas to the power conversion unit.

Results from Coupled Core Kinetics Analysis: Core Neutron Level and Delayed Neutron Precursor Concentration Variations

The coupled core point reactor kinetics program, COUPKIN, calculates the core neutron level and delayed neutron precursor concentrations at any time during operation of the bimodal gaseous core reactor system. The method of solution of the coupled core point reactor kinetics equations employed in COUPKIN is described in detail in Appendix B and a brief description of this solution procedure is given earlier in this Chapter. This section examines the dependence of the core neutron level and the delayed neutron precursor concentration on the PGCR and BPGCR core fuel-gas loading, inner and outer beryllium thickness, core-to-core coupling coefficients, and delay times for the BGCR system. The effect of various cycle times of operation on core neutron level during low power PGCR operation is also examined in this section.

Fueled PGCR cores and unfueled BPGCR core

The effects of variations in inner beryllium thickness, core-to-core coupling coefficients and delay times, and cycle times on PGCR neutron level for low power operation when the PGCR cores are loaded equally and the central BPGCR chamber is unfueled are examined in this section.

Figures 5-23 through 5-26 illustrate typical variations in relative PGCR core neutron level ($N_j(t)/N_j(0)$) and the neutron multiplication factor as a function of cycle time for BGCR systems with inner beryllium thicknesses of 20 cm, 25 cm, 30 cm, and 40 cm, respectively. The cycle time for the 20 cm, 25 cm, and 30 cm inner beryllium thickness cases is 0.20 seconds; for the 40 cm inner beryllium thickness the cycle time is 0.3 seconds. It is assumed that at the start of the cycle the fuel-gas mixture pressure in the PGCR core is 20 atmospheres and can be considered as a residual gas pressure from a previous cycle. The PGCR core gas loading is then raised during the intake phase of operation and the gas is exhausted during the exhaust phase of PGCR operation. For various configurations considered, the core fuel loading

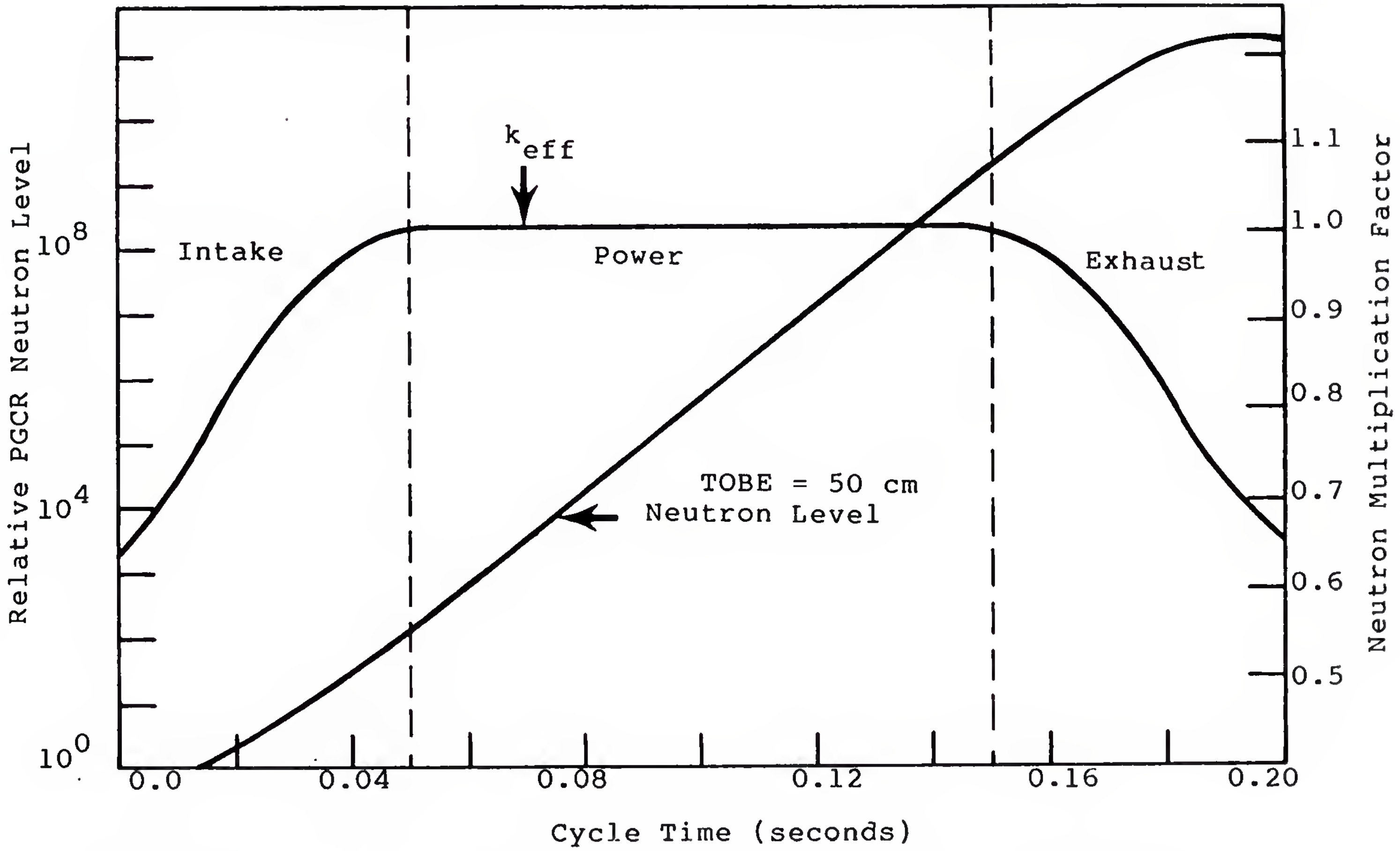

Fiture 5-23. Relative PGCR Neutron Level and k_{eff} as a Function of Time for TIBE of 20 cm.

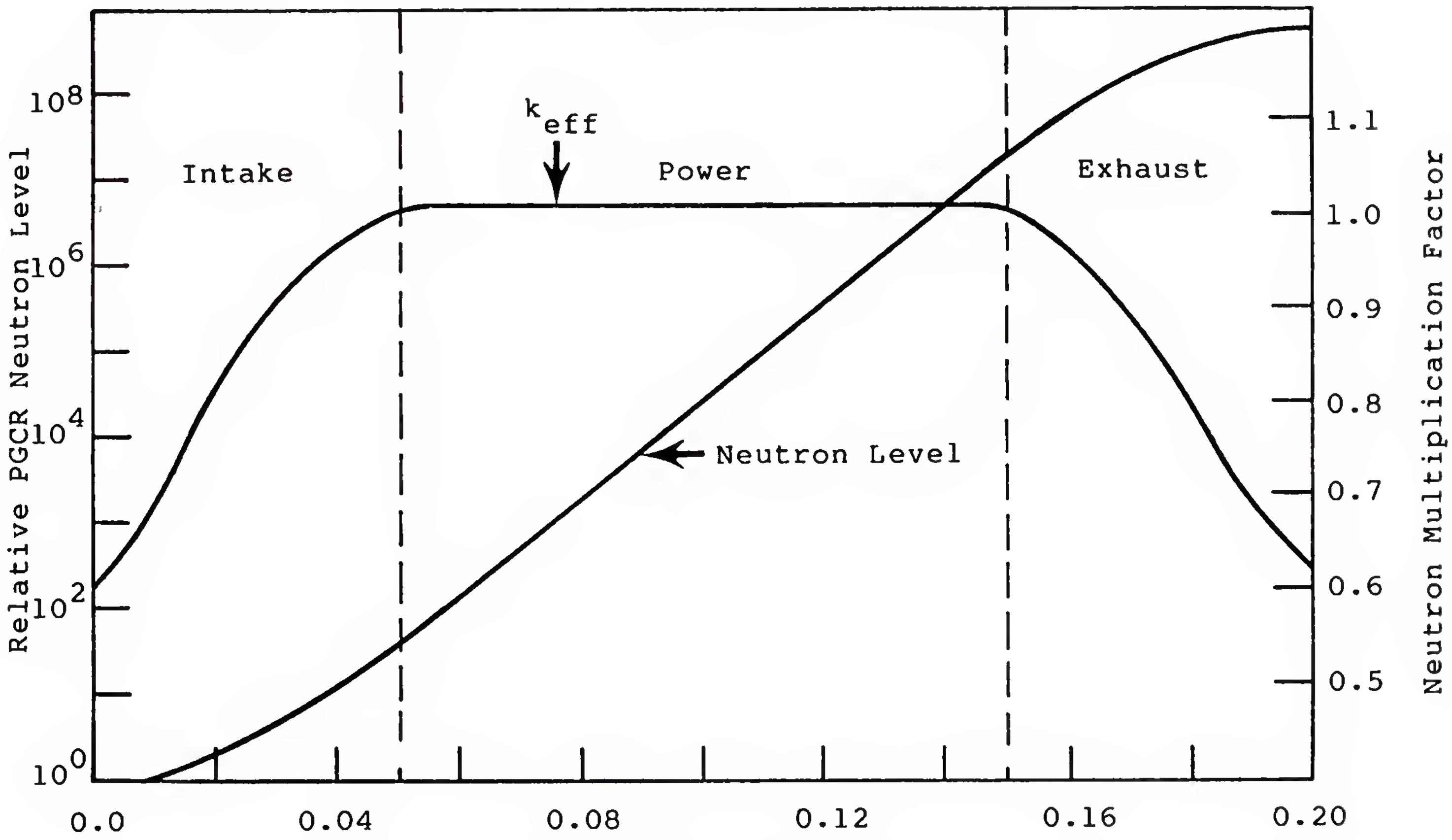

Figure 5-24. Relative PGCR Neutron Level and k_{eff} as a Function of Time for TIBE of 25 cm.

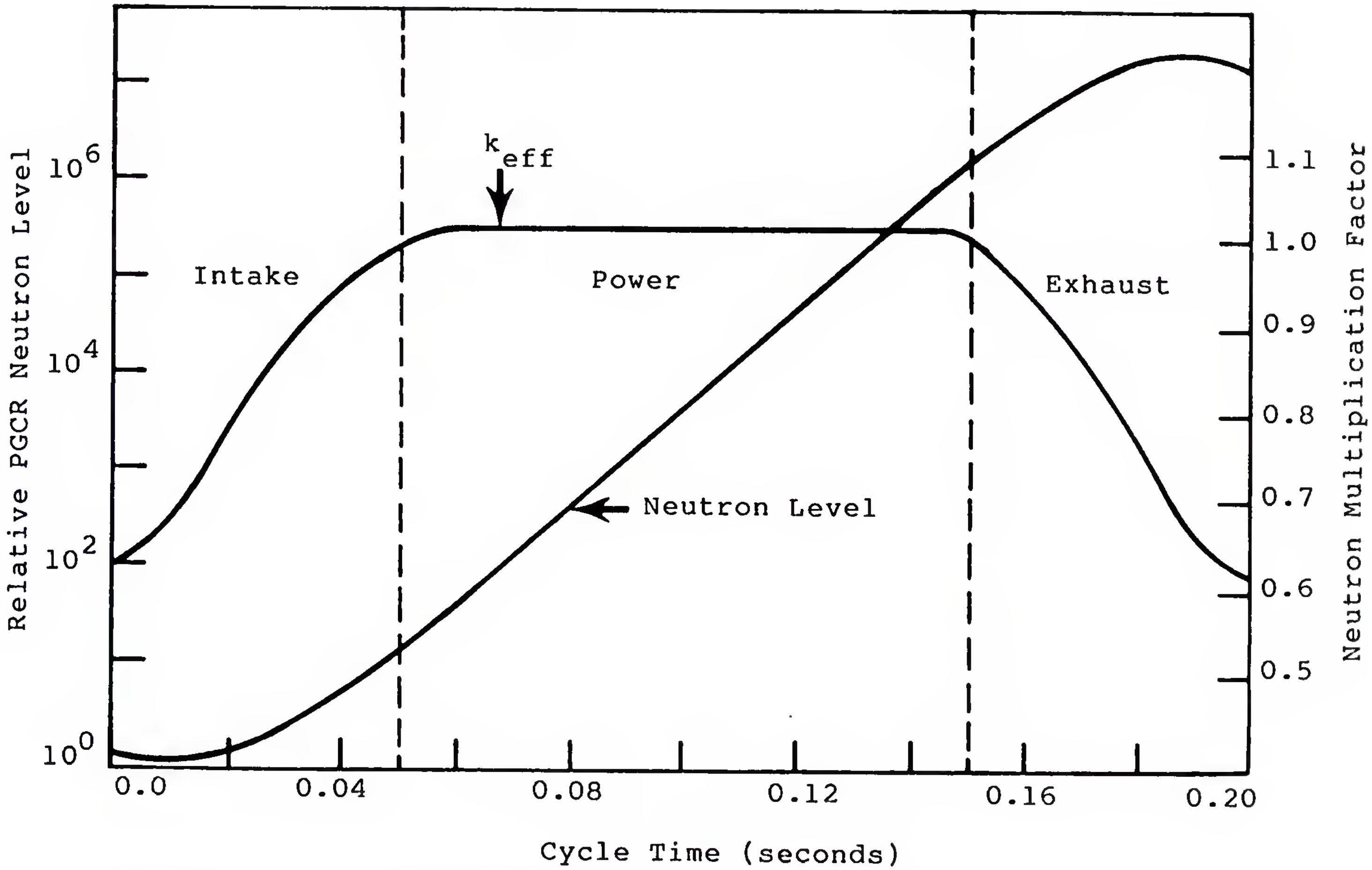

Figure 5-25. Relative PGCR Neutron Level and k_{eff} as a Function of Time for TIBE of 30 cm.

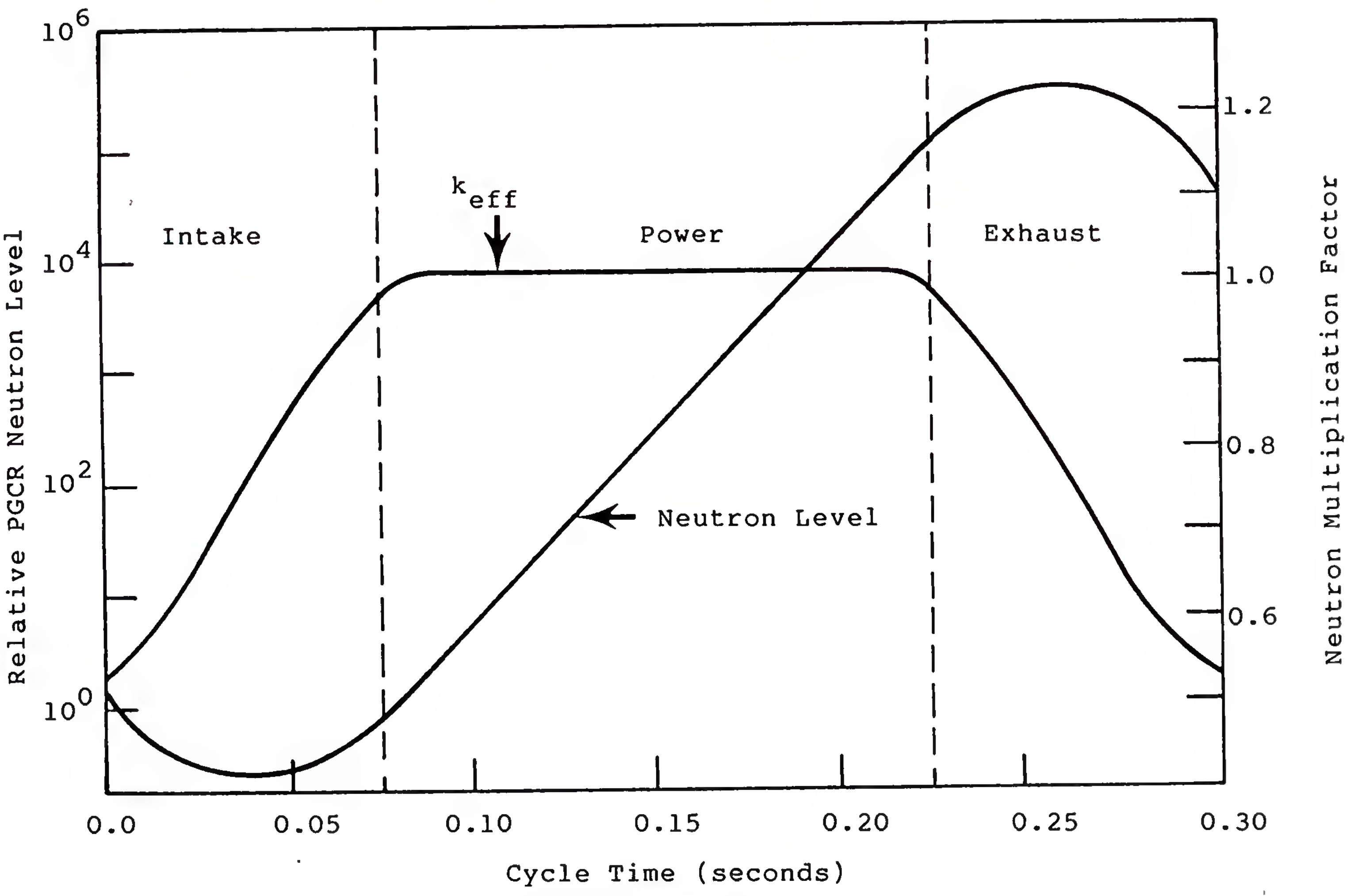

Figure 5-26. Relative PGCR Neutron Level and k_{eff} as a Function of Time for a TIBE of 40 cm.

is adjusted such that the PGCR cores are just critical during the power segment of the cycle. It can be seen from these figures that the relative neutorn level continues to increase (but at a slower rate) even during the PGCR's exhaust phase of operation when the system is far subcritical. This is due to the existence of strong coupling among the PGCR cores during the exhaust phase. The increase in the PGCR neutron level during the exhaust phase can be eliminated by curtailing the core-to-core coupling effects.

Figure 5-27 illustrates the variation of relative PGCR neutron level with cycle time for BGCR systems with inner beryllium thicknesses of 20 cm, 25 cm, 30 cm, and 40 cm. For all the BGCR system configurations illustrated in Figure 5-27, during the exhaust phase of operation the coupling effects among the individual cores are eliminated causing the neutron level to decrease. This is done by setting α_{jk} equal to zero during the solution of the coupled core point reactor kinetics equations in the COUPKIN program.
This can be accomplished in practice by employing properly timed and suitably placed rotating absorbers around the PGCR cores in the moderator.

It can be seen from the plots presented in this section that for BGCR systems with inner beryllium thickness greater than 30 cm, the neutron level decreases during the initial part of the intake phase. This is because of the fact that

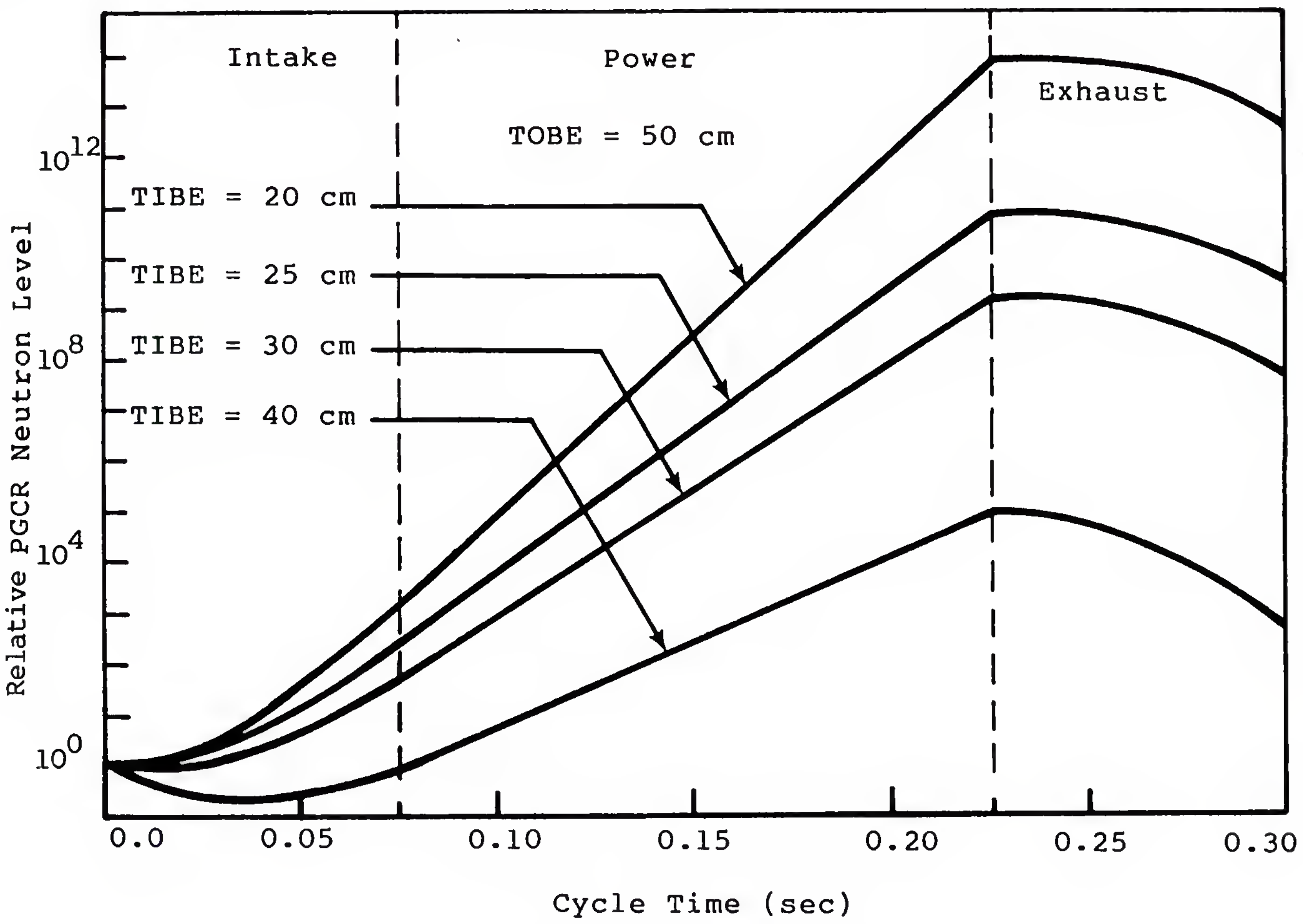

Figure 5-27. Relative PGCR Neutron Level as a Function of Time for a Cycle Time of 0.3 Seconds for BGCR System with Inner Beryllium Thickness of 20 cm, 25 cm, 30 cm, and 40 cm with $\alpha_{jk} = 0$ During Exhaust.

the system is so far subcritical during the initial part of the intake phase and the core-to-core neutronic coupling coefficients, which although larger for low PGCR fuel loading during the initial part of the intake phase than for higher PGCR loading, are insufficient to make the coupling source term in the coupled core kinetics equations large enough to produce a neutron level increase. However, the neutron level increases during the latter part of the intake phase even when the system is still subcritical due to a combination of both an increase in fuel loading (increase in k_{eff}) and the presence of increased neutronic coupling effects among the cores.

The rise in relative PGCR neutron level during the cycle of operation of the system is found to be sharper for system configurations with smaller inner beryllium thickness. This is due to the fact that as the inner beryllium thickness decreases, the coupling coefficients among the PGCR cores increase. It can be seen from Figure 5-27 that as the inner beryllium thickness increases, the peak neutron levels achieved by the PGCR cores decrease (the PGCR core k_{eff} is 1.0 during the power phase in all cases). An increase in the inner beryllium thickness by 10 cm reduces the peak PGCR neutron level at the end of the power phase operation of the system by as much as four orders of magnitude. BGCR systems with larger inner beryllium thicknesses will have weaker neutronic core-to-core coupling and consequently smaller increases in neutron level during any given cycle (assuming a given gas loading or k_{eff} during the power phase) than systems with smaller inner reflectors. If the BGCR system neutron level increase during a cycle is too large, increasing the inner reflector thickness to obtain a smaller neutron level increase may not always be practical. At some point, the increased inner reflector thickness will result in an increased system mass that is undesirable for the space based power system. Effective control of the peak neutron level or power level can, in fact, be achieved by limiting the fuel loading in the cores rather than by designing systems with large inner beryllium thickness.

Figure 5-28 illustrates the variation of relative PGCR neutron level and neutron multiplication factor as a function of time for a cycle time of 0.3 seconds for a BGCR system with inner beryllium thickness of 30 cm. Figure 5-29 shows the variation in PGCR relative neutron level for a cycle time of 0.4 seconds for a BGCR system with an inner beryllium thickness of 40 cm. Figure 5-29 and the plot for a TIBE of 40 cm in Figure 5-27 indicate that for a TIBE of 40 cm, an increase in cycle time from 0.3 seconds to 0.4 seconds raises the relative peak PGCR neutron level from 10^5 to $5x10^6$, i.e., a factor of 50 increase in peak neutron level. From Figure 5-23 and the plot for a TIBE of 20 cm in Figure 5-27, it can be seen that for a TIBE of 20 cm, an

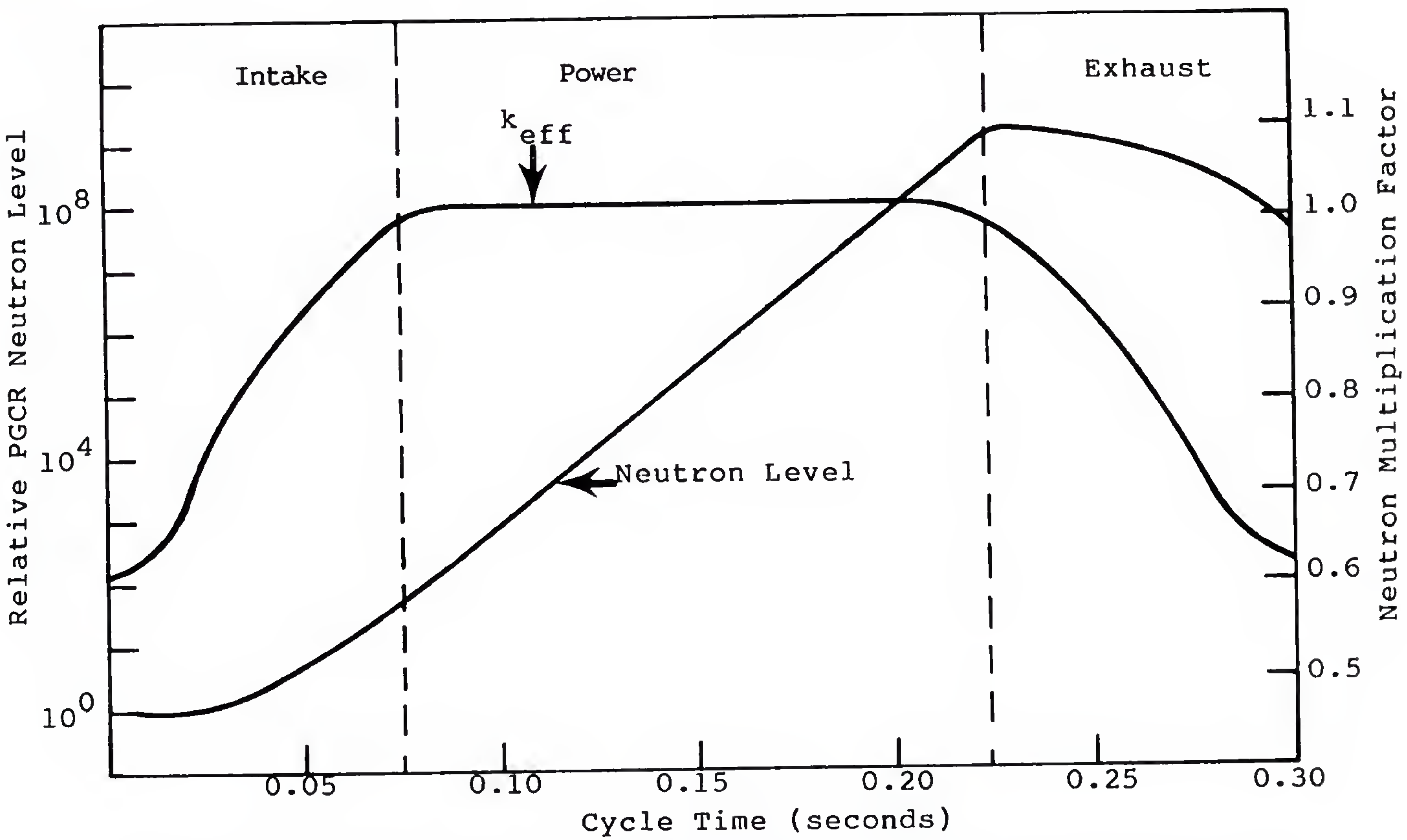

Figure 5-28. Relative PGCR Neutron Level and k_{eff} as a Function of Time for a TIBE of 30 cm and Cycle Time of 0.3 Seconds with $\alpha_{ij} = 0$ During Exhaust.

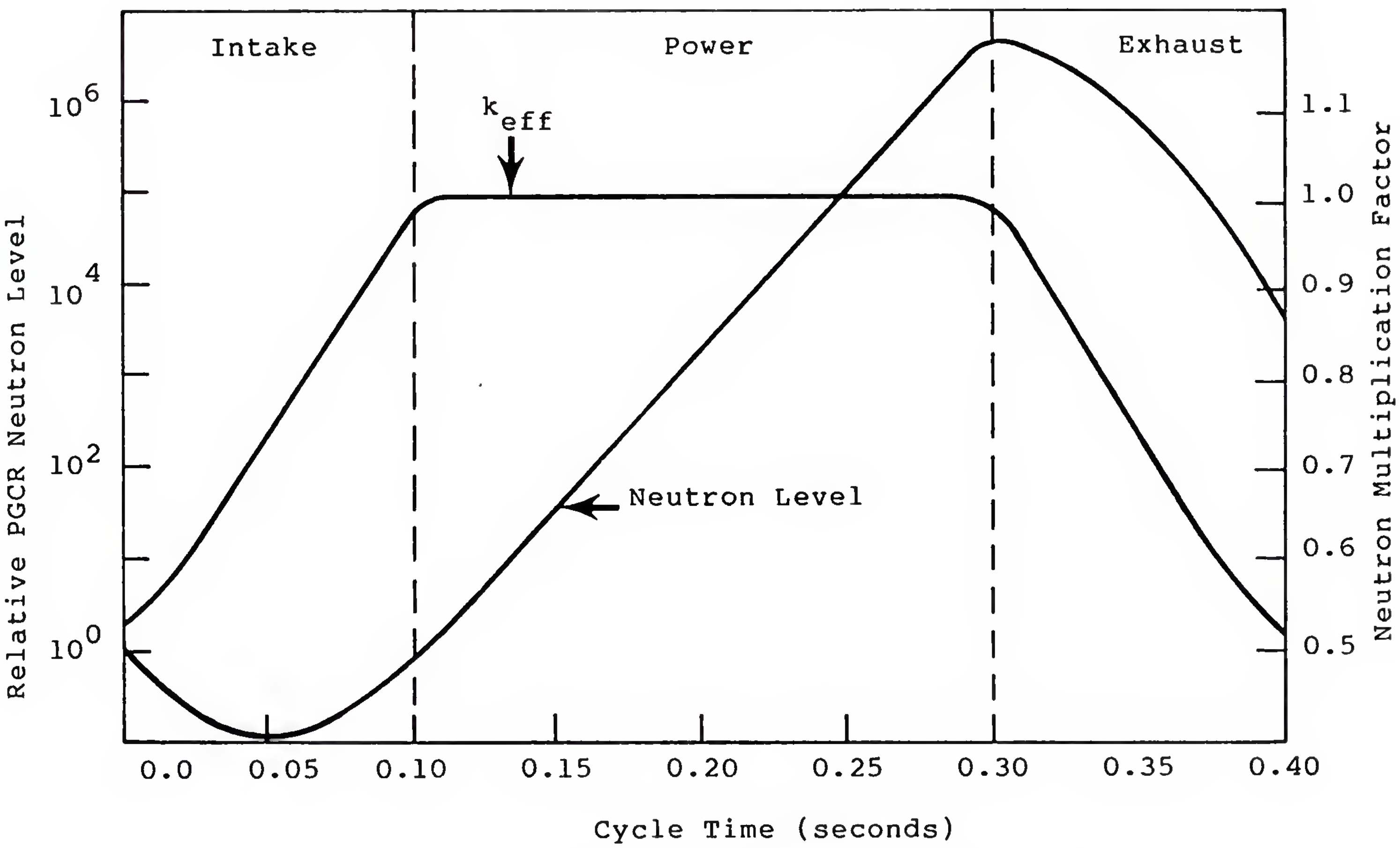

Figure 5-29. Relative PGCR Neutron Level and k_{eff} as a Function of Time for a TIBE of 40 cm with $\alpha_{ij} \equiv 0$ During Exhaust.

increase in cycle time from 0.2 seconds to 0.3 seconds causes the relative neutron level at the end of neutron level phase to increase from $1.6\text{x}10^9$ to $1.6\text{x}10^{14}$. The increase in relative neutron level at the end of the neutron level phase for a TIBE of 30 cm is found to be from $1.3\text{x}10^6$ to $1.56\text{x}10^9$ as the cycle time is raised from 0.2 seconds to 0.3 seconds (see Figures 5-25 and 5-27). Thus, it can be seen that cycle time of operation is another factor which can be used to regulate the neutron level or power level that can be achieved by the system during the PGCR operation.

Figures 5-30 and 5-31 illustrate the variation of PGCR neutron level with time for BGCR systems of inner beryllium thicknesses of 30 cm and 40 cm, respectively. Each of these figures presents plots of the relative PGCR neutron level variations for different values of the core-to-core coupling coefficients. Similar results are obtained for BGCR configurations with other values of inner beryllium thickness. It can be seen from these figures that reduction in the coupling coefficients during the operation of the system (e.g. by means of rotating absorbers between the PGCR cores) can be used to regulate the PGCR neutron level.

Figures 5-32 and 5-33 illustrate the variation of relative PGCR neutron level with cycle time for BGCR systems with inner beryllium thicknesses of 30 cm and 40 cm, respectively. These two figures present plots for the

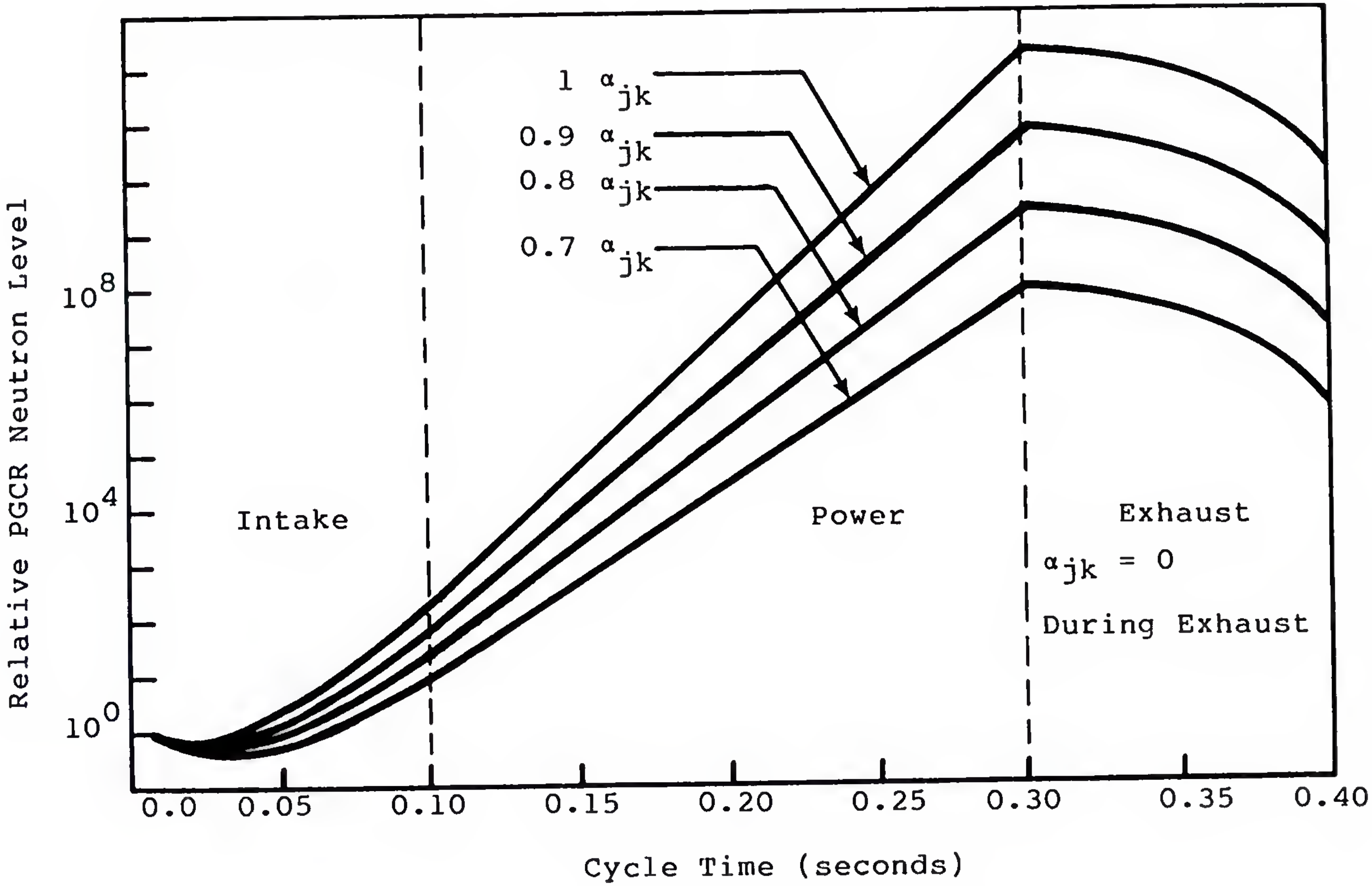

Figure 5-30. Relative PGCR Neutron Level as a Function of Cycle Time for a BGCR System with TIBE of 30 cm for Various Values of Coupling Coefficients (α_{jk}).

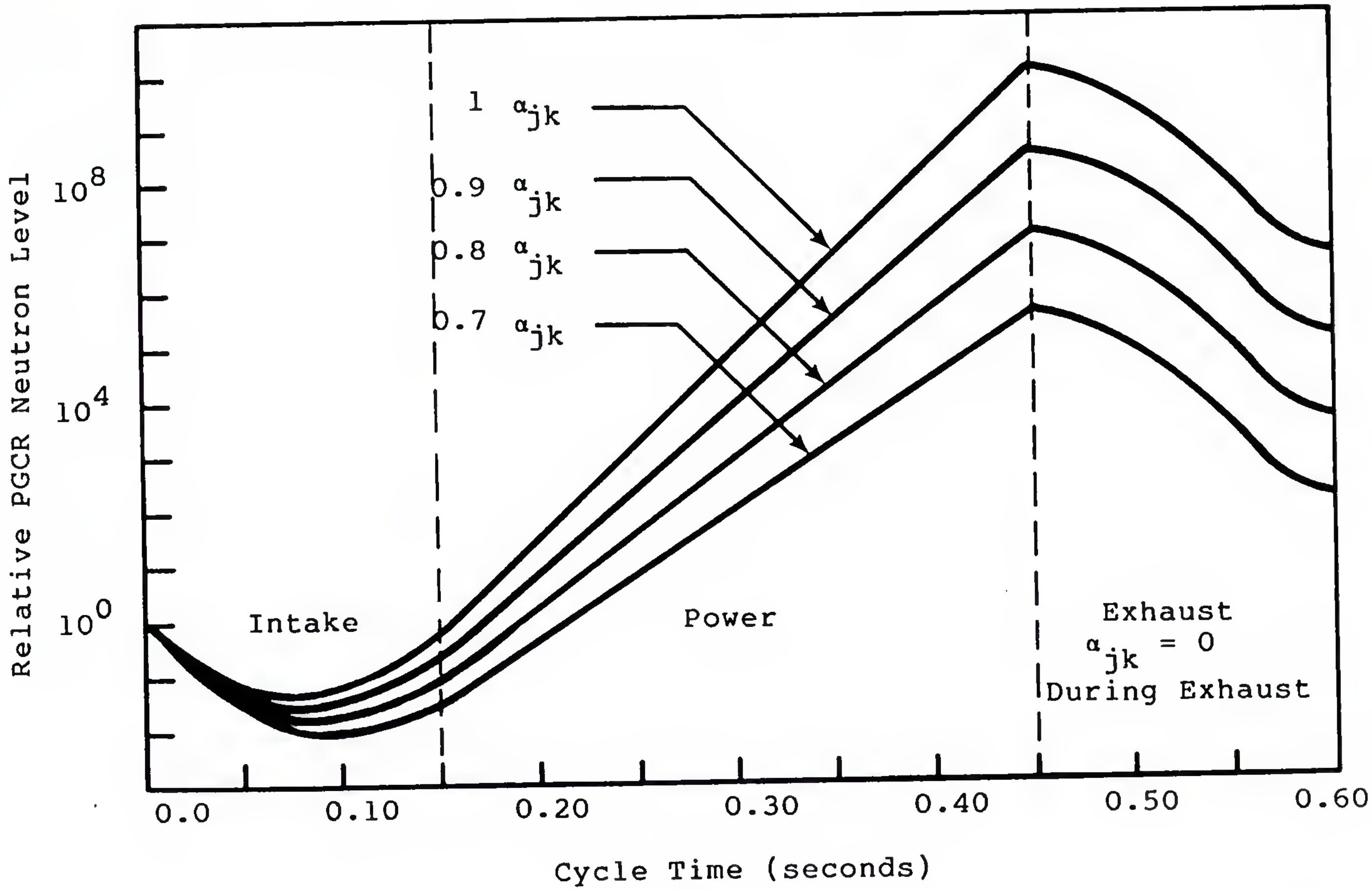

Figure 5-31. Relative PGCR Neutron Level as a Function of Time For a BGCR with TIBE of 40 cm at Various Values of Coupling Coefficients.

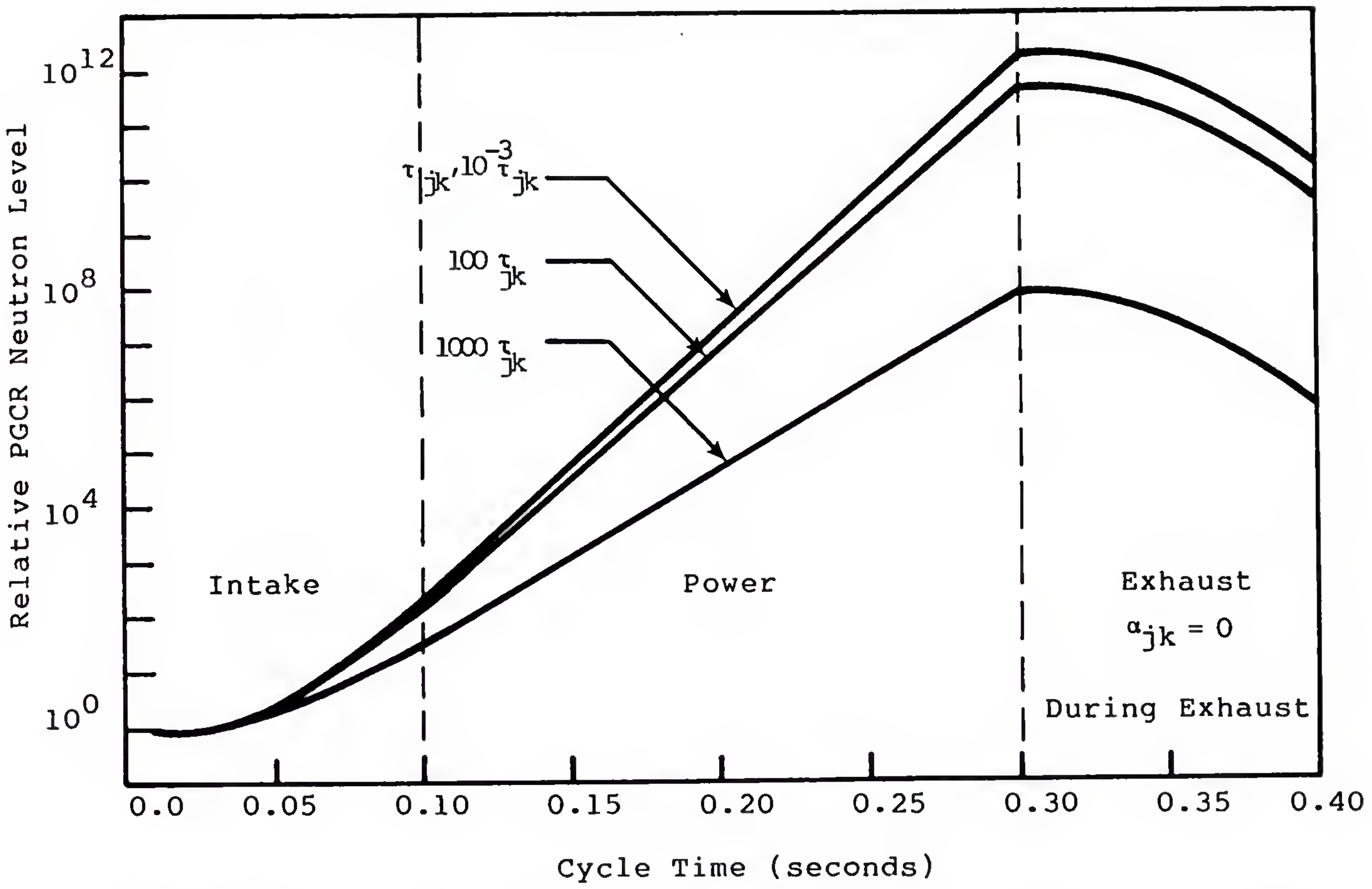

Figure 5-32. Relative PGCR Neutron Level as a Function of Cycle Time for a BGCR with a TIBE of 30 cm for Various Values of Core-to-Core Delay Times (τ_{jk}).

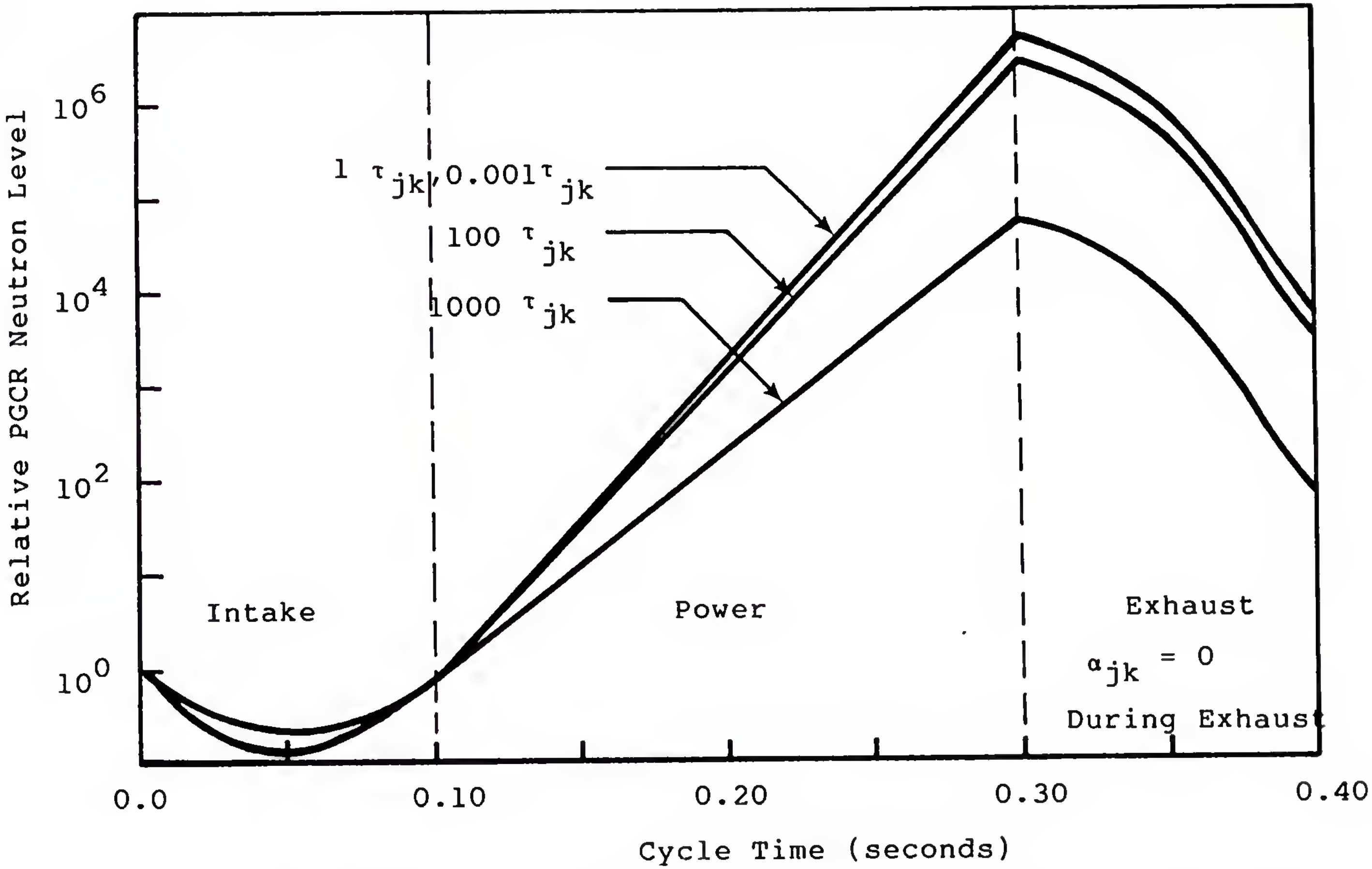

Figure 5-33. Relative PGCR Neutron Level as a Function of Cycle Time for a BGCR with a TIBE of 40 cm for Various Values of Core-to-Core Delay Times (τ_{jk})

relative PGCR neutron level variation for different values of the core-to-core delay times, τ_{jk}. It can be seen that any reduction in core-to-core delay times or a modest increase in the core-to-core delay times has no significant effect on the PGCR core neutron levels. But, when the delay times are increased to the extent that they are comparable to or larger than the neutron generation time ($100\tau_{jk}$ to $1000\tau_{jk}$), the PGCR core neutron levels are significantly reduced.

Figure 5-34 illustrates the variation of relative PGCR neutron level with cycle time for BGCR configurations of inner beryllium thicknesses of 20 cm, 25 cm, 30 cm, and 40 cm for the core-to-core delay times set equal to zero. Comparing Figures 5-34 and 5-27 ($\tau_{jk} \neq 0$) it is to be noted that elimination of delay time for the core-to-core coupling neutrons has no significant effect on the core neutron level.

Figure 5-35 illustrate a typical variation of relative PGCR core neutron level ($N_j(t)/N_j(0)$) and relative total delayed neutron precursor level ($C_j(t)/C_j(0)$) predicted by the COUPKIN program as a function of time for two cycles of operation for a BGCR system of inner beryllium thickness of 40 cm with the PGCR cores uncoupled ($\alpha_{jk}=0$) during the exhaust phases of each cycle. The cycle time is 0.4 seconds. It can be seen that with the PGCR cores fully coupled neutronically during the intake and neutron phases of both

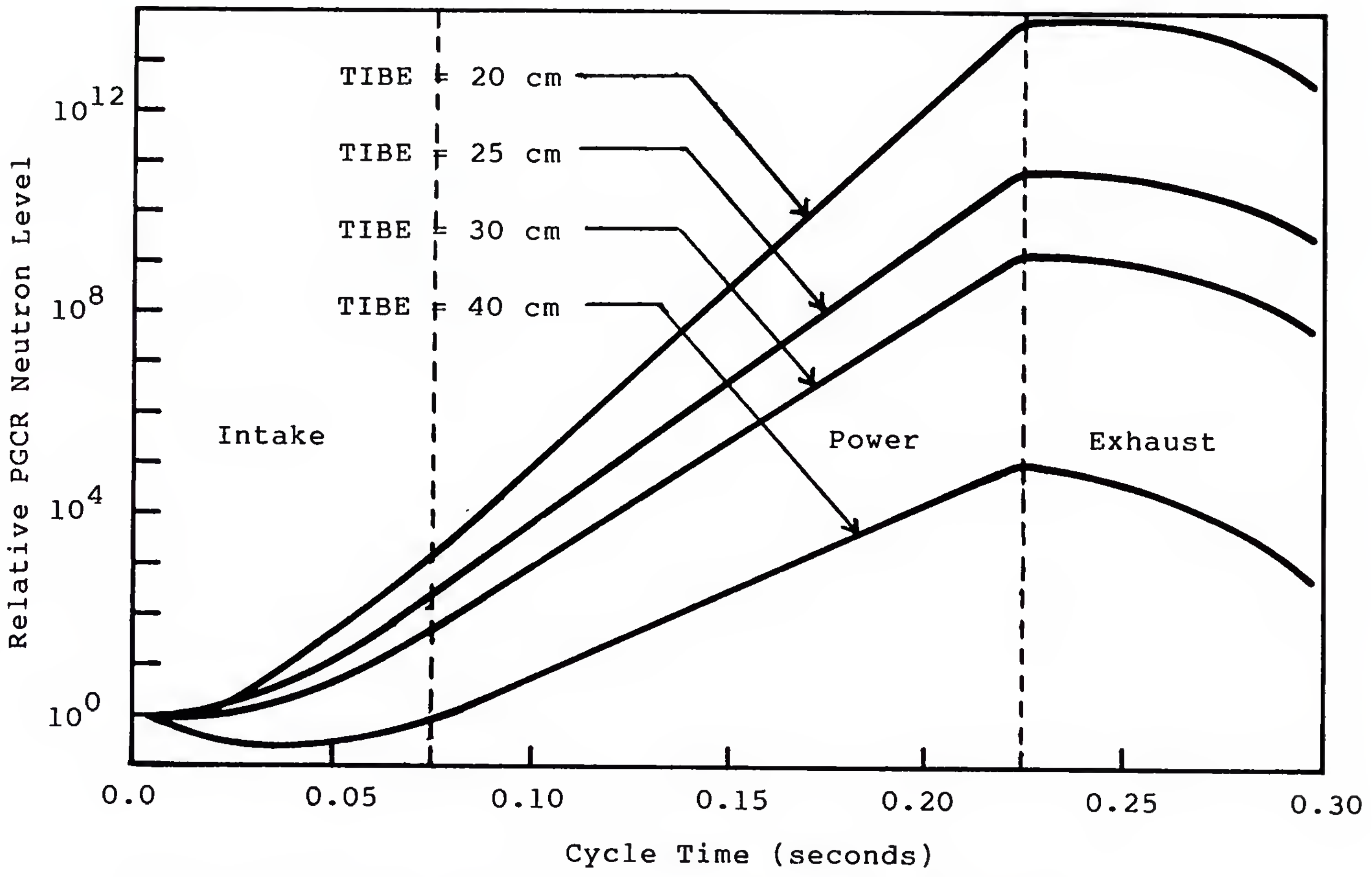

Figure 5-34. Relative PGCR Neutron Level as a Function of Cycle Time for the BGCR System with TIBE of 20 cm, 25 cm, 30 cm and 40 cm with Core-to-Core Delay Time τ_{jk} = 0 sec. and α_{jk} = 0 During Exhaust.

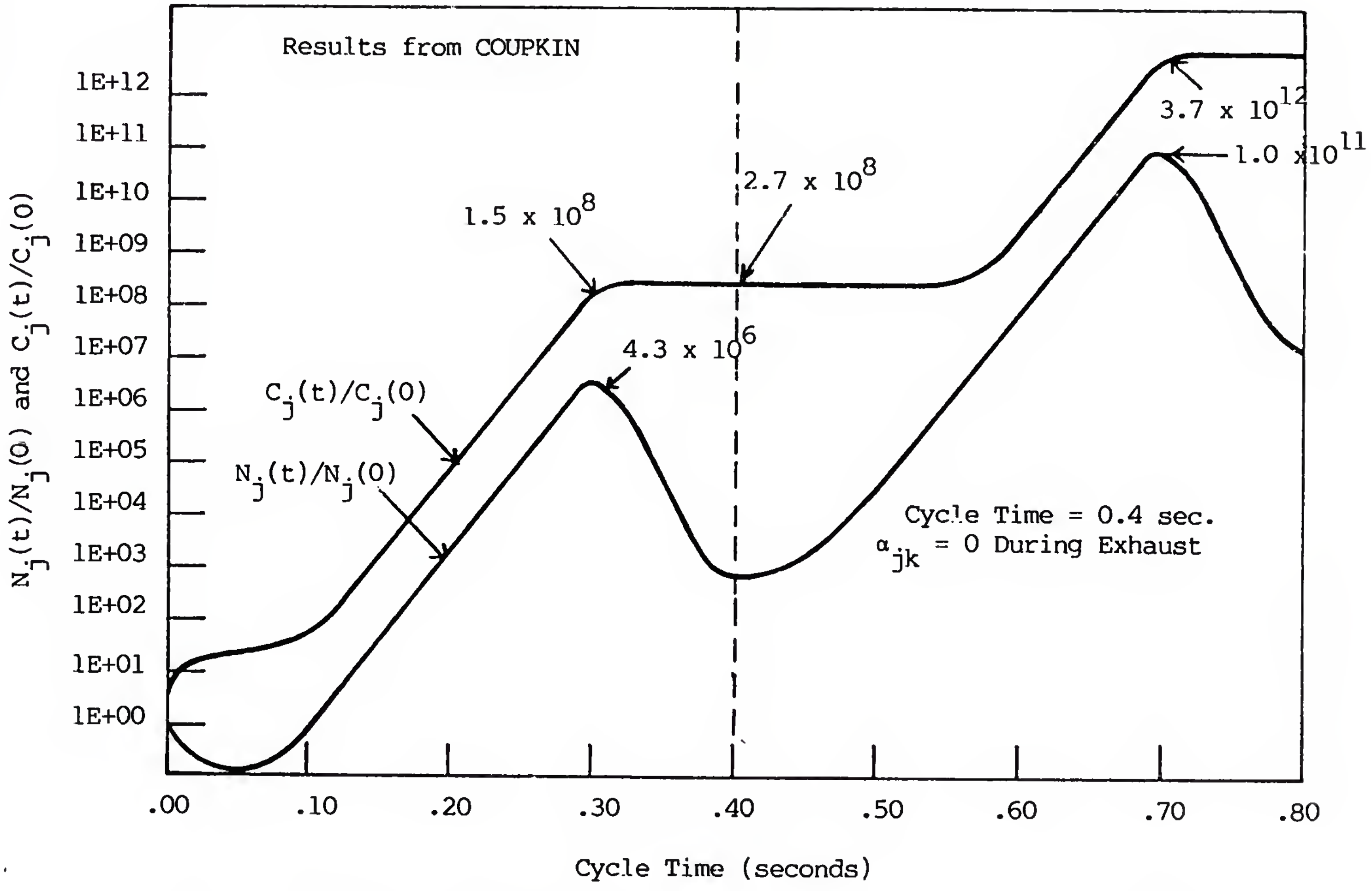

Figure 5-35. $N_j(t)/N_j(0)$ and $C_j(t)/c_j(0)$ for Two Cycles for a BGCR with TIBE of 40 cm with the PGCR Cores Uncoupled (α_{jk} = 0) During Exhaust Phases.

cycles the relative neutron level increases to 4.3×10^6 for the first cycle and to 1.0×10^{11} for the second cycle. During the initial part of the intake phase of the first cycle the neutron level decreases even though the core fuel loading increases. This is due to the fact that the cores are so far subcritical that even the large coupling coefficients at the lower loading are not sufficient to produce an increase in the neutron level. The neutron level, however, increases during the latter part of the intake phase due to a combination of both reactivity increase (due to increased loading) and the presence of increased core-to-core coupling effects. This type of neutron level fluctuation is not observed during the intake phase of the second cycle since the delayed neutron precursor buildup during the first cycle also contributes to the neutron level; the relative neutron level, therefore, increases from the beginning of the second cycle.

Figure 5-36 shows the variation of relative PGCR neutron level $(N_j(t)/N_j(0))$ and the relative total delayed neutron precursor concentration $(C_j(t)/C_j(0))$ as a function of time for two cycles with the PGCR cores uncoupled $(\alpha_{jk}=0)$ during the exhaust phases and the core-to-core coupling reduced to 0.6 times the actual values at all other times. It can be seen that the peak neutron level increases to 4.8×10^2 for the first cycle and to 8.2×10^3 for the second cycle, are greatly reduced relative to the results of Figure

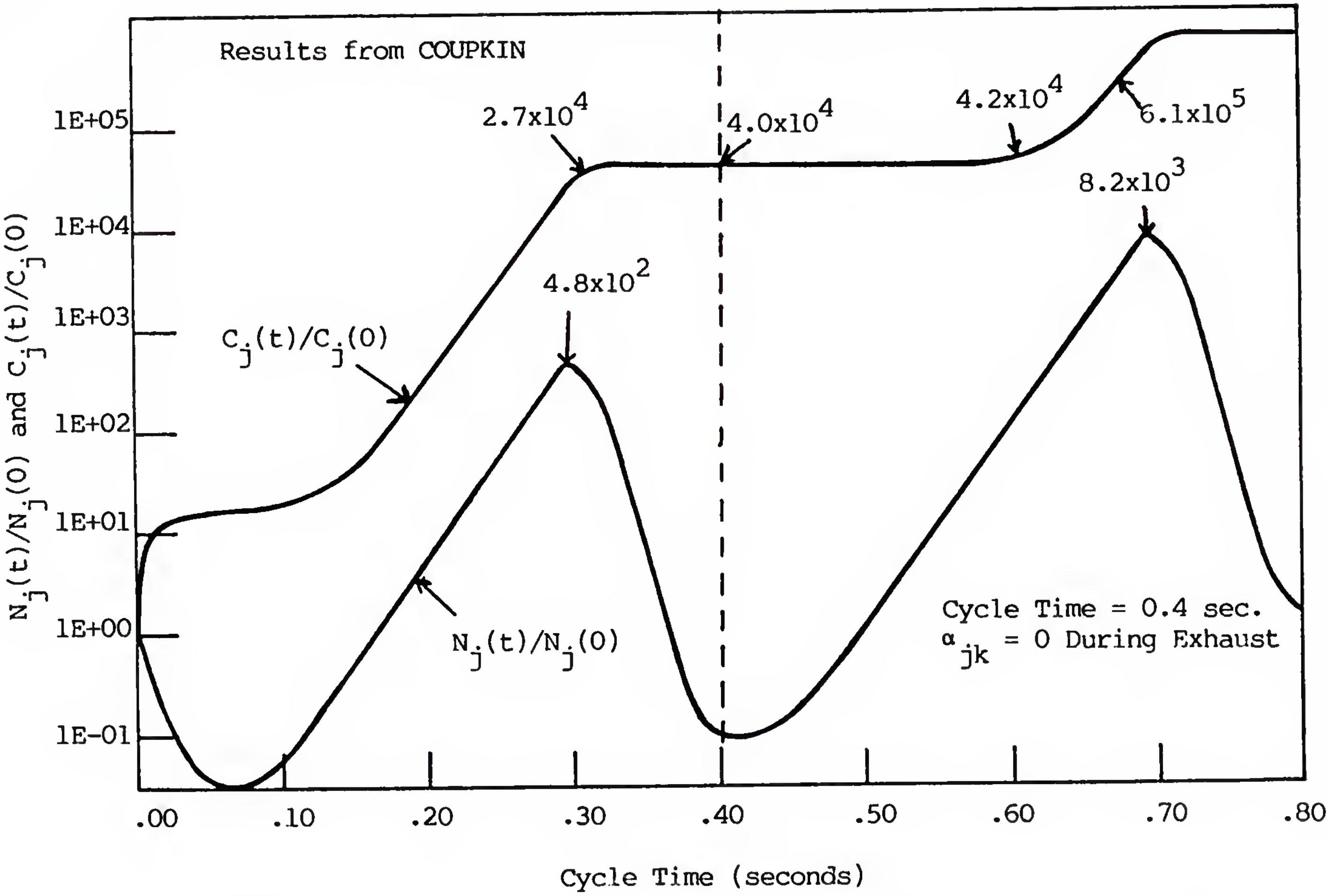

Figure 5-36. $N_j(t)/N_j(0)$ and $C_j(t)/C_j(0)$ for Two Cycles for a BGCR with TIBE of 40 cm with Core-to-Core Coupling Reduced to 0.6 times the Actual Values.

5-35. Figure 5-37 shows the variation of relative PGCR neutron level and the relative total delayed neutron precursor level as a function of time for five cycles for a BGCR system with inner beryllium thickness of 40 cm, with uncoupled PGCR cores (α_{jk}=0) during the exhaust phases and the coupling coefficients further reduced to 0.55 times the actual values at all other times. The cycle-to-cycle peak neutron level undergoes a more moderate increase than in the previous case. Figure 5-38 shows the variation of the same two quantities with time for four cycles (cycle time= 0.3 seconds) for a BGCR system with TIBE of 30 cm with uncoupled PGCR cores (α_{jk}=0) during the exhaust phases and the coupling coefficients reduced to 0.5 times the actual values at all other times.

Figures 5-36 through 5-38 indicate that a desired PGCR neutron level can be achieved by adjusting the neutronic coupling effects among the PGCR cores. The coupling coefficients are strong functions of PGCR core fuel loading; the coefficients decrease as the core fuel loading increases. The coupling coefficients can be regulated either independently, by placing suitable rotating absorbers in the reflector region surrounding the PGCR cores, or by adjusting the core fuel loading. The core fuel loading affects both the coupling coefficients and the core reactivity. Therefore, in order to rapidly bring the PGCR cores to any desired peak neutorn level or power level, a procedure by

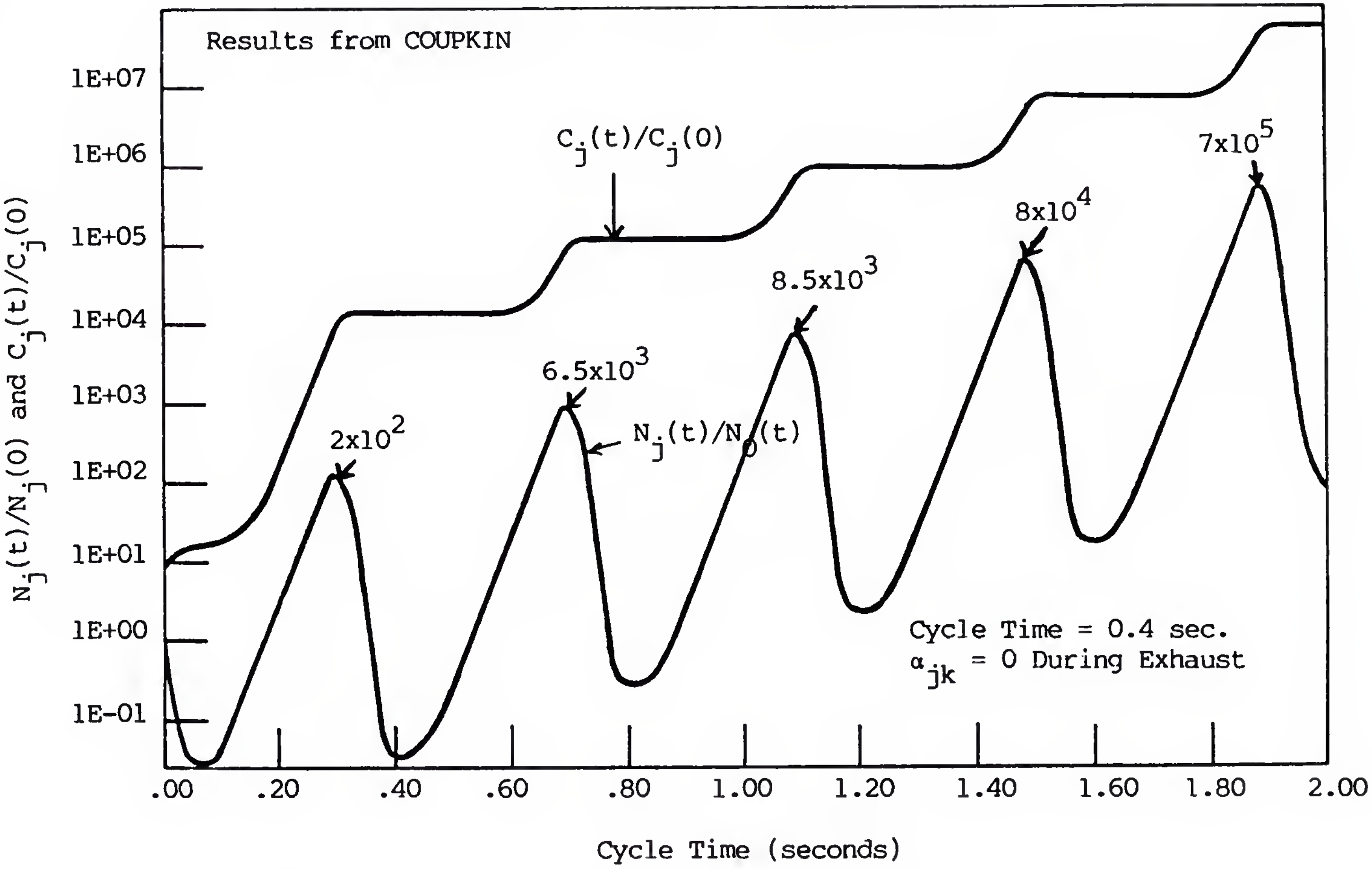

Figure 5-37. $N_j(t)/N_j(0)$ and $C_j(t)/C_j(0)$ for Five Cycles for a BGCR with TIBE of 40 cm with Core-to-Core Coupling Coefficients Reduced to 0.55 times the Actual Values.

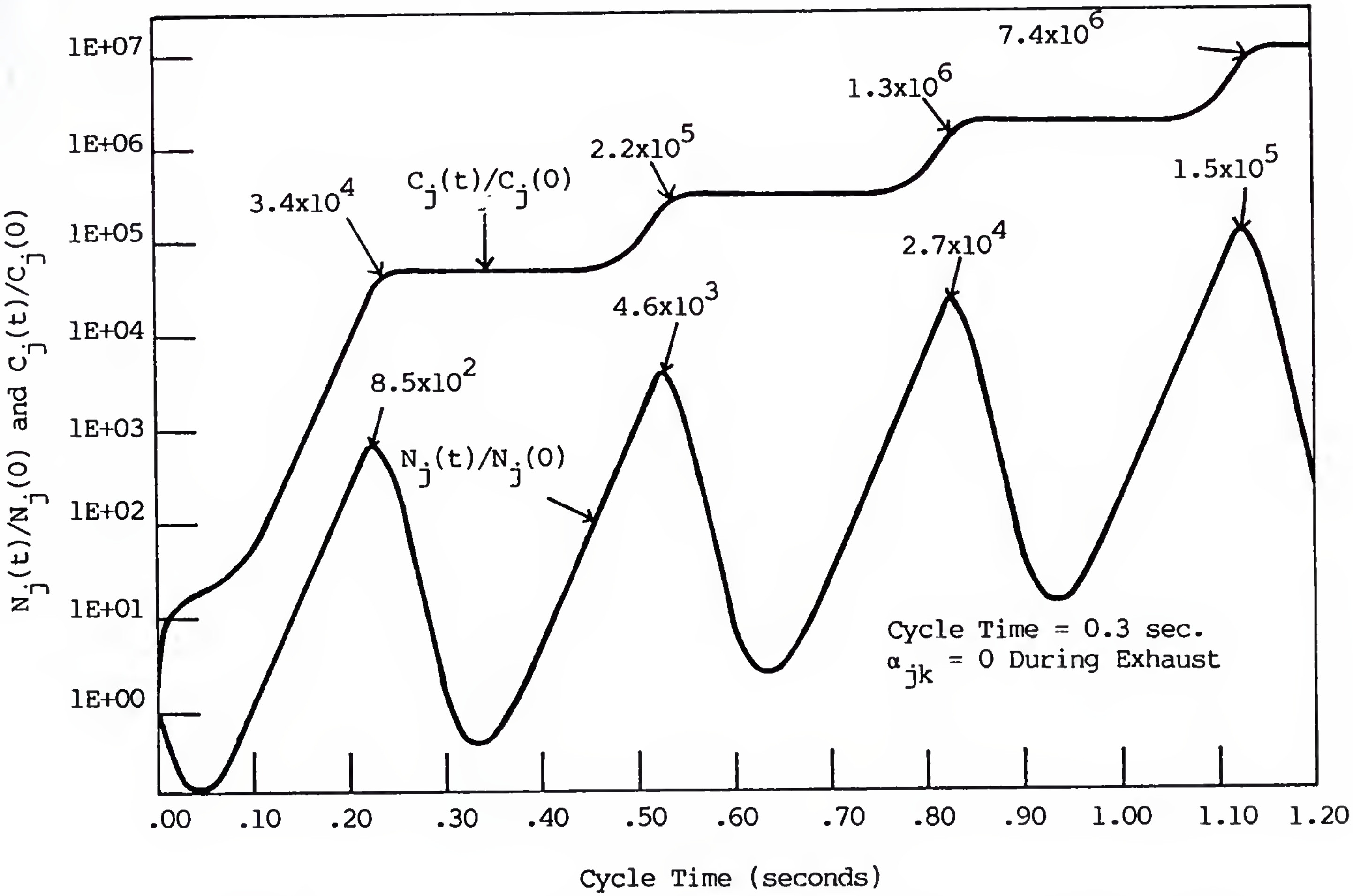

Figure 5-38. $N_j(t)/N_j(0)$ and $C_j(t)/C_j(0)$ for Four Cycles for a BGCR with a TIBE of 30 cm with Core-to-Core Coupling Reduced to 0.5 times the Actual Values.

which both the core fuel loading and the coupling coefficients can be iteratively or simultaneously adjusted for the desired neutron level should be very effective. This procedure can be simulated in the COUPKIN program.

Fueled PGCR cores and nominally fueled BPGCR core

This section examines the relative PGCR core neutron level and relative delayed neutron precursor level variations for a BGCR system in which the PGCR core fuel loading is varied equally while the central BPGCR chamber is nominally fueled at 25 atmospheres.

Figure 5-39 illustrates the variation of relative PGCR core and BPGCR core neutron levels with cycle time for the BGCR system with inner beryllium thickness of 30 cm. Figure 5-40 illustrates the variation of neutron multiplication factor with of the PGCR cores with time for the cycle examined for the Figure 5-39. The PGCR core fuel loading is increased from 10 atmospheres to around 50 atmospheres so that the k_{eff} increases from 0.53 to 0.90. Figure 5-39 illustrates that the PGCR core neutron level increases to a peak relative neutron level of $6x10^6$ even if the core is subcritical. This is due to the neutronic coupling influence of the remaining PGCR cores and the central BPGCR chamber on the specific PGCR core. It can be seen that even if the relative reactivity worth of the BPGCR core decreases as the PGCR core fuel loading increases and the BPGCR core is subcritical, the BPGCR core neutron level also increases.

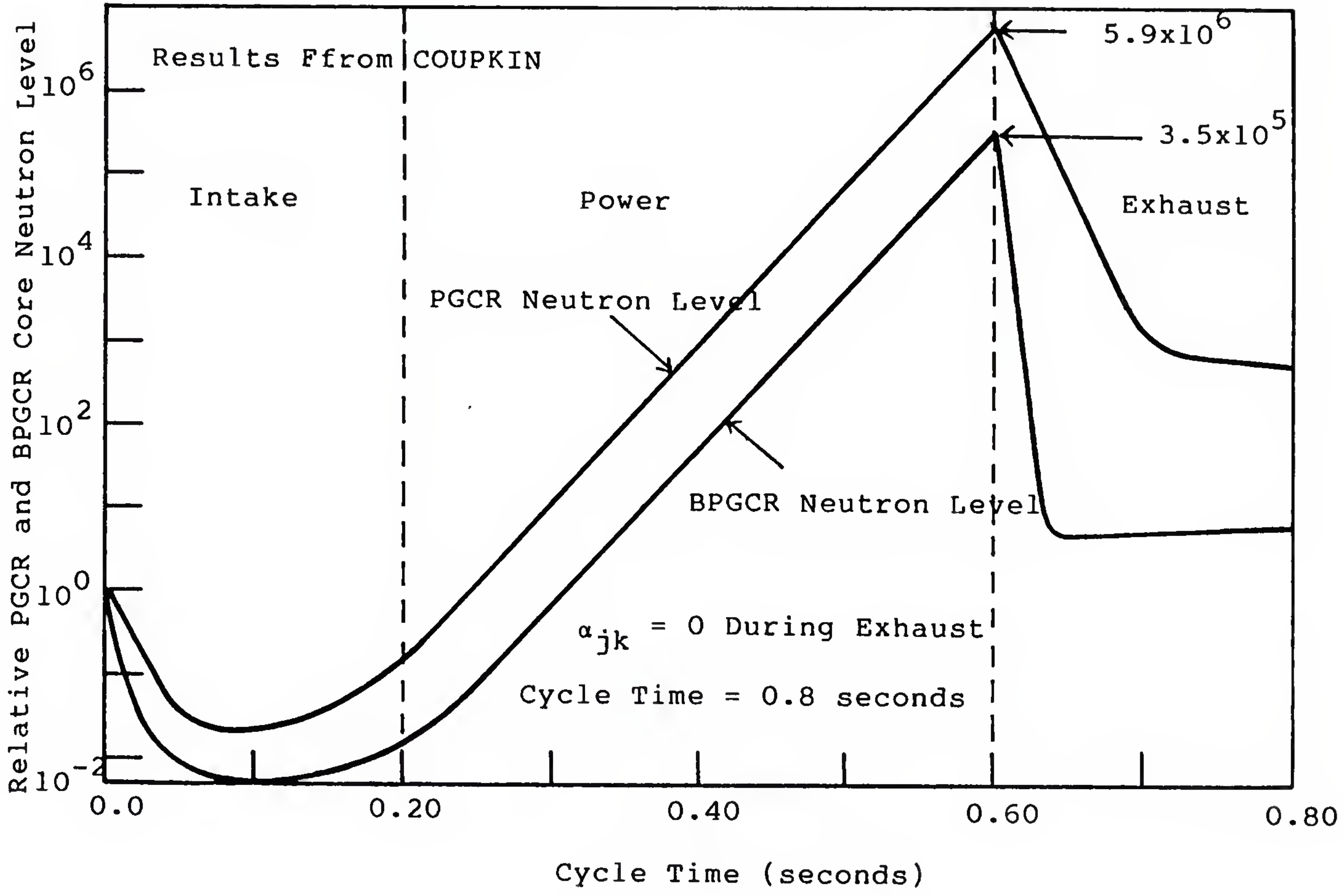

Figure 5-39. Relative PGCR and BPGCR Neutron Levels as a Function of Cycle Time for a BGCR with a TIBE of 30 cm with Coupled PGCR and BPGCR Cores.

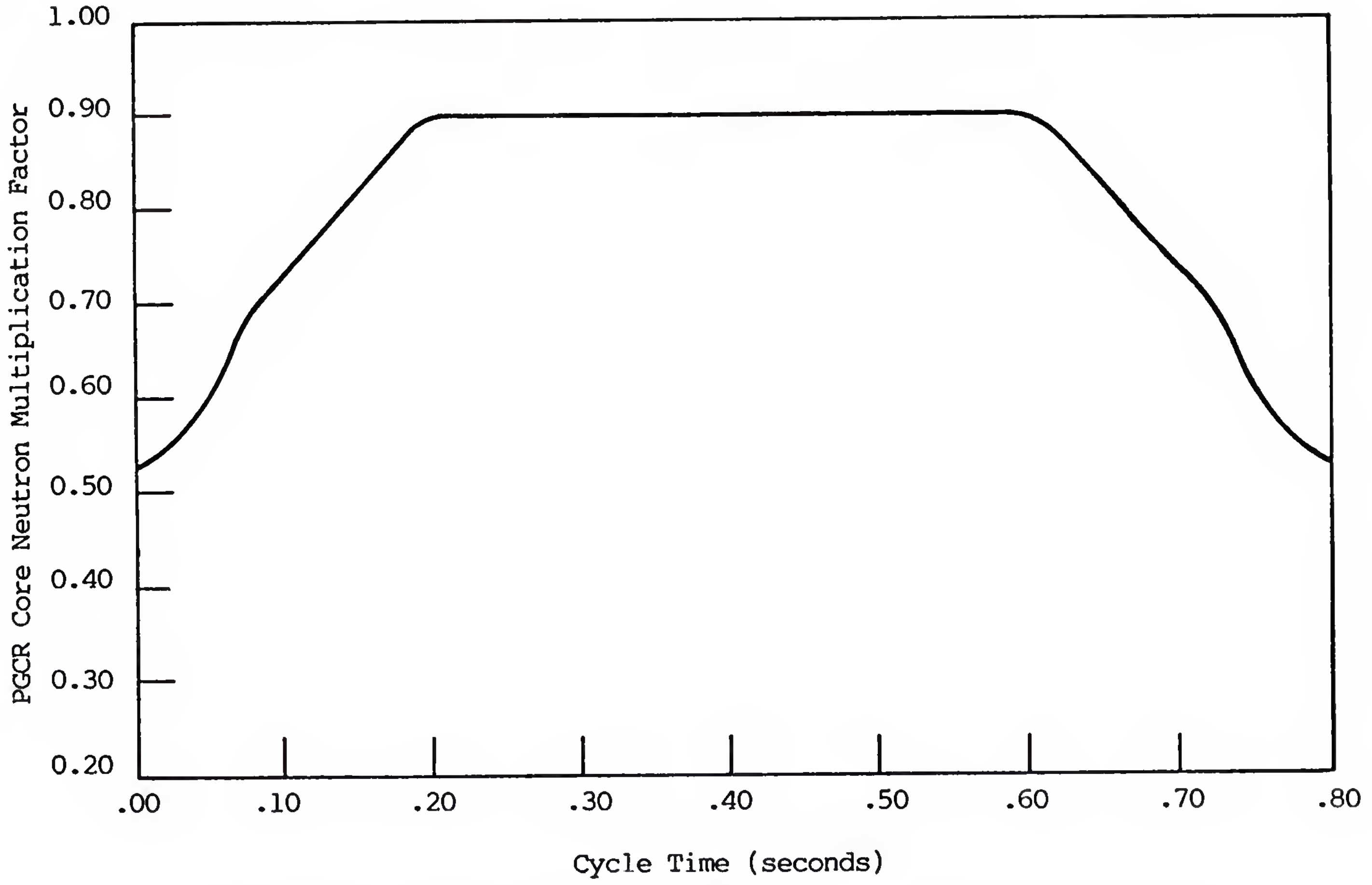

Figure 5-40. PGCR Core Neutron Multiplication Factor as a Function of Cycle Time for a BGCR System with TIBE of 30 cm.

This is due to the fact that the neutronic coupling influence of each of the PGCR cores on the BPGCR core increases as the PGCR core fuel loading increases (see Figure 5-19 and Tables 5-12 and 5-13). Figure 5-41 illustrates the variation of relative PGCR and BPGCR core neutron levels with time for a BGCR of TIBE 30 cm with PGCR cores uncoupled from BPGCR core ($\alpha_{PGCR \leftarrow BPGCR}=0$ and $\alpha_{BPGCR \leftarrow PGCR}=0$). It can be seen that the BPGCR neutron level drops drastically. The relative PGCR core neutron level continues to increase to a slightly lower peak relative neutron (3.2×10^6). Even though the PGCR cores are uncoupled from the BPGCR chamber, the PGCR core neutron level increases due to both the increase in core fuel loading (and reactivity) and the presence of PGCR core-to-core neutronic coupling effects.

Figures 5-42, 5-43, and 5-44 represent the variation of the same data as that of the Figures 5-39 through 5-41, respectively, but for a BGCR system of inner beryllium thickness of 20 cm. The cycle time for this case is 0.4 seconds. The PGCR loading in this case is adjusted such that the k_{eff} during the neutron phase is 0.90. The relative PGCR core neutron level at the end of the neutron phase in this case is greater than the respective peak neutron for the case of TIBE of 30 cm. This is due to the fact that the average coupling coefficients are larger for a TIBE of 20 cm than for a TIBE of 30 cm.

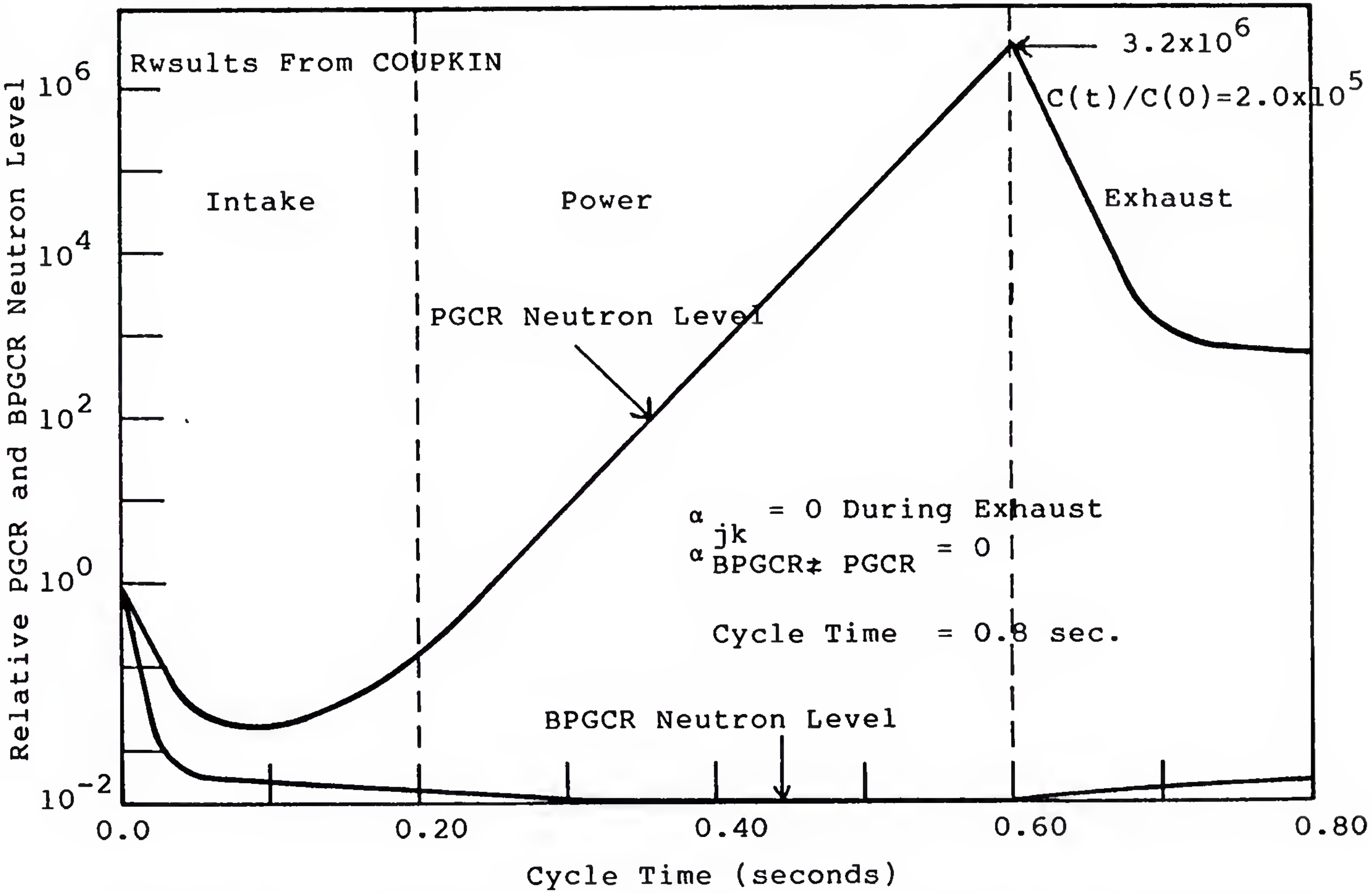

Figure 5-41. Relative PGCR and BPGCR Neutron Levels as a Function of Cycle Time for a BGCR with TIBE of 30 cm with PGCR Cores Uncoupled from BPGCR Core

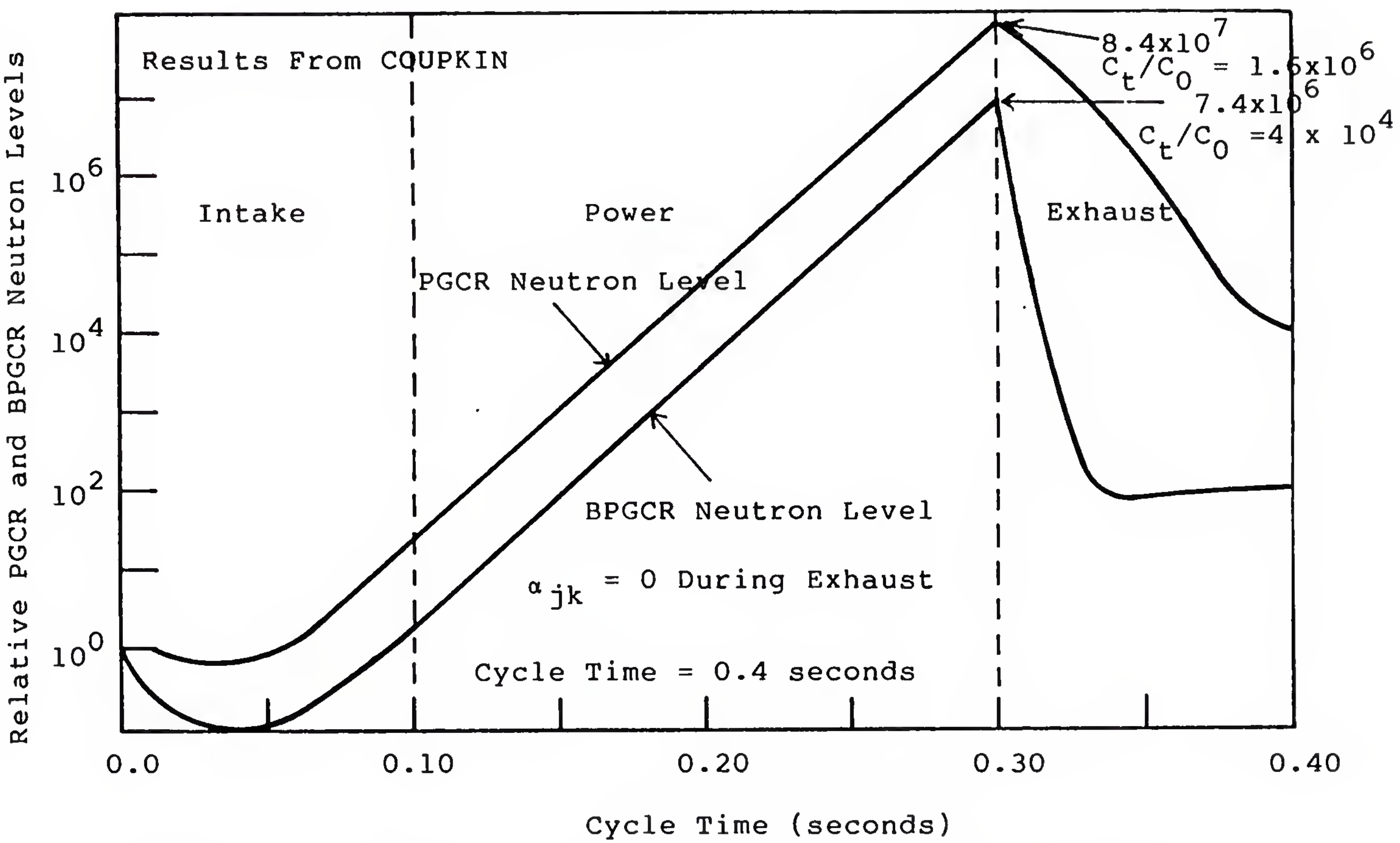

Figure 5-42. Relative PGCR Core and BPGCR Neutron Levels as a Function of Cycle Time for a BGCR with TIBE of 20 cm with Coupled PGCR and BPGCR Cores.

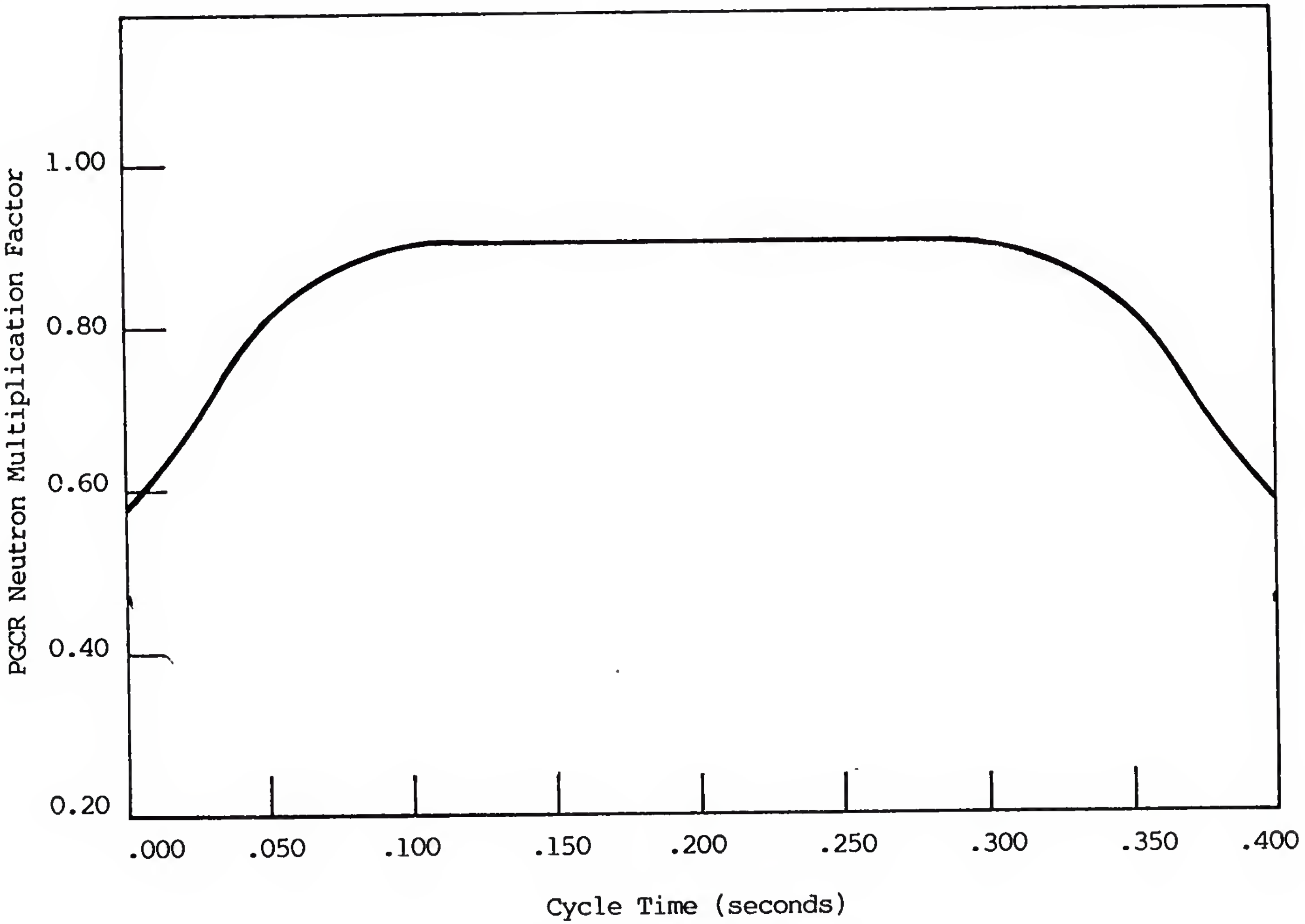

Figure 5-43. PGCR Core Neutron Multiplication Factor as a Function of Cycle Time for a BGCR System with a TIBE of 20 cm.

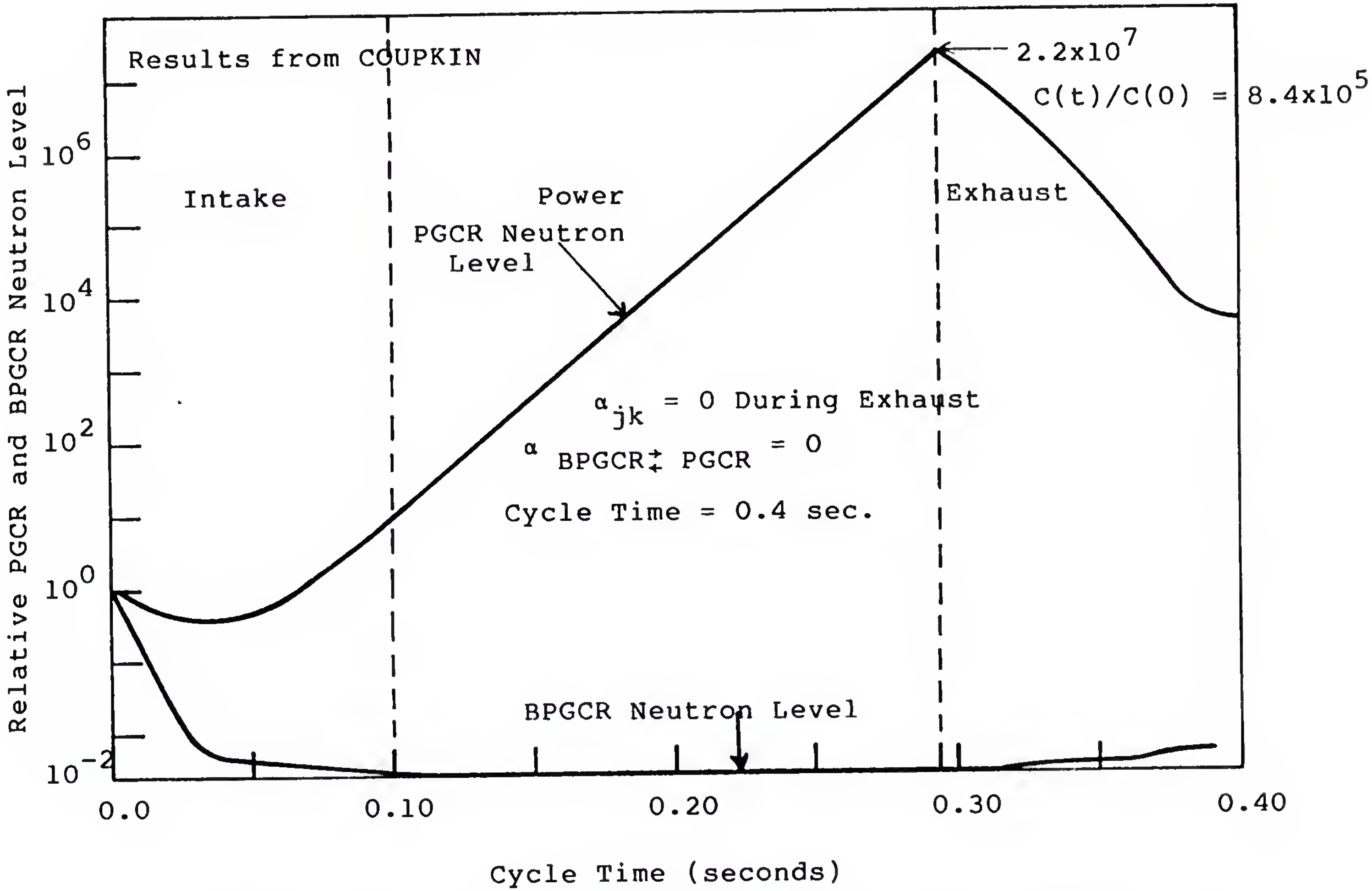

Figure 5-44. Relative PGCR and BPGCR Neutron Levels as a Function of Cycle Time for a BGCR with TIBE of 20 cm with PGCR Cores Uncoupled from BPGCR Core.

Summary

The effects of inner beryllium thickness, core loadings, and various core loading patterns on system reactivity, system neutron generation time, and core-to-core coupling coefficients have been examined in this Chapter. The core loading patterns include various PGCR core loadings both without fuel in the central chamber and with nominal fuel in the central BPGCR chamber and various BPGCR chamber loadings both with a nominal amount of fuel in the PGCR cores and with unequal loading among the PGCR cores. Each of the core loading patterns is repeated for different inner and outer beryllium thicknesses. The three-dimensional, Monte Carlo transport code, MCNP has been used to calculate the integral kinetics parameters of the BGCR system at each core fuel-gas loading for various configurations of the system. Even though computer time limitations have resulted in relatively large uncertainty in some quantities calculated by MCNP, the fact that the exact geometry of the system and probabilities of interaction can be simulated in the MCNP code provides the capability to estimate the integral kinetics parameters, especially the coupling coefficients, with high degree of confidence.

This Chapter also presents results from preliminary kinetics studies of two core loading patterns of the BGCR system: various PGCR fuel loadings both with unfueled BPGCR chamber and with nominally fueled BPGCR chamber. The kinetics analysis is done by using the coupled core point reactor kinetics program, COUPKIN which is developed as part of this research. The integral kinetics parameters such as reactivity, neutron generation time, and the average coupling coefficients which are required in the COUPKIN program are calculated from the appropriate quantities obtained from the MCNP code.

For the BGCR system with PGCR cores loaded and the BPGCR chamber unfueled, the core-to-core coupling coefficients decrease with an increase in the core fuel loading for any specific TIBE. The coupling coefficients are found to decrease with an increase in the inner beryllium thickness for any specific PGCR fuel loading. The neutron generation time decreases with an increase in the PGCR core fuel loading, but is essentially independent of the inner beryllium thickness for any specific PGCR gas loading.

When the PGCR core fuel loading is increased while the BPGCR chamber is nominally fueled, the PGCR core-to-core coupling coefficients are less than the coefficients when the central chamber is unfueled. In this case the BPGCR-to-PGCR coupling coefficients decrease while the PGCR-to-BPGCR coupling coefficients increase moderately with an increase in the PGCR fuel loading. The system neutron generation time is less for the case when the BPGCR chamber is nominally fueled than for the case when the BPGCR chamber is unfueled.

When the BPGCR chamber is fueled while the PGCR cores have a fixed nominal amount of fuel the BPGCR-to-PGCR coupling coefficients initially undergo a moderate increase (for BPGCR loadings up to about 55 atmospheres) and thereafter the coefficients are essentially independent of the BPGCR loading. For this case, the PGCR-to-BPGCR coupling coefficients decrease with an increase in the BPGCR gas loading. The PGCR core-to-core coupling coefficients are essentially independent of the BPGCR loading when the PGCR cores are nominally fueled. The neutron generation time decreases with an increase in BPGCR fuel loading; while the generation time is independent of inner beryllium thickness for any specific BPGCR fuel loading.

The dynamic analysis of the BGCR has shown that the core-to-core coupling coefficients contribute significantly to the power behavior of any chamber during the BGCR operation. The core neutron level can be effectively controlled by either adjusting the coupling effects among the cores (e.g. by placing rotating neutron absorbers around the cores in the reflector) or by regulating the core fuel loading. Any decrease in the core-to-core delay times has no effect on the core neutron level while an increase in the delay times to values comparable to the neutron generation time significantly reduces the core neutron levels.

CHAPTER 6
CONCLUSIONS, RECOMMENDATIONS AND AREAS OF FURTHER RESEARCH

Introduction

The preliminary static and dynamic neutronic analysis of the bimodal gaseous core reactor presented in this dissertation provides a basic understanding of the effects of various parameters such as core loading, core loading patterns, and inner and outer beryllium moderator/reflector thicknesses on the system neutron multiplication factor, neutron removal lifetime, core-to-core neutronic coupling coefficients, core neutron levels, and the delayed neutron precursor concentration level. The neutronic analysis has shown that the PGCR's of the BGCR system are capable of pulsed operation for low power production and the central BPGCR is capable of high power production. It has shown that with multiple PGCR chambers and their proper timing of operation, the low power system should be able to provide an essentially continuous source of hot pressurized gas for the low power energy conversion system. It has also shown that due to the strong core-to-core neutronic coupling, steady state operation and even power increases can be achieved with all of the cores operating in the subcritical condition. This chapter highlights some of the important conclusions drawn from this study and examines some areas of further research required for a comprehensive neutronic and fluid flow/heat transfer analysis of the bimodal gaseous core reactor system.

Summary of Conclusions

A series of static neutronic calculations for different core loading patterns and inner and outer beryllium thicknesses has been performed. The core loading patterns investigated in this work include PGCR fuel loading variations in which all PGCR cores are loaded equally when the central BPGCR chamber is un fueled and nominally fueled; BPGCR chamber loading variations when the outer PGCR cores are nominally fueled; and PGCR core loading variations in which PGCR chambers are not all loaded equally when the BPGCR chamber is fueled and unfueled. The dynamic neutronic analysis has been done on the bimodal system for selected loading patterns, namely, the low power system with PGCR cores fueled while the central BPGCR chamber is either unfueled or nominally fueled and the high power system with the central BPGCR chamber fueled while the PGCR cores have nominal fuel loading. The dynamic analysis has also been performed on the system for the case when the PGCR cores are unequally loaded. The conclusions that can be drawn from the static and dynamic neutronic analysis of the BGCR system are briefly summarized below.

Variation in PGCR Fuel Loading (20 - 60 atm) and Inner Be Thickness (10 - 40 cm),Unfueled BPGCR Chamber

i) The System k_{eff} is found to increase with an increase in PGCR fuel loading for any specific inner beryllium thickness while the system k_{eff} decreases with an increase in the inner Be thickness for any specific PGCR core fuel loading. Critical fuel loading increases with an increase in inner Be thickness. (Figures 4-7, 4-8 and 4-9)

ii) The system neutron removal lifetime (ℓ) is essentially independent of the inner Be thickness while decreases with an increase in PGCR core fuel loading. The system neutron generation time also decreases with an increase in the core fuel loading. (Figures 4-10 and 5-9)

Effect of Outer Be Thickness Variation (20-70 cm)

i) The system k_{eff} increases sharply with an outer Be thickness increase in the 20-50 cm range and thereafter k_{eff} remains essentially independent of any outer Be thickness increase. (Figures 4-11 and 4-12)

ii) The neutron removal lifetime follows the same trend as the variation of k_{eff} with the outer Be thickness. Neutron generation time also increases with an outer beryllium thickness increase in the 20-50 cm range. For outer beryllium thickness above 50 cm, the neutron generation time is essentially independent of the outer beryllium thickness. (Figures 5-6 and 5-7)

iii) The core-to-core neutronic coupling coefficients increase moderately with an increase in outer Be thickness initially (up to 30 cm) and thereafter the coupling coefficients are essentially independent of the outer Be thickness. (Figure 5-10)

Variation in BPGCR Fuel Loading (25-100 atm) and Inner Be Thickness (10-40 cm), Fixed PGCR Fuel Loading (10 atm)

i) The system k_{eff} increases moderately to a maximum value and then decreases with an increase in inner Be thickness. This optimum inner Be thickness increases moderately with an increase in BPGCR fuel loading. (Figures 4-17 and 4-18)

ii) The neutron removal lifetime increases slightly with inner beryllium thickness for values up to about 20 cm for the lower BPGCR gas loading range of 25-50 atmospheres. For this range of BPGCR gas loading, the neutron removal lifetime is essentially independent of inner beryllium thickness beyond about 20 cm for the range of TIBE examined. For higher BPGCR gas loading (60-100 atmospheres) the neutron removal lifetime is essentially independent of the inner beryllium thickness (10-40 cm). (Figure 4-19)

iii) The BPGCR-to-PGCR coupling coefficients increase initially up to a BPGCR core loading of 50 atmospheres and thereafter are essentially independent of BPGCR gas loading. (Tables 5-8 through 5-11)

iv) For the nominal PGCR fuel loading of 10 atmospheres, the BPGCR-to-PGCR coupling coefficients are considerably larger than the PGCR-to-BPGCR coupling coefficients due to the larger reactivity worth of the central BPGCR chamber.

v) The neutron generation time decreases with an increase in the BPGCR fuel loading. The neutron generation time is independent of the inner beryllium thickness for values up to about 20 cm and then increases moderately with inner beryllium thickness for the range of TIBE examined for low BPGCR gas loading of 25-50 atmospheres; the increase in neutron generation time is a consequence of the resultant decrease in k_{eff}. For higher BPGCR gas loading (> 50 atmospheres) the neutron generation time is essentially independent of the inner beryllium thickness. (Figure 5-15)

Variation in PGCR Core Loading (10-50 atm) and Inner Be Thickness (20-30 cm), Fixed BPGCR Chamber Loading (25 atm)

i) The optimum inner Be thickness at which k_{eff} peaks remains the same, at 10 cm, irrespective of the PGCR core loading. (Figure 4-22)

ii) The BPGCR-to-PGCR coupling coefficients decrease with an increase in the PGCR gas loading whereas the PGCR-to-BPGCR coupling coefficients increase with an increase in PGCR core fuel loading. (Figures 5-18 and 5-19)

iii) The PGCR-to-PGCR coupling coefficients are higher than for the case where the central BPGCR chamber is unfueled. (Figure 5-20)

iv) The neutron generation time is smaller than for the case when the BPGCR chamber is unfueled. (Figure 5-21)

Unequal PGCR Core Loading

i) Static and dynamic neutronic analysis of the BGCR with unequal PGCR core fuel loading has shown that a continuous low power output can be obtained from the BGCR by loading the PGCR cores in a staggered pattern. (The staggered loading pattern simulates the situation in which groups of PGCR cores are in different phases of operation, namely, intake, power, and exhaust.)

ii) The neutronic coupling contribution from a core of higher fuel loading to a core of lower fuel loading is larger than the contribution from a core of lower fuel loading to a core of higher fuel loading due to the different reactivity worths of the cores. (Tables 5-14 through 5-19)

For all the various configurations of the BGCR system and loading patterns considered for the dynamic neutronic analysis, the following general conclusions can be drawn.

- The core-to-core coupling effects contribute significantly to the power output of any chamber during the BGCR operation.
- The core neutron level can increase even during the time when the system is subcritical due to the strong neutronic coupling that exists among the BGCR cores.
- The core power level can be controlled by adjusting the individual core fuel gas loading which in turn controls both the core reactivity and the core-to-core neutronic coupling effects. The neutronic coupling effects among the cores can be independently controlled by placing rotating absorbers around the cores in the reflector.
- A decrease in the core-to-core delay time has no effect on the core neutron level while an increase in the delay time to values comparable to the system neutron generation time significantly reduces the core neutron level. (Figure 5-32)

A comprehensive and accurate treatment of the static and dynamic neutronic and fluid flow/heat transfer behavior of the complete bimodal system and optimization of the various parameters such as inner and outer moderator/reflector thickness, fuel loading patterns, fuel enrichment, helium mole fraction in the fuel gas mixture, number and size of the PGCR chambers, cycle time for the pulsing operation of the low power PGCR's etc. will not only be difficult but expensive. Although some relatively elementary models are employed in this investigation, such as the coupled core point reactor kinetics equations for the dynamic analysis, this work provides a good starting point on the basis of which more sophisticated models can be developed.

Comparative evaluation of the results from the single core point reactor kinetics program, ANCON (5), and the coupled core point reactor kinetics program (reduced to analyze single core kinetics), COUPKIN, performed in Appendix D has shown that even for systems that are superpromt critical, the ANCON and COUPKIN results agree reasonably well. Since the dynamic neutronic analysis is done for BGCR system configurations with individual cores that range from subcritical to slightly above critical it is concluded that the basic point reactor kinetics equations and their solution method employed in COUPKIN are valid. However, in order to run COUPKIN for analyzing different operational transients more efficiently, the following modifications should to be implemented.

i) The COUPKIN program currently employs fixed time steps in the calculation of core power level and delayed neutron precursor concentration. The program is currently capable of using different time steps during the intake, power and exhaust phases of operation. COUPKIN algorithm is stable for time steps as large as 5×10^{-2} seconds for transients for critical and slightly above critical systems whose neutron generation time is in the range of 1 to 3 milliseconds. However, a variable time step which depends on the core power level behavior during any transient needs to be implemented in the program. This variable time step will further improve the computation efficiency without loosing accuracy.

ii) The COUPKIN program is capable of performing dynamic calculations for short term operational transients which involve a few operational cycles. However, an iterative procedure should be incorporated into the COUPKIN algorithm so that a desired neutron level can be achieved by adjusting the core reactivity and/or the neutronic coupling effects among the individual cores.

iii) Presently COUPKIN is capable of handling only the delayed neutron feedback. In order to make the coupled core kinetics analysis more general and comprehensive in nature, other feedback effects such as core fuel gas mass flow feedback and moderator and fuel temperature feedbacks have to be included in the kinetics treatment.

The following sections point out other limitations of some of the methods and models used in this study, examine various areas of this work that require still further investigation and suggest possible refinements for some of the procedures employed. These sections also discuss some areas for further research on selection of different fuels and moderating/reflector materials.

Static and Dynamic Neutronic Models for the Bimodal Gaseous Core Reactor System

Steady State Neutronic Analysis

The three dimensional geometry, continuous energy, Monte Carlo transport code, MCNP, has been successfully used in the static neutronic calculations of the BGCR for various system configurations and core loading patterns. With the use of only a few of the variance reduction techniques such as, energy and time cutoff, weight cutoff, geometry splitting and Russian roulette, and energy splitting and Russian roulette it was possible to reduce the uncertainty in the system neutron multiplication factors and neutron removal lifetimes to about 1% or less while the uncertainty in the flux calculation was about 2% and the uncertainty in the core-to-core coupling coefficients was about 4% or higher; for the latter, the uncertainty is least for adjacent cores and increases as the distance between cores increases. In order to further decrease the uncertainty in the k_{eff} and neutron fluxes, sophisticated MCNP variance reduction techniques such as forced collisions, weight window, exponential transform etc. will be required. These variance reduction techniques attempt to decrease the uncertainties by either producing or destroying particles and have to be used cautiously in order to minimize the time per particle history to obtain more efficient results.

The gaseous core of the BGCR is a low scattering medium surrounded by beryllium which is a high scattering medium. The large neutron mean free path in the gaseous core and the lack of any significant above thermal neutron interactions in the gaseous core cause Monte Carlo codes such as MCNP to take considerably less computer time for the transport of neutrons in the gaseous core than for transport of neutrons in the beryllium moderator region. In order to reduce the relatively large computer time required for the static Monte Carlo neutronic analysis of the beryllium moderated BGCR system and to take advantage of the fact that the Monte Carlo calculations are much faster in the gaseous core than in beryllium, a gaseous core specific Monte Carlo scheme should be developed. This scheme would involve specially selected combinations of variance reduction methods for the Monte Carlo analysis which would be married to an analysis with selected approximation to the transport equation with suitable acceleration techniques. This hybrid method should be developed to couple the low scattering gas core region, treated by the Monte Carlo method, with the high scattering beryllium moderator region subjected to a selected transport theory approximation.

It has been found that convergence for one-dimensional or even two-dimensional diffusion or transport theory calculations for externally moderated gaseous core reactors is comparatively slow and such calculations are consequently quite expensive. The significant neutron flux variation in the highly scattering reflector region and particularly in the "boundary layer" at the interface between the gaseous core and the reflector leads to a situation in which conventional solution methods are not very effective and thus time consuming. It is, therefore, suggested that development and implementation of a gaseous core specific transport theory approximation or a combination of transport and diffusion theory calculation schemes with suitable acceleration techniques would increase the speed of convergence of BGCR system neutronic calculations. A good starting point would be the one-dimensional, discrete ordinates transport theory code, ONEDANT (32). For example, a gaseous core reactor specific neutronic scheme which should lead to significant reductions in computation time is to employ different approximations to the neutron transport equation in different regions of the reactor. Discrete ordinates transport theory calculations can be performed both in the gaseous core and in the gaseous core-reflector interface "boundary layer" which extends into the reflector a few mean free paths and diffusion theory calculations would be performed in the remaining reflector region. Modifications made in ONEDANT can be extended to two-dimensional calculations with the discrete ordinates code, TWODANT (33). ONEDANT and TWODANT numerically solve, respectively, the one-dimensional and two-dimensional, multi-group form of the Boltzmann transport equation using the discrete ordinates form of approximation for treating angular variation of neutron distribution and the diamond difference scheme for space discretization. Both inner and outer iterations are accelerated using the diffusion synthetic acceleration technique (32,33).

Integral Kinetics Parameters for Individual Coupled Cores

The solution of the coupled core point reactor kinetics equations (B-1 and B-2) of Appendix B requires integral parameters such as reactivity and neutron generation time for the individual coupled cores. The core reactivity (ρ_j) and core neutron removal lifetime cannot be directly obtained from either MCNP or any other two-dimensional transport calculations unless modifications are made to the available codes. For the present work, the individual core reactivity and neutron generation time have been estimated from the global system reactivity and neutron removal lifetime. Appropriate methods need to be developed to determine the exact reactivity worth and neutron generation time of individual cores in the coupled core BGCR system.

The precise value of the integral parameters such as k_{eff} and ℓ for the individual cores in the coupled core system can be determined from either Monte Carlo or discrete ordinates transport calculations. In a Monte Carlo transport calculation separate ledgers for sources and fission neutrons for each core have to be maintained. This will involve simultaneous tracking of generations of neutrons for each of the separate cores in the coupled core reactor system. This can be achieved by utilizing the parallel computation capability of modern supercomputers such as the Cray-X/MP or IBM 3090. The MCNP code can be modified to accommodate this feature.

Discrete ordinates transport calculations for individual core kinetics parameters can be performed by dividing the system geometry into zones which contain each core and the surrounding moderator material. Each zone will be separated from the adjacent zone by a "pseudo boundary". Each of the cores and the associated moderator region of the zone will have their own transport equations with boundary conditions specified for the "pseudo boundary". This set of equations have to be simultaneously solved for fluxes and core multiplication factors for each of the core zones.

Neutron Kinetics Calculations

The kinetics calculations for the multiple cavity gas core reactor system have been performed by using the coupled core point reactor kinetics equations. The integral kinetics parameters are obtained from the steady state neutronic calculations at various instants of time during the operation of the reactor. The neutron flux shape, the multiplication factor, the neutron removal lifetime, and the core-to-core coupling coefficients undergo significant variation during the loading of the individual cores. Even though the coupled point reactor kinetics equations constitute a reasonably good treatment for a preliminary dynamic analysis of the BGCR, a complete space-time dependent analysis, particularly during the intake and exhaust phases of the PGCR operation must be performed, to accurately incorporate the significant variations of the integral parameters during these phases of operation of the BGCR system into the dynamic analysis. These space-time dependent calculations must eventually include all the different feedback effects discussed below.

Feedbacks due to Temperature Changes

The feedback effects due to temperature changes in the moderator/reflector and fuel need to be included in the kinetics calculations.

The effects of moderator temperature changes on the neutron spectrum and reactivity of the multiple core gaseous core reactor system have to be examined. The MCNP cross section library for beryllium and beryllium oxide contains data sets for only four temperatures: 300 K, 600 K, 800 K, and 1200 K. This library will have to be expanded to include sets of cross sections at additional temperatures so that a study of the neutron spectrum and reactivity variation due to moderator temperature changes can be performed in much finer detail. The NJOY/TRANSX (34) nuclear data processing system can be used to generate cross sections from ENDF/B files for various moderator materials such as beryllium and beryllium oxide at more temperatures than are presently available for use with the MCNP, ONEDANT, and TWODANT codes.

The effects of fuel temperature changes on reactivity through Doppler broadening should be included in the coupled core kinetics calculations. The fuel temperature coefficient of reactivity for 100% enriched UF_6 for a range of temperature 300 K to 1500 K was found to be small and positive ($\approx 6\text{x}10^{-7}$ $\Delta k/k$ per K) and for 80% enrichment the fuel temperature coefficient of reactivity for the same range of temperature was found to be small and negative ($\approx -1.98\text{x}10^{-7}$ $\Delta k/k$ per K) (30). The beryllium moderator temperature coefficient of reactivity for the range of temperature 300 K to 1200 K was found to be significant and negative ($\approx -1.7\text{x}10^{-5}$ $\Delta k/k$ per K). Even though moderator temperature changes have more pronounced effects on reactivity than highly enriched fuel temperature variations for externally moderated gaseous core reactors, the fuel temperature effect cannot be completely neglected for any detailed or comprehensive coupled core kinetics studies.

Moderator Reflector Studies

Beryllium has been the only moderating material considered for the BGCR system in this study. In the previous gas core reactor studies conducted at the University of Florida (30), H_2O and graphite were found to be unsuitable candidates as possible moderating materials for externally moderated gaseous core reactors, H_2O because of its large thermal absorption cross section and graphite because of its large thermal diffusion lengths and excessive slowing down length. H_2O and D_2O are not very desirable materials to be used as moderators for any space based reactors. Both beryllium and beryllium oxide are excellent moderator materials from a neutronics standpoint.

Be and BeO are capable of providing some structural integrity for the reactor system. BeO is more desirable than Be for high power systems because of its much higher melting point. The inner moderator surface will have to be coated with a suitable liner material to protect the moderator reflector from the corrosive UF_6.

Since beryllium oxide is a better moderator for both low power and high power reactor systems, the static and dynamic neutronic calculations will have to be performed with BeO moderator at many temperatures and thicknesses with suitable liner materials. The optimization of the moderator region will have to be based not only on neutronic characteristics but also on heat transfer and structural properties.

Fuel Studies

Calculations in this study have been performed for 85% enriched U^{235} fuel. The neutronic studies should be extended to lower and higher fuel enrichments to determine the effect of fuel enrichments on fuel loading requirements for the coupled gas core reactor system.

It has been predicted that UF_6 begins to dissociate in the reactor cores at around 2000 K and partial pressure of about 10 atmospheres. In view of this, uranium tetrafluoride (UF_4) is being considered as the reactor fuel especially for the high power and high temperature cores. Therefore, the neutronic studies of the coupled gaseous core reactor should be performed with UF_4 as the reactor fuel for both static and dynamic performance of the reactor system.

Neutronic studies should also be extended to include U^{233} and Pu fuels. U^{233} is neutronically more desirable than U^{235} since the critical loading for the BGCR system will be reduced. The reduction in loading requirements is a desirable aspect for any space based power system.

Gas Flow/Heat Transfer Studies For the Bimodal Gaseous Core Reactor

In order to determine the temperature distribution in the gaseous core and the reflector regions an appropriate fluid flow model for the gaseous core region coupled with a conduction heat transfer model for the reflector region need to be developed.

The temperature distribution in the reflector region is calculated by taking into consideration the fission energy deposition in the core, the convective and radiative heat transfer from the gas core to the reflector wall region as well as energy deposition in the reflector from photons and neutrons. Since the reflector temperature exerts a major influence on the neutronic behavior of the gaseous core, the reflector temperature distribution needs to be accurately determined. In order to maintain the moderator temperature at a desired level the necessary coolant flow through coolant channels in the reflector has to be established. An iterative procedure between the neutronic calculation for power output and energy deposition and the fluid flow/heat transfer analysis for the gaseous core and the reflector region temperature distribution will produce a comprehensive neutronic-energetics analysis of the coupled BGCR system.

Summary

Static and dynamic neutronics of the coupled multiple chamber beryllium moderated bimodal gaseous core reactor, capable of generating both low and high power for space applications, have been investigated in this dissertation. It is found that the core-to-core neutronic coupling effects contribute significantly to the power behavior of any chamber during both low power and high power operation. As a consequence of the strong coupling, steady state operation and even power increases can be achieved with all of the cores operating in a subcritical condition. The core power levels can be controlled by the core fuel loadings as well as the neutronic coupling effects among the cores. The neutronic coupling influence can be controlled by suitably placed and properly timed rotating absorbers located in the reflector region.

This chapter has identified some of the key conclusions drawn from the static and dynamic analysis of the coupled core bimodal gaseous core reactor system. It has also examined some of the limitations associated with the dynamic analysis methods used in this study and suggested ways to refine some of these analysis methods. Some areas of further research required for a comprehensive neutronic, fluid flow, and heat transfer analysis of the BGCR system were also suggested.

The three-dimensional, continuous energy, Monte Carlo transport theory code, MCNP, has been successfully used in the steady state neutronic analysis of the BGCR. Simulation of the exact geometry of the complex BGCR and of the probabilities of particle (neutron) interaction in MCNP have permitted estimation of global kinetics parameters such as system neutron multiplication factors and neutron removal lifetime and core specific parameters such as the coupling coefficients to be performed with a high degree of confidence. The coupled core point reactor kinetics equations and their solution method used in this analysis are found to be adequate for preliminary neutron kinetics studies of the BGCR system.

The primary use of such a bimodal reactor system would be for a space based system which requires low power for long term station keeping/surveillance purpose and high or burst power for shorter periods of time, on the order of few hours.

APPENDIX A
MCNP-A GENERAL MONTE CARLO CODE FOR NEUTRON AND PHOTON TRANSPORT

MCNP is a general purpose, continuous energy, generalized geometry, time dependent, coupled neutron-photon Monte Carlo transport code. It solves neutral particle transport problems and may be used in any of three modes: neutron transport only; photon transport only; or combined neutron/photon transport when photons are produced by neutron interactions. This appendix enumerates the basic features of the MCNP code and discusses typical input for both a multicore bimodal gaseous core reactor system and a single core gaseous core reactor system. Details regarding the features and capabilities of MCNP are given in references (3, 35-38).

Nuclear Data

Five classes of nuclear data tables are available for MCNP. They are:

i) Continuous energy and thinned continuous energy neutron interaction data;

ii) Discrete reaction neutron interaction data;

iii) Photon interaction data;

iv) Neutron dosimetry cross sections;

v) Neutron $S(\alpha,\beta)$ data;

Continuous and Thinned Continuous Energy Neutron Cross Section Data

MCNP neutron and photon cross section data have been processed into ACE (A Compact ENDF) format by using NJOY (34) for evaluated data in ENDF/B format and MCPOINT (39) for ENDL data. Continuous and thinned continuous energy cross sections for each reaction are given on one energy grid, which is sufficiently dense that linear-linear interpolation between points reproduces the evaluated cross sections within a specified tolerance that is generally less than 1%. Depending on the number of resolved resonances for each isotope, the resulting energy grid may contain as few as ≈250 points (eg. for hydrogen) or as many as ≈22,500 points (eg. for the ENDF/B-V version of Au-197). Other information such as total absorption cross section, total photon production cross section,and average heating number for energy deposition calculations are also tabulated on the same energy grid.

Angular distributions of scattered neutrons are included in the neutron interaction tables for all non-absorption reactions. The distributions are given in the center of mass system for elastic scattering and discrete level scattering, and in the laboratory system for all other inelastic interactions. Recently-processed data sets contain photon production cross sections and photon angular distributions for each reaction that produces secondary photons. Evaluated angular distributions of secondary neutrons and photons are approximated on MCNP data tables by 32 equally probable cosine bins.

Since the original continuous energy cross section files are very long, a shortened or "thinned" set of cross sections in ACE format is also available for the same ENDF/B materials. This thinned set preserves the flat weighted integral of the total cross section to within 0.5%. When the original continuous and thinned cross sections are plotted on vastly expanded energy scales, one can see that the thin, narrow resonances have been smoothed over or even eliminated in the thinned cross sections; however, it is not possible to see any difference between the two curves if the two sets are plotted on a normal energy scale. The broadening of resonances and changes in the cross section values manifest in other ways. For example, multigroup cross sections are larger when calculated from the thinned set rather than from the original set. Multigroup cross sections confirm that original and thinned cross section sets differ primarily in the resonance region. The thinned cross section set has been developed in order to hold down the size of the cross section files. For problems in which exact detail in the resonance region is essential, it is clearly necessary to use the original continuous cross section set.

Discrete Reaction Neutron Cross Sections

Since even the thinned cross section storage and running time requirements for an MCNP problem can be quite large, a smaller pointwise discrete reaction neutron cross section data table has been included in the MCNP package. This pointwise cross section set has been averaged over 262 energy groups using a flat weighting function. This has shrunk the total size of the individual cross section files by a factor of seven. These discrete reaction cross sections are not multigroup libraries but are given as histograms rather than as continuous curves. Discrete reaction data are provided primarily for reducing the data storage requirements in order to enhance the ability to run MCNP on small machines or in a time sharing environment. These tables are useful for preliminary, scoping calculations. They are not recommended as a substitute for the continuous energy cross section when performing final design calculations, particularly for problems involving transport through the resonance region.

Photon Interaction Data

Photon interaction data that are required for all photon problems are stored in the library MCPLIB. Cross sections as a function of energy are given on the photon tables for coherent scattering, pair production, and the photoelectric effect. Energy grids are tailored specifically for each element and contain about 40 to 60 points. Photon heating numbers are tabulated on the same energy grids as cross sections. Angular distributions of secondary photons are introduced through form factors for coherent scattering functions and scattering functions for incoherent scattering.

Very few approximations are made in the processing codes to transfer photon data from ENDF into the format of MCNP photon interaction data. Form factors and scattering functions are reproduced as given; heating numbers are calculated from evaluated data and fluorescence data are extracted from sources other than ENDF.

Dosimetry Cross Sections

Dosimetry cross sections are provided in the MCNP package for calculating reaction rates by multiplying an energy dependent fluence by the appropriate cross sections. Data contained on dosimetry tables are simply energy-cross section pairs for some reactions with energy grids for all reactions independent of each other.

Neutron Thermal $S(\alpha,\beta)$ Cross Sections

Thermal $S(\alpha,\beta)$ cross sections that are required for a complete representation of thermal neutron scattering by molecules and crystalline solids are from a special set of ENDF tapes; they are processed through the THERMR and ACER modules of the NJOY (34) system into a format appropriate for MCNP. Data on the current library, TMCCS2, are for neutron energies less than 4 eV.

Cross sections are tabulated on a table-dependent energy grid; inelastic scattering cross sections are always given; elastic scattering cross sections are sometimes given. Corrected energy-angle distributions are provided for inelastically-scattered neutrons. Elastic scattering data are derived from either a coherent or incoherent approximation. In the coherent case, cosine bins are tabulated for each of the several incident energies while for the incoherent case, scattering cosines are determined from a set of Bragg energies derived from the lattice parameters.

The current thermal cross section data library, TMCCS2, available at the San Diego Supercomputer Center (SDSC) Cray XMP/48 includes light water, hydrogen and zirconium in ZrHx, polyethylene, benzene, beryllium metal, beryllium oxide,and graphite.

Validation of and Choosing Cross Sections

Several successful benchmark calculations have been carried out using MCNP with the associated cross section data in order to establish the validity of the MCNP cross section library (40). These calculations have been done on thermal critical assemblies, light water moderated uranium metal fueled assemblies, heavy water moderated uranium metal fueled assemblies, various magnetic fusion reactor designs,and fast reactor concepts. A differential data checking in which the point-wise data files themselves as processed into ACE format by the NJOY code has also been performed. In the differential data checking procedure, sets of multigroup cross sections are calculated from the original ENDF/B cross sections and from cross sections in ACE format using the same weighting function. Even though one does not expect the corresponding multigroup cross sections to be identical due to the effects of linearization of the original data and due to thinning, the larger than expected anomaly is attributed to some sort of problem in the data translation (35).

The selection of appropriate neutron interaction data is highly user and problem dependent. The easiest choice for the user is not to specify anything in which case MCNP is forced to select the default tables that are found first in the cross section directory file, XSDIR. Some guidelines and observations that can be followed in the selection of appropriate cross section files are listed below.

i) Discrete reaction cross sections are not a bad approximation for high energy problems. The detailed continuous energy cross section set is essential for problems influenced strongly by transport through the resonance region.

ii) The differences in philosophies of cross section data evaluators must be taken into account by the MCNP user. The evaluation by the Physical Data Group at Livermore (ENDL) reflect the philosophy of representing the experimental data with the fewest possible points whereas the evaluations by the Nuclear Science Group at Los Alamos are frequently complex because they are the most thorough.

iii) The resonance data that have been Doppler broadened to the appropriate temperature have to be used in the calculation.

iv) Preliminary sensitivity studies of the problem set must be carried out and differences in the results, if any, must be investigated.

v) The continuous energy cross section data require larger memory and greater execution time than the discrete reaction cross section data. One of the criteria for the selection of appropriate cross section data is the affordability of computer system CPU and storage by the user.

Geometry

Cells

The basic unit of MCNP geometry is the cell. Surfaces are used to create cells in the ordinary Cartesian coordinate system using the sense of space on either side. Combinations of sense-signed surfaces are used to define regions of space encompassed by a cell.

The Boolean geometry operators are used in MCNP to construct cells. The intersection of common regions of a space with respect to surfaces is the default operator. The union of space with respect to surfaces is designated by a colon (:). A complement operator (#) is used to remove portions of space defined by either cells or surfaces. Parentheses are used to control the order of execution of the three geometry operators.

MCNP cells are required for various aspects of the transport calculation such as construction of the appropriate model, specification of the appropriate materials in the cells and for definition of variance reduction parameters. Volumes of most cells are analytically calculated automatically in MCNP. Other volumes are calculated stochastically.

Surfaces

MCNP uses 26 different types of surfaces defined by first-, second-, and certain fourth- order equations to create three dimensional geometries. These surfaces are separated into seven classes: four planes, five spheres, six cylinders, six cones of either one or two sheets, simple quadratics which have their axes parallel to a coordinate axis, general quadratics whose axes are not parallel to a coordinate axis, and elliptical tori with an axis parallel to a coordinate axis. Each of the 26 types of surfaces has a descriptive one or two letter mnemonic. All surfaces are defined by specifying the appropriate equation coefficients.

Table (A-1) illustrates the surface types, their equations, their mnemonics, and the order of the card entries.

Any surface may be designated a reflecting surface by preceding its number on the surface card with an asterisk. Any particle hitting a reflecting surface is specularly reflected. Reflecting planes are useful in introducing symmetry into the geometry of the problem.

Variance Reduction Techniques

The MCNP code is rich in variance reduction techniques. These are computational tools that make it possible for the code user to better sample statistical events in the regions of interest and to reduce wasted effort in unimportant regions thereby reducing the computer time to obtain results of sufficient precision.

Geometry Splitting and Roulette

The problem geometry is divided into a number of geometric regions or cells each of which is assigned a cell importance by the user on the MCNP data input card depending on a variety of factors such as the physics of the problem. In geometry splitting a particle crossing into a cell of higher importance is split whereas a particle crossing into a cell of lower importance undergoes Russian roulette. When a particle of weight WGT passes from a cell of importance I to one of higher importance I', the particle is split into a a number of identical particles of lower weight according to

Table A-1. MCNP Surface Cards.

Mnemonic	Type	Description	Equation	Card Entries
P	Plane	General	$Ax+By+Cz-D=0$	A B C D
PX		Normal to X-axis	$x-D=0$	D
PY		Normal to Y-axis	$Y-D=0$	D
PZ		Normal to Z-axis	$z-D=0$	D
SO	Sphere	Centered at Origin	$x^2+y^2+z^2-R^2=0$	R
S		General	$(x-\bar{x})^2+(y-\bar{y})^2+(z-\bar{z})^2-R^2=0$	$\bar{x}$ $\bar{y}$ $\bar{z}$ R
SX		Centered on X-axis	$(x-\bar{x})^2+y^2+z^2-R^2=0$	$\bar{x}$ R
SY		Centered on Y-axis	$x^2+(y-\bar{y})^2+z^2-R^2=0$	$\bar{y}$ R
SZ		Centered on Z-axis	$x^2+y^2+(z-\bar{z})^2-R^2=0$	$\bar{z}$ R
C/X	Cylinder	Parallel to X-axis	$(y-\bar{y})^2+(z-\bar{z})^2-R^2=0$	$\bar{y}$ $\bar{z}$ R
C/Y		Parallel to Y-axis	$(x-\bar{x})^2+(z-\bar{z})^2-R^2=0$	$\bar{x}$ $\bar{z}$ R
C/Z		Parallel to Z-axis	$(x-\bar{x})^2+(y-\bar{y})^2-R^2=0$	$\bar{x}$ $\bar{y}$ R
CX		On X-axis	$y^2+z^2-R^2=0$	R

Table A-1. Continued.

Mnemonic	Type	Description	Equation	Card Entries
CY		On Y-axis	$x^2+z^2-R^2=0$	R
CZ		On Z-axis	$x^2+y^2-R^2=0$	R
K/X	Cone	Parallel to X-axis	$\sqrt{(y-\bar{y})^2+(z-\bar{z})^2}-t(x-\bar{x})=0$	$\bar{x}$ $\bar{y}$ $\bar{z}$ t^2 ±1
K/Y		Parallel to Y-axis	$\sqrt{(x-\bar{x})^2+(z-\bar{z})^2}-t(y-\bar{y})=0$	$\bar{x}$ $\bar{y}$ $\bar{z}$ t^2 ±1
K/Z		Parallel to Z-axis	$\sqrt{(x-\bar{x})^2+(y-\bar{y})^2}-t(z-\bar{z})=0$	$\bar{x}$ $\bar{y}$ $\bar{z}$ t^2 ±1
KX		On X-axis	$\sqrt{y^2+z^2}-t(x-\bar{x})=0$	$\bar{x}$ t^2 ±1
KY		On Y-axis	$\sqrt{x^2+z^2}-t(y-\bar{y})=0$	$\bar{y}$ t^2 ±1
KZ		On Z-axis	$\sqrt{x^2+y^2}-t(z-\bar{z})=0$	$\bar{z}$ t^2 ±1 =1 used only for 1 sheet cone
SQ	Ellipsoid Hyperboloid Paraboloid	Axes parallel to X-, Y-, or Z- axis	$A(x-\bar{x})^2+B(y-\bar{y})^2+C(z-\bar{z})^2$ $+2D(x-\bar{x})+2E(y-\bar{y})$ $+2F(z-\bar{z})+G=0$	A B C D E F G $\bar{x}$ $\bar{y}$ $\bar{z}$
CQ	Cylinder Cone Ellipsoid Hyperboloid Paraboloid	Axes not parallel to X-, Y-, or Z- axis	$Ax^2+By^2+Cz^2+Dxy+Eyz$ $+Fzx+Gx+Hy+Jz+K=0$	A B C D E F G H J K

Table A-1. Continued.

Mnemonic	Type	Description	Equation	Card Entries
TX	Elliptical or circular torus. Axis is parallel to X,Y or Z axis.	$(x-\bar{x})^2/B^2+(\sqrt{(y-\bar{y})^2+(z-\bar{z})^2}-A)^2/C^2-1=0$		$\bar{x}$ $\bar{y}$ $\bar{z}$ A B C
TY		$(y-\bar{y})^2/B^2+(\sqrt{(x-\bar{x})^2+(z-\bar{z})^2}-A)^2/C^2-1=0$		$\bar{x}$ $\bar{y}$ $\bar{z}$ A B C
TZ		$(z-\bar{z})^2/B^2+(\sqrt{(x-\bar{x})^2+(y-\bar{y})^2}-A)^2/C^2-1=0$		$\bar{x}$ $\bar{y}$ $\bar{z}$ A B C

the following manner. If I'/I is an integer n ($n \geq 2$), the particle is split into n identical particles each weighing WGT/n. Weight is preserved in the splitting process. If I'/I is not an integer, but still greater than 1, splitting is done probabilistically so that the expected number of splits is equal to the importance ratio. For example, if I'/I is 2.75, 75% of the time the splitting is 3-for-1 and 25% of the time the splitting is 2-for-1.

If the particle weight of WGT passes from a cell of importance I to one of lower importance I' so that I'/I < 1, Russian roulette is played with the probability of 1-(I'/I) or the particle is followed further with the probability I'/I and weight WGT*I/I'. Figure A-1 illustrates the geometry splitting and Russian roulette variance reduction technique.

The original cell importances can have any values; they are not limited to integers. However, adjacent cells with vastly different importances will produce unreliable sampling. It is generally best to keep the ratio of importances of adjacent cells to within a factor of a few and to have cells in the penetration direction with optical thickness less than about two mean free paths.

Weight Cutoff

Weight cutoff is one of the variance reduction techniques in MCNP by which particles are killed if their weights fall below a specified minimum weight in any

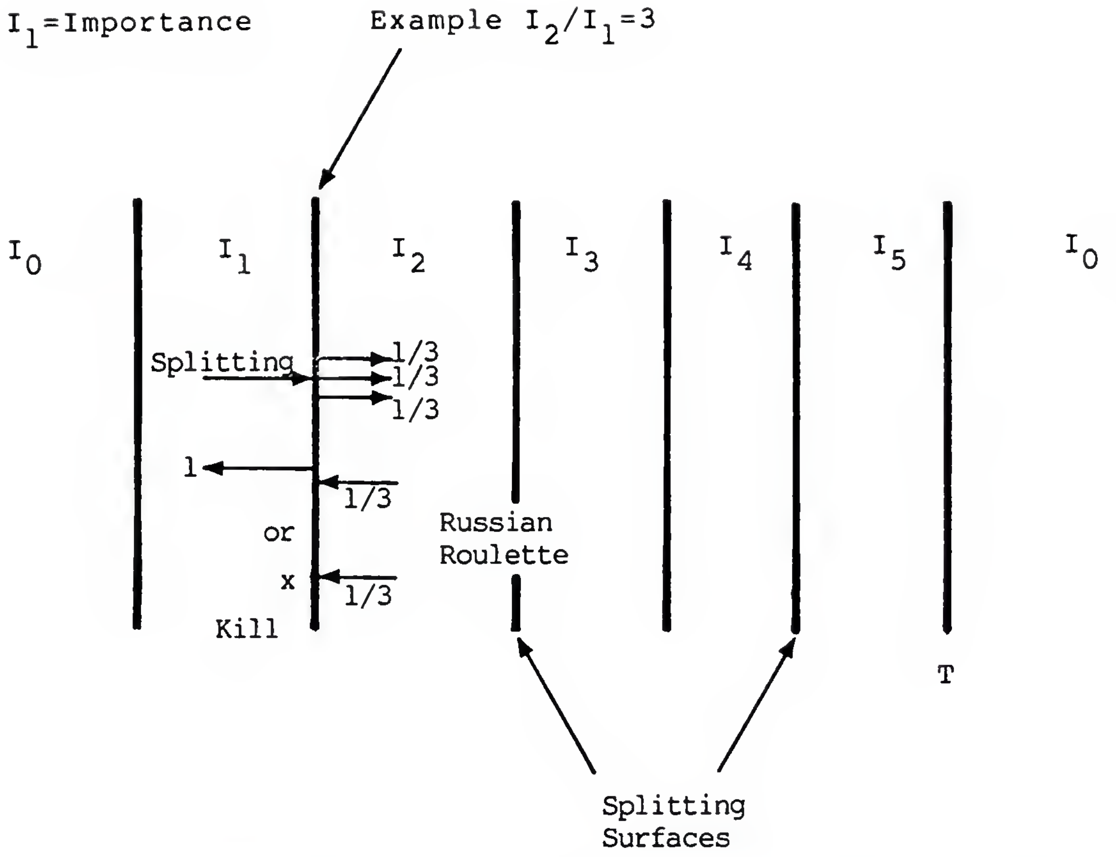

Figure A-1. Geometry Splitting/Russian Roulette Technique in MCNP.

specific region. This avoids the loss of time following very low weight and, hence, unimportant particles.

Time and Energy Cutoffs

A MCNP run can be truncated with a time cutoff that discontinues particle tracking below a specified energy range. The Energy cutoff technique must be used cautiously so that the specified cutoff energy conforms with the nature of the problem.

Exponential Transform

Exponential transform is another variance reduction method that can be used to bias particles towards the tally region. The exponential transform allows particle walks to move in a preferred direction by artificially reducing the macroscopic cross section in the preferred direction and increasing the cross section in the opposite direction according to

$$\Sigma^*_t = \Sigma_t(1 - p\mu) \qquad \text{(A-1)}$$

where Σ^*_t = fictitious transformed cross section

Σ_t = true total cross section

p = exponential transform parameter used to vary the degree of biasing

μ = cosine of the angle between the preferred direction and the particle velocity.

This method which is also known as "path length stretching" does not work well when the particle population does not have an exponential distribution. It is reported that the exponential transform works best in highly absorbing media and very poorly in scattering media (3).

Implicit Capture

In implicit capture a particle's weight is reduced by the capture probability at each collision rather than being killed with the capture probability as in the analog case. In implicit capture the particle always survives the collision and followed with new weight:

$$\mathrm{WGT}\left(1 - \frac{\sigma_{ai}}{\sigma_{ti}}\right)$$

where, σ_{ti} is the total microscopic cross section and σ_{ai} is the microscopic absorption cross section for nuclide i. Implicit capture can be considered as a splitting process where the particle is split into an absorbed weight (which is not followed further) and a surviving weight.

In analog capture, the particle is killed with the probability σ_a/σ_t, where σ_a and σ_t are the microscopic absorption and total cross section of the collision nuclide at the incoming neutron energy.

Weight Window

The weight window method is a space-energy-dependent splitting and Russian roulette technique. This is illustrated in Figure A-2. Each region is assigned a set of upper and lower weight window bounds. Particles with weights above the upper bounds are split so that their

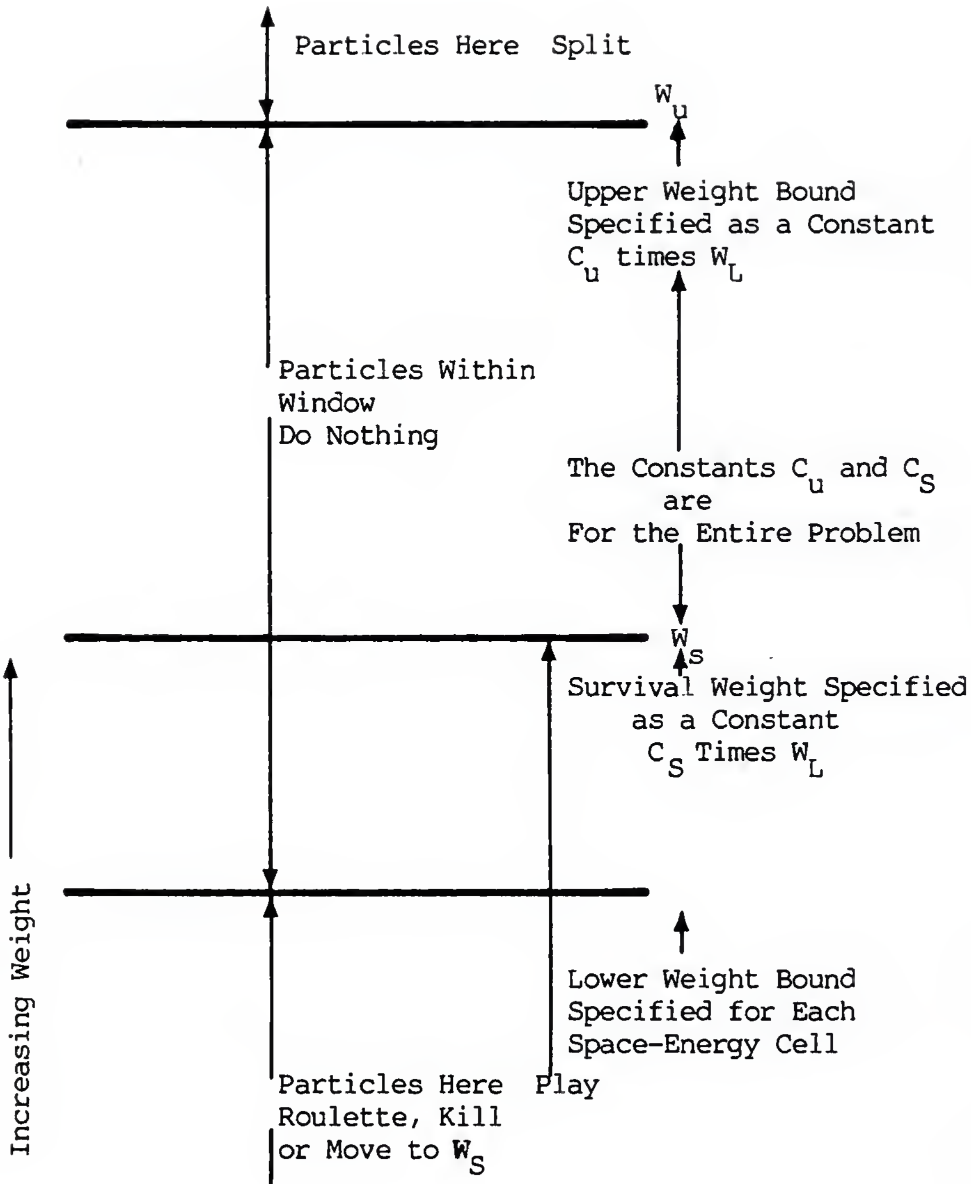

Figure A-2. Detail of the Weight Window

weight drops into the window; particle with weight below the lower bounds are rouletted and the particle's weight is either increased to a value within the window or the particle is terminated. No action is taken for particles within the window. In addition to causing the particle to migrate towards the tally region, the weight window method also provides effective weight control. The weight window game may be played on either surfaces, collisions or both. The energy and geometry dependence of the weight window game render this more powerful than the traditional combination of geometric splitting and Russian roulette and weight cutoff.

In order to alleviate the difficulty in providing a large number of input importance functions for the code for a multiregion problem, provisions are being made in the future versions of MCNP code to automatically select the input importance function (41).

Forced Collisions

Forced collisions method is used to reduce the variance by forcing particle collisions in regions where collisions are unlikely. The MCNP forced collision algorithm causes particles entering a spatial region to be split into a collided and an uncollided part with the appropriate weight adjustments. The uncollided part exits the current cell without collision and is stored in the bank until later when its track is continued at the cell boundary. The collided part may undergo Russian roulette, if desired, in order to limit the number of additional particles.

Source Energy and Angle Bias

The source energy and angle biasing is a variance reduction technique through which provision is made for biasing the MCNP sources in any or all of the variables specified. This method works by artificially starting more of the source particles in the direction and energy regime of most importance and then adjusting the weight of the particle as follows:

$$w_s = p/p^* \qquad \text{(A-2)}$$

where w_s = weight adjustment factor for the source particle that was modeled.

p = the value of the true probability function for the source particle.

and p^* = the value of the artificial probability density function that was used in sampling the particle.

Problem efficiency can be improved by orders of magnitude by invoking source biasing for problems where the source sampling is a major component of the total problem solution. However, overuse of source biasing may cause unacceptably large weight fluctuation.

In MCNP, the user has several choices of arbitrary probability density functions for source biasing. For source energy biasing, the user has several options to select the energy range and the probability functions to sample the energy ranges.

For source angle biasing, the user specifies a preferred direction vector that is an arbitrary vector in space. The two options in source angle biasing are the cone biasing and exponential biasing. In cone biasing, a cone which divides the angular domain into two pieces is specified; one inside and one outside the cone. The user then specifies the fractions of the particles to be started inside the cone and outside the cone. The particles started inside the cone have the same weight and all those started outside the cone have a different weight. If a significant weight discontinuity occurs at the surface of the cone, the exponential source biasing should be used at the cone surface to eliminate this discontinuity in weight.

The exponential source biasing is a continuous angle bias because the sampled density is exponential in the cosine of the angle with respect to a reference direction. The probability density function for the exponential source biasing is

$$p(\mu) = Ce^{k\mu} \qquad \text{(A-3)}$$

where $\mu=\cos\theta$, k is user selected biasing parameter $0.01 \le k \le 3.5$, C is the normalization constant and θ is the angle between the reference direction and the cone. The normalized constant is given by

$$C = \frac{k}{e^{k} - e^{-k}} \quad . \qquad \text{(A-4)}$$

It can be seen that the exponential angle biasing has no weight discontinuities and large weight fluctuation can be introduced by setting k too large.

Tallies

MCNP provides six neutron tallies and five photon tallies to make it easy for the user to obtain the desired result (flux, current, heating etc.) as a function of cell or surface, energy, time, angle, flagged cell or surface, segmented portions of cell or surface, tally multipliers, and any other user modifications for a tally.

Table A-2: Basic MCNP Tallies

Tally Mnemonic	Description
F1:N or F1:P	Surface Current
F2:N or F2:P	Surface Flux
F4:N or F4:P	Flux by Track Length per unit Volume.
F5a:N or F5a:P	Flux at a Point
F6:N or F6:N,P or F6:P	Track Length Estimate of Energy Deposition
F7	Track Length Estimate of Fission Energy Deposition

In addition to the basic tallies given in Table A-2 there are several standard tally modifiers that allow easy tally conversion to the quantity of interest. MCNP tallies can be either particles or particle energy; energy-, time-, and angular dependent user specified multipliers are available. General reaction multipliers to any tally are available in MCNP that can be sums or products of any of the various reactions from the data tables. Segmented tallies can be made in a cell or surface by using pseudo surfaces (that are not part of the geometry). Flux and current tallies can be obtained by flagging those particle which have crossed one or more specified cell(s) or surface(s). The cell flagging and surface flagging capability of MCNP allows one to determine the tally contribution of particles from one cell or surface to any other cell or surface of the system. This capability of MCNP is used in this work to determine the coupling coefficients (α_{jk}) for the bimodal gaseous core reactor which are a measure of the degree of influence of the k th core neutron flux on the jth core neutron flux.

Error Analysis in MCNP

MCNP provides extensive error analysis procedures which give statistical error or uncertainty associated with the results. The user not only gains an insight into the quality of the results, but also can determine if a tally is well behaved. If a tally is not well behaved, the estimated error associated with the result will not reflect the true confidence interval of the result and, thus the answers could be completely erroneous.

The Monte Carlo mean x is estimated by

$$\bar{x} = \frac{1}{N} \sum_{i=1}^{N} x_i \qquad \text{(A-5)}$$

where x_i is the tally from the i th history and N is the total number of histories.

The variance of the population of x values which is a measure of the spread of these values is given by

$$S^2 = \frac{1}{N-1} \sum_{i=1}^{N} (x_i - x)^2 \approx \bar{x}^2 - \overline{x^2} \qquad \text{(A-6)}$$

where

$$\overline{x^2} = \frac{1}{N} \sum_{i=1}^{N} x_i^2 \qquad \text{(A-7)}$$

The quantity S is the standard deviation of the population x based on the values of x_i that were actually sampled.

The estimated variance of $\bar{x}$, $S_{\bar{x}}$, is given by

$$S_{\bar{x}}^2 = \frac{S^2}{N} \qquad \text{i.e., } S_{\bar{x}} \;\alpha\; \frac{1}{\surd N} \qquad \text{(A-8)}$$

which means that in order to halve S_x, four times the original number of histories must be calculated, a process that can be expensive. The quantity S_x can also be reduced for a specified N by reducing S, i.e., by reducing the spread of tally x. This can be accomplished by using variance reduction techniques such as those described earlier in this appendix.

All standard MCNP tallies such as fluxes, currents, neutron multiplication factor (k_{eff}), neutron removal lifetime (ℓ) etc. are normalized to be per starting particle and printed in the output with a second number which is the estimated relative error which is defined as

$$R = \frac{S_{\bar{x}}}{\bar{x}} = \left[\frac{1}{N}\left(\frac{\overline{x^2}}{\bar{x}^2} - 1\right)\right]^{\frac{1}{2}}$$

$$= \left[\frac{\sum_{i=1}^{N} x_i^2}{\left(\sum_{i=1}^{N} x_i\right)^2} - \frac{1}{N}\right]^{\frac{1}{2}} \qquad \text{(A-9)}$$

where, x_i and x_i^2 are updated at the end of each history in MCNP to include the history correlations. Experience has shown that reliable confidence intervals are generated when the relative error is less than 0.10.

Since R^2 is proportional to 1/N and the problem computer time T is proportional to N a figure of merit (FOM) for a tally is defined as

$$\mathrm{FOM} = 1/R^2T \qquad \text{(A-10)}$$

The numerical value of the FOM, which is approximately a constant, will increase as the problem becomes more efficient because R^2T will decrease. This means that more efficient tallies will have a larger FOM. In addition, the FOM can be used for estimating the amount of computer time required to achieve a desired relative error. Tally fluctuation charts which contain the FOM for one user specified tally bin of each tally as a function of the number of histories are automatically printed at the end of each MCNP problem.

Criticality Calculations

MCNP has the capability to calculate the k_{eff} eigenvalue and neutron removal lifetime for both subcritical and supercritical systems, and their associated relative errors. The calculation is performed as a series of generations or cycles of neutrons, estimating both k_{eff} and removal lifetimes. These quantities are estimated for every active cycle as well as averaged over all previous active cycles. k_{eff} is estimated basically in three ways and removal lifetimes in two ways. The basic k_{eff} calculations are collision, absorption, and track length estimators and the removal lifetime calculations are collision and absorption estimators. These estimates are combined and correlated so that the user can select the combined tally with the lowest relative error.

There are seven total estimators for k_{eff}: collision, absorption, track length, and four combinations of these single estimators. The three removal lifetime estimators are collision, absorption, and a combined collision absorption estimator. Covariances are included in the calculation of the relative errors of the combined estimates.

Program Flow

Because criticality calculations involve running successive generations of particles, they have a different program flow than other MCNP problems and require a criticality source (KCODE) incompatible with the other standard MCNP sources. The MCNP criticality calculation stream consists of three stages, namely, initiation stage, transport stage, and cycle termination.

Initiation Stage

The user is required to supply the following information on the KCODE card in the MCNP input file.

i) the nominal number of source particles,N

ii) an initial k_{eff} guess

iii) the number of cycles, l_c, to skip before tally accumulation

iv) the total number of cycles in the problem

v) an initial spatial distribution as a set of triplets of points in all regions with fissile material

vi) a flag for tally normalization

The initial source points are duplicated enough times so that the total number of points (M) in the source spatial distribution is approximately equal to the nominal source size N. The energy for the source particles is sampled from a generic thermal fission distribution probability if it is not available from a SRCTP file for a previous run of the same or a similar problem.

Transport stage

For each cycle, M source particles are started isotropically from the source. For the first cycle these M points are from the initiation stage while for the subsequent cycles these points originate at collision sites from the previous cycles. The weight of each particles is N/M, so that normalization occurs as if N rather than M particles started in each cycle. Source particles are transported through the MCNP geometry and the fission is treated as an analog or implicit capture. At each collision point the following is done:

i) removal lifetime by absorption is estimated

ii) if fission is possible, the k_{eff} data are accumulated and n fission sites are stored for use as source points in the next cycle.

$$\bar{n} = W\ \bar{\nu}(\sigma_f/\sigma_t)\ (1/k_{eff}) \qquad \text{(A-11)}$$

W = particle weight

$\bar{\nu}$ = average number of neutrons produced by fission

σ_f = microscopic fission cross section

σ_t = microscopic total cross section

$M = \Sigma n$ = number of source points to be used in the next cycle

iii) The collision nuclide and reaction are sampled but the fission reaction is not allowed to occur because fission is not treated as capture.

Cycle termination

At the completion of each cycle a set of M source particles are written from fissions in that cycle to the SRCTP fission source file which can be used as an initial source in a subsequent criticality calculation with the same or similar geometry.

After the first l_c "settle" cycles, which is a user specified number of source cycles to be skipped before tally accumulation, the source spatial distribution is assumed to be in equilibrium. During the "active" cycles the tallies are accumulated. The problem is terminated either on the user-specified total number of cycles or time limit of the problem.

Criticality calculations with MCNP suffer from two potential problems. The first is the failure of the source to converge from its initial guess to a distribution fluctuating around the eigenmode solution. In order to correct this problem, it is recommended to make an initial run with a relatively small number of source particles per generation (cycle) and allow a large number of cycles so that the eigenvalue appears to be fluctuating about a constant value. The source file, SRCTP from the last cycle of the initial run can then be used as the source for the final production run to be made with a large number of source neutrons per generation.

The second problem with the criticality calculation is the fact that the algorithm produces a bias in the estimated eigenvalue. It is known that the bias varies as 1/N, where N is the number of source particles per generation. The total running time is proportional to $1/\sqrt{N l_t}$, where l_t is the number of cycles contributing to the eigenvalue estimation. By examining the results of the convergence or initial run the total number of histories necessary to achieve the desired variance may be estimated.

Steady state calculation with MCNP has shown that the gaseous core reactor system is a very slowly converging system. In order to have the criticality calculations converge to a reasonable eigenvalue, it was necessary to run MCNP for many more cycles with a larger number of source particles per cycle than would have been required for a solid core.

Sample Input

The MCNP input file contains three major sections with each separated by a blank card: i) cell definitions with material number, density and sense labeled surfaces; ii) surface cards; and iii) data cards which define all other aspects of the problem. All cards have free-field form input with mnemonic or cell/surface numbers in columns 1 through 5 and data in columns 6 through 72. Useful input-card aids are available for interpolating, repeating, multiplying, and jumping over data entries. To minimize user input errors, MCNP performs over 200 checks on the input file and produces warning and/or fatal error messages in the output file. A fatal error terminates the problem while a warning message should be carefully examined and appropriate action may need be taken even if the problem continues to run.

Two test problem input files for the Cray X-MP/48 machine at the San Diego Supercomputer Center are given below. Both are for UF_6-fueled gaseous core reactor systems; one for the bimodal multiple chamber gaseous core reactor system; and the second for a simple, single core pulsed gaseous core reactor.

Input for Multicore Bimodal Gaseous Core Reactor System

This section describes typical MCNP input for the bimodal gaseous core reactor with both the central BPGCR and the surrounding PGCR's fueled and with beryllium as the inner and outer moderator reflector material. This input set is for MCNP version 3A and the computer system is the Cray X-MP/48 at the San Diego Supercomputer Center.

Figure A-3a gives the cross sectional view of the bimodal reactor system seen from the side and Figure A-3b gives the cross sectional view of the reactor system seen from the top. The numbers within circles denote the cell numbers and numbers within parentheses are the surface

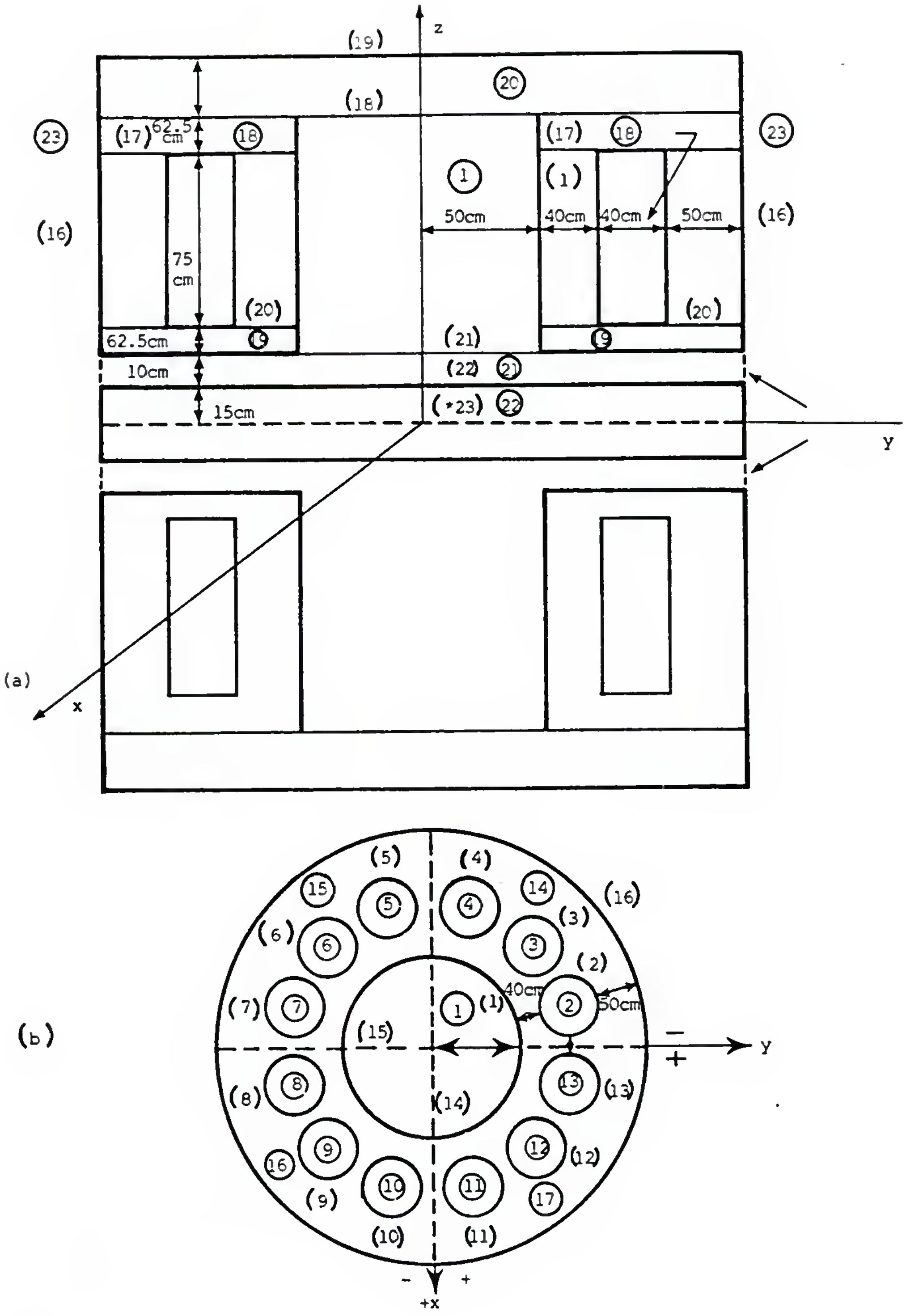

Figure A-3. Cross Sectional View of Bimodal Gaseous Core Reactor (a) Side-View (b) Top View.

numbers for the surfaces which border the cells. Table A-3 lists the input cards for the problem.

The initial run input file has the following general form.

```
Message Block
Blank Line Delimiter
Title Cards
Cell Cards
.................
Blank Line Delimiter
Surface Cards
.................
.................
Blank Line Delimiter
Data Cards
.................
.................
Blank Line Delimiter
Anything Else
```

Message and title cards

The optional message block starts with a card which must have the string MESSAGE: in columns 1-8. The message block ends with a blank line delimiter before the title card. There can be one or more optional message continuation cards between the first card and the blank card. Everything in columns 1-80 on continuation cards is interpreted as a message by MCNP.

The first card after the optional message block (card 1 in the given input set) is the required problem title card. It is limited to one line from column 1 through 80 and is used as a title in various places in MCNP. The title card in the given input set identifies the problem as the BPGCR/PGCR bimodal gaseous core reactor system with an inner

Table A-3. Input Cards for the Bimodal Gaseous Core Reactor System.

```
bpgcr/pgcr tibe=40 cm.  tobe=50 p(bp)=90 atm.
p(pg)=10 (bp9040in)
1      3  3.12354e-4  -1    -18  21
2      1  8.0115e-05  -2    20   -17
3      1  8.0115e-05  -3    20   -17
4      1  8.0115e-05  -4    20   -17
5      1  8.0115e-05  -5    20   -17
6      1  8.0115e-05  -6    20   -17
7      1  8.0115e-05  -7    20   -17
8      1  8.0115e-05  -8    20   -17
9      1  8.0115e-05  -9    20   -17
10     1  8.0115e-05  -10   20   -17
11     1  8.0115e-05  -11   20   -17
12     1  8.0115e-05  -12   20   -17
13     1  8.0115e-05  -13   20   -17
14     2   0.121251  1   -16 -15  14   2   3   4   20   -17
15     2   0.121251  1   -16 -15 -14   5   6   7   20   -17
16     2   0.121251  1   -16  15 -14   8   9  10   20   -17
17     2   0.121251  1   -16  14  15  11  12  13   20   -17
18     2   0.121251  17 -16 -18   1
19     2   0.121251  21 -16 -20   1
20     2   0.121251  18 -16 -19
21     3   3.12354e-4  22  -16  -21
22     2   0.121251    23  -16  -22
23     0                16: 19:  -23

1      cz    50.0
2      c/z  -28.470    106.252   20.0
3      c/z  -77.782    77.782    20.0
4      c/z  -106.252   28.470    20.0
5      c/z  -106.252  -28.470    20.0
6      c/z  -77.782   -77.782    20.0
7      c/z  -28.470   -106.252   20.0
8      c/z   28.470   -106.252   20.0
9      c/z   77.782   -77.782    20.0
10     c/z   106.252  -28.470    20.0
11     c/z   106.252   28.470    20.0
12     c/z   77.782    77.782    20.0
13     c/z   28.470    106.252   20.0
14     py    0.0
15     px    0.0
16     cz    180.0
17     pz    162.5
18     pz    225.0
19     pz    275.0
20     pz    87.50
21     pz    25.0
22     pz    15.0
```

Table A-3. -Continued

```
 *23   pz    0.0

imp:n 2  12r  1  6r  2  1  0
vol   13j  1.47851e+06  3r  6j
kcode 2000  1.00  2  0  4500
ksrc    10   10   20   10   10   40   20   20 60 15 15 100
      -28  106  125  -78   78  125  -106  28  125
      -106 -28  125  -78 -78  125  -28 -106  125
       28 -106  125   78 -78  125   106 -28  125
       106  28  125   78  78  125   28  106  125
f2:n  1  2  3  4  5  6  7  8  9  10  11  12
      13  16
fq2   e  f
f4:n  1  14  15  16  17  18  19  20  21  22
fq4   e   f
f6:n  14  15  16  17  18  19  20  21  22  2  3
      6  8  10
fq6   e   f
f7:n  2  3  4  5  6  7  8  9  10  11  12  13
fq7   e  f
f14:n 1  2  3  4  5  6  7  8  9  10  11  12  13
cf14  1
f24:n 1  2  3  4  5  6  7  8  9  10  11  12  13
cf24  2
f34:n 1  2  3  4  5  6  7  8  9  10  11  12  13
cf34  3
f44:n 1  2  3  4  5  6  7  8  9  10  11  12  13
cf44  4
f54:n 1  2  3  4  5  6  7  8  9  10  11  12  13
cf54  5
f64:n 1  2  3  4  5  6  7  8  9  10  11  12  13
cf64  6
f74:n 1  2  3  4  5  6  7  8  9  10  11  12  13
cf74  7
f84:n 1  2  3  4  5  6  7  8  9  10  11  12  13
cf84  8
f94:n 1  2  3  4  5  6  7  8  9  10  11  12  13
cf94  9
f104:n 1  2  3  4  5  6  7  8  8  10  11  12  13
cf104  10
f114:n 1  2  3  4  5  6  7  8  9  10  11  12  13
cf114  11
f124:n 1  2  3  4  5  6  7  8  9  10  11  12  13
cf124  12
f134:n 1  2  3  4  5  6  7  8  9  10  11  12  13
cf134  13
fq0    f  e  d
```

```
f144:n 2  3  4  5  6  7  8  9  10  11  12  13
fc144  corrected neutron flux  total neutron fluence;
       total fissions; total fission neutrons and
       fission heating, total absorptions,
       neutron heating
fm144  (0.50) (9.42478e+04) (-9.42478e+04 1 (-6)
       (-6 -7) (-6 -7 -8) (-2)) (-378.212 1 1 -4)
fq144  f  e  m
f154:n 1
fc154  corrected neutron flux;total neutron fluence;
       total fissions,total fission neutrons,
       fission heating, neutron absorptions
       and total heating.
fm154  (0.50) (1.5708e+06) (-1.5708e+06 1 (-6)
       (-6 -7) (-6 -7 -8) (-2)) (-97.01739 3 1 -4)
fq154  f  e  m
f164:n 14  15  16  17
fc164  corrected flux; fluence; absorptions;
       and heating.
fm164  (0.50)  (1.47851e+06) (-1.47851e+06 2 -2)
       (-0.55109 2 1 -4)
fq164 f  e  m
e0     1.86e-06  2.75e-04  5.53e-03  3.34e-01
       8.21e-01  1.65  14.9183
m1    92235.50c  0.04191  92238.50c  0.0074
      9019.51c 0.29576  2004.50c   0.65493
m2     4009.50c  1.0
m3     92235.18c  0.041905  92238.50c  0.007394
       9019.51c 0.295771  2004.50c  0.654930
totnu
phys:n 14.9183  0.0
tmp1   13j  6.8936e-08  6r  1j  6.8936e-08  1j
tmp2   13j  6.8936e-08  6r  1j  6.8936e-08  1j
thtme  1.0e+8  1.0e+09
mt2    be.05t
cut:n  1.0e+16  0.0  .01
print
```

beryllium thickness, TIBE, of 40 cm; outer beryllium thickness, TOBE, of 50 cm; total gas-fuel mixture pressure in the BPGCR, P(bp), of 90 atmospheres and total gas-fuel mixture pressure in the PGCR, P(pg), of 10 atmospheres. The name of the input file is bp9040in.

Cell cards

Cards 2 through 24 are the cell cards. Each cell card has entries in the form

j m d geom parms

where j is the cell number ($1 \le j \le 9999$), m is the material number (zero if the cell is void), d is the material density, geom are the geometry specifications of the cell that consists of signed surface numbers and Boolean operators that specify how the regions bound by the surfaces are to be connected, and parms are optional cell parameters. A signed surface number stands for the region on the side of the surface where the points have the indicated sense. The plus sign for positive is optional. The regions are combined by Boolean operators: intersection (no symbol); union (symbol is :) and complement (symbol is #). If the entry for the material density is positive it is interpreted as the atomic density in units of 10^{24} atoms/cm^3; and if the entry is negative it is interpreted as the mass density in units of grams/cm^3.

Cell 1 is the upper half of the central burst power gaseous core reactor (BPGCR) cylindrical cell bound by the cylindrical surface 1 and plane surfaces 18 and 21; it contains material number 3 (UF_6-He mixture) the composition of which is given on the material card. The atomic density of material 3 is $3.124x\ 10^{-4}$ atoms/barns-cm.

Cells 2 through 13 are the upper PGCR cells each of which are bound by the respective cylindrical surfaces 2 through 13, top plane surface 17, and bottom plane surface 20. Each of the PGCR cells contains material number 1 (UF_6-He mixture) of atomic density 8.012×10^{-5} atoms/barn-cm.

Cells 14 through 20 and 22 are the beryllium moderator cells. Material number 2 is beryllium. Cells 14 through 17 are the beryllium moderator cells which radially surround the PGCR cells; they are bound by the upper plane surface 17, lower plane surface 20 outside cylindrical surface 16, inner cylindrical surface 1, and outside the cylindrical surfaces of the respective PGCR cores in the cells 14 through 17 (cells 2, 3, and 4 in cell 14; cells 5, 6, and 7 in cell 15; cells 8, 9 and 10 in cell 16; cells 11, 12, and 13 in cell 17).

Cell 21 is the MHD region. Cell 23 is the outside space which is formed by the union of surfaces 16, 19, and the negative sense of 23.

Surface cards

Cards 26 through 48 are the surface cards. A surface card contain entries in the form

j n a list

where j is the surface number ($1 \leq j \leq 99999$), with asterisk if it is a reflecting surface, n is absent if there is no coordinate transformation, a is the surface mnemonic from Table A-1 and the list contains one to ten entries. To specify a surface, the mnemonic for the specific surface and the coefficients for the surface equation from Table A-1 are entered in the list.

Card 26 denotes the cylindrical surface on the z axis with a radius of 50 cm. Cards 27 through 38 represent the cylindrical surfaces of the 12 PGCR cells surrounding the central cylindrical BPGCR cell surface. These surfaces are parallel to the z axis (mnemonic, c/z). The three numerical entries for each of these surfaces are the x and y coordinates of the geometric center of the cylinders and the radius of the cylinder, respectively. Cards 39 and 40 represent the plane surfaces 14 and 15 which are normal to the y and x axes, respectively, and pass through the origin of the coordinate system. Card 41 represents the outer cylindrical surface 16 on the z-axis and its radius is 180 cm. Cards 42 through 48 represent the plane surfaces 17 through 23 all of which are normal to the z-axis. The numerical entries for these surfaces represent the normal distances from the origin to the planes (D in the equation $z-D=0$). The asterisk preceding surface number 23 designates this surface as a reflecting surface indicating that the reactor has symmetry about a horizontal plane through the origin. Any particle hitting the reflecting surface is specularly reflected. It is recommended that the reflecting surface be used cautiously in MCNP and the tally results must be accordingly adjusted.

Data cards

Card 50 assigns importance for neutrons in each of the cells. The general form of the card is

$$\text{imp:n} \quad x_1\ x_2\ ..x_i...x_n$$

where n=N for neutrons, n= P for photons, and x_i is the importance for cell i= 1,2,....... . Card 50 assigns an importance of 2 for cells with the fissile material, 1 for the moderator reflector cells, and zero for the outside world. Card 51 enters the volume of the cells 14 through 17. MCNP usually calculates the volumes of all cells that are rotational symmetric (generated by surface of revolution) about any axis. As a biproduct of the volume calculation, areas of surfaces and masses of cells are also calculated. These volumes, areas of surfaces and masses of cells are printed in the MCNP output file. Since the cells 14 through 17 have no symmetry about any axis it is mandatory that the user supplies the volumes of these cells in the VOL card.

KCODE and KSRC cards are required for the criticality problem. The KCODE card entries are in the form

KCODE NSRCK RKK IKZ KCT MSRK KNRM

where NSRCK = nominal source size per cycle

RKK = initial guess for k_{eff}

IKZ = number of cycles to be skipped before tally accumulation

KCT = number of cycles to be done

MSRK = number of source points to allocate storage for

and KNRM = method of source normalization

0 means normalize tallies by weight

1 means normalize tallies to number of particles.

The NSRCK entry is the nominal source size for each cycle and should be in the range of 300 to 3000. The IKZ entry is the number of initial cycles to be skipped before tally accumulation begins. This entry is important if the initial source guess is poor. The KCT entry specifies the total number of cycles to be done in the problem. A zero entry means never terminate on cycles but terminate on time. The MSRK entry is the maximum number of source points for which storage will be allocated, usually not more than 1.5 times nsrck.

For the current problem, the nominal source size is 2000, the initial k_{eff} guess is 1.00, 2 cycles are to be skipped before tally accumulation, the problem terminates on time allocated for the problem, and the storage is 4500.

Card 53 is the KSRC card which can contain NSRCK (x,y,z) triplets, which are the locations of initial source points for the KCODE criticality calculation. At least one source point must be provided in a cell containing fissile material. MCNP will quickly calculate and use the new fission source distribution from the initial source points. The energy of the source is sampled from a fission spectrum hardwired into MCNP. If a problem has a lot in common with respect to geometry with a previous MCNP problem the KSRC card can be replaced by the SRCTP file from that problem.

Cards 54 through 88 are tally cards which have the numbers 2, 4, 6, 7 with particle designators N for neutrons. Tallies can be assigned numbers as above or in increments of 10. The fqn card that follows each tally card specifies the print hierarchy for the tally in the MCNP output file.

Card 54 instructs MCNP to provide tallies that contain the flux averaged over the surfaces whose numbers are entered in the card.

Card 56 asks for the track length averaged neutron flux over the cells whose numbers are indicated in the card.

Cards 58 and 60 are heating tally cards. The F6 card entries are cell numbers whose neutron heating contribution is requested whereas the F7 card entries are cells with fissile material for which MCNP is to provide fission heating data in those cells. The F7 tally includes the gamma heating where the gammas are assumed to be deposited locally. The F6 tally does not include gamma heating.

Of the cards 63 through 88 the F4 cards are the track length averaged neutron flux cards and the respective CF4 cards are the cell flagging cards. The cell flagging cards are in the form

$$CF_n \quad C_1 \ldots . C_i \ldots \ldots C_k$$

where n is the tally number and C_i are the problem cell numbers whose tally contributions are flagged.

The F4 tally (track length estimate of particle flux) contribution from cells 1 through 13 are flagged so that when the particles leave the designated cells, their contribution to the Fn tally are listed separately in addition to the normal total tally. For example, consider the tally cards 62 and 63. In addition to the track length averaged particle flux in cells 1 through 13, the contributions from cell 1 to each of the cells 1 through 13 are also listed separately. This cell flagging capability of MCNP has been used to determine the coupling coefficients among the coupled cores of the system. The fq0 card (card 88) sets up the print hierarchy in the order f, cell; e, energy; and d, flagged contribution.

Cards 89 through 100 contain FMn cards which are the multiplier cards. Card 91 (FM144) causes MCNP to calculate the quantities described by the FC144 tally comment card by multiplying the track length estimate of neutron flux in cells 2 through 13 specified by the F144 card by the quantities entered in the FM144 card. The corrected neutron flux in each of the PGCR cells is obtained by multiplying the cell averaged flux by 0.50 since there is a reflecting surface for half symmetry. The volume of each PGCR cell is 9.425×10^4 cm^3 and is used to obtain the total fluence. The negative sign in front of the volume causes the atom density to be included in the calculation. The numbers in parentheses (-6) (-6 -7), (-6 -7 -8), and (-2) cause MCNP to combine the atom density of material 1 and the respective ENDF nuclear data to produce total fissions, total fission neutrons, fission heating, and total absorption in each of the PGCR cells. The number 378.212, which is the reciprocal of the mass density of material 1, when combined with the ENDF specifications in the last parentheses of card 91 gives the total heating in the cells 2 through 13.

Cards 93 through 96 cause MCNP to calculate the quantities described in the FC154 tally comment card for the central BPGCR chamber cell. Similarly cards 97 through 100 cause MCNP to calculate quantities specified in the FC164 comment card for the beryllium cells surrounding the PGCR cells.

Card 101 (E0) establishes the energy bins for the tallies in the order of increasing magnitude in Mev. The general form of the energy bin card is

$$E_n \quad E_1 \ldots E_i \ldots . E_k$$

where n is the tally number and E_i is the upper bound for the i th energy bin for tally n. In this problem the E0 card sets up a single default energy bin structure for all tallies. A specific En card will over ride the default structure for the tally n. Cards 102 through 104 are the material cards that give the composition of the materials specified in the cell cards. The material card has the form

Mn $ZAID_1$ $fraction_1$...$ZAID_i$ $fraction_i$...

where n corresponds to the material number on the cell cards, $ZAID_i$ is the identifier in the form ZZZAAA.nnX from the directory file for the cross section data included in the MCNP package. Quantity ZZZ is the atomic number, AAA is the atomic mass, nn is the library identifier, and X is the class of data. $Fraction_i$ is the atomic fraction (or weight fraction if entered as a negative number) of the constituent isotope i in the material.

Material M1 is the UF_6-He mixture in the PGCRs, material M2 is beryllium, and material M3 is the UF_6-He mixture in the central BPGCR cell.

Card 105 is the TOTNU card which requires MCNP to use the total nu for the fissionable nuclides. If NO is present in this card MCNP will use the prompt nu (ν) for the fissile materials.

Card 106 is the energy physics cutoff card. It is in the form

PHYS:n E_{max} EMNCF

where E_{max} is the upper limit for neutron energy in Mev and EMNCF is the energy boundary (Mev) above which neutrons are treated with implicit capture and below which they are treated with analog capture. The current problem sets the upper energy as 14.92 Mev and all neutron energies are treated with implicit capture.

Cards 107 and 108 are the free gas thermal temperature cards. The general form of these cards is

TMPn T_{1n} T_{2n}......T_{in}......T_{ln}

where n is the index of time on the THTME card and T_{in} is the temperature of the i th cell at time n and l is the number of cells in the problem. The present problem specifies that at 10^8 and 10^9 shakes (1 shake = 10^{-8} seconds) the beryllium cell temperatures are at 800 K. (= 6.8936×10^{-8} Mev)

The MT2 card specifies that $S(\alpha,\beta)$ thermal data be used for beryllium (material 2) at 800 K for thermal scattering calculations.

Card 111 is the problem cutoff card and has the general form

CUT:n T E WC1 WC2 SWTM

where n = N for neutrons, P for photons

T = time cutoff in shakes

E = lower energy cutoff in Mev

WC1, WC2 = weight cutoffs

and SWTM = minimum source weight.

The PRINT card with no entries allows MCNP to produce a full output print. The table numbers can be given on this card for specific tables to be printed in the output file.

Input for Single Core Gaseous Core Reactor System

This section gives typical MCNP input for a single core cylindrical gaseous core reactor with UF_6-He mixture as the working fluid and beryllium as the moderator reflector material. Figure A-4 gives the cross sectional view of the reactor system seen from the side. The Table A-4 lists the input cards.

Card 1 is the title card which specifies the problem as a large cylinder which is equivalent in volume to the 24 small PGCR cylinders in the previous problem. The radius of the large PGCR is 84.85 cm and its height is 100 cm.

Cards 2 through 5 are the cell cards. Card 2 specifies that cell 1, which is the large PGCR cell, contains material number 1 with atomic density of 4.006×10^{-4} atoms/barn-cm and is bound by the cylindrical surface 1, top plane surface 3, and lower reflecting surface 5. Cells 2 and 3 are beryllium (material 2) with number density 0.121 atoms/b-cm and bound by the surfaces indicated in these cards. Cell 4 is outside the reactor system.

Card 7 through 11 are the surface cards. Surfaces 1 and 2 are the cylindrical surfaces on the z axis whose radii are 84.85 cm and 134.85 cm respectively. Surfaces 3 and 4

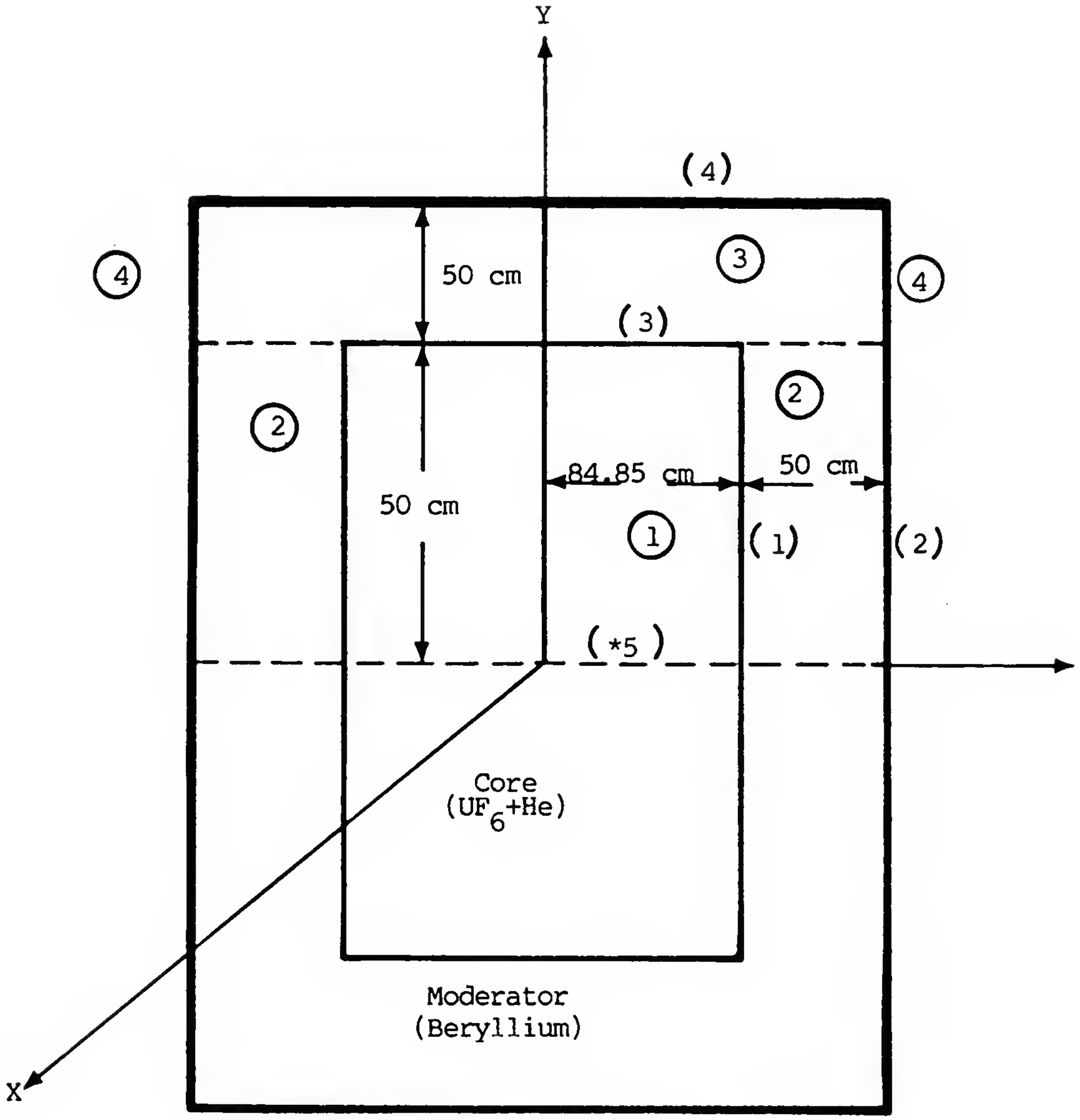

Figure A-4. Cross Sectional View of Single Core PGCR.

Table A-4. MCNP Input for a Single Core PGCR.

```
large cylinder p. g. c. r. (eq. to 24 mini.)
(r(c)=84.85,h=100 cm)
1     1     4.00575e-04   -1  -3  5
2     2     0.121251       1  -2  -3  5
3     2     0.121251       3  -2  -4
4     0                    2: 4: -5

1     cz   84.85
2     cz   134.85
3     pz   50.0
4     pz   100.0
*5    pz   0.0

imp:n 4  1  1  0
kcode 2000  1.00  2  0  4500
ksrc  5  5  5  10  10  10
f4:n  1  2  3
fq4   e  f
f14:n 1
cf14  2
fq14  f  e  d
f24:n 1
cf24  3
fq24  f  e  d
f6:n  1  2  3
f7:n  1
fq6   e  f
f34:n  1
fc34  corrected neutron flux; total neutron fluence;
      total fissions; fission neutrons; fission
      heating,neutron absorption and neutron heating.
fm34  (.50)  (1.13089e+06)  (-1.131e+06  3  (-6)
      (-6 -7) (-6 -7 -8)  (-2))  (-76.642 1 1 -4)
fq34   f  e  m
e0    1.86e-06  2.75e-04  5.53e-03  3.34e-01
      8.21e-01 1.65  14.9183
m1    92235.50c  .04191  92238.50c  .0074
      9019.51c 0.29576 2004.50c  .65493
m2    4009.50c  1.00
m3    92235.50c  1.67875e-05
      92238.50c  2.9625e-06
totnu
phys:n 14.9183  0.0
tmp1   1j  6.8936e-08  1r  1j
tmp2   1j  6.8936e-08  1r  1j
thtme  1.0e+08  1.0e+10
mt2    be.05t
cut:n  1.0e+16  0.0  .01
print
```

are plane surfaces normal to z axis and are at 50 cm and 100 cm from the origin of the coordinate system. Surface 5 is a reflecting surface which establishes half-symmetry for the problem.

Card 13 assigns an importance of 4 to the core cell, 1 to the beryllium cells and zero to the outside cell.

KCODE card specifies the nominal size of the source to be 2000, an initial k_{eff} guess of 1.00, two cycles to be done before tally accumulation, and allows the problem to be terminated on time. The maximum storage allowed is 4500.

The KSRC card allows two points (5,5,5) and (10,10,10) as the initial source points in the core.

Cards 16 through 26 are the tally cards. The F4 card calculates the track length estimate of neutron flux in the cells 1, 2, and 3. The F14 and F24 cards allow MCNP to calculate the track length estimate of neutron flux in cell 1 and corresponding cell flagging cards, CF14 and CF24, allow MCNP to calculate the contribution from cells 2 and 3 to cell 1. The F6 and F7 tally cards call for the total and fission heating quantities, respectively, for the cells specified in these cards.

FM34 (card 29) causes MCNP to calculate the quantities specified in the FC34 comment card for the PGCR cell.

The E0 card specifies the single energy bin structure for all tallies. The material cards M1 and M2 specify the composition of the materials on the cell cards.

Material M3 which is used only for the tally f34 contains the U^{235} and U^{238} isotopes from material M1.

Cards 37 through 39 specify the time and temperature of the beryllium cells for the free gas thermal treatment. The MT2 card (card 40) allows MCNP to use $S(\alpha,\beta)$ thermal data for beryllium at 800 K.

APPENDIX B
COUPLED CORE POINT REACTOR KINETICS EQUATIONS AND THE SOLUTION PROCEDURE

Time dependent neutronic behavior of various types of coupled core reactors has been modeled by many authors and can be found in the references cited in this dissertation (6-24). In most cases a set of coupled point reactor kinetics equations is derived from either the time dependent Boltzmann's transport equation or the time dependent diffusion equation. The detailed derivation of coupled point reactor kinetics equations is not reproduced here; instead, this appendix lists the coupled point reactor kinetics equations used in the analysis of the kinetic behavior of the bimodal gaseous core reactor system along with the conventional expressions for the integral parameters which appear in the coupled point reactor kinetics equations. Since these parameters are obtained from the static neutronic analysis of the system at intermediate instants of time during any cycle or at various instants of times during the operation of the system (more than one cycle) using MCNP and other codes, appropriate interpretations of these integral parameter expressions are also given. Finally the solution method adopted for the coupled point reactor kinetics equations is explained in this appendix.

The coupled core point reactor kinetics equations for MC coupled cores can be written in the form,

$$\frac{dN_j(t)}{dt} = \frac{(\rho_j(t) - \bar{\beta}_j(t))}{\Lambda_j(t)} N_j(t) + \sum_{i=1}^{ND} \lambda_{ji} C_{ji}(t) + \sum_{\substack{k=1 \\ k \neq j}}^{MC} \frac{\alpha_{jk}(t) N_k(t-\tau_{jk})}{\Lambda_j(t)} + Q_j(t) \qquad \text{(B-1)}$$

$$\frac{dC_{ji}(t)}{dt} = \frac{\bar{\beta}_{ji}(t)}{\Lambda_j(t)} N_j(t) - \lambda_{ji} C_{ji}(t) \qquad \text{(B-2)}$$

$j = 1, 2, \ldots\ldots, MC$
$i = 1, 2, \ldots\ldots, ND$

Equation (B-1) describes the time dependent behavior of the j th core neutron level and Equation (B-2) describes the time dependent variation of the i th group delayed neutron precursor concentration in the j th core of the bimodal gaseous core reactor system.

In describing the time dependent behavior of the bimodal gaseous core reactor system by means of equations (B-1) and (B-2), the delayed neutron precursor loss from the cores due to the circulation of the gaseous fuel is neglected. The circulation of the fuel causes a fraction of the delayed neutron precursors to be swept along with the fuel into the external loop, where some delayed neutrons are emitted and lost to the reactor cores. The delayed neutron loss depends on the fuel residence time in the individual cores and on the external loop circulation time. Changes in either of these parameters change the number of delayed neutron precursors which undergo decay while they are in the external loop. Those precursors which do not decay in the loop, upon reentering the cores act as a neutron source.

The effect of photoneutron production in the beryllium reflector is significant though much less important than the delayed neutron effect. It was determined by Dugan (30) that the fraction of the photoneutron gamma rays which penetrate from the gaseous core of the PNP to the beryllium moderator and to eventually induce photoneutrons is 0.3. For beryllium moderated PNP and PGG system the maximum neutron multiplication factor, when delayed neutrons and photoneutrons were included was 1.055. When photoneutrons were neglected the maximum neutron multiplication factor had to be increased to 1.061 in order to maintain the system performance level. When both delayed neutrons and photoneutrons were neglected, the maximum neutron multiplication factor had to be increased to 1.091 in order to maintain the system performance level (28). Because of the small effect of photoneutrons on the power level of the gaseous cores the photoneutrons are ignored in this study.

The third term in the equation (B-1) represents the neutronic coupling contribution from other cores to core j. In this treatment the coupling effect is introduced as an effective source $\sum_{\substack{k=1 \\ k \neq j}}^{MC} \frac{\alpha_{jk}(t) N_k(t-\tau_{jk})}{\Lambda_j(t)}$. The assumption in this treatment is that the reactivity associated with the j th core, ρ_j, does not include the contribution due to the neutronic coupling effects of other cores on j. The term α_{jk} is the coupling coefficient for neutrons diffusing from the k th to the j th core and causing fission in the j th core and τ_{jk} is the corresponding delay time associated with the neutrons diffusing from the k th to the j th core. It can be seen that this formulation explicitly introduces the nonlinear power coupling between the individual cores through the coupling terms $N_k(t-\tau_{jk})$ with the retarded time arguments. Since there is a finite time lapse from the birth of a fission neutron in one core, its slowing down to thermal energy in the moderator, and its capture in another core causing fission, the core neutron levels in the coupling terms have been assigned a retarded time argument.

Integral Parameters

Integral parameters in equations (B-1) and (B-2), namely, $\rho_j(t)$, $\overline{\beta}_j(t)$, $\Lambda_j(t)$, $C_{ji}(t)$, $\alpha_{jk}(t)$, etc., are defined below. Quantity ND is the number of delayed neutron groups and MC is the total number of cores in the bimodal gaseous core reactor system.

The reactivity, $\rho_j(t)$, of the core j is given by the expression:

$$\rho_j(t) = \frac{1}{F_j} \{<[\chi(E')(1-\overline{\beta}_j) + \sum_{i=1}^{ND} \overline{\beta}_{ji} f_i(E')]\, w(\overline{r},E,t)$$

$$\nu\Sigma_f(\overline{r},E',t),\ \psi_{pj}(\overline{r},E,\overline{\Omega},t)>$$

$$- <w(\overline{r},E,t),\overline{\Omega}.\nabla\psi_{pj}(\overline{r},E,\overline{\Omega},t)>$$

$$- <w(\overline{r},E,t),\ \Sigma_a(\overline{r},E,t)\ \psi_{pj}(\overline{r},E,\overline{\Omega},t)>\} \ . \qquad (B-3)$$

The i th group effective delayed neutron fraction for the j th core is given by

$$\overline{\beta}_{ji}(t) = \frac{1}{F_j} <f_i(E')\ \overline{\beta}_{ji}\ \nu\Sigma_f(\overline{r},E,t),w(\overline{r},E,t)$$

$$\psi_{pj}(\overline{r},E,\overline{\Omega},t)> \qquad (B-4)$$

and the effective total delayed neutron fraction for the j th core is given by

$$\overline{\beta}_j(t) = \sum_{i=1}^{ND} \overline{\beta}_{ji}(t). \qquad (B-5)$$

Prompt neutron generation time for the j th core, Λ_j, is given by

$$\Lambda_j(t) = \frac{1}{F_j} <\frac{1}{v(E)}\ w(\overline{r},E,t),\ \psi_{pj}(\overline{r},E,\overline{\Omega},t)>. \qquad (B-6)$$

The i th group delayed neutron effectve concentration for the j th core is given by

$$C_{ji}(t) = \frac{1}{\Lambda_j F_j} [\ <w(\overline{r},E,t),\ f_i(E)\ c_{ji}(\overline{r},t)>\ ] \qquad (B-7)$$

The source term $Q_j(t)$ in Equation (B-1) is given by

$$Q_j(t) = \frac{1}{\Lambda_j F_j} [< w(\bar{r},E,t),\ q(\bar{r},E,\bar{\Omega},t) >] \qquad \text{(B-8)}$$

and

$$\begin{aligned} F_j &= F_j(t) \\ &= < [\chi(E')(1-\bar{\beta}_j) + \sum_{i=1}^{ND} \bar{\beta}_j f_i(E')]\ \nu\Sigma_f(\bar{r},E,t), \\ &\qquad w(\bar{r},E,t)\ \psi_{pj}(\bar{r},E,\bar{\Omega},t) >. \qquad \text{(B-9)} \end{aligned}$$

The effective source term $\sum_{\substack{k=1 \\ k \neq j}}^{MC} \frac{\alpha_{jk}(t) N_k(t-\tau_{jk})}{\Lambda_j(t)}$ which represents the neutronic contribution from other cores to core j can be represented by the integral expression

$$s_j(t) = \frac{1}{\Lambda_j F_j} < w(\bar{r},E,t),\ S_j(\bar{r},E,t) >. \qquad \text{(B-10)}$$

$S_j(\bar{r},E,t)$ can be interpreted as the source distribution function which consists of a sum of a series of terms representing the neutronic coupling of the core j with all other cores in the reactor system. Since the neutronic coupling between core j and other cores is associated with a finite time lapse, the expression for $S_j(\bar{r},E,t)$ is given by

$$S_j(\bar{r},E,t) = \sum_{\substack{k=1 \\ k \neq j}}^{MC} \epsilon_{jk}(\bar{r},E,t)\ \psi_{pj}(\bar{r},E,\bar{\Omega},t) N_k(t-\tau_{jk}) \qquad \text{(B-11)}$$

where $\epsilon_{jk}(\bar{r},E,t)$ is the probability that a neutron escaping the core k will cause fission at a point r and at energy E in the j th core. The product $\epsilon_{jk}(\bar{r},E,t)\ \psi_{pj}(\bar{r},E,\bar{\Omega},t)$ can be considered as a new shape function resulting from the effective source of coupling neutrons.

Comparing the effective source term $\sum_{\substack{k=1\\k\neq j}}^{MC} \frac{\alpha_{jk}(t)N_k(t-\tau_{jk})}{\Lambda_j(t)}$

and equations (B-10) and (B-11) the expression for $\alpha_{jk}(t)$ can be written as

$$\alpha_{jk}(t) = \frac{1}{F_j} < w(\bar{r},E,t),\ \epsilon_{jk}(\bar{r},E,t)\ \psi_{pj}(\bar{r},E,\bar{\Omega},t). \tag{B-12}$$

The term N(t) appearing in equations (B-1) and (B-2) is generally termed the amplitude function or amplitude factor which accounts for all the growth and decay of the angular flux $\Phi_j(\bar{r},E,\bar{\Omega},t)$. The relationship between amplitude factor and the angular flux is given by

$$\Phi(\bar{r},E,\bar{\Omega},t) = N_j(t)\ \psi_{pj}(\bar{r},E,\bar{\Omega},t) \tag{B-13}$$

In the expressions (B-3), (B-4), (B-6), (B-7), (B-8), (B-9), and (B-10) the notation < , > denotes the integration over the phase space $(\bar{r},E,\bar{\Omega})$.

The factor $F_j(t)$ given by equation (B-9) in the above expressions is an arbitrary normalization factor which does not influence the solution of the coupled core point kinetics equation (B-1) and (B-2). However F is chosen so that the various parameters expressed above can be given a consistent physical interpretation. Equation (B-9) for $F_j(t)$ indicates that F_j can be considered as a production operator in the expression for the various integral parameters.

The term $w(\bar{r},E,t)$ appearing in the above expressions is an appropriate weighting function.

Reactivity $\rho_j(t)$ is given by the expression (B-3). With the term $F_j(t)$ given by the Equation (B-9) considered as a production term, the expression for reactivity, $\rho(t)$ can be considered as the ratio of net production of neutrons to the total production of neutrons in the core. The expression for $\rho(t)$, (B-3), is very similar to that for the relative change in the effective neutron multiplication factor, i. e.,

$$= \frac{\text{Production - (absorption + leakage)}}{\text{Production}}$$

$$= \frac{k_{eff} - 1}{k_{eff}} = \frac{\Delta k_{eff}}{k_{eff}} \quad . \tag{B-14}$$

The neutron generation time, $\Lambda(t)$, given by Equation (B-6) is the mean time for one neutron to cause fission, i. e., the average time between two successive generations of neutrons. The system neutron removal lifetime which is the mean time for one neutron to be removed from the system by absorption or leakage is obtained directly from MCNP. The expression for the neutron generation time, $\Lambda(t)$, in terms of the neutron removal lifetime, ℓ, and the effective system neutron multiplication factor, k_{eff}, can be written as

$$\Lambda(t) = \frac{\ell(t)}{k_{eff}(t)} \qquad \text{(B-15)}$$

and can be calculated at various instants of time during any cycle of operation of the gaseous core reactor system.

Coupling coefficients (α_{jk}) that appear in the coupled core kinetics equation (B-1) are given by the Equation (B-12). In Equation (B-12), the term $\epsilon_{jk}(r,E,t)$ is the probability that a neutron escaping from the core k will cause fission at a point r and at energy E in the $_j$ th core. The coupling coefficients, $\alpha_{jk}(t)$, as given by Equation (B-12) can be interpreted as the fraction of neutrons in core j that diffuse from any core k and enter core j and cause fission in core j.

In terms of the quantities that are obtained directly from the MCNP code, α_{jk} can be expressed in the form,

$$\alpha_{jk}(t) = \frac{(SO_{jk})_{th}(t)}{(SO_j)_{tot}(t)} \left(\frac{\Sigma_f}{\Sigma_a} \right) \qquad \text{(B-16)}$$

where $(SO_{jk})_{th}$ is the thermal neutron contribution from core k that is absorbed in core j, $(SO_j)_{tot}$ is the total source neutrons in core j, Σ_f is the total macroscopic fission cross section, and Σ_a is the total macroscopic absorption cross section.

Solution of Coupled Point Reactor Kinetics Equations

Numerical solution of coupled point reactor kinetics equations (B-1) and (B-2) is briefly described in this section.

One approach in the solution of the coupled reactor kinetics equation is to neglect the core-to-core delay time τ_{jk} entirely. This is not an unreasonable assumption under certain conditions where the delay times are very short compared to very long prompt neutron generation time, Λ_j. Another method of solution leading to more general results is to approximate the coupling term $N_k(t-\tau_{jk})$ in equation (B-1) by a Taylor series expansion about time t. Since the delay times are inherently small for the BPGCR/PGCR system, the first two terms of the expansion provide a good approximation.

$$N_k(t-\tau_{jk}) \approx N_k(t) - \tau_{jk}\, N'_k(t) \qquad \text{(B-17)}$$

Substitution of (B-17) into equations (B-1) yields

$$\frac{dN_j(t)}{dt} + \sum_{\substack{k=1 \\ k\neq j}}^{MC} \frac{\alpha_{jk}(t)\ \tau_{jk}}{\Lambda_j(t)} \frac{dN_k(t)}{dt} =$$

$$\frac{\rho_j(t) - \overline{\beta}_j(t)}{\Lambda_j(t)} N_j(t) + \sum_{i=1}^{ND} \lambda_{ji} C_{ji}(t) +$$

$$\sum_{\substack{k=1 \\ k\neq j}}^{MC} \frac{\alpha_{jk}(t)}{\Lambda_j(t)} N_k(t) + Q_j(t)\ . \qquad \text{(B-18)}$$

The time derivatives in equations (B-2) and (B-18) are approximated by forward finite differences so that,

$$\frac{dN_j(t)}{dt} = \frac{N_j^{n+1} - N_j^{n}}{\Delta t_n} \qquad \text{(B-19a)}$$

$$\frac{dN_k(t)}{dt} = \frac{N_k^{n+1} - N_k^{n}}{\Delta t_n} \qquad \text{(B-19b)}$$

and

$$\frac{dC_{ji}(t)}{dt} = \frac{C_{ji}^{n+1} - C_{ji}^{n}}{\Delta t_n} \qquad \text{(B-19c)}$$

for $t_n \leq t \leq t_{n+1}$. All other terms are approximated by a "theta differencing" technique

$$\rho_j N_j(t) = \theta \rho_j^{n+1} N_j^{n+1} + (1-\theta)\rho_j^{n} N_j^{n} \qquad \text{(B-20a)}$$

$$N_j(t) = \theta\, N_j^{n+1} + (1-\theta)\, N_j^{n} \qquad \text{(B-20b)}$$

$$N_k(t) = \theta\, N_k^{n+1} + (1-\theta)\, N_k^{n} \qquad \text{(B-20c)}$$

$$C_{ji}(t) = \theta_d\, C_{ji}^{n+1} + (1-\theta_d) C_{ji}^{n} \qquad \text{(B-20d)}$$

$$Q_j(t) = \theta\, Q_j^{n+1} + (1-\theta)\, Q_j^{n} \qquad \text{(B-20e)}$$

where $0 \leq \theta \leq 1$ and $0 \leq \theta_d \leq 1$. Note that if $\theta=\theta_d=1$, we have fully implicit differencing, if $\theta=\theta_d=\frac{1}{2}$ we have central differencing and if $\theta=\theta_d=0$ we have fully explicit differencing.

Equations (B-19a) through (B-19c) and (B-20a) through (B-20e) are substituted into (B-18) and (B-2). C_{ji} for the (n+1) th time step from the resulting latter equation is then substituted into the resulting former equation to obtain the coupled finite difference equations for the BPGCR/PGCR cores in the form:

$$\left\{1 - \frac{\theta\Delta t_n}{\Lambda_j}\rho_j^{n+1} + \frac{\theta\Delta t_n}{\Lambda_j}\bar{\beta}_j - \theta_d\Delta t_n \sum_{i=1}^{ND}\left[\frac{\lambda_{ji}\theta\Delta t_n\bar{\beta}_{ji}}{\Lambda_j(1+\theta_d\lambda_{ji}\Delta t_n)}\right]\right\} N_j^{n+1}$$

$$+ \left[\sum_{\substack{k=1\\k\neq j}}^{MC}\frac{\alpha_{jk}\tau_{jk}}{\Lambda_j} - \theta\Delta t_n\sum_{\substack{k=1\\k\neq j}}^{MC}\frac{\alpha_{jk}}{\Lambda_j}\right] N_k^{n+1}$$

$$= \left\{1 + \frac{(1-\theta)\Delta t_n}{\Lambda_j}\rho_j^{n} - \frac{(1-\theta)\Delta t_n}{\Lambda_j}\bar{\beta}_j\right.$$

$$\left. + \theta_d\,\Delta t_n\sum_{i=1}^{ND}\lambda_{ji}\left[\frac{(1-\theta)\,\Delta\, t_n\,\bar{\beta}_{ji}}{\Lambda_j(1+\theta_d\lambda_{ji}\Delta t_n)}\right]\right\} N_j^{n}$$

$$+ \left[\sum_{\substack{k=1\\k\neq j}}^{MC}\frac{\alpha_{jk}\tau_{jk}}{\Lambda_j} + (1-\theta)\Delta t_n\sum_{\substack{k=1\\k\neq j}}^{MC}\frac{\alpha_{jk}}{\Lambda_j}\right] N_k^{n} + (1-\theta_d)\Delta t_n\sum_{i=1}^{ND}\lambda_{ji}C_{ji}^{n}$$

$$+ \theta d\;\Delta t_n\sum_{i=1}^{ND}\lambda_{ji}\left[\frac{1-(1-\theta_d)\Delta t_n\,\lambda_{ji}}{(1+\theta_d\,\lambda_{ji}\,\Delta t_n)}\right] C_{ji}^{n} + \theta\Delta t_n Q_j^{n+1} + (1-\theta)\Delta t_n Q_j^{n} \qquad \text{(B-21)}$$

$j = 1, 2, \ldots\ldots\ldots, MC$

$$\text{and}\quad C_{ji}^{n+1} = \left[\frac{1-(1-\theta_d)\;\Delta t_n\;\lambda_{ji}}{\Lambda_j(1+\theta_d\;\lambda_{ji}\;\Delta t_n)}\right] C_{ji}^{n} + \left[\frac{\theta\Delta t_n\bar{\beta}_{ji}}{\Lambda_j(1+\theta_d\;\lambda_{ji}\;\Delta t_n)}\right] N_j^{n+1}$$

$$+ \left[\frac{(1-\theta)\;\Delta t_n\bar{\beta}_{ji}}{\Lambda_j(1+\theta_d\;\lambda_{ji}\Delta t_n)}\right] N_j^{n}. \qquad \text{(B-22)}$$

$j = 1, 2, \ldots\ldots, MC$

The set of equations (B-21) can be arranged in a matrix form

$$\underline{A}\ \underline{x} = \underline{b} \qquad \text{(B-23)}$$

where x is vector $[N_1, N_2, \ldots\ldots\ldots, N_{MC}]^T$ at the (n+1) th time step and b is the constant vector. Equation (B-23) is iteratively solved for the coupled core neutron levels vector x at all time intervals during any cycle. The time dependent delayed neutron precursor concentration $C_{ji}(t)$ is obtained from equation (B-22).

Effect of Circulating Fuel

The bimodal gas core reactor system, which is the main focus of this study is a circulating fuel reactor. The circulation of the fuel causes a fraction of the delayed neutron precursors to be swept along with the fission products into the external loop. The delayed neutrons emitted by the delayed neutron precursors while in the external loop are lost to the reactor cores. The delayed neutron source depends on the fuel residence time in the individual cores and on the external loop circulation time. Changes in either of these parameters changes the number of delayed neutron precursors which undergo decay while they are in the external loop. Those precursors which do not decay in the external loop, upon reentering the cores, decay and act as extra neutron sources.

The coupled core point reactor kinetics equations which accounts for fuel circulation can be written as (42),

$$\frac{dN_j(t)}{dt} = \frac{\rho_j(t) - \bar{\beta}_j(t)}{\Lambda_j(t)} N_j(t) + \sum_{i=1}^{ND} \lambda_{ji} C_{ji}(t)$$

$$+ \sum_{\substack{k=1 \\ k \neq j}}^{MC} \frac{\alpha_{jk}(t) N_k(t-\tau_{jk})}{\Lambda_j(t)} + Q_j(t) \qquad \text{(B-24)}$$

and

$$\frac{dC_{ji}(t)}{dt} = \frac{\bar{\beta}_{ji}(t)}{\Lambda_j(t)} N_j(t) - \lambda_{ji} C_{ji}(t) - \lambda_{jc} C_{ji}(t)$$

$$+ \lambda_{jc} \exp(-\lambda_{jc}/\lambda_{jL})\, C_{ji}(t - 1/\lambda_{jL}). \qquad \text{(B-25)}$$

The Equation for the rate of variation of neutron level $N_j(t)$ in the coupled core kinetics equation (B-1) remains the same, but is rewritten as Equation (B-24). The difference in Equation (B-25) for the delayed neutron precursor level change with time from Equation (B-2) is the addition of two terms to account for the delayed neutron precursors which are leaving and reentering the reactor cores. In Equation (B-25), $-\lambda_{jc}\, C_{ji}(t)$ is the rate of removal of the i th group delayed neutron precursors C_{ji} from the core j. The quantity λ_{jc} is the inverse of the residence time of the delayed neutron emitters in core j.

The last term in Equation (B-25) represents the rate at which the i th group delayed neutron precursors reenter the core j after being in the external loop for $1/\lambda_{jL}$ seconds. These delayed neutron precursors have been reduced by a factor of $\exp(-\lambda_{ji}/\lambda_{jL})$ since they decay exponentially with the decay constant λ_{ji} during the time $1/\lambda_{jL}$ seconds they spend in the external loop. Quantity λ_{jL} is the reciprocal of the average circulation time of the i th group delayed neutron precursors of the j th core in the external loop.

Solution of the coupled core point reactor kinetics equations (B-24) and (B-25) involves linearization of the terms $N_k(t-\tau_{jk})$ in Equation (B-24) and $C_{ji}(t-1/\lambda_{jL})$ in Equation (B-25) by truncated Taylor series expansions, approximating the time derivatives in the resulting set of equations by forward finite differences, applying the "theta differencing" technique to all the other terms and finally iterative solution of the coupled core equations for core neutron levels and the delayed neutron precursor concentrations. Linearization of the term $C_{ji}(t-1/\lambda_{jL})$ in Equation (B-25) by a truncated Taylor series expansion around time t gives

$$C_{ji}(t-1/\lambda_{jL}) \approx C_{ji}(t) - \frac{1}{\lambda_{jL}} \frac{dC_{ji}(t)}{dt} . \qquad \text{(B-26)}$$

Substitution of (B-26) into Equation (B-25) yields

$$\frac{dC_{ji}(t)}{dt} + \frac{\lambda_{jc}}{\lambda_{jL}} \exp(-\lambda_{ji}/\lambda_{jL}) \frac{dC_{ji}(t)}{dt} = \frac{\bar{\beta}_{ji}}{\Lambda_j(t)} N_j(t)$$
$$- \lambda_{ji}C_{ji}(t) - \lambda_{jc}C_{ji}(t) + \lambda_{jc} \exp(-\lambda_{ji}/\lambda_{jL}) C_{ji}(t) .$$
$$\text{(B-27)}$$

The time derivatives in Equations (B-18) and (B-27) are approximated by forward finite differences as given by Equations (B-19a) through (B-19c) and all the other terms are approximated by the "theta differencing" technique as given by Equations (B-20a) through (B-20e). The resulting equation for C_{ji} at the (n+1) th time step from Equation (B-27) is substituted into the resulting equation for N_j at the (n+1) th time step from Equation (B-18). The final coupled finite difference equations are in the form

$$\{1 - \frac{\theta \Delta t_n}{\Lambda_j} \rho_j^{n+1} + \frac{\theta \Delta t_n}{\Lambda_j} \bar{\beta}_j - \theta_d \, \Delta t_n \sum_{i=1}^{ND} \lambda_{ji} \frac{\bar{\beta}_{ji} \, \theta \Delta t_n}{\Lambda_j \, (DEN)} \} N_j^{n+1}$$

$$+ \{ \sum_{\substack{k=1 \\ k \neq j}}^{MC} \frac{\alpha_{jk} \tau_{jk}}{\Lambda_j} - \theta \Delta t_n \sum_{\substack{k=1 \\ k \neq j}}^{MC} \frac{\alpha_{jk}}{\Lambda_j} \} \, N_k^{n+1}$$

$$= \{1 + \frac{(1-\theta) \Delta t_n}{\Lambda_j} \rho_j^{n+1} - \frac{(1-\theta) \Delta t_n}{\Lambda_j} \bar{\beta}_j + \theta_d \, \Delta t_n \sum_{i=1}^{ND} \lambda_{ji} \frac{\bar{\beta}_{ji} (1-\theta) \Delta t_n}{\Lambda_j (DEN)} \} \, N_j^{n}$$

$$+ \{ \sum_{\substack{k=1 \\ k \neq j}}^{MC} \frac{\alpha_{jk} \tau_{jk}}{\Lambda_j} + (1-\theta) \Delta t_n \sum_{\substack{k=1 \\ k \neq j}}^{MC} \frac{\alpha_{jk}}{\Lambda_j} \} N_k^{n} + (1-\theta_d) \Delta t_n \sum_{i=1}^{ND} \lambda_{ji} C_{ji}^{n}$$

$$+ \theta_d \Delta t_n \sum_{i=1}^{ND} \lambda_{ji} \frac{(NUM)1 - (NUM)2}{(DEN)} C_{ji}^{n} + \theta \Delta t_n \, Q_j^{n+1} + (1-\theta) \Delta t_n Q_j^{n}$$

$j = 1, 2, \ldots\ldots, MC$ (B-28)

and $$C_{ji}^{n+1} = \frac{(NUM)1-(NUM)2}{(DEN)} C_{ji}^{n} + \frac{\bar{\beta}_{ji}\theta\Delta t_n}{\Lambda_j (DEN)} N_j^{n+1} + \frac{\bar{\beta}_{ji}(1-\theta)\Delta t_n}{\Lambda_j (DEN)} N_j^{n}$$

$$i = 1, 2, \ldots\ldots, ND$$

$$j = 1, 2, \ldots\ldots, MC \qquad (B-29)$$

where $(NUM)1 = 1 + [(\lambda_{jc}/\lambda_{jL}) + \lambda_{jc}(1-\theta_d)\ \Delta t_n]\ \exp(-\lambda_{jc}/\lambda_{jL})$

$(NUM)2 = (\lambda_{jc}/\lambda_{jL})\ (1-\theta_d)\Delta t_n$

and $(DEN) = 1+[(\lambda_{jc}/\lambda_{jL})-\lambda_{jc}\theta_d\Delta t_n]\exp(-\lambda_{jc}/\lambda_{jL}) + (\lambda_{ji} +\lambda_{jc})\ \theta_d\ \Delta t_n.$

NOMENCLATURE

c_{ji}	i th group delayed neutron precursor concentration for the j the core.
C_{ji}	Effective i th group delayed neutron precursor concentration for the j th core.
E	Symbol for the energy variable
F_j	Production operator for the j th core.
f_i	Energy spectrum for the delayed fission neutron of the i th group.
k_{eff}	System neutron multiplication factor.
ℓ	System neutron removal lifetime.
MC	Number of coupled cores in the BGCR system.
N_j, N_k	Core neutron levels for j th and k th cores.
ND	Number of delayed neutron groups.
q	Inhomogeneous neutron source.
Q_j	Weighted inhomogeneous neutron source for the j th core.
r	Symbol for vector variable indicating position
t	Symbol for time.
Δt	Time step.
v	Neutron speed.
w	Weighting function.
α_{jk}	Coupling coefficients for neutrons diffusing from core k to core j causing fission in core j.

$\bar{\beta}_{ji}$	Effective delayed neutron fraction for the i th group of precursors in the j th core.
$\bar{\beta}_j$	Total effective delayed neutron fraction in the j th core.
ϵ_{jk}	Probability that a neutron escaping the core k will cause fission in core j.
θ	Parameter (1,0 or 1/2) that determines whether the numerical scheme is fully implicit, fully explicit or average implicit.
λ_{jc}	Inverse of residence time of the delayed neutron precursors in core j.
λ_{ji}	The decay constant for the i th group of delayed neutron precursors in the j th core.
λ_{jL}	Inverse of the average circulation time of the delayed neutron precursors of the j th core in the external loop.
Λ_j	Prompt neutron generation time for the jth core.
ν	Average number of neutrons released per fission.
ρ	Reactivity of the system.
ρ_j	Reactivity of the j th core.
σ_f	Microscopic fission cross section.
Σ_f	Macroscopic fission cross section.
σ_a	Microscopic absorption cross section.
Σ_a	Macroscopic absorption cross section.
τ_{jk}	Average time delay associated with neutrons diffusing from k th core to the j th core.
χ	Energy spectrum for the prompt fission neutrons.
ψ	Shape function for the neutron flux.
Ω	Symbol for the vector indicating direction or angle.

APPENDIX C
BENCHMARK CALCULATIONS WITH XSDRNPM AND MCNP CODES ON REFERENCE SPHERICAL AND CYLINDRICAL GAS CORE REACTOR SYSTEMS

Steady state neutronic analysis of the multiple cavity bimodal gas core reactor system for this work has been done by using the Monte Carlo Neutron Photon (MCNP) transport code (3) and the one dimensional, discrete ordinates (S_N) transport code, XSDRNPM (4). Neutronic calculations for the multi-region bimodal gas core reactor system with XSDRNPM are done by mocking up the three-dimensional BGCR geometry with an one-dimensional spherical configuration (Figure 4-1) which has an equivalent volume core and an equivalent thickness moderator. Even though the k_{eff} values obtained from XSDRNPM have been used mainly as initial k_{eff} guesses for the respective MCNP runs, the XSDRNPM k_{eff} values for different configurations have also been used for comparative study of the static neutronics of the system. This Appendix compares the results from static neutronic calculations on a reference single chamber, cylindrical gas core reactor. One-dimensional XSDRNPM calculations are performed using both cylindrical geometry and a spherical mockup configuration. The XSDRNPM k_{eff} values are then compared with one another and with results from three-dimensional, cylindrical geometry, continuous energy MCNP calculations.

Continuous energy MCNP calculations are also performed on the spherical mockup configuration. The cylindrical geometry XSDRNPM calculations have been done with four-group and 26-group cross section structures and the spherical mockup XSDRNPM calculations have been done with four-group, 26-group, and 123-group cross section structures.

The reference cylindrical GCR system selected for these benchmark XSDRNPM and MCNP calculations has a core of radius 71.7 cm and a height of 140 cm. The cylindrical core is surrounded by 50 cm thick beryllium moderator on the side, top, and bottom of the gaseous core. The spherical mockup of the cylindrical system consists of a spherical core of radius 81.4 cm surrounded by 50 cm thick beryllium moderator.

Table C-1 gives the system neutron multiplication factor (k_{eff}) for the reference gas core reactor from XSDRNPM 4-group and 26-group cylindrical geometry calculations at various beryllium temperatures. Table C-2 gives the XSDRNPM system k_{eff} values for the spherical mockup of the reference system at different beryllium temperatures. The k_{eff} results from MCNP calculations for the reference GCR for various moderator temperatures are given in Table C-3. MCNP calculations for beryllium temperatures of 700 K and 1000 K are not done since the MCNP nuclear data library does not contain the cross section data for beryllium at these temperatures. Similarly the XSDRNPM nuclear data library does not have the neutron

Table C-1. System k_{eff} from XSDRNPM Benchmark Calculations for the Reference Gaseous Core Reactor-Cylindrical Geometry.

Core Radius = 71.7 cm
Core Height = 140 cm
Beryllium Thickness = 50 cm

Geometry	Number of Neutron Groups	Beryllium Temp (K)	k_{eff}^{*}	Deviation from XSDRNPM Spherical Mockup Calc. (%)	Deviation from MCNP Calc. (%)
Cylinder (1-D)	4	300	1.2933	+10.36	+14.36
		600	1.2940	+10.70	+12.37
		700	1.2919	+10.74	--
		800	1.2919	+10.72	+13.06
		1000	1.2879	+10.82	--
Cylinder (1-D)	26	300	1.2399	+9.67	+9.64
		600	1.2563	+10.70	+9.11
		700	1.2567	+11.02	--
		800	1.2582	+11.19	+10.10
		1000	1.2556	+11.64	--

*Convergence Criteria for XSDRNPM is 10^{-5}.

Table C-2. System k_{eff} from XSDRNPM Benchmark Calculations for the Reference Gaseous Core Reactor-Spherical Geometry Mockup.

Core Radius = 81.4 cm
Beryllium Thickness = 50 cm

Geometry	Number of Neutron Groups	Beryllium Temp (K)	k_{eff}*	Deviation from 123 Group Calc (%)	Deviation from MCNP Cyl. Geometry Calc (%)
Sphere (1-D)	4	300	1.1718	+5.36	+3.6
		600	1.1688	+3.58	+1.51
		700	1.1666	--	--
		800	1.1668	+3.95	+2.11
		1000	1.1621	+3.66	--
Sphere (1-D)	26	300	1.1305	+1.65	-0.025
		600	1.1341	+0.50	-1.51
		700	1.1319	--	--
		800	1.1316	+0.81	-0.98
		1000	1.1246	+0.32	--
Sphere (1-D)	123	300	1.1121		-1.65
		600	1.1284		-1.99
		800	1.1225		-1.77
		1000	1.1210		--

*Convergence Criteria for XSDRNPM Calculation is 10^{-5}.

Table C-3. System k_{eff} from MCNP Benchmark Calculation for the Reference Gaseous Core Reactor System.

Cylinder
Core Radius = 71.7 cm
Core Height = 140 cm
Beryllium Thickness = 50 cm

Spherical Mockup:
Core Radius = 81.4 cm
Beryllium Thickness = 50 cm

Geometry	Number of Neutron Groups	Beryllium Temperature (K)	k_{eff}*
"Equivalent" Sphere (3-D)	Continuous	800	1.1379**(.50)
Cylinder(3-D)	Continuous	300	1.1308(.41)
Cylinder(3-D)	Continuous	600	1.1515(.59)
Cylinder(3-D)	Continuous	800	1.1427(.45)
Cylinder(3-D)	Continuous	1200	1.1139(.57)

*Uncertainty (%) in k_{eff} and ℓ calculation given in parenthesis.

**Deviation from Cylindrical Geometry MCNP calculation is -0.42%.

cross section for beryllium at 1200 K and, hence, the calculations are not done at this temperature. The convergence level required for XSDRNPM k_{eff} is 10^{-5} and the uncertainty in k_{eff} values from MCNP is around 0.5%; uncertainty values are given in parenthesis for each k_{eff} in Table C-3. Tables C-4 and C-5 give, respectively, the 26-group and 4-group XSDRNPM neutron group structures.

The inherent difference in the MCNP and XSDRNPM schemes can be established from the MCNP spherical mockup and 123-group XSDRNPM spherical mockup results. The "equivalent" spherical mockup, 123 group XSDRNPM k_{eff} (= 1.1225) at a beryllium temperature of 800 K from Table C-2 is 1.35% less than the MCNP spherical mockup k_{eff} (= 1.1379) at a beryllium temperature of 800 K. This discrepancy in k_{eff} results from MCNP Monte Carlo transport theory versus XSDRNPM discrete ordinates calculations and MCNP continuous energy cross section library versus the AMPX multi-group cross section library for XSDRNPM calculations. The continuous energy MCNP neutron cross section library is obtained by processing the ENDF/B-V cross section files into the ACE (A Compact ENDF) format with the ACER module of the NJOY nuclear data processing system from the Los Alamos National Laboratory. The multi-group XSDRNPM cross section library is processed from the ENDF/B-IV files by the XLACS module in the AMPX package from the Oak Ridge National Laboratory.

Table C-4. XSDRNPM Collapsed 26-Group Structures.

Group	E(lower) (eV)	E(upper) (eV)
1	7.408+06	14.918+06
2	3.012+06	7.408+06
3	2.231+06	3.012+06
4	1.653+06	2.231+06
5	1.353+06	1.653+06
6	8.208+05	1.353+06
7	4.978+05	8.208+05
8	3.337+05	4.978+05
9	1.831+05	3.337+05
10	1.227+05	1.831+05
11	5.247+04	1.227+05
12	1.171+04	5.247+04
13	5.531+03	1.171+04
14	3.354+03	5.531+03
15	9.611+02	3.354+03
16	2.754+02	9.611+02
17	7.889+01	2.754+02
18	2.260+01	7.889+01
19	6.476+00	2.260+01
20	1.860+00	6.476+00
21	1.125+00	1.860+00
22	6.500-01	1.125+00

Table C-4. Continued.

Group	E(lower) (eV)	E(upper) (eV)
23	2.500-01	6.500-01
24	1.200-01	2.500-01
25	5.000-02	1.200-01
26	5.000-03	5.000-02

Table C-5. XSDRNPM Collapsed 4-Group Structure.

Group	E(lower) (eV)	E(upper) (eV)
1	8.208+05	14.918+06
2	5.531+03	8.208+05
3	1.860+00	5.531+03
4	5.000-03	1.860+00

The results of Table C-1 indicate that the XSDRNPM cylindrical geometry k_{eff} values for both the 26-group and 4-group reference GCR calculations are about 10-11% higher than the corresponding values from the XSDRNPM spherical mockup calculations. Table C-1 also indicates that the 4-group XSDRNPM cylindrical geometry k_{eff} values are on the average 12-14% higher and the 26-group XSDRNPM values about 9-10% higher than the corresponding values from the MCNP calculations. The large deviation (overestimate) of cylindrical geometry XSDRNPM k_{eff} values relative to the XSDRNPM spherical mockup calculation results is due to the inability of the one-dimensional XSDRNPM cylindrical geometry calculations to account for the perpendicular leakage from the system. The cylinder is considered to be of infinite height in the calculations (zero perpendicular leakage); since the flux does not "buckle" in the gas core, perpendicular bucklings cannot be used to account for perpendicular leakages.

The results for the spherical mockup XSDRNPM calculations given in Table C-2 indicate that the system k_{eff} values for four-group, 26-group and 123-group calculations are closer to the MCNP results than the results for the XSDRNPM cylindrical calculations of Table C-1. The 4-group XSDRNPM results are about 1-3% higher and the 26-group results are about 0.03-1.5% lower than the MCNP results. The 123-group results are about 1.6 to 2% lower than the MCNP results. It is to be noted that at a beryllium temperature of 800 K the k_{eff} value from the four-group XSDRNPM spherical mockup is about 2% higher than the corresponding k_{eff} value from the MCNP calculation. The static MCNP and four-group XSDRNPM results presented in Chapter 4 are done at a beryllium temperature of 800 K. The better k_{eff} results for the XSDRNPM spherical mockup calculations as compared to the cylindrical geometry results is due to the fact that the spherical mockup better simulates the two-dimensional cylindrical geometry because one-dimensional, cylindrical geometry calculations are unable to account for transverse leakage effects. Also, the 26-group and 123-group XSDRNPM spherical mockup results show improvement over the four-group XSDRNPM calculations since the 26-group and 123-group cross section structures have better resolution in the thermal energy range and in the high energy range. The larger number of low energy groups (six in the 26-group and 30 in the 123-group structure) helps to model the thermal scattering well and the larger number of high energy cross section groups can better take care of the important (n,2n) reaction in beryllium.

It is to be noted that the deviation of 123-group XSDRNPM k_{eff} values are slightly greater than the deviation of 26-group XSDRNPM k_{eff} values from MCNP cylindrical k_{eff} values. As shown above, the combination of cross section library differences and Monte Carlo transport theory versus discrete ordinates transport theory calculational differences leads to XSDRNPM inherently underestimating the k_{eff} by about 1.35% relative to k_{eff} from an otherwise identical MCNP calculation. From Table C-3 it is also observed that the spherical mockup MCNP calculations lead to a 0.4% underestimate in k_{eff} relative to the value obtained from the true cylindrical geometry calculations. This combination of factors is responsible for the approximate 1.8% underestimate of k_{eff} by 123 group XSDRNPM spherical mockup calculations that is seen in Table C-2. When analyzing thermal reactors, a collapsing from many groups to fewer groups almost always results in an increase in k_{eff}. The fewer group structure (especially fewer thermal groups) has a tendency to overemphasize the more productive lower energy group(s) at the expense of less productive higher energy groups. In Table C-2, collapsing from 123 to 26-groups results in a 0.3% to 1.7% overestimate in k_{eff}. When this is combined with the inherent ≈1.8% k_{eff} underestimate for (many group) XSDRNPM spherical calculations, the result is a ≈0% to 1.5% underestimate for k_{eff}. Similarly, in Table C-2 a collapsing from 123 to 4 groups results in about a 4% overestimate in k_{eff}. When this is combined with the inherent ≈1.8% k_{eff} underestimate for (many group) XSDRNPM spherical calculations, the result is about a 2 to 3% overestimate for k_{eff}.

The system k_{eff} values from MCNP given in Table C-3 indicate that at a moderator temperature of 800 K, the k_{eff} from the spherical mockup of the GCR is about 0.4% less than the k_{eff} obtained when cylindrical geometry is employed. By including the uncertainty of about 0.5% in the MCNP k_{eff} values, this discrepancy can be in the range of +0.1% to -0.9%.

The benchmark calculations presented in this appendix in Tables C-1 through C-3 have shown that the k_{eff} values from the one-dimensional XSDRNPM spherical mockup calculations are closer to the three-dimensional MCNP cylindrical geometry results than are the one-dimensional cylindrical geometry XSDRNPM k_{eff} values. Even though 26-group or 123-group XSDRNPM calculations are inherently more accurate than the four-group XSDRNPM calculations, it would have been prohibitively expensive to undertake 26-group or 123-group XSDRNPM calculations for all the cases that are presented in Chapters 4 and 5. Since the results from XSDRNPM are used only as either initial guesses for the respective MCNP runs and/or to explain trends in the neutronic behavior of different configurations of the BGCR, 4-group spherical mockup XSDRNPM calculations are found to be sufficient for these purposes.

APPENDIX D

COMPARISON OF RESULTS FROM COUPKIN AND ANCON CODES

In order to establish the validity of the basic point reactor kinetics equations and the solution method used in this dissertation, the results from the COUPKIN program for a few reference single core reactor transients are compared with the results from the ANCON code (5).

The COUPKIN program solves the coupled core point reactor kinetics equations (B-1 and B-2) for core power levels and delayed neutron precursor concentrations. The solution procedure used in the COUPKIN program is given in detail in Appendix B. In order to compare the results from the COUPKIN program directly with those from the single core kinetics code, ANCON, the coupled core kinetics equations in COUPKIN are reduced to one set of equations for a single core without the coupled source term.

The ANCON (ANalytic CONtinuation) code solves the point reactor kinetics equations, including thermal feedback, by a method known as continuous analytic continuation (43-44). For this comparative evaluation of the results from the COUPKIN and ANCON programs, the thermal feedback calculations are not included in the ANCON code. The functional form of the reactivity input for the ANCON code includes both impressed reactivity and reactivity feedback. The options for impressed reactivity include a constant reactivity, constant reactivity with a sinusoidal driving term with or without linear thermal feedback, polynomials in time as the driving terms and nonlinear thermal feedback including Doppler feedback. For this comparative evaluation of the ANCON and COUPKIN results, the reactivity input for the ANCON code is constant.

The continuous analytic continuation method consists of expanding the dependent variables, neutron level (N(t)) and delayed neutron precursor concentrations (C(t)), in Taylor series, with a truncation error criterion, over successive intervals on the time axis. The order of the Taylor expansion is specified in the input. The time steps are obtained by requiring that the absolute value of the fractional truncation error for each expansion be, at most, equal to an input truncation error criterion.

The neutron generation time, delayed neutron fraction, and delayed neutron precursor decay constants are input to the ANCON code. The initial values for the delayed neutron precursor concentrations can either be read in or the code can compute values from the equilibrium conditions.

Comparison of results from ANCON and COUPKIN is made for four cases: subcritical, supercritical, and two superprompt critical systems. Tables D-1 through D-4 show the relative neutron levels (N(t)/N(0)) as a function of time for the four reference cases as calculated by the ANCON and COUPKIN programs. The results shown in these Tables are the relative power levels from ANCON and COUPKIN calculations at times calculated by ANCON code. The ANCON code employs a variable time step which is determined by the input truncation error ctriterion. The relative power levels from the COUPKIN code given in these tables are at the ANCON time steps and are interpolated from the COUPKIN results since the COUPKIN time steps do not correspond to those of ANCON.

Table D-1 shows the variation of relative neutron level, N(t)/N(0), with time for a supercritical system of neutron multiplication factor 1.0058 and neutron generation time 1.896×10^{-3} second. The COUPKIN results agree completely with the ANCON results for the first five seconds of the transient. It can be seen that the COUPKIN results are slightly less (0.01% to 0.05%) than the ANCON results during the remaining time period (5.5 to 9.5 seconds) of the transient.

Table D-2 shows the variation of the relative neutron level with time for a subcritical system of neutron multiplication factor 0.928 and neutron generation time 2.563×10^{-3} second. It can be seen that except during the initial 0.13 seconds, the COUPKIN and ANCON results agree with each other.

Table D-1. Relative Neutron Level (N(t)/N(O)) as a Function of Time as Predicted by ANCON and COUPKIN for a System of Neutron Multiplication Factor 1.0058.

Neutron Generation Time = 1.896E-03 seconds
Reactivity = 0.005767

Time (sec)	Rel. Neutron Level (N(t)/N(O))		Percentage Deviation of COUPKIN Results
	ANCON	COUPKIN	
0.0	1.0	1.0	0
0.1455	1.432	1.432	0
0.4877	2.417	2.417	0
1.1965	4.670	4.670	0
1.5117	5.895	5.895	0
1.9015	7.704	7.704	0
2.3894	1.057+01	1.057+01	0
3.0909	1.639+01	1.639+01	0
3.9557	2.775+01	2.775+01	0
4.6837	4.299+01	4.299+01	0
5.5501	7.217+01	7.216+01	-0.011
6.2848	1.118+02	1.117+02	-0.04
7.1488	1.869+02	1.868+02	-0.05
7.8873	2.898+02	2.898+02	0
8.7480	4.833+02	4.832+02	-0.02
9.4896	7.506+02	7.505+02	-0.01

Table D-2. Relative Neutron Level (N(t)/N(O)) as a Function of Time as Predicted by ANCON and COUPKIN for a System of Neutron Multiplication Factor 0.9280.

Neutron Generation Time = 2.563E-03 seconds
Reactivity = -0.07759

Time (sec)	Rel. Neutron Level (N(t)/N(O))		Percentage Deviation of COUPKIN Results
	ANCON	COUPKIN	
0.0	1.0	1.0	---
0.0201	0.555	0.555	---
0.0675	1.774-01	1.785-01	+0.62
0.1267	8.984-02	9.000-02	+0.18
0.2052	7.462-02	7.462-02	0
0.6963	6.425-02	6.425-02	0
1.0325	5.971-02	5.971-02	0
2.2851	4.822-02	4.822-02	0
3.5323	4.080-02	4.080-02	0
4.2720	3.742-02	3.742-02	0
5.0389	3.446-02	3.446-02	0

Tables D-3 and D-4 give the relative neutron level (N(t)/N(0)) as a function of time, respectively, for two superprompt critical systems: Table D-3 for a system of neutron multiplication factor 1.042 and generation time $1.829\text{x}10^{-3}$ second and Table D-4 for a system of neutron multiplication factor 1.117 and generation time $1.767\text{x}10^{-3}$ second. It can be seen from Table D-3 that the COUPKIN results are about 0.04% to 0.45 % greater than the respective ANCON results. For a superprompt critical system of neutron multiplication factor 1.117, the results of Table D-4 indicate that COUPKIN predicts a higher power level (by 1.6%-5.5%) than does ANCON during the examined period.

Comparative evaluation of the ANCON and COUPKIN results performed in this Appendix indicates that even for systems which are superprompt critical, the ANCON and COUPKIN results agree reasonably well. In view of this, since the dynamic neutronic analysis is done for BGCR system configurations with individual cores that range from subcritical to slightly above critical, it is concluded that the basic point reactor kinetics equations and the solution method employed in COUPKIN are valid.

Table D-3. Relative Neutron Level (N(t)/N(O)) as a Function of Time as Predicted by ANCON and COUPKIN for a System of Neutron Multiplication Factor 1.0421.

Neutron Generation Time = 1.829E-03 seconds
Reactivity = 0.0404

Time (sec)	Rel. Neutron Level (N(t)/N(O))		Percentage Deviation of COUPKIN Results
	ANCON	COUPKIN	
0.0	1.0	1.0	---
0.0495	2.793	2.794	+0.04
0.1248	1.189+01	1.194+01	+0.42
0.2005	4.909+01	4.913+01	+0.08
0.5036	1.379+04	1.385+04	+0.43
0.7056	5.908+05	5.934+05	+0.44
1.0087	1.656+08	1.659+08	+0.18
1.2108	7.093+09	7.104+09	+0.15
1.3118	4.642+10	4.656+10	+0.30
1.4128	3.037+11	3.049+11	+0.39
1.5138	1.988+12	1.997+12	+0.45
2.0190	2.386+16	2.391+16	+0.20

Table D-4. Relative Neutron Level (N(t)/N(O)) as a Function of Time as Predicted by ANCON and COUPKIN for a System of Neutron Multiplication Factor 1.1171.

Neutron Generation Time = 1.767E-03 seconds
Reactivity = 0.1048

Time (sec)	Rel. Neutron Level (N(t)/N(O))		Percentage Deviation of COUPKIN Results
	ANCON	COUPKIN	
0.0	1.0	1.0	---
0.0168	2.641	2.700	+2.2
0.0504	1.758+01	1.792+01	+1.9
0.1011	2.952+02	3.000+02	+1.6
0.2023	8.275+04	8.555+04	+3.4
0.5061	1.822+12	1.900+12	+4.2
0.7508	1.498+18	1.536+18	+2.5
0.9027	7.031+21	7.366+21	+4.7
1.0040	1.970+24	2.078+24	+5.4

LIST OF REFERENCES

1. N.J. Diaz, E.T. Dugan, C.C. Oliver, E.E. Carroll, Jr., and E.D. Whitney, "Studies of Pulsed Gaseous Core Nuclear Systems," Annual Report, NSF Grant Number 77-28034, University of Florida, Gainesville (March 1979).

2. N.J. Diaz, E.T. Dugan, C.C. Oliver, E.E. Carroll, Jr., and E.D. Whitney, "Basic Feasibility Studies of Pulsed Gaseous Core Nuclear Systems," Annual Report, NSF Grant Number 77-28034, University of Florida, Gainesville (March 1980).

3. J.F. Breismeister, Ed. "MCNP-A General Monte Carlo Code for Neutron and Photon Transport, Version 3A," LA-7396, Revision 2, Los Alamos National Laboratory, Los Alamos (1986).

4. L.M. Petrie and N.M. Greene, "XSDRNPM: AMPX Module with One-Dimensional S_n Capability for Spatial Weighting," AMPX: A Modular Code System for Generating Coupled Multigroup Neutron-Gamma Libraries from ENDF/B, Oak Ridge National Laboratory, Oak Ridge (March 1976).

5. John C. Vigil, "ANCON User's Manual," LA-4616, VC-32, TID-4500, Los Alamos National Laboratory, Los Alamos (May 1971).

6. R. Avery, "Theory of coupled Reactors," Proc. of the Second United Nations International Conference on the Peaceful Uses of Atomic Energy, Geneva 1958, Vol. 12, pp. 182-191, United Nations, New York (1958).

7. R. Avery, "Coupled Fast-Thermal Power Breeder," Nucl. Sci. Eng., Vol. 3, pp. 120-144 (1958).

8. Masaoki Komato, "An Attempt of Applying Reactor Theory to Time-Dependent Multi-Region System," Coupled Reactor Kinetics - Proc. of the National Topical Meeting on Coupled Reactor Kinetics at Texas A and M University, College Station, Texas, January 1967, CONF-670107, pp. 129-152, University of Texas, College Station (1967).

9. S. Kaplan, A.F. Henry, S.G. Margolis, and J.J. Taylor, "Space-Time Reactor Dynamics," Proc. of Third International Conference on Peaceful Uses of Atomic Energy, Geneva 1964, Vol. 4, p. 31, United Nations, New York (1964).

10. A. Bellani-Morante, "The Kinetic Behavior of a Reactor Composed of Two Loosely Coupled Cores: Integral Formulation," J. of Nuclear Energy Parts A/B, Vol. 18, pp. 547-559 (1964).

11. G.E. Hansen, "Kinetics Equation for a Cluster of Rover Reactors," Los Alamos National Laboratory Office memorandum N-2-7967, Los Alamos National Laboratory, Los Alamos (1965).

12. R.G. Cockrell and R.B. Perez, "On the Kinetic Theory of Spatial and spectral Coupling of the Reactor Neutron Field," Proc. Symposium Neutron Dynamics and Control, pp. 323-341, University of Arizona, Tucson (April 1965).

13. S.J. Gage, F.T. Adler, and P.N. Powers, "Investigations on Nonlinear Stability of Coupled Nuclear Systems," Proc. Symposium Neutron Dynamics and Control, pp. 45-76, University of Arizona, Tucson (April 1965).

14. D. Schwalm, "On a Multigroup Kinetics," EUR2285E (1965).

15. D. Schwalm, "On a Derivation of the Multigroup Kinetic Equations of Coupled Reactors," EUR2416E (1965).

16. R.L. Seale, "Coupled Core Reactors," LAMS-2967, Los Alamos National Laboratory, Los Alamos (1964).

17. R.L. Seale, "Investigation of Coupled Rover Cores," LAMS-2968, Los Alamos National Laboratory, Los Alamos (1964).

18. E.P. Gyftopoulos, "Point Reactor Kinetics and Stability Criteria," Proc. Third International Conference on Peaceful Uses of Atomic Energy, Geneva, 1964, pp. 3-9, United Nations, New York (1964).

19. H. Plaza and W.H. Kohler, "Coupled Core Kinetics Equations," Nucl. Sci. Eng., Vol. 26, pp. 419-423 (1966).

20. G.C. Baldwin, "Kinetics of a Reactor Composed of Two Loosely Coupled Cores," Nucl. Sci. Eng., Vol. 6, pp. 320-327 (1959).

21. R.L. Seale and G.E. Hansen, "Calculation of Interaction Parameters for Loosely Coupled Reactor Systems," Coupled Reactor Kinetics - Proc. of the National Topical Meeting on Coupled Reactor Kinetics at Texas A and M University, College Station, Texas, January 1967, pp. 218-230, CONF-670107, University of Texas, College Station (1967).

22. A.F. Henry, "The Application of Reactor Kinetics to the Analysis of Experiments", Nucl. Sci. Eng., Vol. 37, pp. 52-70 (1958).

23. G.I. Bell, S. Glasstone, Nuclear Reactor Theory, Robert E. Kreiger Publishing Company, Malabar, Florida (1970)..

24. C.G. Chezem and H.H. Helmick, "Pulsed Neutron Analysis in the Los Alamos Coupled Reactor Experiment," LA-3263-MS , Los Alamos National Laboratory, Los Alamos (1965).

25. L.D.P. King, "Description of the KIWI-TNT- Excursion", Trans. Am. Nucl. Soc., Vol. 8, p. 126 (1965).

26. W.R. Stratton, D.M. Peterson, and P.M. Altomare, "Analysis of the KIWI-TNT Experiment," Trans. Am. Nucl. Soc., Vol. 8, p. 126 (1965).

27. C.D. Kylstra, J.L. Cooper, Jr., and B.E. Miller, "UF_6 Plasma Engine," 2nd Symposium on Uranium Plasmas: Research and Applications - A Collection of Technical Papers, pp. 283-290, Atlanta, Georgia, November 1971, AIAA, New York (1971).

28. E.T. Dugan, N.J. Diaz, and C.C. Oliver, "Neutronics and Energetics of Pulsed Gaseous Core Nuclear Systems," NSF Final Report, Grant Number ENG-75-01437, University of Florida, Gainesville (April 1978).

29. N.J. Diaz, Edward T. Dugan, and Calvin C. Oliver, "Cyclic Gas Core Reactor Power Systems," Atomkernenergic Kerntechnk, Vol. 36, pp. 191-194 (1980).

30. E.T. Dugan, "The Nuclear Piston Engine and Pulsed Gaseous Core Reactor Power System," Ph.D. Dissertation, University of Florida, Gainesville (1976).

31. Edward T. Dugan, Nils J. Diaz, and Edward E. Carroll, Jr., "Gas Core Reactor Neutronics - Theoretical Modeling and Experimental Verification," Nuclear Technology, Vol. 69, pp. 134-153 (1985).

32. R. Douglas O'Dell, Forrest W. Brinkley, and Duane R. Marr, "User's Manual for ONEDANT: A Code Package for One-Dimensional, Diffusion-Accelerated, Neutral-Particle Transport," LA-6941-MS, Los Alamos National Laboratory, Los Alamos (1982).

33. Ray E. Alcouffe, Forrest W. Brinkley, Duane R. Marr and R. Douglas O'Dell, "User's Guide for TWODANT: A Code Package for Two-Dimensional, Diffusion-Accelerated, Neutron-Particle Transport," LA-10049-M, Revision 1, Los Alamos National Laboratory, Los Alamos (1984).

34. R.E. MacFarlane, D.W. Muir, and R.M. Boicouit, "The NJOY Nuclear Data Processing System, Volume 1: User's Manual, Volume II: The NJOY, RECONR, BROADR, HEATR and THERMR Modules," LA-9303-M, Los Alamos National Laboratory, Los Alamos (May 1982).

35. R.A. Forster and T.N.K. Godfrey, "MCNP-A General Monte Carlo Code for Neutron and Photon Transport," Monte Carlo methods and Application in Neutronics, Photonics and Statistical Physics - Lecture Notes in Physics 240, pp. 33-55, Springer Verlag, New York (1985).

36. Robert C. Little and Robert E. Seamon, "Nuclear Data for MCNP," Monte Carlo Methods and Applications in Neutronics, Photonics and Statistical Physics - Lecture Notes in Physics 240, pp. 13-25, Springer Verlag, New York (1985).

37. J.S. Hendricks and T.E. Booth, "MCNP Variance Reduction Overview," Monte Carlo Methods and Application in Neutronics, Photonics and Statistical Physics - Lecture Notes in Physics 240, pp. 83-92, Springer Verlag, New York (1985).

38. Thomas E. Booth, "A Sample Problem for Variance Reduction in MCNP," LA-10363-MS, VC-32, Los Alamos National Laboratory, Los Alamos (October 1985).

39. R.J. Hoverton, R.E. Dye, P.C. Giles, J.R. Kimlinger, S.T. Perkins, and E.F. Plechaty, "Omega Documentation," UCRL-50400, Vol. 25, Lawrence Livermore National Laboratory, Livermore (August 1983).

40. R.E. Prael, "Summary of Thermal Reactor Benchmark Calculations Using MCNP with ENDF/B Version IV Data," LA8232-PR, p. 3, Los Alamos National Laboratory, Los Alamos (February 1980).

41. T.E. Booth and J.S. Hendricks, "Importance Estimation in Forward Monte Carlo Calculations," Nucl. Tech./Fusion, Vol. 5, p. 90 (1984).

42. John MacPhee, "The Kinetics of Circulation Fuel Reactors," Nucl. Sci. Eng. Vol. 4, pp. 588-597 (1958).

43. H.T. Davis, Introduction to Nonlinear Differential and Integral Equations, Dover Publications, New York (1962).

44. J.C. Vigil, "Solution of the Reactor Kinetics Equation by Analytic Continuation," Nucl. Sci. Eng., Vol. 29, pp. 392-401 (1967).

BIOGRAPHICAL SKETCH

Mathew M. Panicker was born on August 19, 1945, in Kerala, India. In 1961, Mathew Panicker matriculated to the University of Kerala and received the degree of Bachelor of Science in physics with first class in 1965. He continued his graduate study in Physics at the University of Kerala and received the Master of Science degree with first class in 1967.

After teaching two years at the Catholicate College, affiliated to the University of Kerala, Mathew Panicker left India in 1969 for Liberia, West Africa, to accept a teaching position in physics and mathematics at Cuttington University College in Liberia. In 1976, he was promoted to Associate Professor of Physics and Chairman of the Science Division at Cuttington University College. In the fall of 1980 Mathew Panicker entered the graduate program in nuclear engineering at the North Carolina State University in Raleigh, North Carolina. In 1983 he obtained the Master of Science degree in nuclear engineering from NCSU. In 1983 the author was awarded admission and a teaching assistantship in nuclear engineering sciences at the University of Florida to pursue the Ph.D. degree.

At the University of Florida, Mathew Panicker continued as teaching assistant in nuclear engineering until May 1985. From June 1985 he has been working as a research assistant in the Innovative Nuclear Space Power Institute.

He is married to the former Annamma Varghese. Their son, Dinesh Panicker, is 9 years old.

I certify that I have read this study and that in my opinion it conforms to acceptable standards of scholarly presentation and is fully adequate, in scope and quality, as a dissertation for the degree of Doctor of Philosophy.

Edward T Dugan

Edward T. Dugan, Chairman
Associate Professor of
Nuclear Engineering Sciences

I certify that I have read this study and that in my opinion it conforms to acceptable standards of scholarly presentation and is fully adequate, in scope and quality, as a dissertation for the degree of Doctor of Philosophy.

Alan M. Jacobs

Alan M. Jacobs,
Professor of Nuclear
Engineering Sciences

I certify that I have read this study and that in my opinion it conforms to acceptable standards of scholarly presentation and is fully adequate, in scope and quality, as a dissertation for the degree of Doctor of Philosophy.

Nils J. Diaz
Professor of Nuclear
Engineering Sciences

I certify that I have read this study and that in my opinion it conforms to acceptable standards of scholarly presentation and is fully adequate, in scope and quality, as a dissertation for the degree of Doctor of Philosophy.

Calvin C. Oliver

Calvin C. Oliver
Professor of Mechanical
Engineering

I certify that I have read this study and that in my opinion it conforms to acceptable standards of scholarly presentation and is fully adequate, in scope and quality, as a dissertation for the degree of Doctor of Philosophy.

Robert J Hanrahan

Robert J. Hanrahan
Professor of Chemistry

This dissertation was submitted to the Graduate Faculty of the College of Engineering and to the Graduate School and was accepted as partial fulfillment of the requirements for the degree of Doctor of Philosophy.

May 1989

Hubert A. Bevis

Dean, College of Engineering

Dean, Graduate School

UNIVERSITY OF FLORIDA
3 1262 08556 8078